12-16-2015 12:00 AM

The Role of Bone Sialoprotein in Periodontal Tissue Development and Bone Repair

Yohannes Soenjaya
The University of Western Ontario

Supervisor
Harvey A. Goldberg
The University of Western Ontario

Graduate Program in Biomedical Engineering
A thesis submitted in partial fulfillment of the requirements for the degree in Doctor of Philosophy

Abstract

Bone development and repair involve complex processes that include interaction between cells and their surrounding matrix. In the body, bone sialoprotein (BSP) expression is up-regulated at the onset of mineralization. BSP is a multifunctional acidic phosphoprotein with collagen-binding, hydroxyapatite nucleating, and integrin recognition (RGD sequence, which is important for cell-attachment and signaling) regions. Mice lacking BSP expression (*Bsp*$^{-/-}$), exhibit a bone phenotype with reductions in bone mineral density, bone length, osteoclast activation, and impaired bone healing. This thesis examined the role of BSP in tooth development and also its potential use as a therapeutic reagent for bone repair. MicroCT and histological analysis of *Bsp*$^{-/-}$ mice revealed significant periodontal tissue breakdown marked by defective acellular cementum formation leading to periodontal ligament detachment, extensive alveolar bone and tooth root resorption, and tooth malocclusion. Substituting hard to soft diet, which minimized applied stress during mastication, did not reduce extent of periodontal tissue breakdown. However, soft diets eliminated the incidence of severe incisor malocclusion and the *Bsp*$^{-/-}$ mice featured normal body weight, long-bone length, and serum alkaline phosphatase activity, suggesting that tooth dysfunction and malnutrition contribute to growth and skeletal defects previously reported.

In the bone repair studies, the effectiveness of BSP-treated nano-hydroxyapatite/poly(ester-urethane) (nHA/PU) scaffolds in promoting bone regeneration was determined using a rat calvarial defect model. Recombinant human bone morphogenetic protein (rhBMP-2), which is a potent growth factor was used as the positive control for repair. Addition of BSP to nHA/PU scaffolds improved cell attachment and differentiation, and the consequent osteogenic mineralization *in vitro*. *In vivo*, at 6 weeks, microCT and histological analysis indicated that the rhBMP-2 treated nHA/PU scaffolds promoted significant new bone repair, in which approximately 70% of the defect, based on bone volume to total defect volume, was filled with new bone. In contrast, both BSP-treated nHA/PU scaffolds and non-treated scaffolds resulted in approximately 20% new bone formed. These findings suggest that BSP plays a non-redundant role in cementum formation, likely involved in initiating mineralization on the root surface. The effectiveness of nHA/PU scaffold as a carrier for

rhBMP-2 and BSP was verified. However, in our system, BSP by itself was not a potent promoter of bone regeneration *in vivo*.

Key words: Bone sialoprotein, cementum, periodontal ligament, bone resorption, malocclusion, hydroxyapatite, poly(ester-urethane), bone morphogenetic protein 2, bone repair

Co-Authorship Statement

Chapter 2 entitled "Deficiency in acellular cementum and periodontal attachment in *Bsp*-null mice" was adapted from Foster et al., 2013. (Published). The manuscript was written by Dr. B.L. Foster with suggestions and edits from Y. Soenjaya, and Drs. M.J. Somerman and H.A. Goldberg. The histological analyses were performed at the NIH facilities under the guidance of Dr. B.L. Foster. The animal breeding and maintenance, preparation of all the specimens, blood serum collection, and imaging analyses were done by Y. Soenjaya.

Chapter 3 entitled "Mechanical forces exacerbate periodontal defects in *Bsp*-null mice" was adapted from Soenjaya et al., 2015. (Published). The manuscript was written by Y. Soenjaya. The histological analyses were performed at the NIH facilities with the guidance of Dr. B.L. Foster. The eruption study was performed by M. Ao with the guidance of Dr. B.L. Foster. All other experiments and analyses including animal breeding and maintenance, preparation of the specimens, blood serum collection, and imaging analyses were done by Y. Soenjaya.

Chapter 4 entitled "Healing of rat calvarial defects with nano-hydroxyapatite/poly(ester-urethane) scaffolds loaded with low dose rhBMP-2" was written by Y. Soenjaya. The poly(ester-urethane)-based scaffolds were provided by Drs. D. Eglin and M. Alini. The mechanical tests were done by Y. Soenjaya with guidance from Dr. T. L. Willett. All other experiments were performed by Y. Soenjaya.

Chapter 5 entitled "Effect of bone sialoprotein treated nano-hydroxyapatite/poly(ester-urethane) scaffolds on bone formation" was written by Y. Soenjaya. The poly(ester-urethane)-based scaffolds were provided by Drs. D. Eglin and M. Alini. All other experiments were performed by Y. Soenjaya.

Chapter 4 and 5 are currently being combined in preparation for a manuscript.

Acknowledgments

The pursuit of this degree has been a journey and humbling experience. It has been a privilege to work with so many people who have supported and helped over the course of my study. First I would like to thank my primary supervisor Dr. Harvey A. Goldberg for the guidance and giving me the opportunity to pursue my passion for research. Under his guidance I have grown personally and professionally through the life lessons and personal discussions that we had over the years. Thank you for giving me the flexibility to design experiments, interpret the data, collaborate with other researchers, and also allowing me to make mistakes along the way. I know that I would not be the person I am today without your mentorship and guidance.

I would like to extend many thanks to my co-supervisor, Dr. Robert. D. Litchfield and advisory committee board, Drs. Graeme K. Hunter and David. W. Holdsworth, for their support, guidance, and mentorship over the course of my study. Special thanks to our great collaborators Drs. Brian L. Foster, Martha J. Somerman, David Eglin, and Mauro Alini. Their input, feedback and guidance during the preparation of experiments and manuscripts were immensely valuable and greatly appreciated.

The completion of this thesis could not be possible without the assistance and support of all my friends and colleagues. Special thanks to Vasek Pitelka for teaching and assisting me in animal surgeries. I would like to thank Linda Jackson and Honghong Chen for assistance in planning and preparing histological samples for analysis. To my labmates and friends: Dr. Erik Holm, Dr. Lauren Solomon, Dr. Michael Pest, Dr. Shawna Kim, Dr. Kim Beaucage, Dr. Chris Norley, Dr. Steven Pollman, Justin Tse, Rose Yee, Lim Chien Tang, Nancy Wang, Ryan Marinovich, Kevin Bartman, Yinyin (Heidi) Liao, and anyone who I might have forgotten, thank you for lending a hand, guidance, and encouragement. You guys have made my time in the lab fun, lively, and always interesting. Especially on topics that are not related to research.

Finally, I thank all of my family and family-in-law members for all of the great encouragement, endless love and support. Thank you for all of your confidence in me.

Special thanks to my wife, Shirleen, for having faith in me, and also our 7 month old son, Matthew, who likes to distract me every day and never fails to make me laugh. Also not to forget, my cousin, Isabela for all her encouragement and support. I am fortunate to have had all these people in my life and throughout the pursuit of this PhD.

Table of Contents

Abstract ii

Co-Authorship Statement iv

Acknowledgments v

Table of Contents vii

List of Tables xii

List of Figures xiii

List of Appendices xvi

List of Abbreviations xvii

CHAPTER 1 1

1 Literature Review 1

1.1 INTRODUCTION 2

1.2 SKELETAL TISSUE DEVELOPMENT 2

1.2.1 Skeletal cell: Osteoblasts 3

1.2.2 Skeletal cell: Osteoclasts 3

1.2.3 Endochondral and intramembranous ossification 4

1.2.4 Bone repair 5

1.2.5 Mouse tooth development 7

1.2.6 Tooth anatomy 11

1.3 BONE SIALOPROTEIN (BSP) 15

1.3.1 BSP structure and function 15

1.3.2 BSP expression and role in biomineralization 18

1.4 BONE MORPHOGENETIC PROTEIN (BMP) 20

1.4.1 Role of BMP in bone regeneration 20

1.4.2 Potential side effects of using high dose of BMPs 22

1.5 BIOMATERIALS FOR TISSUE ENGINEERING 23

1.5.1 Introduction of biomaterials scaffolds 23

1.5.2 Potential use of nanohydroxyapatite/poly(ester-urethane) scaffold as a carrier for growth factors and bioactive proteins 26

1.6 PURPOSE OF THE THESIS 27

1.7 REFERENCES 31

CHAPTER 2 42

2 Deficiency in acellular cementum and periodontal attachment in *Bsp*-null mice 42

2.1 INTRODUCTION 43

2.2 MATERIALS & METHODS 44

2.2.1 Animals 44

2.2.2 Micro-computed tomography (microCT) and scanning electron microscopy (SEM) 44

2.2.3 Histological procedures 45

2.3 RESULTS 46

2.3.1 *Bsp*$^{-/-}$ mice exhibit defective acellular cementum formation 46

2.3.2 Failure of acellular cementum mineralization in *Bsp*$^{-/-}$ mice 55

2.3.3 Periodontal breakdown in *Bsp*$^{-/-}$ mice 60

2.4 DISCUSSION 71

2.4.1 Acellular cementum as a mineralization-sensitive tissue 71

2.4.2 Absence of BSP leads to periodontal breakdown 72

2.5 REFERENCES 74

CHAPTER 3 78

3 Mechanical Forces Exacerbate Periodontal Defects in *Bsp*-null Mice 78

3.1 INTRODUCTION 79

3.2 MATERIALS AND METHODS 80

3.2.1 Animals 80

3.2.2 Blood chemistry 80

3.2.3 Histology 81

3.2.4 Micro-computed tomography 81

3.2.5 Measurement of incisor eruption rate 82

3.2.6 Statistical analyses 82

3.3 RESULTS 83

3.3.1 Soft diet normalized body weight, long-bone length, and incisor malocclusion of *Bsp*$^{-/-}$ mice 83

3.3.2 Altered dentin and enamel formation in incisors of *Bsp*$^{-/-}$ mice 90

3.3.3 Soft diet does not rescue periodontal defects in *Bsp*$^{-/-}$ mice 100

3.4 DISCUSSION 106

3.4.1 Role of altered mechanotransduction in *Bsp*$^{-/-}$ mice periodontal breakdown 106

3.4.2 Malocclusion and altered incisor formation in *Bsp*$^{-/-}$ mice 108

3.4.3 Limiting factors of the studies 110

3.5 CONCLUSION 110

3.6 REFERENCES 111

CHAPTER 4 116

4 Healing of rat calvarial defects with nano-hydroxyapatite/ poly(ester-urethane) scaffolds loaded with low dose rhBMP-2 116

4.1 INTRODUCTION 117

4.2 MATERIALS AND METHODS 118

4.2.1 Scaffold preparation 118

4.2.2 *In vitro* rhBMP-2 release kinetics 119

4.2.3 Cell isolation, culture conditions and cell viability 120

4.2.4 Scanning Electron Microscopy (SEM) analysis 121

4.2.5 Animals and surgery 121
4.2.6 In vivo micro-computed tomography analysis 122
4.2.7 Histological Analysis 123
4.2.8 Mechanical Testing 124
4.2.9 Statistical Analyses 125
4.3 RESULTS 125
4.3.1 Cells adhesion and nHA/PU scaffold properties 125
4.3.2 *In vitro* bioactivity of bound rhBMP-2 125
4.3.3 rhBMP-2 treated nHA/PU scaffolds promote bone repair 133
4.3.4 Mechanical test analysis 143
4.4 DISCUSSION 146
4.4.1 nHA/PU scaffold supports cell attachment and binding of rhBMP-2 146
4.4.2 nHA/PU scaffold treated with low dose rhBMP-2 enhanced repair of calvarial bone defects 148
4.5 REFERENCES 152
CHAPTER 5 158
5 Effect of bone sialoprotein treated nano-hydroxyapatite/ poly(ester-urethane) scaffolds on bone formation 158
5.1 INTRODUCTION 159
5.2 MATERIALS AND METHODS 160
5.2.1 Scaffold preparation 160
5.2.2 BSP expression and purification 161
5.2.3 *In vitro* prBSP binding experiment 163
5.2.4 Cell isolation, culture conditions and cell viability 163
5.2.5 Animals and surgery 165
5.2.6 *In vivo* micro-computed tomography analysis 166
5.2.7 Histological Analysis 167

5.2.8 Statistical Analyses 167

5.3 RESULTS 167

5.3.1 bBSP expression and purification 167

5.3.2 Addition of nHA improved prBSP binding to the PU-based scaffold 172

5.3.3 The addition of BSP improved cell attachment and appeared to have increased mineral formation 176

5.3.4 bBSP treated nHA/PU scaffolds are not effective in promoting bone repair 182

5.4 DISCUSSION 189

5.4.1 The presence of BSP enhanced mineral formation *in vitro*; however, BSP is not effective for bone repair in our *in vivo* model. 189

5.5 REFERENCES 194

CHAPTER 6 200

6 Discussion 200

6.1 DISCUSSION 201

6.2 FUTURE DIRECTION 207

6.3 REFERENCES 211

Appendices 230

Curriculum Vitae 234

List of Tables

Table 2.1. Serum biochemistry for *Bsp*$^{-/-}$ and WT mice. 59

Table 3.1. The effect of diet on the onset of severe malocclusion in *Bsp*$^{-/-}$ mice. 87

Table 3.2. Serum biochemistry for *Bsp*$^{-/-}$ and WT mice. 88

Table 5.1. Estimation of bound prBSP for each treatment group. 175

Table 5.2. The effect of BSP on cell attachment to the nHA/PU scaffold. 178

List of Figures

Figure 1.1. Schematic of mouse tooth development. 9

Figure 1.2. A diagram of tooth anatomy. 10

Figure 1.3. Schematic of a molar tooth cross section. 13

Figure 1.4. Schematic of an incisor cross section. 14

Figure 1.5. Linear schematic of BSP functional regions. 17

Figure 2.1. Bone sialoprotein is required for proper acellular cementum formation. 48

Figure 2.2. Decreased thickness and mineralization of acellular cementum in the *Bsp*$^{-/-}$ mouse molar. 50

Figure 2.3. Loss of BSP compromises mouse incisor cementum development. 52

Figure 2.4. Delayed mineralization in *Bsp*$^{-/-}$ mouse cellular cementum. 54

Figure 2.5. Lack of mineralized acellular cementum ultrastructure on *Bsp*$^{-/-}$ mouse molar teeth. 56

Figure 2.6. Exploration of potential causative factors for lack of acellular cementum formation in *Bsp*$^{-/-}$ mice. 58

Figure 2.7. Periodontal breakdown in *Bsp*$^{-/-}$ mice. 62

Figure 2.8. Progressive loss of PDL organization in *Bsp*$^{-/-}$ mice. 64

Figure 2.9. Progressive epithelial in-growth in *Bsp*$^{-/-}$ mouse molars and incisors. 66

Figure 2.10. Lack of inflammation during periodontal breakdown in *Bsp*$^{-/-}$ mice. 68

Figure 2.11. Increased tooth root and alveolar bone resorption in *Bsp*$^{-/-}$ mice. 70

Figure 3.1. Soft diet normalizes body weight, bone length, and incisor malocclusion in *Bsp*$^{-/-}$ mice. 86

Figure 3.2. Altered incisor dentin and enamel formation in *Bsp*$^{-/-}$ mice. 92

Figure 3.3. Increased incisor dentinogenesis and enamel mineralization in *Bsp*$^{-/-}$ mice. 94

Figure 3.4. Similar enamel thickness was observed between experimental groups. 96

Figure 3.5. *Bsp*$^{-/-}$ mice feature reduced rates of incisor eruption. 98

Figure 3.6. Soft diet does not rescue periodontal phenotype in *Bsp*$^{-/-}$ mice. 102

Figure 3.7. Progressive periodontal breakdown in mandibles of *Bsp*$^{-/-}$ mice. 104

Figure 3.8. Further extensive alveolar bone resorption is seen in older *Bsp*$^{-/-}$ mice. 105

Figure 4.1. SEM images of nHA/PU scaffolds incubated with mesenchymal stromal cells (MSC). 128

Figure 4.2. *In vitro* cumulative release of rhBMP-2 from nHA/PU scaffolds. 129

Figure 4.3A. Control nHA/PU scaffolds show minimal alizarin red staining. 130

Figure 4.3B. The presence of rhBMP-2 in nHA/PU scaffold increased matrix mineralization when cultured with MSC cells. 132

Figure 4.4. MicroCT images of bone repair for nHA/PU and nHA/PU/rhBMP-2 groups. . 136

Figure 4.5. Quantitative microCT analysis of bone repair. 138

Figure 4.6. Histology and microCT analysis of rat calvaria at 6 and 12 weeks. 141

Figure 4.7. Quantitative histological analysis of explanted tissues at 6 and 12 week. 142

Figure 4.8. Mechanical testing of rat calvarias at 6 and 12 weeks. 145

Figure 5.1. Separation of bone proteins by ion exchange chromatography. 169

Figure 5.2. Separation of bBSP using Superdex 200 PG gel filtration column. 170

Figure 5.3. Re-purification of bBSP using Superdex 200 PG gel filtration column. 171

Figure 5.4. SDS-PAGE analysis of prBSP binding to PU scaffold. 173

Figure 5.5. SDS-PAGE analysis of prBSP binding to nHA/PU scaffold. 174

Figure 5.6. The effect of prBSP treated nHA/PU scaffold cultured with C3H10T1/2 cells.177

Figure 5.7. Effect of prBSP on nHA/PU cultured with MSC for 4 weeks. 180

Figure 5.8. Effect of bBSP on nHA/PU cultured with MSC for 4 weeks..... 181

Figure 5.9. Quantitative microCT analysis of bone repair..... 184

Figure 5.10. MicroCT images of bone repair in rat calvarial defects from 0 to 12 weeks post-op..... 186

Figure 5.11. MicroCT images of bone repair in rat calvarial defects after 12 weeks post-op. 187

Figure 5.12. Histological analysis of rat calvaria at 12 weeks..... 188

List of Appendices

Appendix A: Statement of permission for the use of animals for experimental research. .. 230

Appendix B: Statement of permission to re-use Figure 1.2 from A.D.A.M. Education. 230

List of Abbreviations

µA	microampere
µg	microgram
µm	micrometer
ac	acellular cementum
AAV	adeno-associated virus
AB-NFR	alcian blue stain with nuclear fast red
ALP	alkaline phosphatase
ALPL	alkaline phosphatase, tissue-nonspecific isozyme
bBSP	native bovine bone sialoprotein
BCA	bicinchoninic acid
BMC	bone mineral content
BMP	bone morphogenetic protein
bOPN	native bone osteopontin
BQ	bone quality
BR	bone regeneration
BSP	bone sialoprotein
BV	bone volume
cb	cementoblasts
CBV	cortical bone volume

cc	cubic centimeter
cDNA	complementary deoxyribonucleic acid
CF	calcified fibrocartilage
cRNA	complementary ribonucleic acid
DIG	digoxigenin
dpn	days postnatal
E	embryonic day
EDTA	ethylenediaminetetraacetic acid
enam	enamel
FBS	fetal bovine serum
FPLC	fast protein liquid chromatography
GTC	Goldner's trichrome
H & E	hematoxylin and eosin
HA	hydroxyapatite
HBSS	Hank's balanced salt solution
HCl	hydrochloric acid
HD	hard diet
HPP	hypophosphatasia
HU	hounsfield unit
HUVEC	human umbilical vein endothelial cells

IHC	immunohistochemistry
IMDM	Iscove's modified Dulbecco's medium
ISH	in situ hybridization
je	junctional epithelium
kDA	kilo dalton
kN	kilo newton
kVp	peak kilovoltage
mg	milligram
microCT	micro-computed tomography
MIP	maximum intensity projection
mmol	millimolar
mRNA	messenger ribonucleic acid
ms	millisecond
MSC	mesenchymal stromal cells
MT	masson's trichrome
N	newton
ng	nanogram
nHA	nano-sized hydroxyapatite
ob	osteoblasts
OPG	osteoprotegerin

OPN	osteopontin
Osx	osterix
PBS	phosphate buffered saline
PDL	periodontal ligament
pI	isoelectric point
PI	proteinase inhibitor
PPi	pyrophosphate
PLGA	poly(lactic-co-glycolic) acid
PMMA	poly(methyl methacrylate)
PMSF	phenylmethylsulfonyl fluoride
PR	picrosirius red
prBSP	phosphorylated recombinant rat bone sialoprotein
PU	poly(ester-urethane)
QCT	quadriceps tendon
RANKL	receptor activator of nuclear factor kappa-B ligand
ratBSP	native rat bone sialoprotein
rBSP	recombinant rat bone sialoprotein
rhBMP-2	recombinant human bone morphogenetic protein 2
rhBSP	recombinant human bone sialoprotein
ROI	region of interest

Runx2	runt-related transcription factor 2
SD	soft diet
SEM	scanning electron microscopy
SIBLING	small integrin-binding ligand N-linked glycoprotein
SDS	sodium dodecyl sulfate
SDS-PAGE	sodium dodecyl sulfate - polyacrylamide gel electrophoresis
SST	supraspinatus tendon
TGF	transforming growth factor
TNAP	tissue-nonspecific alkaline phosphatase
TNF	tumor necrosis factor
TV	total tissue volume
TRAP	tartrate resistant acid phosphatase
VOI	volume of interest
WT	wild-type

CHAPTER 1

1 Literature Review

1.1 INTRODUCTION

Bone is a complex tissue that undergoes a remodeling process involving resorption and formation of bone. Cell interactions with various hormones and growth factors and the surrounding extracellular matrix are crucial for bone development and bone regeneration. The bioactive protein of interest for this study is bone sialoprotein (BSP), whose expression has been shown to be up-regulated at the onset of mineralization. Various studies have indicated that BSP plays a role in promoting biomineralization during bone development. However, the role of BSP in other mineralized tissues such as those associated with the periodontal tissues is still not fully understood. Furthermore, it has been suggested that BSP may promote bone repair, however there have only been limited studies in this area.

This thesis has two main objectives: 1) to determine the role of BSP in periodontal tissue development and 2) to determine the potential use of BSP as therapeutic agent to enhance bone repair. The literature review that follows covers these two topics.

1.2 SKELETAL TISSUE DEVELOPMENT

Mineralized tissue formation is an essential development of the human body. All mammalian skeletal tissues are comprised of inorganic mineral (mainly hydroxyapatite) that are embedded in an extracellular organic matrix. There are two developmental processes responsible for bone development and growth: endochondral and intramembranous ossification (Cohen, 2000; Olsen et al., 2000; Provot and Schipani, 2005). The main difference between the two is that endochondral ossification has the presence of a cartilaginous intermediate, whereas intramembranous ossification does not. For both developmental processes, cells such as osteoblasts and osteoclasts are important in maintaining balance in order to have normal skeletal tissue development.

1.2.1 Skeletal cell: Osteoblasts

Osteoblasts are cells derived from osteoprogenitor cells within the bone marrow and the periosteum (Olsen et al., 2000; Wagner and Karsenty, 2001). Osteoblastic differentiation is regulated by the transcription factors *Runx2* and Osterix (*Osx*) (Aubin, 2001; Chau et al., 2009). In addition, it can also be induced by various growth factors such as bone morphogenetic proteins (BMPs) (Long, 2012). Osteoblasts are responsible for the production of the osteoid matrix, the non-mineralized matrix, and its subsequent mineralization. During bone formation, osteoblasts have been shown to express a variety of proteins and enzymes including Type I collagen, alkaline phosphatase (ALP), and non-collagenous proteins such as bone sialoprotein (BSP), osteopontin (OPN), osteonectin, and osteocalcin. As the osteoblasts mature, they will either become osteocytes, bone lining cells or undergo apoptosis (Crockett et al., 2011).

Osteocytes are mature osteoblasts trapped within the mineralized bone tissue. These cells are connected with each other through microscopic canals called canaliculi, which function as conduits for transport of nutrients and signaling molecules to maintain proper bone homeostasis. In addition, studies also have shown that the osteocyte network acts as a mechanosensor that is crucial for the bone-remodeling process (Bonewald, 2006; You et al., 2008). In contrast, the bone-lining cells are inert reserve cells at the bone surface that are thought to have a role as osteoprogenitors or involved in coupling of bone resorption and bone formation (Everts et al., 2002).

1.2.2 Skeletal cell: Osteoclasts

Osteoclasts are cells derived from monocytes (Quinn et al., 1998) or macrophages (Udagawa et al., 1990) and are usually found in pits on the bone surface called Howship's lacunae. The differentiation of osteoclasts from hematopoetic lineage cells is regulated by receptor activator of nuclear factor kappa-B ligand (RANKL) and tumor necrosis factor (TNF) (Boyle et al., 2003). These multinucleated cells are responsible for the degradation of both mineral and organic matrix (Blair et al., 1986) in bone during

development, maintenance and repair. Normal healthy bone requires ongoing bone resorption and formation. For resorption, osteoclasts bind to mineralized surfaces in bone where they form a tight seal. Within the sealing zone, due to the activity of the membrane bound proton pumps, the pH becomes acidic which favors dissolution of bone mineral (Baron et al., 1985; Schlesinger et al., 1997). In addition, osteoclasts also secrete enzymes such as tartrate resistant acid phosphatase (TRAP) and cathepsin K that are involved in the breakdown of the extracellular matrix (Boyle et al., 2003; Crockett et al., 2011). Various skeletal disorders such as osteopetrosis and Paget's disease are related to the defective regulation of osteoclast activity or function (Helfrich et al., 2007).

1.2.3 Endochondral and intramembranous ossification

Intramembranous ossification occurs during the formation of flat bones such as the skull, clavicles and the mandible. In this ossification process, no cartilaginous intermediate is present. Ossification sites appear within the fibrous connective tissue membrane. During this stage, mesenchymal stromal cells (MSCs) proliferate and condense to form clusters which differentiate into osteoblasts. Within the fibrous membrane, osteoblasts secrete type I collagen matrix and non-collagenous proteins to form the osteoid, which subsequently is mineralized. The mineralized osteoid is laid down in a random fashion around the blood vessels to form a bone network that is woven in appearance. At the same time, mesenchymal cells on the external surface of the woven bone also condense to become periosteum. The periosteum is a thin non-calcified tissue on the exterior of bone. The periosteum consists of an exterior layer of fibrous connective tissue and an internal osteogenic layer. The exterior layer is primarily composed of collagen fibers and fibroblastic cells. Whereas the inner layer contains the osteoprogenitor cells, which are critical for bone growth and repair. As the osteoprogenitor cells along the inner surface of the periosteum differentiate into osteoblasts, they deposit osteoid matrix parallel to the existing woven bone. These osteogenic cells are responsible for the appositional growth of woven bone, which eventually is replaced by lamellar bone that is organized in appearance. As a result, flat bone will have a unique sandwich structure where the outer

layers are composed of dense cortical bone and the midsection is filled with trabecular bone (Cohen, 2000; Olsen et al., 2000).

Endochondral ossification occurs during the formation of long bones and other bone types. In this process, hyaline cartilage, which is formed first, becomes the platform that will be remodeled and replaced by bone. Initially, periosteum and blood vessels form along the diaphysis of the hyaline cartilage. Then periosteum-derived osteoprogenitor cells proliferate and differentiate into osteoblasts, which secrete osteoid matrix. As the osteoid matrix mineralizes, bony collars are formed around the diaphysis of the hyaline cartilage. Then mineralization of the cartilage matrix occurs at the diaphysis of the hyaline cartilage. The next step involves the formation of a primary ossification site at the center of the diaphysis. At this stage, the periosteal bud begins to invade the primary ossification site carrying blood vessels and cells such as osteoblasts and osteoclasts. Over time, the remaining mineralized cartilage matrix will be broken down by osteoclasts and replaced by trabecular bone formed by the osteoblasts, which in turn will be remodeled into mature lamellar bone. In addition, as blood vessels and cells invade the center of the bone, the diaphysis also starts to elongate. The osteoclasts help to form the medullar cavity by breaking down the newly formed woven bone.

In addition, the blood vessels also penetrate the hyaline cartilage at the epiphysis of the long bones to form the secondary ossification centers. The process of secondary ossification is similar to the primary ossification, except instead of forming lamellar bone, trabecular bone is maintained. At the end of the process, cartilage that remains at the ends of the bones is called articular cartilage. In addition, the diaphysis and both epiphyses of the long bone are separated by epiphyseal plates, the sites responsible for bone elongation (Cohen, 2000; Olsen et al., 2000; Provot and Schipani, 2005).

1.2.4 **Bone repair**

Normal bone repair goes through a sequence of stages including inflammation, callus formation, and remodeling. Damage to bone will result in fairly rapid inflammatory

response involving coagulation of blood and invasion of hematopoietic cells, which is the start of the tissue repair process. For example during a repair of non-critical sized long bone fracture, within days, progenitor cells from the periosteum and bone marrow around the fracture site differentiate into chondroblasts, which generate new cartilage at the wound site. At the same time, distal from the fracture site, other progenitor cells differentiate into osteoblasts, which generate the organic matrix of new osteoid. The two tissues grow separately and eventually unite to create a bridge composed of a combination of cartilage and woven bone, which is known as the callus. Eventually, at the remodeling stage, the callus is resorbed by osteoclasts and replaced with cortical bone by osteoblasts. The remodeled bone will have a similar shape and strength as the original bone (Claes et al., 2012; Einhorn and Gerstenfeld, 2015; Marsell and Einhorn, 2011).

However, in severe bone injury such as tumour excision, non-union trauma and critical-sized defect fractures, normal repair is impaired. In this condition, it may require years for complete healing; in some cases it may never heal completely without intervention. Therefore, various natural or synthetic biomaterials are used in conjunction with growth factors or other bioactive proteins to enhance regeneration and improve the functional state of the damaged tissues.

Various animal models have been used to address the clinical challenge in repairing bone defects. For our study, the rodent calvarial defect model was chosen since this model allows for reproducible defects that can be generated quickly. In addition, the calvarial defect model is more economical compared to the femoral defect models, which require additional fixation procedures to stabilize the long bone. For calvarial defect model, an 8 mm defect is generally accepted as a critical size defect (Spicer et al., 2012). Critical size defects are the smallest size defects that will not completely heal, without intervention, over the lifetime of the animal. Various studies have also used smaller 5 mm defects, with 2 defects per animal, in order to allow for reduced animal usage for a given study. However, these non-critical size defects can heal even without intervention. Nevertheless, this is a good model to determine whether the addition of a specific osteoinductive or osteoconductive agent can enhance the healing process.

1.2.5 Mouse tooth development

Mouse tooth development goes through three well-defined stages - the bud, cap, and bell stages as shown in Figure 1.1 (Caton and Tucker, 2009). Around embryonic day 11.5 (E11.5), at the tooth development site, formation of the dental lamina is observed, marked by the start of epithelial cell proliferation and thickening of the oral epithelium. By E12.5, invagination of the dental epithelium becomes apparent. The invagination will continue further into the underlying neural crest-derived mesenchyme and start to form a bud. At around E13.5, these underlying neural crest mesenchymal cells start to condense around the formed bud. By E14.5, tooth development has reached the cap stage, where the epithelium is further folded and the enamel knot becomes visible. The enamel knot is a transient structure, which will disappear by the end of the cap stage through apoptosis. The cells in the enamel knot are regulated by BMP-4 (Jernvall et al., 1998) and the enamel knot cells have a low proliferation rate. Other studies have shown that these enamel knot cells act like an anchor constricting the movement of cells in the developing tooth (Jernvall et al., 1994; Vaahtokari et al., 1996). During the cap stage, the epithelial cells become the enamel organ and the condensed mesenchyme forms the dental papilla. As for the surrounding tissue, it will become the dental follicle.

By E16.5, these tissues developed further and form the bell stage. During this stage, cells begin to differentiate into their respective lineages. The cells in the enamel organ differentiate into two types of cells - 1) outer enamel cells, which cover the enamel organ and organize a network for the transport of nutrition, and 2) inner enamel cells, which become the ameloblasts that form the enamel. The cells in the periphery of the dental papilla differentiate into odontoblasts that form pre-dentin, the precursor to dentin, which is mineralized. The central region of the dental papilla, which contains undifferentiated mesenchymal cells, will become the dental pulp. As for the dental follicle, this tissue contains progenitor cells that will differentiate into cementoblasts, periodontal ligament fibroblasts, and osteoblasts to form the cementum-periodontal ligament-alveolar bone

structure, respectively as shown in a representative diagram of the tooth anatomy in Figure 1.2.

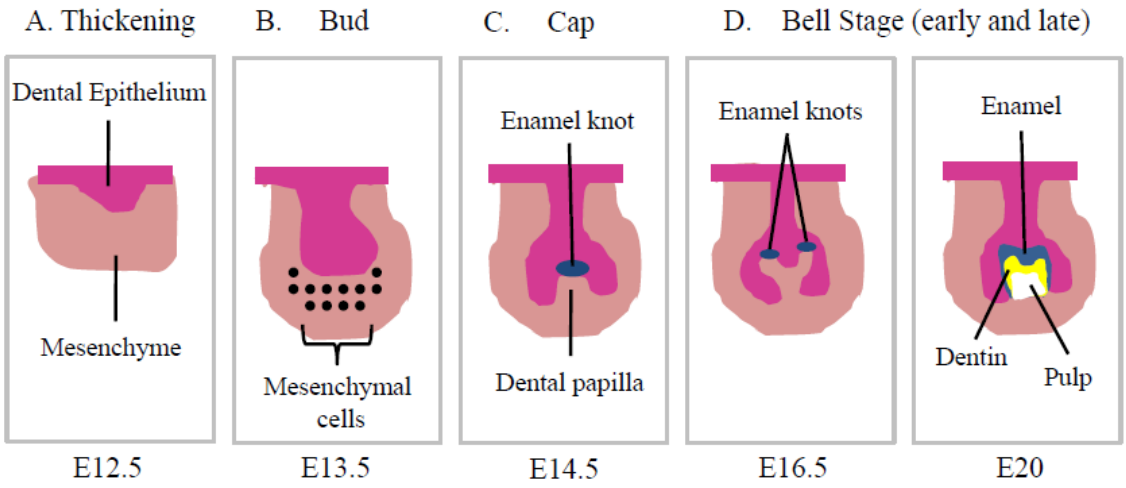

Figure 1.1. Schematic of mouse tooth development.

(A) At embryonic day 12.5 (E12.5), thickening and invagination of the dental epithelium (dark pink) becomes apparent. **(B)** At around E13.5, the neural crest mesenchymal cells (black dots) within the underlying mesenchyme (light pink) start to condense around the formed bud. **(C)** By E14.5, the epithelium is further folded and the enamel knot becomes visible (blue oval). During this cap stage, the condensed mesenchyme forms the dental papilla. **(D)** At E16.5, the tissue development reaches the early bell stage and cells in the dental papilla begin to differentiate into their respective lineages. By E20, the ameloblasts and odontoblasts have started to form enamel (blue) and dentin (yellow) respectively. The central region of the dental papilla, which contains undifferentiated mesenchymal cells, will turn into dental pulp (white). Note: This figure is adapted from (Caton and Tucker, 2009).

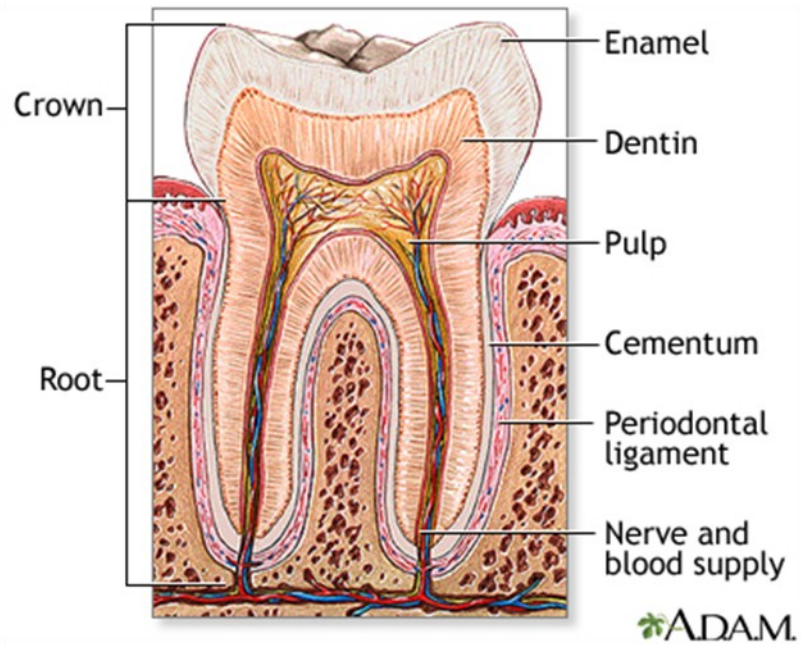

Figure 1.2. A diagram of tooth anatomy.

A cross section of tooth anatomy showing major components of the tooth.

The figure is copied from https://www.nlm.nih.gov/medlineplus/ency/imagepages/1121.htm

(Permission to use the image was acquired from A.D.A.M. Education)

1.2.6 Tooth anatomy

The tooth is made up of four major tissues: enamel, dentin, cementum, and dental pulp as shown in a representative cross section diagram of molar and incisor (Figure 1.2, 1.3 and 1.4). Among the three mineralized tissues, enamel is the hardest and most highly mineralized. Approximately 96% of enamel by weight consists of hydroxyapatite (HA), with the remainder water and organic matrix (Deakins and Volker, 1941; LeFevre and Manly, 1938). Different from dentin, cementum and bone, enamel does not contain collagen. Enamel contains three major structural proteins called amelogenin, ameloblastin, and enamelin (Bartlett, 2013).

Dentin, which is found between the pulp chamber and enamel or cementum, is a mineralized tissue that is formed by odontoblasts. While lower in mineral density than enamel, dentin is composed of 70% HA, 10% water, and 20% organic matrix. Similar to bone, dentin's organic matrix is composed of collagen and a variety of non-collagenous proteins. Within the mineralized matrix of dentin, there are dentinal tubules, which are microscopic channels that radiate outward from the pulp chamber to either the enamel or cementum border (Goldberg et al., 2011).

Cementum is a mineralized tissue found adjacent to the dentin and covers the tooth root. Similar to osteoblasts for bone, cementoblasts are responsible for the formation of the organic matrix of the cementum, and its subsequent mineralization process. Cementum consists primarily of 45% HA, 20% water, and 35% organic matrix (Gonçalves et al., 2005). The main role of the cementum is to act as a medium for the attachment of the periodontal ligament, which stabilizes and anchors the tooth root to the bone. There are two types of cementum - acellular and cellular cementum. The acellular extrinsic fiber cementum is found in the top 40 to 70% of the root surface. This matrix consists of a dense fringe of short collagenous fibers that are oriented perpendicular to the root surface (Gonçalves et al., 2005). As the fibers become elongated and become continuous with the principal PDL fibers, they are called Sharpey's fibers. In addition, two major non-collagenous proteins, bone sialoprotein (BSP) and osteopontin (OPN), are prominently expressed in acellular cementum. BSP is believed to play a role in cell adhesion,

progenitor cell differentiation into cementoblasts, and initiating mineralization (Saygin et al., 2000; Somerman et al., 1990).

The cellular intrinsic fiber cementum contains embedded cementocytes in the mineralized collagenous matrix. This tissue is found at the apical root portion and it maintains the root in its proper position. The collagen fibers in the matrix are oriented mostly parallel to the root surface (Gonçalves et al., 2005). Studies have shown that it also participates in the repair process, however, there is no direct evidence that it plays a role in tooth attachment (Bosshardt and Selvig, 1997).

The dental pulp is a soft connective tissue containing blood and nerve supplies to the tooth, which enters at the apex of the tooth root. Along the boundary of the pulp and dentin, in the pre-dentin layer, odontoblasts are found. Other cells such as pre-odontoblasts and fibroblasts are also present in the pulp chamber.

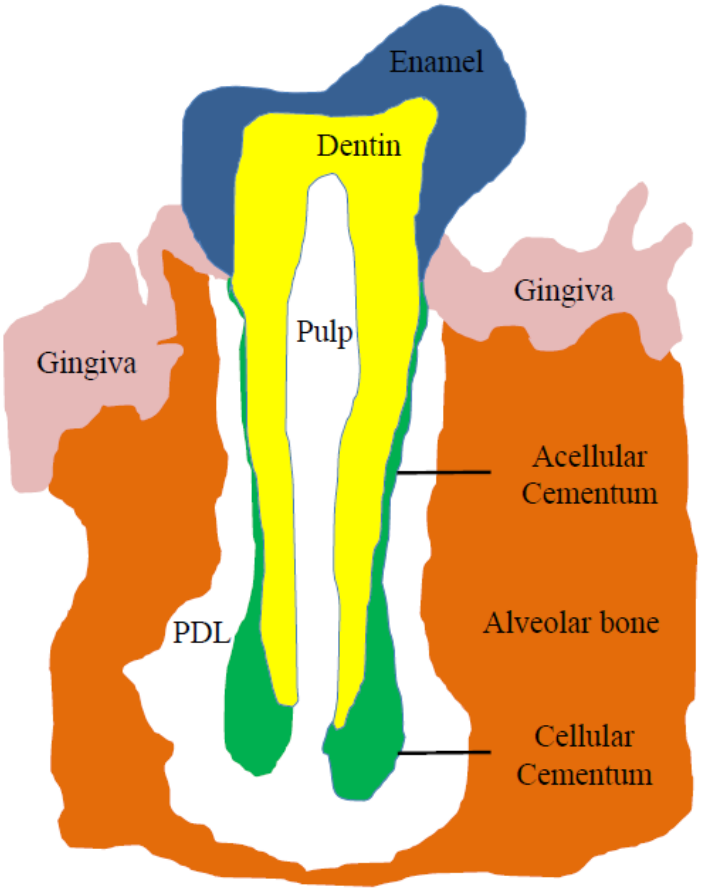

Figure 1.3. Schematic of a molar tooth cross section.

The image represents a cross section (coronal) of the mice tooth, which are emphasized by color codes: enamel (blue), dentin (yellow), cementum (green for both acellular and cellular cementum), alveolar bone (brown), and gingiva (pink). The pulp chamber is located in the core of the tooth. Whereas the periodontal ligament (PDL) is located between the alveolar bone and cementum. Note: This figure is adapted from (Foster, 2012).

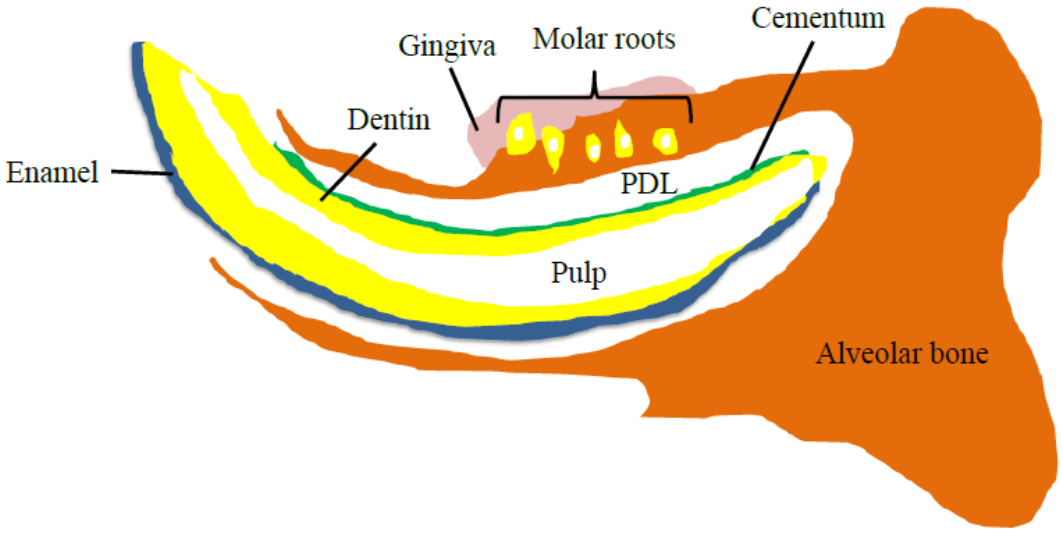

Figure 1.4. Schematic of an incisor cross section.

The image represents a cross section (sagittal) of the mice tooth, which are emphasized by color codes: enamel (blue), dentin (yellow), cementum (green for both acellular and cellular cementum), alveolar bone (brown), and gingiva (pink). The pulp chamber is located in the core of the incisor. Whereas the periodontal ligament (PDL) is located between the alveolar bone and cementum.

1.3 BONE SIALOPROTEIN (BSP)

1.3.1 BSP structure and function

Bone sialoprotein (BSP), an acidic phosphoprotein, is a member of the Small Integrin-Binding Ligand N-Linked Glycoprotein (SIBLING) family of proteins and a major component of non-collagenous proteins in bone. BSP is highly conserved and found in all vertebrate species with mineralized tissue. BSP has been isolated from a wide range of animals such as bovine (Fisher et al., 1983; Franzen and Heinegard, 1985), pig (Zhang et al., 1990), rat (Gorski and Shimizu, 1988), rabbit (Kinne and Fisher, 1987), chicken (Yang et al., 1995), frogs (Shintani et al., 2008), and humans (Fisher et al., 1987). The calculated molecular weight of human BSP based on mass spectroscopy was determined to be approximately 49 kDa (Wuttke et al., 2001) and 52.5 kDa (Zaia et al., 2001). The variability in the average mass of BSP is likely due to its heterogeneous post-translational modifications. Furthermore, BSP has a flexible structure which is intrinsically disordered with no secondary or tertiary structure (Fisher et al., 2001; Wuttke et al., 2001). The flexible nature of BSP is likely important since it may allow for simultaneous interaction with other proteins, cells and minerals as previously discussed by Fisher *et al* (Fisher et al., 2001). On average, BSP contains around 327 amino acid residues including the 16 residue signal sequence and within it, a high concentration of acidic amino acid residues, glutamic acid and aspartic acid, as well as the negatively charged sialic acid residues (Zaia et al., 2001), which contributes to the overall negative charge of BSP [isoelectric point (pI) of 3.9].

BSP has been determined to have three main functional regions: 1) collagen-binding region, 2) two hydroxyapatite (HA)-nucleating regions, and 3) an integrin recognition region (Figure 1.5). These functional regions are highly conserved and always found in BSP regardless of species (Goldberg and Hunter, 2012). The collagen-binding region (spanning residues 18-45) is a hydrophobic region located near the N-terminus (Tye et al., 2005). The two nucleating regions (spanning residues 42-100 and 133-205), each containing a contiguous glutamate sequence, were found to be critical for HA nucleation (Hunter and Goldberg, 1993) and binding (Goldberg et al., 2001; Stubbs et al., 1997). Of

the two HA-nucleating regions, the second sequence in rat (BSP 133-205) has been determined to be more potent than the first one (Harris et al., 2000; Tye et al., 2003). Previous studies have shown that even the short BSP133-148 sequence containing a poly-glutamate sequence and a phosphorylated serine residue, possesses HA-nucleation activity (Baht et al., 2010). In addition, using a steady state collagen-gel system, it has been demonstrated that the HA nucleation potency of BSP is enhanced when it is bound to collagen (Baht et al., 2008). The integrin recognition region (RGD; spanning residues 273-275) is located near the C-terminus (Wuttke et al., 2001). This RGD motif of BSP has been shown to mediate cell attachment and signaling that contributes to osteoprogenitor cell differentiation and migration (Gordon et al., 2007). The RGD motif interacts with the $\alpha_v\beta_3$ integrin, which is a cell-surface receptor present in osteoblasts (Oldberg et al., 1988) and osteoclasts (Helfrich et al., 1992). The overexpression of BSP in MC3T3-E1 osteogenic cells has been shown to increase the level of osteoblast differentiation signaling markers and formation of matrix mineralization nodules *in vitro* (Gordon et al., 2007). However, when the RGD sequence is mutated to KAE, the cell-integrin binding capabilities have been shown to be diminished or abolished in osteoblasts (Gordon et al., 2007), fibroblasts (Harris et al., 2000), chondrocytes (Gill et al., 2008) and endothelial cells (Bellahcène et al., 2000). Furthermore, overexpression of the BSP in rat primary calvarial pre-osteoblasts containing the KAE mutation did not result in enhanced osteoblastic differentiation *in vitro* (Gordon et al., 2007).

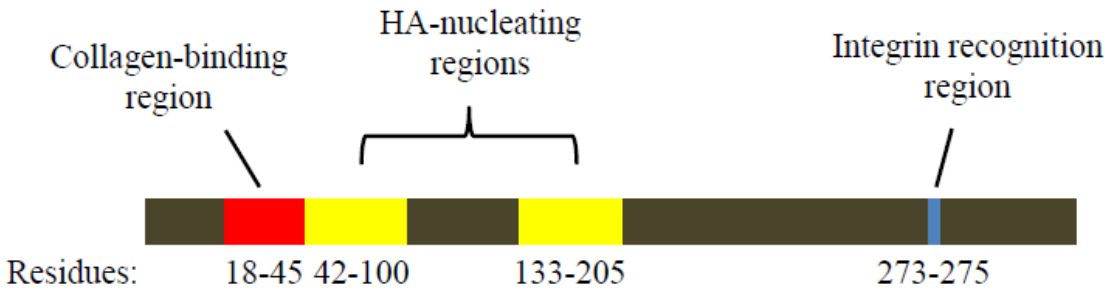

Figure 1.5. Linear schematic of BSP functional regions.

BSP contains on average 327 amino acid residues and has three main functional regions. The first region is the collagen-binding region (red), which is located near the N-terminus. The second region consists of two hydroxyapatite (HA)-nucleating regions, which are rich in poly-glutamic acid sequences (yellow). The last region is an integrin recognition region consisting of the RGD sequence that has been shown to promote cell adhesion and signaling.

1.3.2 BSP expression and role in biomineralization

BSP appears to be expressed in all mineralized tissues. For example, it is highly expressed in bone, cementum, and calcified cartilage (Ganss et al., 1999). Other studies have also suggested that BSP is expressed in dentin at low level (Fujisawa et al., 1993; Qin et al., 2001). BSP expression has been demonstrated in cells that produce a matrix that mineralizes such as osteoblasts, hypertrophic chondrocytes, cementoblasts, ameloblasts, and odontoblasts (Bianco et al., 1991; Chen et al., 1998). This suggests that BSP may play an important role in osteogenic mineral formation. In the osteoblasts, BSP is detected in the Golgi apparatus where it is post-translationally modified before being secreted (Bianco et al., 1993). A potential reason for BSP being a potent nucleator for HA is likely due to its highly acidic sequences that attract and immobilize calcium ions in a specific orientation. Therefore when phosphate ions bind, a template for mineral formation is established. This concept is further supported by a previous study that demonstrated that the phosphorylation of the Serine-136 residue, but not other potential serine sites in BSP, enhances HA nucleation potency of the protein (Baht et al., 2010). Interestingly, the Ser-136 residue is adjacent to a poly-glutamic sequence in BSP. Of relevance to the potential role of BSP in mineral formation, other studies have shown BSP is associated with pathological calcification such as the microcalcifications observed in breast cancer tissue (Bellahcene et al., 1994) and lung cancer tissue (Bellahcene et al., 1997). Furthermore, various cancer cells, including breast, lung and prostate, express high levels of BSP (Bellahcene et al., 2008).

A number of *in vivo* studies have also shown the physiological importance of BSP including its functional relevance in skeletal development. Mice with the *Bsp* gene ablated ($Bsp^{-/-}$) have impaired bone growth and mineralization. $Bsp^{-/-}$ mice were reported to have shortened long bones, decreased bone mineral density, delayed mineral formation, thinner cortical bones, and greater trabecular bone volume as compared to wild type (WT) mice (Malaval et al., 2008). In addition, studies also indicate that reduction in osteoclast formation and activities were observed in $Bsp^{-/-}$ mice, which

resulted in low bone turnover (Boudiffa et al., 2010; Malaval et al., 2008). In a long bone defect model, *Bsp*$^{-/-}$ mice also displayed delayed bone repair compared to WT control (Malaval et al., 2009; Monfoulet et al., 2010). These phenotypes observed in *Bsp*$^{-/-}$ mice suggest that BSP plays a crucial role in bone development and mineralization. In addition, BSP may also be important for maintaining the homeostasis of both osteoblasts and osteoclasts in number and activities. Of relevance, studies have demonstrated that in the presence of BSP and RANKL, the differentiation of osteoclast from monocyte/macrophage cells is greater compared to that without BSP (Valverde et al., 2005). In addition, previous studies on transgenic mouse line with overexpression of BSP demonstrated increased osteoclast formation and activity level (Valverde et al., 2008).

Studies have shown the therapeutic potential for BSP to induce bone repair *in vivo* (Wang et al., 2006; Xu et al., 2007). The authors used a bovine BSP treated-collagen scaffold which was implanted into rat calvarial defects. At 4 days post-surgery, the BSP-collagen scaffold induced recruitment of osteoblasts and promoted early mineralization. However, no bone repair was observed when denatured collagen was used as a scaffold (Xu et al., 2007). Other *in vitro* studies were also able to confirm that BSP binding affinity to denatured collagen is less than to native collagen (Baht et al., 2008). The outcomes of these studies indicate that the collagen-binding region in BSP potentially has an important role in biomineralization.

On the other hand, there are a couple of studies that indicate BSP was not effective in promoting bone repair. For example, when recombinant human BSP- (rhBSP) coated polymeric scaffolds [porous β-tricalcium phosphate scaffold (Skelite ^{TM}) and synthetic polymer (Polyactive ^{TM})] were used in an *in vivo* subcutaneous model in nude mice, the presence of BSP did not improve the efficiency of bone tissue formation compared to the control group (Schaeren et al., 2010).

Studies on BSP also look at its potential role in enhancing osteointegration of implants into biological tissues. BSP coating of a hydroxyapatite-based titanium implant (TICER ®) with rough surface improved its osteoinductive properties and enhanced attachment of

bone marrow derived cells *in vitro* (Graf et al., 2008). Another study on bovine BSP coating of titanium femoral implants demonstrated enhanced osteoinductive properties with evidence of abundant osteoid, elongated osteoblasts and neovascularisation around the implant-bone interface (O'Toole et al., 2004). However, when subjected to mechanical pullout test, the BSP coating was unable to enhance the strength of the implant-bone integration.

1.4 BONE MORPHOGENETIC PROTEIN (BMP)

1.4.1 Role of BMP in bone regeneration

Bone morphogenetic proteins (BMPs) are multifunctional cytokines that belong to the transforming growth factor (TGF)-β superfamily (Abe, 2006). BMPs are potent growth factors that have been widely investigated for use in the clinical setting for bone repair. For example, BMP-2, -4, and -7 have been shown to have strong osteogenic properties (Chen et al., 2012). These BMPs are currently the standard growth factor used in combination with various carriers for bone tissue regeneration. The BMPs possess the ability to stimulate osteoblastic differentiation (Canalis et al., 2003; Schmitt et al., 1999).

Previous studies have shown that the growth factors BMP-2,4 and 7 are expressed by the mesenchymal stromal cells (MSC), osteoprogenitors cells, osteoblasts, endothelial cells, fibroblasts and chondrocytes at fracture sites and during the inflammatory phase of bone repair (Bostrom et al., 1995; Canalis et al., 2003; Martinovic et al., 2004; Nakase et al., 1994; Onishi et al., 1998; Zhang and Li, 2005). After being secreted, the extracellular matrix temporarily stores the BMPs, which are then released during bone repair and remodeling. BMPs bind to BMP receptors types I and II, which are important for signal transduction to activate the transcription factor Smad cytoplasmic proteins. The binding of BMP catalyzes phosphorylation of Smads 1,5,8, which are also associated with the activation of Smad-4 which translocates into the cell nucleus. Smad-4 regulates the

expression of *Runx2* and *Osx* genes, which are gene markers of osteoblastic differentiation (Chen et al., 2012).

Other studies have also suggested that BMPs play a role in promoting angiogenesis via the Wnt pathways (de Jesus Perez et al., 2009; Guo and Wang, 2009). During intramembranous ossification, these BMPs are expressed by the proliferating osteoblasts. Whereas during chondrogenesis and endochondral ossification, these BMPs are expressed by both the proliferating chondrocytes and osteoblasts near the ossification front (Sfeir et al., 2005).

The inactivation of the various BMP genes leads to a variety of phenotypes. For example, BMP-2-null mice have an embryonic lethal phenotype prior to the formation of the skeleton. This mutation also caused defects in amnion, chorion, and cardiac development (Zhang and Bradley, 1996). Similarly, BMP-4-null mice have an early embryonic lethal phenotype with defects in mesoderm development (Winnier et al., 1995). As for the elimination of BMP-7 gene, null mice also revealed a lethal phenotype due to developmental abnormalities in the kidney, eye and skeletal structure (Jena et al., 1997; Luo et al., 1995). These studies confirmed the important role of BMPs in development of a variety of tissues, including skeletal tissue.

In addition, the use of BMP as a therapeutic growth factor to enhance bone repair has been accepted clinically as a standard procedure. Previous studies using various animal models, including rats (Sawyer et al., 2009), rabbits (Murakami et al., 2002), dogs (Asamura et al., 2010), sheep (Geiger et al., 2003), and non-human primates (Suh et al., 2002), have been used to evaluate the addition of BMPs to heal bone defects. All of these studies have shown that the presence of BMPs accelerates bone formation at the defect sites.

1.4.2 Potential side effects of using high dose of BMPs

Currently, there are two FDA-approved recombinant human BMPs (rhBMPs) 2 and 7, which are obtained by molecular cloning of their respective cDNAs and expressed using the Chinese hamster ovary cell line, for clinical use in humans (Wozney, 2002). For this study, we focused on the use of rhBMP-2 since it has been extensively evaluated in numerous studies for bone repair (Chen et al., 2004). For example, commercialized rhBMP-2 is delivered with a bovine collagen sponge (INFUSE Bone Graft, Medtronic) for posterior-lateral spine, tibia and specific craniofacial applications.

Recent studies have reported wound complications in the use of rhBMP-2 for anterior cervical fusion and non-union fractures (Cahill et al., 2009; Papakostidis et al., 2008; Williams et al., 2011). These complications include superficial and deep wound infections, and epidural hematoma or seroma. In addition, there have also been reports of intense inflammation and bone resorption in children patients treated with BMPs for cleft lip and palate repair (Neovius et al., 2013) and symptomatic ulnar nonunion repair (Ritting et al., 2012). However, there are no clear studies that indicate the observed complication is directly caused by usage of BMP as opposed to normal surgical complication. Another potential problem is that the commercially available BMP-2 is also clinically used "off-label".

For *in vitro* studies, the utilization of BMP-2 is generally at very low dosages (5-20 ng/mL). However, for *in vivo* or clinical treatments, commercially available rhBMP-2 are usually packaged in large dosage (up to 40 mg), which depend on the size of the defect. High doses of BMP-2 are usually needed to be clinically effective due to poor retention of the BMPs to its carrier. In addition, the high cost of rhBMPs for clinical use is another factor to consider. Of relevance, animals studies have shown that rhBMP-2 has a short half-life of 7-16 minutes systemically (Poynton and Lane, 2002), however if bound to collagen scaffold, the residence time of rhBMP-2 was determined to be approximately 8 days; with a half-life of 5.6 days (Sellers et al., 2000). Another main concern of using rhBMPs at large dosage is that it will pose risks to patients due to its potential for significant side effects including heterotopic bone formation, significant

immune responses and potential to be carcinogenic (Carragee et al., 2011; Epstein, 2013). In spite of all of these controversial results, the use of BMPs is still the best solution for promoting bone repair in defects that do not respond to normal therapies or procedures. In orthopedics, the challenge is to use a much lower dose of BMPs without compromising the overall effectiveness in promoting bone regeneration. Therefore, there is a necessity of designing a biomaterial scaffold that can retain and systematically release BMPs over time. Thus, the selection of the carrier for BMPs and the dose used should be studied carefully in animal models.

1.5 BIOMATERIALS FOR TISSUE ENGINEERING

Large bone defects due to tumour excision, non-union fracture and critical-sized defect fractures affect millions of people worldwide each year. Normal bone remodeling requires a number of factors that involve cell migration, adhesion, proliferation, and differentiation as well as the extracellular matrix and growth factors. In critical sized defects, normal repair is impeded where in the majority of cases successful healing does not occur without intervention. Various biomaterials have been developed with the goal to regenerate and improve the functional state of damaged tissues.

1.5.1 Introduction of biomaterials scaffolds

The use of autogenous and allogenic bone grafts are among the most common clinical procedures to promote bone regeneration. These bone grafts have their own advantages and disadvantages. Autograft tissue is the safest and has the fastest healing potential without dealing with issues such as tissue rejection due to immune response. Clinically, it is the "gold standard" treatment for bone defects. The source of autograft tissue, usually from the iliac crest, has the potential to facilitate new bone formation due to the endogenous presence of growth factors, which can promote angiogenesis and

osteogenesis (Soucacos et al., 2008). However, additional surgical procedures are required to harvest the autograft from a secondary site within the patient body, leading to extended recovery time and potential risk of infection (Younger and Chapman, 1989). The secondary site (for example iliac crest) could also be uncomfortable and painful for years after the surgical procedure (Lementowski et al., 2010; Palmer et al., 2008). Lastly, there is a limited supply of autograft material since over-harvesting can cause destabilization of the secondary site. In contrast, allografts are obtained from human donors (cadavers) and do not require additional surgical procedures to the receiving individuals. However, proper screening for pathogens and risk factors for diseases are necessary for the use of allografts. Limited supplies and tissue rejection are also additional concerns for using allografts.

In tissue engineering, the best surgical procedures to treat non-union bone fractures and spinal fusion involve the use of bone graft substitutes. In addition, these substitutes need to be osteoconductive, osteoinductive and have mechanical properties allowing them to withstand normal *in vivo* loads (Bauer and Muschler, 2000). There has been an emphasis on the use of synthetic biomaterials that can replace autogeneous and allogenic bone grafts for large bone defects. Below are brief descriptions of these synthetic biomaterials for bone grafts, which can be divided into 3 main categories: metals, ceramics, and polymers.

Metals implants are widely used for load-bearing applications such as fracture fixation plates or screws. However, in some cases they are required to be removed after the bone heals, which can be inconvenient and painful for patients. Another potential concern is that metals can corrode, due to chemical reaction with enzymes and acids in the body, and the metals ions can be toxic to the body. However, there are medical grade metals such as titanium, which are naturally resistant to corrosion.

Ceramics are also used for bone implants, in particular those containing calcium phosphates, the primary inorganic phase of bone minerals. Ceramics are chemically inert and have high compressive strength. However, they are also brittle and lack the toughness needed to bear cyclic loading (Ducheyne, 1987; Yaszemski et al., 1996).

However, bioceramic scaffolds comprised of porous β-tricalcium phosphate matrix combined with hydroxyapatite (HA) nano particles show a compressive strength similar to that of cancellous bone (Lu et al., 2002; Metsger et al., 1993; Ramay and Zhang, 2004).

Various polymers are widely used as biomaterials and they can be easily manufactured and modified for any application. There are two broad categories of polymers that are used for biomaterials: 1) natural and 2) synthetic. Natural materials such as type I collagen are usually derived from animals, which is the main matrix component of many connective tissues including bone and skin. Natural materials are generally not toxic to the body and biocompatible. In addition, natural materials may carry specific protein binding sites and elicit biochemical signals that promote tissue regeneration. However, occasionally, these materials can also be subject to tissue rejection due to immune response. One potential problem with natural materials such as unmodified type I collagen is their limited mechanical stiffness and strength for load bearing applications; especially when the scaffold is in aqueous condition.

A variety of synthetic polymers are used in tissue engineering, which include poly(lactic-co-glycolic) acid (PLGA), poly(methyl methacrylate) (PMMA), and polyesters. Some modification can often be done on these synthetic polymers so that they can be hydrolytically degraded. Unfortunately, in some cases, the degraded particles potentially may lead to an inflammatory response (Bostman et al., 1990; Vert et al., 1994). Overall, some advantages of both natural and synthetic polymer scaffolds are the ability of them to be easily modified, adsorb proteins and retain solutions quite well.

In general, synthetic biomaterials do not possess the three required properties for tissue engineering applications in bone repair, which includes being osteoconductive, osteoinductive and load-bearing. Therefore, additional modifications to the synthetic biomaterials are required to achieve this goal. To improve the osteoinductive property the most common technique is to combine the biomaterials with growth factors and other bioactive proteins that are able to promote angiogenesis and osteogenesis (Itoh et al., 2001; Li et al., 2009; Schliephake et al., 2008). In general the goal is to use the scaffold

as a carrier for slow release of the growth factors at the defect site. For improvement in load-bearing properties, composites are used for tissue engineering application. These composites are usually made up of a combination of polymers and bioceramics. For example, studies were able to create scaffolds made up of collagen and HA that have the strength and stiffness comparable to trabecular bone (Itoh et al., 2002; Kikuchi et al., 2001).

1.5.2 Potential use of nanohydroxyapatite/poly(ester-urethane) scaffold as a carrier for growth factors and bioactive proteins

Over the years, polyurethane has been shown to be safe, and easily molded into various shapes. However, for most applications, pure polyurethane is a poor candidate for use in drug delivery due to its resistance to degradation. The introduction of ester bonds into the polymer backbone resolves the resistance to degradation issue (Ulery et al., 2011). In general, polyurethane is composed of hard and soft copolymer segments that can undergo microphase separation, which allows these polymers to handle physical stress very well and improves its mechanical strength. Typically, biodegradable poly(ester-urethanes) (PU) are synthesized by polycondensation of diisocyanates with polyester diol or triols, which are composed of either glycilide, lactide or caprolactone, to create the soft segment of the polymer. For the hard segment, the typical copolymers are composed of polypeptides or diols or triols of 3-hydroxybutyrate (Guelcher, 2008; Henry et al., 2007).

In the literature, different forms of PU-based scaffolds have been used extensively in tissue engineering applications such as regeneration of bone (Hofmann et al., 2008; Kavlock et al., 2007; Li et al., 2009), cartilage (Dresing et al., 2014; Lee et al., 2005), and other soft tissues (Gogolewski et al., 2008; Guan et al., 2005; Guelcher, 2008; Guelcher et al., 2008). For bone tissue engineering, another important aspect for a successful biomaterial is its capability to bind growth factors, such as rhBMP-2, to promote bone repair. Of relevance, previous *in vitro* studies have shown that rhBMP-2 binds well to

PU-based scaffolds (Li et al., 2009). Based on this study, we postulate that the novel PU scaffolds used in the study may also be an effective carrier for rhBMP-2.

Previous studies have demonstrated that the novel PU scaffolds have porous interconnected three-dimensional environment for cell and blood vessel infiltration (Laschke et al., 2009; Laschke et al., 2013). These PU scaffolds are biocompatible and have viscoelastic properties, which are important for load bearing applications (Hofmann et al., 2008; Laschke et al., 2009; Laschke et al., 2013; Lee et al., 2005; Pirvu et al., 2015). In addition, the PU scaffolds were shown to have the capability of supporting the co-culture of primary human osteoblasts and human umbilical vein endothelial cells (HUVEC) (Hofmann et al., 2008). Using a novel *in vivo* subcutaneous model, the authors showed that the PU scaffolds are osteoconductive and also allow for blood vessels formation within its 3D matrix.

For our study, modifications were made by incorporating nano-sized hydroxyapatite (nHA) particles into the PU matrix to make a novel scaffold (nHA/PU). A 10% weight ratio of nHA to the PU was selected since it gave the best improvement in material stiffness, increased by 30%, compared to PU scaffold alone (Boissard et al., 2009). The addition of nHA was also shown to increased the scaffold capacity to bind proteins such as serum albumin and fibrinogen (Laschke et al., 2010b). The presence of nHA may potentially enhance binding affinity of growth factors and bioactive proteins to the nHA/PU scaffold. The incorporation of nHA did not affect its biocompatibility or inhibit its ability to allow vascularization as previously shown by Laschke et al (Laschke et al., 2009).

1.6 PURPOSE OF THE THESIS

The role of BSP in skeletal tissue development has been studied using *in vitro* culture and transgenic mouse models. BSP has been suggested to promote osteoprogenitor cell differentiation leading to bone formation. One study has also shown that the addition of

BSP-treated collagen scaffolds to critical sized defects promoted bone repair. In addition, BSP is also present in mineralized periodontal tissues, especially in cementum, the mineralized tissue lining the tooth root. However, the role of BSP in the periodontal tissues is unknown.

The studies in this thesis are separated into two main objectives. The first objective focused on the role of BSP in mineralized periodontal tissues. The second objective focused on the potential use of BSP as a therapeutic agent, with a novel poly(ester) urethane (PU) scaffold, for bone repair.

Hypothesis 1: *The absence of BSP in periodontal tissues, specifically acellular cementum, will result in a significant periodontal tissue phenotype.*

Rationale: Previous studies have shown that the absence of BSP in mice results in abnormal bone phenotypes indicated by reduced bone growth, mineralization and repair (Malaval et al., 2008; Malaval et al., 2009; Monfoulet et al., 2010). Other than bone, BSP has also been shown to be present in the mineralized tissues of the tooth, especially cementum (McKee et al., 1996; Somerman et al., 1990). It has been postulated that BSP plays an important, though undefined, role in the formation and mineralization of the cementum (Somerman et al., 1990).

In chapter 2 of the thesis, characterization of the *Bsp*$^{-/-}$ mouse periodontium was conducted to determine whether there were periodontal tissue abnormalities. In brief, the study confirmed that BSP is present in normal cementum and also demonstrated that the *Bsp*$^{-/-}$ mouse has defective acellular cementum, which leads to periodontal tissue breakdown. Histological, SEM, and microCT analyses were utilized to describe the observed phenotype.

In chapter 3, the study focused in part on the additional characterization of the periodontal phenotype and the determination of the potential mechanisms that lead to the abnormalities observed in the *Bsp*$^{-/-}$ mouse. Substitution of hard-pellet diet to soft powdered diet was introduced to verify whether the reduction in occlusal force required

during mastication of the hard diet prevents or reduces the PDL detachment observed in the *Bsp*$^{-/-}$ mouse, which is described in chapter 2. MicroCT and histological analyses were performed. In addition, detailed morphometric measurements were performed to characterize the periodontal tissue destabilization and breakdown.

Hypothesis 2: *BSP treated poly(ester-urethane) scaffolds promote bone repair.*

Rationale: The implantation of BSP treated fibrillar type I collagen scaffolds has been previously shown to promote bone repair (Wang et al. 2006). Previous studies (Goldberg's group), however, were not able to reproduce these results using rat BSP and various types of collagen scaffolds. Based on the efficacy of BSP in promoting biomineralization in a variety of *in vitro* studies as well as the published findings of the Glimcher group (Wang et al., 2006), it was believed that the delivery of BSP to the bone defect site may be the critical factor.

In a collaborative study (Drs. David Eglin and Mauro Alini, AO Foundation), novel scaffolds composed of poly(ester) urethane mixed with nano-hydroxyapatite (nHA/PU) were prepared. Previous studies by our collaborators demonstrated the effectiveness of the nHA/PU scaffold for tissue engineering applications because of its osteoconductive property and its ability to bind bioactive proteins (Boissard et al., 2009; Laschke et al., 2009). The applicability of the nHA/PU scaffold in conjunction with BSP for bone repair is the focus of our studies.

There were 2 main objectives:

The first goal (chapter 4) was to confirm that nHA/PU scaffolds can safely be used as a carrier of bioactive growth factors to promote bone repair. The growth factor used was rhBMP-2, a clinically established therapeutic for bone repair. In brief, using a rat calvarial defect model, this study indicated that the nHA/PU scaffolds bound rhBMP-2 well, and the treated scaffolds enhanced bone formation. MicroCT and histological analyses were used to monitor bone repair.

Based on the enhanced bone repair observed with rhBMP-2 treated nHA/PU scaffolds, our second goal was to determine the efficacy of BSP-treated nHA/PU scaffolds in promoting repair (chapter 5). BSP was shown to bind to nHA/PU scaffolds, and the BSP-treated scaffolds apparently promoted osteoprogenitor cell adhesion, however bone repair *in vivo* was not enhanced. MicroCT and histological analyses were used to monitor the bone repair.

1.7 REFERENCES

Abe E. 2006. Function of BMPs and BMP antagonists in adult bone. Ann N Y Acad Sci. 1068(41-53.

Asamura S, Mochizuki Y, Yamamoto M, Tabata Y, Isogai N. 2010. Bone regeneration using a bone morphogenetic protein-2 saturated slow-release gelatin hydrogel sheet: evaluation in a canine orbital floor fracture model. Ann Plast Surg. 64(4):496-502.

Aubin JE. 2001. Regulation of osteoblast formation and function. Rev Endocr Metab Disord. 2(1):81-94.

Baht GS, Hunter GK, Goldberg HA. 2008. Bone sialoprotein–collagen interaction promotes hydroxyapatite nucleation. Matrix Biol. 27(7):600-608.

Baht GS, O'Young J, Borovina A, Chen H, Tye CE, Karttunen M, Lajoie GA, Hunter GK, Goldberg HA. 2010. Phosphorylation of Ser^{136} is critical for potent bone sialoprotein-mediated nucleation of hydroxyapatite crystals Biochem J. 428(385-395.

Bartlett JD. 2013. Dental enamel development: proteinases and their enamel matrix substrates. ISRN Dent. 2013(684607.

Bauer TW, Muschler GF. 2000. Bone graft materials. An overview of the basic science. Clin Orthop Relat Res. 371):10-27.

Bellahcene A, Merville MP, Castronovo V. 1994. Expression of bone sialoprotein, a bone matrix protein, in human breast cancer. Cancer Res. 54(11):2823-2826.

Bellahcene A, Maloujahmoum N, Fisher LW, Pastorino H, Tagliabue E, Menard S, Castronovo V. 1997. Expression of bone sialoprotein in human lung cancer. Calcif Tissue Int. 61(3):183-188.

Bellahcene A, Castronovo V, Ogbureke KU, Fisher LW, Fedarko NS. 2008. Small integrin-binding ligand N-linked glycoproteins (SIBLINGs): multifunctional proteins in cancer. Nat Rev Cancer. 8(3):212-226.

Bellahcène A, Bonjean K, Fohr B, Fedarko NS, Robey FA, Young MF, Fisher LW, Castronovo V. 2000. Bone Sialoprotein Mediates Human Endothelial Cell Attachment and Migration and Promotes Angiogenesis. Circ Res. 86(8):885-891.

Bianco P, Fisher LW, Young MF, Termine JD, Robey PG. 1991. Expression of bone sialoprotein (BSP) in developing human tissues. Calcif Tissue Int. 49(6):421-426.

Bianco P, Riminucci M, Silvestrini G, Bonucci E, Termine JD, Fisher LW, Robey PG. 1993. Localization of bone sialoprotein (BSP) to Golgi and post-Golgi secretory

structures in osteoblasts and to discrete sites in early bone matrix. J Histochem Cytochem. 41(2):193-203.

Boissard CIR, Bourban PE, Tami AE, Alini M, Eglin D. 2009. Nanohydroxyapatite/poly(ester urethane) scaffold for bone tissue engineering. Acta Biomaterialia. 5(9):3316-3327.

Bonewald LF. 2006. Mechanosensation and Transduction in Osteocytes. Bonekey Osteovision. 3(10):7-15.

Bosshardt DD, Selvig KA. 1997. Dental cementum: the dynamic tissue covering of the root. Periodontol 2000. 13(41-75.

Bostman O, Hirvensalo E, Makinen J, Rokkanen P. 1990. Foreign-body reactions to fracture fixation implants of biodegradable synthetic polymers. J Bone Joint Surg Br. 72(4):592-596.

Bostrom MP, Lane JM, Berberian WS, Missri AA, Tomin E, Weiland A, Doty SB, Glaser D, Rosen VM. 1995. Immunolocalization and expression of bone morphogenetic proteins 2 and 4 in fracture healing. J Orthop Res. 13(3):357-367.

Boudiffa M, Wade-Gueye NM, Guignandon A, Vanden-Bossche A, Sabido O, Aubin JE, Jurdic P, Vico L, Lafage-Proust MH, Malaval L. 2010. Bone sialoprotein deficiency impairs osteoclastogenesis and mineral resorption in vitro. J Bone Miner Res. 25(12):2669-2679.

Boyle WJ, Simonet WS, Lacey DL. 2003. Osteoclast differentiation and activation. Nature. 423(6937):337-342.

Cahill KS, Chi JH, Day A, Claus EB. 2009. Prevalence, complications, and hospital charges associated with use of bone-morphogenetic proteins in spinal fusion procedures. JAMA. 302(1):58-66.

Canalis E, Economides AN, Gazzerro E. 2003. Bone morphogenetic proteins, their antagonists, and the skeleton. Endocr Rev. 24(2):218-235.

Carragee EJ, Hurwitz EL, Weiner BK. 2011. A critical review of recombinant human bone morphogenetic protein-2 trials in spinal surgery: emerging safety concerns and lessons learned. The Spine Journal. 11(6):471-491.

Caton J, Tucker AS. 2009. Current knowledge of tooth development: patterning and mineralization of the murine dentition. J Anat. 214(4):502-515.

Chau JF, Leong WF, Li B. 2009. Signaling pathways governing osteoblast proliferation, differentiation and function. Histol Histopathol. 24(12):1593-1606.

Chen D, Zhao M, Mundy GR. 2004. Bone morphogenetic proteins. Growth Factors. 22(4):233-241.

Chen G, Deng C, Li Y-P. 2012. TGF-β and BMP Signaling in Osteoblast Differentiation and Bone Formation. International Journal of Biological Sciences. 8(2):272-288.

Chen J, Sasaguri K, Sodek J, Aufdemorte TB, Jiang H, Thomas HF. 1998. Enamel epithelium expresses bone sialoprotein (BSP). Eur J Oral Sci. 106(S1):331-336.

Cohen MM, Jr. 2000. Merging the old skeletal biology with the new. I. Intramembranous ossification, endochondral ossification, ectopic bone, secondary cartilage, and pathologic considerations. J Craniofac Genet Dev Biol. 20(2):84-93.

Crockett JC, Rogers MJ, Coxon FP, Hocking LJ, Helfrich MH. 2011. Bone remodelling at a glance. J Cell Sci. 124(Pt 7):991-998.

de Jesus Perez VA, Alastalo TP, Wu JC, Axelrod JD, Cooke JP, Amieva M, Rabinovitch M. 2009. Bone morphogenetic protein 2 induces pulmonary angiogenesis via Wnt-beta-catenin and Wnt-RhoA-Rac1 pathways. J Cell Biol. 184(1):83-99.

Deakins M, Volker JF. 1941. Amount of Organic Matter in Enamel From Several Types of Human Teeth. J Dent Res. 20(2):117-121.

Dresing I, Zeiter S, Auer J, Alini M, Eglin D. 2014. Evaluation of a press-fit osteochondral poly(ester-urethane) scaffold in a rabbit defect model. Journal of Materials Science: Materials in Medicine. 25(7):1691-1700.

Ducheyne P. 1987. Bioceramics: material characteristics versus in vivo behavior. J Biomed Mater Res. 21(A2 Suppl):219-236.

Epstein NE. 2013. Complications due to the use of BMP/INFUSE in spine surgery: The evidence continues to mount. Surgical Neurology International. 4(Suppl 5):S343-S352.

Everts V, Delaissé JM, Korper W, Jansen DC, Tigchelaar-Gutter W, Saftig P, Beertsen W. 2002. The Bone Lining Cell: Its Role in Cleaning Howship's Lacunae and Initiating Bone Formation. J Bone Miner Res. 17(1):77-90.

Fisher LW, Whitson SW, Avioli LV, Termine JD. 1983. Matrix sialoprotein of developing bone. J Biol Chem. 258(20):12723-12727.

Fisher LW, Hawkins GR, Tuross N, Termine JD. 1987. Purification and partial characterization of small proteoglycans I and II, bone sialoproteins I and II, and osteonectin from the mineral compartment of developing human bone. J Biol Chem. 262(20):9702-9708.

Fisher LW, Torchia DA, Fohr B, Young MF, Fedarko NS. 2001. Flexible structures of SIBLING proteins, bone sialoprotein, and osteopontin. Biochem Biophys Res Commun. 280(2):460-465.

Foster BL. 2012. Methods for studying tooth root cementum by light microscopy. Int J Oral Sci. 4(3):119-128.

Franzen A, Heinegard D. 1985. Isolation and characterization of two sialoproteins present only in bone calcified matrix. Biochem J. 232(3):715-724.

Fujisawa R, Butler WT, Brunn JC, Zhou HY, Kuboki Y. 1993. Differences in composition of cell-attachment sialoproteins between dentin and bone. J Dent Res. 72(8):1222-1226.

Ganss B, Kim RH, Sodek J. 1999. Bone sialoprotein. Crit Rev Oral Biol Med. 10(1):79-98.

Geiger M, Li RH, Friess W. 2003. Collagen sponges for bone regeneration with rhBMP-2. Adv Drug Deliv Rev. 55(12):1613-1629.

Gill KS, Beier F, Goldberg HA. 2008. Rho-ROCK signaling differentially regulates chondrocyte spreading on fibronectin and bone sialoprotein. Am J Physiol Cell Physiol. 295(1):C38-49.

Gogolewski S, Gorna K, Zaczynska E, Czarny A. 2008. Structure–property relations and cytotoxicity of isosorbide-based biodegradable polyurethane scaffolds for tissue repair and regeneration. Journal of Biomedical Materials Research Part A. 85A(2):456-465.

Goldberg HA, Warner KJ, Hunter GK. 2001. Binding of bone sialoprotein, osteopontin and synthetic polypeptides to hydroxyapatite. Connect Tissue Res. 42(1):25-37.

Goldberg HA, Hunter GK. 2012. Functional domains of bone sialoprotein.In: Phosphorylated extracellular matrix proteins of bone and dentin. M Goldberg editor^editors. Oak Park (IL): Bentham Science Publishers; p. 266-282.

Goldberg M, Kulkarni AB, Young M, Boskey A. 2011. Dentin: Structure, Composition and Mineralization: The role of dentin ECM in dentin formation and mineralization. Frontiers in Bioscience (Elite Edition). 3(711-735.

Gonçalves PF, Sallum EA, Sallum AW, Casati MZ, de Toledo S, Nociti Jr FH. 2005. Dental cementum reviewed: development, structure, composition, regeneration and potential functions. Brazilian Journal of Oral Science. 4(12):651-658.

Gordon JAR, Tye CE, Sampaio AV, Underhill TM, Hunter GK, Goldberg HA. 2007. Bone sialoprotein expression enhances osteoblast differentiation and matrix mineralization in vitro. Bone. 41(3):462-473.

Gorski JP, Shimizu K. 1988. Isolation of new phosphorylated glycoprotein from mineralized phase of bone that exhibits limited homology to adhesive protein osteopontin. J Biol Chem. 263(31):15938-15945.

Graf HL, Stoeva S, Armbruster FP, Neuhaus J, Hilbig H. 2008. Effect of bone sialoprotein and collagen coating on cell attachment to TICER® and pure titanium implant surfaces. Int J Oral Maxillofac Surg. 37(7):634-640.

Guan J, Fujimoto KL, Sacks MS, Wagner WR. 2005. Preparation and characterization of highly porous, biodegradable polyurethane scaffolds for soft tissue applications. Biomaterials. 26(18):3961-3971.

Guelcher SA. 2008. Biodegradable polyurethanes: synthesis and applications in regenerative medicine. Tissue Eng Part B Rev. 14(1):3-17.

Guelcher SA, Srinivasan A, Dumas JE, Didier JE, McBride S, Hollinger JO. 2008. Synthesis, mechanical properties, biocompatibility, and biodegradation of polyurethane networks from lysine polyisocyanates. Biomaterials. 29(12):1762-1775.

Guo X, Wang XF. 2009. Signaling cross-talk between TGF-beta/BMP and other pathways. Cell Res. 19(1):71-88.

Harris NL, Rattray KR, Tye CE, Underhill TM, Somerman MJ, D'Errico JA, Chambers AF, Hunter GK, Goldberg HA. 2000. Functional analysis of bone sialoprotein: identification of the hydroxyapatite-nucleating and cell-binding domains by recombinant peptide expression and site-directed mutagenesis. Bone. 27(6):795-802.

Helfrich MH, Nesbitt SA, Dorey EL, Horton MA. 1992. Rat osteoclasts adhere to a wide range of RGD (Arg-Gly-Asp) peptide-containing proteins, including the bone sialoproteins and fibronectin, via a beta 3 integrin. J Bone Miner Res. 7(3):335-343.

Helfrich MH, Crockett JC, Hocking LJ, Coxon FP. 2007. The pathogenesis of osteoclast diseases: Some knowns, but still many unknowns. IBMS BoneKEy. 4(2):61-77.

Henry JA, Simonet M, Pandit A, Neuenschwander P. 2007. Characterization of a slowly degrading biodegradable polyester-urethane for tissue engineering scaffolds. J Biomed Mater Res A. 82(3):669-679.

Hofmann A, Ritz U, Verrier S, Eglin D, Alini M, Fuchs S, Kirkpatrick CJ, Rommens PM. 2008. The effect of human osteoblasts on proliferation and neo-vessel formation of human umbilical vein endothelial cells in a long-term 3D co-culture on polyurethane scaffolds. Biomaterials. 29(31):4217-4226.

Hunter GK, Goldberg HA. 1993. Nucleation of hydroxyapatite by bone sialoprotein. Proc Natl Acad Sci U S A. 90(18):8562-8565.

Itoh S, Kikuchi M, Takakuda K, Koyama Y, Matsumoto HN, Ichinose S, Tanaka J, Kawauchi T, Shinomiya K. 2001. The biocompatibility and osteoconductive activity of a novel hydroxyapatite/collagen composite biomaterial, and its function as a carrier of rhBMP-2. J Biomed Mater Res. 54(3):445-453.

Itoh S, Kikuchi M, Koyama Y, Takakuda K, Shinomiya K, Tanaka J. 2002. Development of an artificial vertebral body using a novel biomaterial, hydroxyapatite/collagen composite. Biomaterials. 23(19):3919-3926.

Jena N, Martin-Seisdedos C, McCue P, Croce CM. 1997. BMP7 null mutation in mice: developmental defects in skeleton, kidney, and eye. Exp Cell Res. 230(1):28-37.

Jernvall J, Kettunen P, Karavanova I, Martin LB, Thesleff I. 1994. Evidence for the role of the enamel knot as a control center in mammalian tooth cusp formation: non-dividing cells express growth stimulating Fgf-4 gene. Int J Dev Biol. 38(3):463-469.

Jernvall J, Aberg T, Kettunen P, Keranen S, Thesleff I. 1998. The life history of an embryonic signaling center: BMP-4 induces p21 and is associated with apoptosis in the mouse tooth enamel knot. Development. 125(2):161-169.

Kavlock KD, Pechar TW, Hollinger JO, Guelcher SA, Goldstein AS. 2007. Synthesis and characterization of segmented poly(esterurethane urea) elastomers for bone tissue engineering. Acta Biomater. 3(4):475-484.

Kikuchi M, Itoh S, Ichinose S, Shinomiya K, Tanaka J. 2001. Self-organization mechanism in a bone-like hydroxyapatite/collagen nanocomposite synthesized in vitro and its biological reaction in vivo. Biomaterials. 22(13):1705-1711.

Kinne RW, Fisher LW. 1987. Keratan sulfate proteoglycan in rabbit compact bone is bone sialoprotein II. J Biol Chem. 262(21):10206-10211.

Laschke MW, Strohe A, Scheuer C, Eglin D, Verrier S, Alini M, Pohlemann T, Menger MD. 2009. In vivo biocompatibility and vascularization of biodegradable porous polyurethane scaffolds for tissue engineering. Acta Biomaterialia. 5(6):1991-2001.

Laschke MW, Strohe A, Menger MD, Alini M, Eglin D. 2010. In vitro and in vivo evaluation of a novel nanosize hydroxyapatite particles/poly(ester-urethane) composite scaffold for bone tissue engineering. Acta Biomaterialia. 6(6):2020-2027.

Laschke MW, Schank TE, Scheuer C, Kleer S, Schuler S, Metzger W, Eglin D, Alini M, Menger MD. 2013. Three-dimensional spheroids of adipose-derived mesenchymal stem cells are potent initiators of blood vessel formation in porous polyurethane scaffolds. Acta Biomaterialia. 9(6):6876-6884.

Lee C, Grad S, Gorna K, Gogolewski S, Goessl A, Alini M. 2005. Fibrin–Polyurethane Composites for Articular Cartilage Tissue Engineering: A Preliminary Analysis. Tissue Engineering. 11(9-10):1562-1573.

LeFevre ML, Manly RS. 1938. Moisture, Inorganic and Organic Contents of Enamel and Dentin from Carious Teeth*. The Journal of the American Dental Association and The Dental Cosmos. 25(2):233-242.

Li B, Yoshii T, Hafeman AE, Nyman JS, Wenke JC, Guelcher SA. 2009. The effects of rhBMP-2 released from biodegradable polyurethane/microsphere composite scaffolds on new bone formation in rat femora. Biomaterials. 30(35):6768-6779.

Long F. 2012. Building strong bones: molecular regulation of the osteoblast lineage. Nat Rev Mol Cell Biol. 13(1):27-38.

Lu J, Descamps M, Dejou J, Koubi G, Hardouin P, Lemaitre J, Proust JP. 2002. The biodegradation mechanism of calcium phosphate biomaterials in bone. J Biomed Mater Res. 63(4):408-412.

Luo G, Hofmann C, Bronckers AL, Sohocki M, Bradley A, Karsenty G. 1995. BMP-7 is an inducer of nephrogenesis, and is also required for eye development and skeletal patterning. Genes Dev. 9(22):2808-2820.

Malaval L, Wade-Guéye NM, Boudiffa M, Fei J, Zirngibl R, Chen F, Laroche N, Roux J-P, Burt-Pichat B, Duboeuf F et al. 2008. Bone sialoprotein plays a functional role in bone formation and osteoclastogenesis. J Exp Med. 205(5):1145-1153.

Malaval L, Monfoulet L, Fabre T, Pothuaud L, Bareille R, Miraux S, Thiaudiere E, Raffard G, Franconi J-M, Lafage-Proust M-H et al. 2009. Absence of bone sialoprotein (BSP) impairs cortical defect repair in mouse long bone. Bone. 45(5):853-861.

McKee MD, Zalzal S, Nanci A. 1996. Extracellular matrix in tooth cementum and mantle dentin: Localization of osteopontin and other noncollagenous proteins, plasma proteins, and glycoconjugates by electron microscopy. Anat Rec. 245(2):293-312.

Metsger DS, DePhilip RM, Hayes TG. 1993. An autoradiographic study of calcium phosphate ceramic bone implants in turkeys. Clin Orthop Relat Res. 291):283-294.

Monfoulet L, Malaval L, Aubin JE, Rittling SR, Gadeau AP, Fricain J-C, Chassande O. 2010. Bone sialoprotein, but not osteopontin, deficiency impairs the mineralization of regenerating bone during cortical defect healing. Bone. 46(2):447-452.

Murakami N, Saito N, Horiuchi H, Okada T, Nozaki K, Takaoka K. 2002. Repair of segmental defects in rabbit humeri with titanium fiber mesh cylinders containing recombinant human bone morphogenetic protein-2 (rhBMP-2) and a synthetic polymer. J Biomed Mater Res. 62(2):169-174.

Nakase T, Nomura S, Yoshikawa H, Hashimoto J, Hirota S, Kitamura Y, Oikawa S, Ono K, Takaoka K. 1994. Transient and localized expression of bone morphogenetic protein 4 messenger RNA during fracture healing. J Bone Miner Res. 9(5):651-659.

Neovius E, Lemberger M, Docherty Skogh AC, Hilborn J, Engstrand T. 2013. Alveolar bone healing accompanied by severe swelling in cleft children treated with bone morphogenetic protein-2 delivered by hydrogel. J Plast Reconstr Aesthet Surg. 66(1):37-42.

O'Toole GC, Salih E, Gallagher C, FitzPatrick D, O'Higgins N, O'Rourke SK. 2004. Bone sialoprotein-coated femoral implants are osteoinductive but mechanically compromised. J Orthop Res. 22(3):641-646.

Oldberg A, Franzen A, Heinegard D, Pierschbacher M, Ruoslahti E. 1988. Identification of a bone sialoprotein receptor in osteosarcoma cells. J Biol Chem. 263(36):19433-19436.

Olsen BR, Reginato AM, Wang W. 2000. Bone development. Annu Rev Cell Dev Biol. 16(191-220.

Onishi T, Ishidou Y, Nagamine T, Yone K, Imamura T, Kato M, Sampath TK, ten Dijke P, Sakou T. 1998. Distinct and overlapping patterns of localization of bone morphogenetic protein (BMP) family members and a BMP type II receptor during fracture healing in rats. Bone. 22(6):605-612.

Papakostidis C, Kontakis G, Bhandari M, Giannoudis PV. 2008. Efficacy of autologous iliac crest bone graft and bone morphogenetic proteins for posterolateral fusion of lumbar spine: a meta-analysis of the results. Spine (Phila Pa 1976). 33(19):E680-692.

Pirvu T, Blanquer SBG, Benneker LM, Grijpma DW, Richards RG, Alini M, Eglin D, Grad S, Li Z. 2015. A combined biomaterial and cellular approach for annulus fibrosus rupture repair. Biomaterials. 42(0):11-19.

Provot S, Schipani E. 2005. Molecular mechanisms of endochondral bone development. Biochem Biophys Res Commun. 328(3):658-665.

Qin C, Brunn JC, Jones J, George A, Ramachandran A, Gorski JP, Butler WT. 2001. A comparative study of sialic acid-rich proteins in rat bone and dentin. Eur J Oral Sci. 109(2):133-141.

Ramay HR, Zhang M. 2004. Biphasic calcium phosphate nanocomposite porous scaffolds for load-bearing bone tissue engineering. Biomaterials. 25(21):5171-5180.

Ritting AW, Weber EW, Lee MC. 2012. Exaggerated inflammatory response and bony resorption from BMP-2 use in a pediatric forearm nonunion. J Hand Surg Am. 37(2):316-321.

Sawyer AA, Song SJ, Susanto E, Chuan P, Lam CXF, Woodruff MA, Hutmacher DW, Cool SM. 2009. The stimulation of healing within a rat calvarial defect by mPCL–TCP/collagen scaffolds loaded with rhBMP-2. Biomaterials. 30(13):2479-2488.

Saygin NE, Giannobile WV, Somerman MJ. 2000. Molecular and cell biology of cementum. Periodontol 2000. 24(73-98.

Schaeren S, Jaquiéry C, Wolf F, Papadimitropoulos A, Barbero A, Schultz-Thater E, Heberer M, Martin I. 2010. Effect of bone sialoprotein coating of ceramic and synthetic

polymer materials on in vitro osteogenic cell differentiation and in vivo bone formation. Journal of Biomedical Materials Research Part A. 92A(4):1461-1467.

Schliephake H, Weich HA, Dullin C, Gruber R, Frahse S. 2008. Mandibular bone repair by implantation of rhBMP-2 in a slow release carrier of polylactic acid—An experimental study in rats. Biomaterials. 29(1):103-110.

Schmitt JM, Hwang K, Winn SR, Hollinger JO. 1999. Bone morphogenetic proteins: an update on basic biology and clinical relevance. J Orthop Res. 17(2):269-278.

Sellers RS, Zhang R, Glasson SS, Kim HD, Peluso D, D'Augusta DA, Beckwith K, Morris EA. (2000). Repair of articular cartilage defects one year after treatment with recombinant human bone morphogenetic protein-2 (rhBMP-2). J Bone Joint Surg Am 82(2)*:*151-160.

Sfeir C, Ho L, Doll BA, Azari K, Hollinger JO. 2005. Fracture Repair.In: Bone Regeneration and Repair: Biology and Clinical Applications. JR Lieberman and GE Friedlaender editor^editors. Totowa, NJ: Humana Press Inc; p. 21-44.

Shintani S, Kamakura N, Kobata M, Toyosawa S, Onishi T, Sato A, Kawasaki K, Weiss KM, Ooshima T. 2008. Identification and characterization of integrin-binding sialoprotein (IBSP) genes in reptile and amphibian. Gene. 424(1-2):11-17.

Somerman MJ, Shroff B, Agraves WS, Morrison G, Craig AM, Denhardt DT, Foster RA, Sauk JJ. 1990. Expression of attachment proteins during cementogenesis. J Biol Buccale. 18(3):207-214.

Soucacos PN, Johnson EO, Babis G. 2008. An update on recent advances in bone regeneration. Injury. 39 Suppl 2(S1-4.

Stubbs JT, 3rd, Mintz KP, Eanes ED, Torchia DA, Fisher LW. 1997. Characterization of native and recombinant bone sialoprotein: delineation of the mineral-binding and cell adhesion domains and structural analysis of the RGD domain. J Bone Miner Res. 12(8):1210-1222.

Suh DY, Boden SD, Louis-Ugbo J, Mayr M, Murakami H, Kim HS, Minamide A, Hutton WC. 2002. Delivery of recombinant human bone morphogenetic protein-2 using a compression-resistant matrix in posterolateral spine fusion in the rabbit and in the non-human primate. Spine (Phila Pa 1976). 27(4):353-360.

Tye CE, Rattray KR, Warner KJ, Gordon JAR, Sodek J, Hunter GK, Goldberg HA. 2003. Delineation of the Hydroxyapatite-nucleating Domains of Bone Sialoprotein. J Biol Chem. 278(10):7949-7955.

Tye CE, Hunter GK, Goldberg HA. 2005. Identification of the Type I collagen-binding domain of bone sialoprotein and characterization of the mechanism of interaction. J Biol Chem. 280(14):13487-13492.

Ulery BD, Nair LS, Laurencin CT. 2011. Biomedical Applications of Biodegradable Polymers. J Polym Sci B Polym Phys. 49(12):832-864.

Vaahtokari A, Aberg T, Jernvall J, Keranen S, Thesleff I. 1996. The enamel knot as a signaling center in the developing mouse tooth. Mech Dev. 54(1):39-43.

Valverde P, Tu Q, Chen J. 2005. BSP and RANKL induce osteoclastogenesis and bone resorption synergistically. J Bone Miner Res. 20(9):1669-1679.

Valverde P, Zhang J, Fix A, Zhu J, Ma W, Tu Q, Chen J. 2008. Overexpression of bone sialoprotein leads to an uncoupling of bone formation and bone resorption in mice. J Bone Miner Res. 23(11):1775-1788.

Vert M, Mauduit J, Li S. 1994. Biodegradation of PLA/GA polymers: increasing complexity. Biomaterials. 15(15):1209-1213.

Wagner EF, Karsenty G. 2001. Genetic control of skeletal development. Curr Opin Genet Dev. 11(5):527-532.

Wang J, Zhou H-Y, Salih E, Xu L, Wunderlich L, Gu X, Hofstaetter J, Torres M, Glimcher M. 2006. Site-Specific *In Vivo* Calcification and Osteogenesis Stimulated by Bone Sialoprotein. Calcif Tissue Int. 79(3):179-189.

Williams BJ, Smith JS, Fu KM, Hamilton DK, Polly DW, Jr., Ames CP, Berven SH, Perra JH, Knapp DR, Jr., McCarthy RE et al. 2011. Does bone morphogenetic protein increase the incidence of perioperative complications in spinal fusion? A comparison of 55,862 cases of spinal fusion with and without bone morphogenetic protein. Spine (Phila Pa 1976). 36(20):1685-1691.

Winnier G, Blessing M, Labosky PA, Hogan BL. 1995. Bone morphogenetic protein-4 is required for mesoderm formation and patterning in the mouse. Genes Dev. 9(17):2105-2116.

Wozney JM. 2002. Overview of bone morphogenetic proteins. Spine (Phila Pa 1976). 27(16 Suppl 1):S2-8.

Wuttke M, Muller S, Nitsche DP, Paulsson M, Hanisch FG, Maurer P. 2001. Structural characterization of human recombinant and bone-derived bone sialoprotein. Functional implications for cell attachment and hydroxyapatite binding. J Biol Chem. 276(39):36839-36848.

Xu L, Anderson AL, Lu Q, Wang J. 2007. Role of fibrillar structure of collagenous carrier in bone sialoprotein-mediated matrix mineralization and osteoblast differentiation. Biomaterials. 28(4):750-761.

Yang R, Gotoh Y, Moore MA, Rafidi K, Gerstenfeld LC. 1995. Characterization of an avian bone sialoprotein (BSP) cDNA: comparisons to mammalian BSP and identification of conserved structural domains. J Bone Miner Res. 10(4):632-640.

Yaszemski MJ, Payne RG, Hayes WC, Langer R, Mikos AG. 1996. Evolution of bone transplantation: molecular, cellular and tissue strategies to engineer human bone. Biomaterials. 17(2):175-185.

You L, Temiyasathit S, Lee P, Kim CH, Tummala P, Yao W, Kingery W, Malone AM, Kwon RY, Jacobs CR. 2008. Osteocytes as mechanosensors in the inhibition of bone resorption due to mechanical loading. Bone. 42(1):172-179.

Younger EM, Chapman MW. 1989. Morbidity at bone graft donor sites. J Orthop Trauma. 3(3):192-195.

Zaia J, Boynton R, Heinegard D, Barry F. 2001. Posttranslational modifications to human bone sialoprotein determined by mass spectrometry. Biochemistry (Mosc). 40(43):12983-12991.

Zhang H, Bradley A. 1996. Mice deficient for BMP2 are nonviable and have defects in amnion/chorion and cardiac development. Development. 122(10):2977-2986.

Zhang Q, Domenicucci C, Goldberg HA, Wrana JL, Sodek J. 1990. Characterization of fetal porcine bone sialoproteins, secreted phosphoprotein I (SPPI, osteopontin), bone sialoprotein, and a 23-kDa glycoprotein. Demonstration that the 23-kDa glycoprotein is derived from the carboxyl terminus of SPPI. J Biol Chem. 265(13):7583-7589.

CHAPTER 2

2 Deficiency in acellular cementum and periodontal attachment in *Bsp*-null mice

2.1 INTRODUCTION

Bone sialoprotein (BSP, or integrin binding sialoprotein) is an extracellular matrix protein in the Small Integrin Binding Ligand N-linked Glycoprotein (SIBLING) family, associated with mineralized tissues of the skeleton and dentition (Fisher and Fedarko, 2003; Ganss et al., 1999). Like other SIBLING proteins, BSP is multifunctional, with roles in cell attachment and migration (through the integrin-binding RGD motif), cell signaling, collagen binding, and hydroxyapatite nucleation. The ability of BSP to act as a positive regulator for hydroxyapatite precipitation has been demonstrated *in vitro* (Hunter and Goldberg, 1993), and is of particular interest in terms of regulating mineralized tissue development. Mice null for the *Bsp* gene ($Bsp^{-/-}$) feature delayed bone growth and mineralization (Malaval et al., 2008).

In addition to its inclusion in bone extracellular matrix, BSP is present in both acellular and cellular cementum (MacNeil et al., 1994; McKee et al., 1996). Acellular cementum is the thin, mineralized tissue covering the cervical portion of the tooth root, important for attachment of the periodontal ligament (PDL) to the root surface (Bosshardt, 2005; Foster et al., 2007). Cellular cementum is a more bone-like tissue covering apical portions of roots. Developmental factors directing cementogenesis remain poorly defined, hampering progress towards more effective therapies for cementum regeneration. The finding that BSP was present in cementum and strongly expressed by cementoblasts led to speculation that this protein might contribute to cementum formation and mineralization (MacNeil et al., 1995; Somerman et al., 1990), however this hypothesis has remained untested in the two decades since these findings. Here, we analyzed the function of BSP in cementogenesis and periodontal stability by determining effects of lack of BSP on tooth formation.

2.2 MATERIALS & METHODS

2.2.1 Animals

Animal procedures were performed in accordance with guidelines of the Canadian Council on Animal Care and Animal Care and Veterinary Services, University of Western Ontario. Preparation and genotyping procedures of *Bsp*$^{-/-}$ and wild-type (WT) mice were described previously (Malaval et al., 2008). All of the mice were maintained on a mixed 129/CD1 background and fed a standard mouse diet (2018 Tekland Global 18% protein diet, Harlan Laboratories, USA). Three to six animals were analyzed per genotype at ages 14, 26, 30, and 60 days postnatal (dpn) to determine abnormal phenotypes. Serum biochemistry was analyzed using standard assays by NIH Veterinary Services Clinical Chemistry (Bethesda, MD). For this study, all comparison were made between *Bsp*$^{-/-}$ and WT littermate pairs.

2.2.2 Micro-computed tomography (microCT) and scanning electron microscopy (SEM)

MicroCT of formalin-fixed hemi-mandibles was performed using eXplore Locus SP (GE Healthcare, Canada). 2D images were acquired at 80 kVp and 80 μA, using an integration time of 1600 ms/frame, 4 frames/view, and a total of 900 views at an increment of 0.4 degrees. Images were constructed at a spatial resolution of 13 μm and calibrated with a cortical bone phantom (SB3; Gamex RMI, Wisconsin, USA) having a hydroxyapatite equivalent of 1,100 mg/cc (White, 1978). Data were analyzed using MicroView ABA version 2.2 (GE Healthcare).

For SEM analysis, extracted and cleansed molars were osmium coated. For fracture analysis, an ultra-fine diamond burr (Brassfler DET6UF-31) was used to drill through crowns, and teeth were fractured longitudinally. SEM images were analyzed in

secondary electron mode at 1-10 kV on a Leo 1540 XB FIB/SEM (Carl Zeiss, Western Nanofabrication Facility).

2.2.3 Histological procedures

Procedures for histology, *in situ* hybridization (ISH), and immunohistochemistry (IHC) were previously described on Bouin's fixed, decalcified, paraffin-embedded samples (Foster, 2012; Foster et al., 2012). Histomorphometry was used to quantify cementum, root-lining cells (cementoblasts) (D'Errico et al., 1997), and epithelial attachment, and statistical analysis was performed by independent samples t-test.

For the ISH of *Bsp* mRNA, digoxigenin (DIG)-labeled cRNA probe (Marian Young, NIDCR, Bethesda, MD) with NBT/BCIP substrate were utilized. As for the IHC, biotinylated secondary antibodies and peroxidase substrate were utilized. A variety of primary antibodies were used in the study, which included rabbit anti-BSP (1:200; Renny Franceschi, University of Michigan, Ann Arbor), rat anti-alkaline phosphatase (TNAP/ALPL, 1:200; R&D Systems, Minneapolis, MN), LF-175 rabbit anti-osteopontin (OPN; 1:200) (Larry Fisher, NIDCR), rabbit anti-cytokeratin (Abcam, Cambridge, MA), goat anti-RANKL (1:50; Santa Cruz Biotechnology, Santa Cruz, CA), and rat anti-neutrophil antibody (1:200; NIMP-R14; Abcam).

As for undecalcifed, glutaraldehyde/formalin fixed tissues, they were either LR white-embedded for ultramicrotome sectioning (1 μm) for von Kossa staining (Everts et al., 2012), or processed and methylmethacrylate-embedded for microtome sectioning (6 μm) for Goldner's trichrome staining (Kacena et al., 2004). For all ISH and IHC sections, negative and positive controls were always stained to verify no background staining.

The histology sections stained with alcian blue were used to measure the thickness of the acellular cementum (dark blue in appearance). All of the measurement were done within the top 2/3 of the root. Three random measurements were conducted and then the average values were calculated for each mouse.

2.3 RESULTS

2.3.1 *Bsp*$^{-/-}$ mice exhibit defective acellular cementum formation

Bsp mRNA is highly expressed by cementoblasts during tooth root formation, as well as osteoblasts of the alveolar bone (Figure 2.1A). BSP protein is localized to alveolar bone, and acellular and cellular cementum covering the cervical and apical portions of the molar, respectively (Figure 2.1B-C). Absence of BSP immunostaining was confirmed in *Bsp*$^{-/-}$ mice (Figure 2.1D-E).

Over the course of root development, *Bsp*$^{-/-}$ mouse molar teeth displayed deficiency in acellular cementum formation. At 14 days postnatal (dpn), a basophilic layer of acellular cementum covered the root dentin in WT mice (Figure 2.1F-G), while in *Bsp*$^{-/-}$ molars, this layer was thinner (Figure 2.1H-I). At 26 dpn, WT acellular cementum had grown thicker and inserted PDL fibers radiated from the surface of the cervical root (Figure 2.1J-K). Conversely, *Bsp*$^{-/-}$ acellular cementum showed no additional growth (Figure 2.1L-M). It was common to find PDL disorganization in *Bsp*$^{-/-}$ molars, and a structural defect in the cementum-PDL interface was indicated by detachment in all *Bsp*$^{-/-}$ samples (possibly partly due to tissue processing, but not present in WT samples). By 60 dpn, acellular cementum remained stunted in *Bsp*$^{-/-}$ mice, and PDL detachment was present in all *Bsp*$^{-/-}$, but not WT, samples (Figure 2.1N vs. P). Histomorphometry confirmed that the apparent acellular cementum thickness was significantly reduced in *Bsp*$^{-/-}$ compared to WT molars (Figure 2.1R). Alcian blue staining supported diminished acellular cementum and Goldner's trichrome staining indicated a lack of mineralized cementum matrix on *Bsp*$^{-/-}$ molar surfaces (Figure 2.2). The continuously erupting mouse incisor features acellular cementum on the lingual root analog, and *Bsp*$^{-/-}$ incisors featured reduced cementum thickness and PDL disorganization (Figure 2.3), contributing to a high rate of incisor malocclusion observed in *Bsp*$^{-/-}$ mice. The quantity of cellular cementum covering the apical molar root was unaffected at 60 dpn in *Bsp*$^{-/-}$ compared to WT molars (Figure 2.1O vs. Q), though at 26 dpn mineralization was delayed in this layer (Figure 2.4).

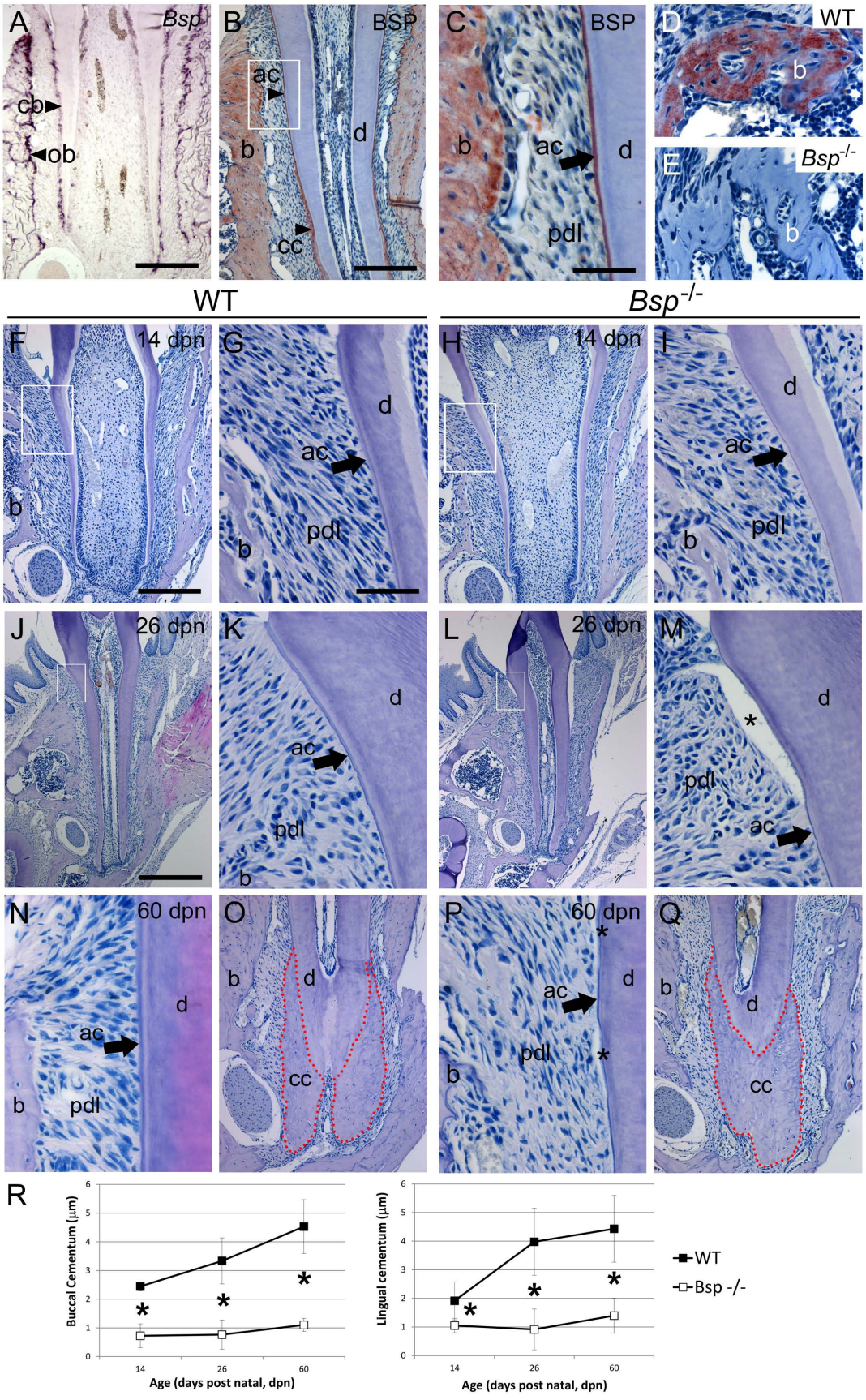
A
Bsp
cb
ob
B
BSP
ac
b
d
cc
C
BSP
b
ac
d
pdl
D
WT
b
E
Bsp-/-
b
WT
Bsp-/-
F
14 dpn
b
G
d
ac
pdl
b
H
14 dpn
I
d
ac
pdl
b
J
26 dpn
K
d
ac
pdl
b
L
26 dpn
M
d
*
pdl
ac
N
60 dpn
d
ac
b
pdl
O
b
d
cc
P
60 dpn
*
ac
d
pdl
*
b
Q
b
d
cc
R
Buccal Cementum (µm)
Age (days post natal, dpn)
Lingual cementum (µm)
Age (days post natal, dpn)
WT
Bsp -/-

Figure 2.1. Bone sialoprotein is required for proper acellular cementum formation.

(A) *Bsp* mRNA is expressed by cementoblasts (cb) and osteoblasts (ob) during molar tooth root development at 14 dpn. **(B, C)** BSP protein is localized to alveolar bone (b), acellular cementum (ac), and cellular cementum (cc) at 26 dpn. White box in B is shown at higher magnification in C to highlight acellular cementum. BSP immunolabeling in **(D)** WT alveolar bone is absent in **(E)** $Bsp^{-/-}$ mice. **(F, G)** Newly formed acellular cementum anchors periodontal ligament (pdl) attachment in WT molars. **(H, I)** Acellular cementum in $Bsp^{-/-}$ molars is thin compared WT. In contrast to the thickened acellular cementum in **(J, K)** WT at 26 dpn, **(L, M)** $Bsp^{-/-}$ molars feature stunted acellular cementum, and regions of PDL detachment from the tooth (*) were common, indicating defects in cementum-PDL interface. PDL detachment is observed in all of the $Bsp^{-/-}$ mice, whereas in all of the WT mice the PDL attachment appeared normal. The well organized attachment of the acellular cementum, PDL, and bone in **(N)** WT molars at 60 dpn is severely degraded in **(P)** $Bsp^{-/-}$ molars, where stunted acellular cementum is associated with PDL disorganization. In contrast, cellular cementum in **(O)** WT and **(Q)** $Bsp^{-/-}$ at 60 dpn is not different in size. **(R)** Both buccal and lingual acellular cementum are significantly reduced in thickness in $Bsp^{-/-}$ mice compared to WT counterparts (* indicated significant difference, $p < 0.05$). Scale bar is 200 μm in panels A, B, F, H, O, and Q (original 100X), 50 μm in panels C, D, E, G, I, K, M, N, and P (original 400X), and 400 μm in panels J and L (original 50X). n=6

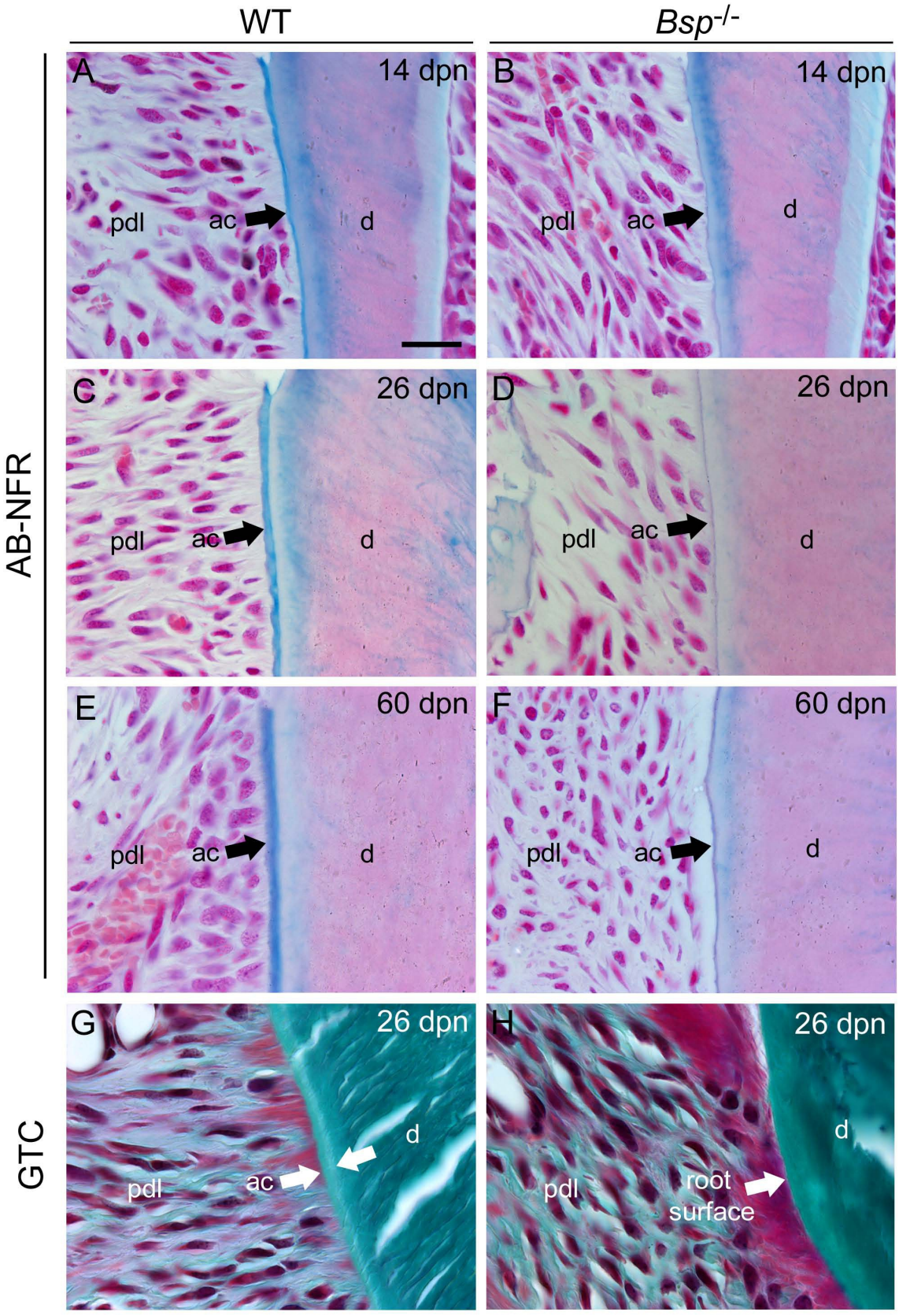
WT
Bsp-/-
AB-NFR
GTC
A
14 dpn
pdl
ac
d
B
14 dpn
pdl
ac
d
C
26 dpn
pdl
ac
d
D
26 dpn
pdl
ac
d
E
60 dpn
pdl
ac
d
F
60 dpn
pdl
ac
d
G
26 dpn
d
pdl
ac
H
26 dpn
d
pdl
root
surface

Figure 2.2. Decreased thickness and mineralization of acellular cementum in the *Bsp*$^{-/-}$ mouse molar.

(A-F) Alcian blue and nuclear fast red (AB-NFR) staining was used to visualize acellular cementum in WT and *Bsp*$^{-/-}$ first molars at 14, 26, and 60 dpn because we found it to be a sensitive stain for cementum (Methods are described in detail in: Foster, 2012). Briefly, Bouin's fixed, demineralized, and paraffin-embedded sections were stained with Alcian blue stain, followed by counter-staining with nuclear fast red, rendering acellular cementum bright blue. **(A, C, E)** Compared to the steady appositional growth of acellular cementum (ac) in the WT from 14 to 60 dpn, **(B, D, F)** *Bsp*$^{-/-}$ molars feature thin cementum that does not increase in size over this time. **(G-H)** Goldner's trichrome (GTC) staining was used to indicate the relative mineralization of dental tissues, where mineralized tissues (e.g. bone, dentin) stain green and unmineralized fibrous-collagenous tissues (e.g. osteoid) stain pink to red. Briefly, undecalcified glutaraldehyde/formaldehyde fixed tissues were methylmethacrylate-embedded, and sections stained by a standard protocol for Goldner's trichrome. **(G)** Whereas WT mouse molars at 26 dpn feature a mineralized acellular cementum layer (light green, flanked by white arrows), **(H)** *Bsp*$^{-/-}$ molar teeth exhibit no visible layer between root dentin (d) and periodontal ligament (pdl), suggesting the thin cementum layer identified by histology is unmineralized. Tears that appear in the tissue are artifacts from undecalcified sectioning. Scale bar is 20 μm in panels A-H (original 630X). n=6

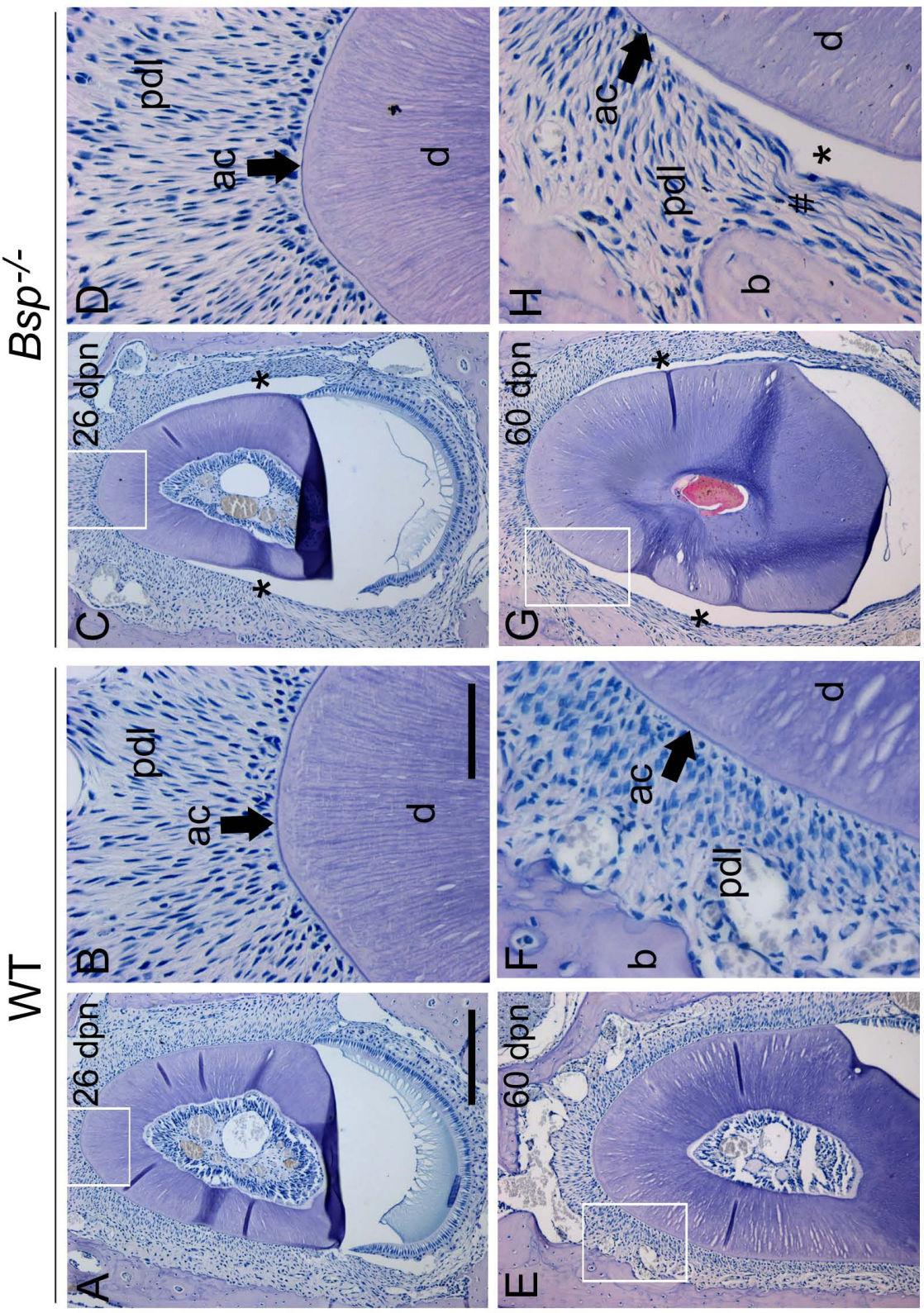
WT
Bsp-/-
A
26 dpn
B
pdl
ac
d
C
26 dpn
*
*
D
pdl
ac
d
*
E
60 dpn
F
b
pdl
ac
d
G
60 dpn
*
*
H
ac
pdl
#
*
b
d

Figure 2.3. Loss of BSP compromises mouse incisor cementum development.

(A, B, E, F) Mouse continually erupting incisors feature a layer of acellular cementum (ac) on the lingual root analogue. **(C, D, G, H)** In *Bsp*$^{-/-}$ mice, incisors display a thin cementum layer, PDL fiber disorganization (#), and PDL detachment from the root surface (*) indicating cementum-PDL structural defects. PDL detachment is observed in all of the *Bsp*$^{-/-}$ mice, whereas in all of the WT mice the PDL attachment appeared normal. Scale bar is 200 μm in panels A, C, E, and G (original 100X), and 50 μm in panels B, D, F, and H (original 400X). n=6

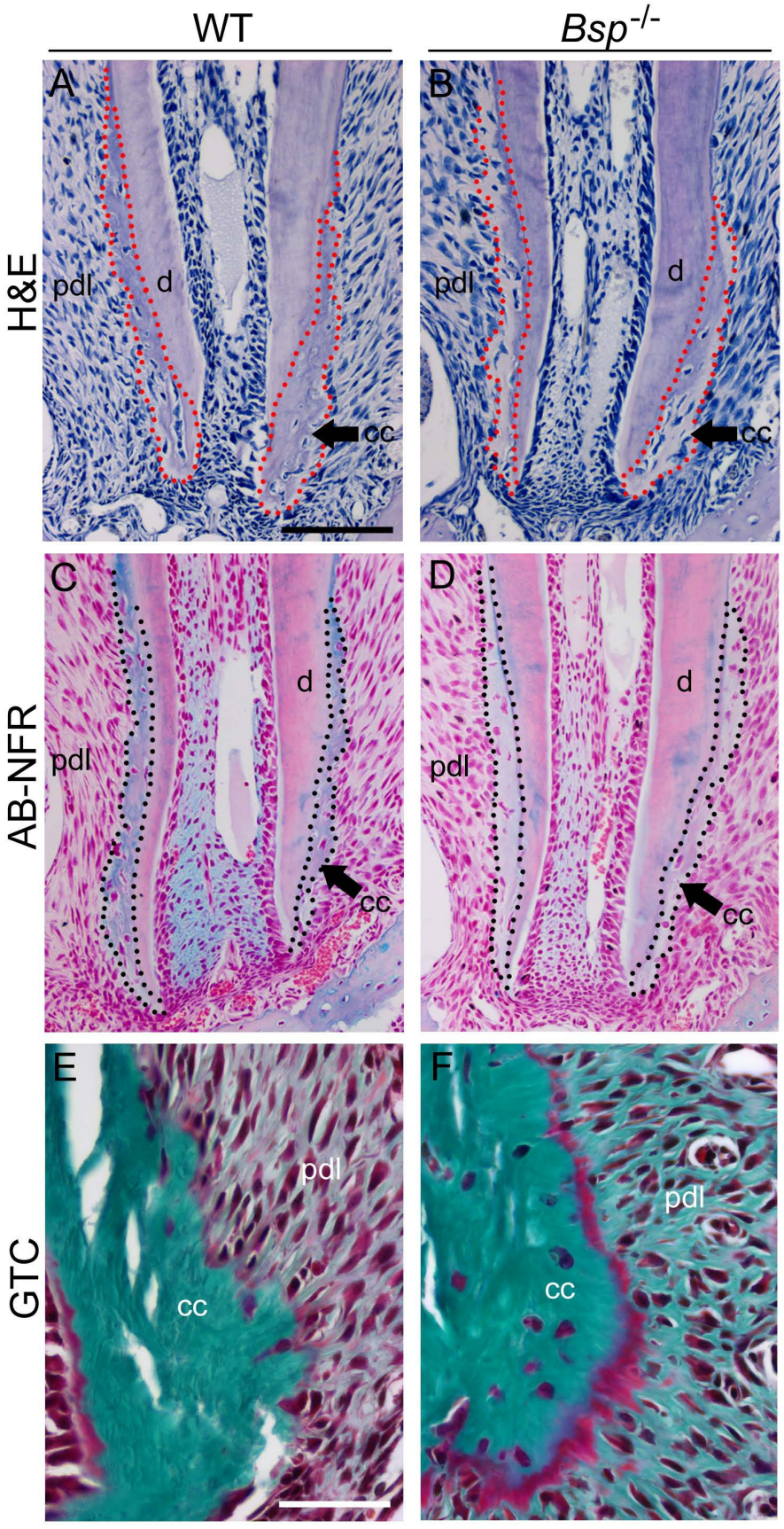
WT
Bsp-/-
H&E
AB-NFR
GTC
A
B
C
D
E
F
pdl
d
cc

Figure 2.4. Delayed mineralization in *Bsp*$^{-/-}$ mouse cellular cementum.

Mineralization of the apical cellular cementum (cc) appeared delayed in *Bsp*$^{-/-}$ compared to WT at 26 dpn as evaluated by **(A, B)** H&E stain and **(C, D)** Alcian blue stain with nuclear fast red (AB-NFR) stain (see Figure 2.2 caption for description of methods). **(E,F)** Goldner's trichrome (GTC) staining of undecalcified sections at 30 dpn confirmed increased cementoid (red layer) at the cellular cementum surface in *Bsp*$^{-/-}$ compared to WT molars. Tears that appear in the tissue are artifacts from undecalcified sectioning. Abbreviations: d=dentin; pdl=periodontal ligament. Scale bar is 100 μm for panels E-F (original 200X) and 50 μm for panels E-F (original 400X). n=6

2.3.2 Failure of acellular cementum mineralization in *Bsp*$^{-/-}$ mice

SEM analysis supported histochemical observations that the thin layer of acellular cementum on *Bsp*$^{-/-}$ molar roots was not mineralized, as no mineralized cementum ultrastructure could be identified on the cervical root surfaces of *Bsp*$^{-/-}$ molars at 60 dpn, in contrast to the mineralized cementum layer on age-matched WT molars (Figure 2.5).

We considered developmental possibilities predisposing to inhibition of cementum formation in *Bsp*$^{-/-}$ mice. Dentin, required as a foundation for cementum deposition, appeared sound and well-mineralized in *Bsp*$^{-/-}$ mice by histology (Figure 2.1) and von Kossa staining (Figure 2.6A-B). Acellular cementum formation requires migration of dental follicle/cementoblast precursors to the nascent root surface. Root lining cells were present in similar numbers in *Bsp*$^{-/-}$ versus WT first molar roots at 14 dpn (Figure 2.6C). PDL fringe fibers at the root surface suggested that the proper acellular cementum matrix was present for cementogenesis (Figure 2.6D-E). Immunostaining revealed deposition of osteopontin (OPN) on the root surface, confirming functional cementoblasts in *Bsp*$^{-/-}$ mice (Figure 2.6F-I). Markers of local and systemic mineral metabolism were assayed. TNAP immunolabeling in *Bsp*$^{-/-}$ versus WT molars (Figure 2.6J-M), and serum alkaline phosphatase, calcium, and phosphorus, were undiminished in *Bsp*$^{-/-}$ mice (Table 2.1), ruling out systemic mineral ion disturbance as an underlying cause of the cementum defect.

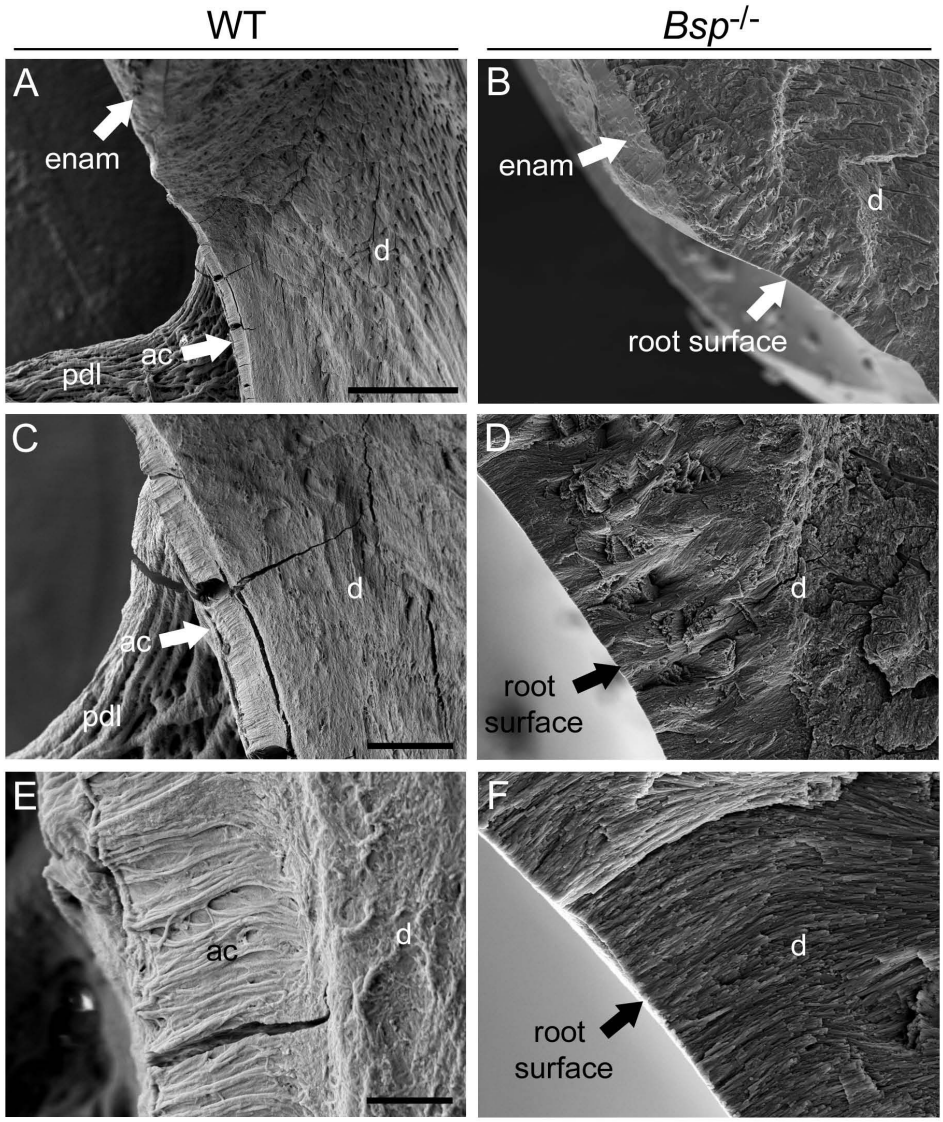

Figure 2.5. Lack of mineralized acellular cementum ultrastructure on *Bsp*$^{-/-}$ mouse molar teeth.

Secondary electron SEM analysis on fractured first molars at 60 dpn indicates that, compared to the mineralized acellular cementum layer visible in WT molars at various magnifications **(A, C, E)**, no mineralized cementum ultrastructure can be identified on the roots of *Bsp*$^{-/-}$ molars **(B, D, F)**. Some cracking is evident as an artifact of sample preparation. Abbreviations: enam=enamel; ac=acellular cementum; pdl=periodontal ligament. Scale bar is 50 μm in panels A and B (original 500X), 10 μm in panels C and D (original 2,000X), and 2 μm in panels C and D (original 10,000X). n=3

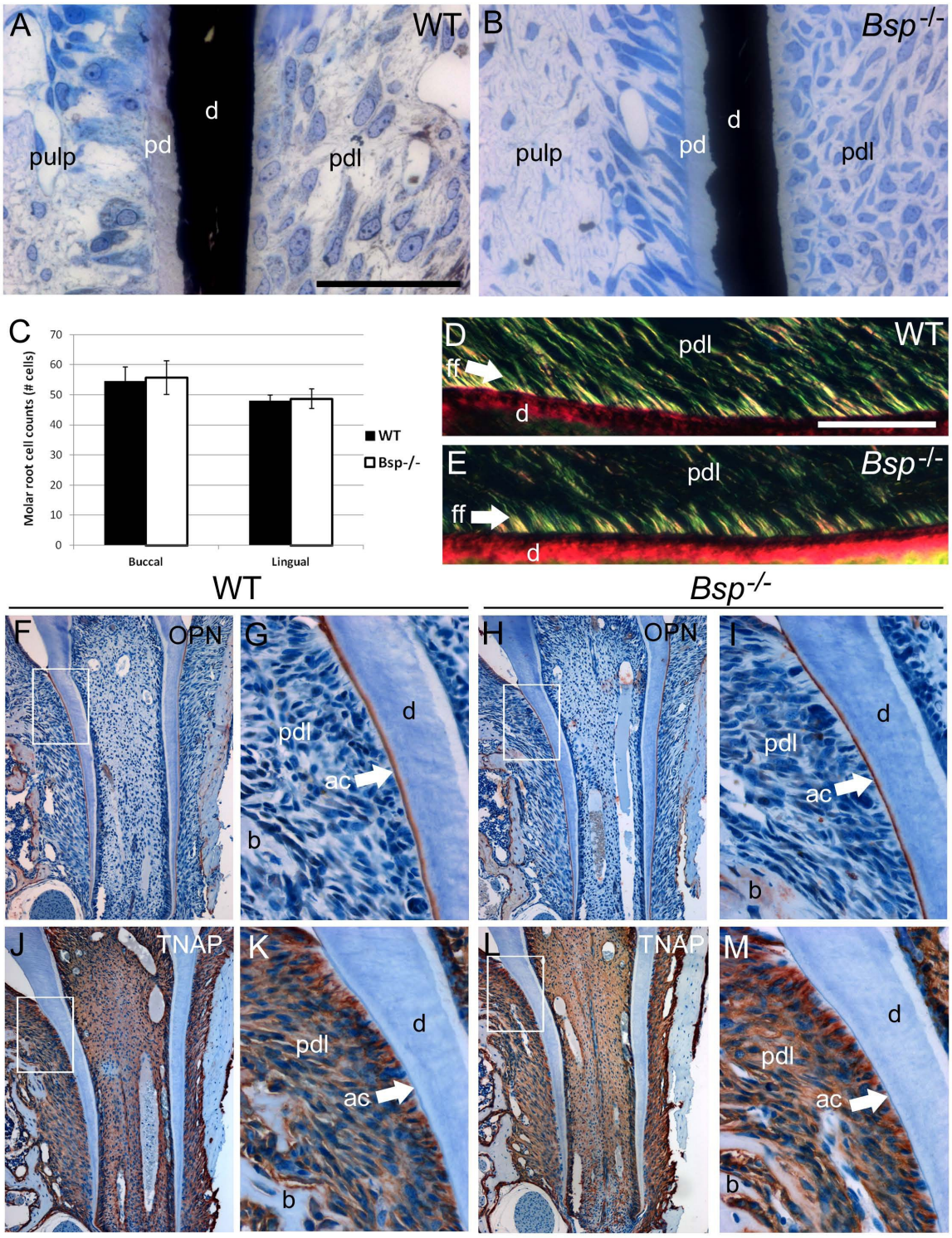
A
WT
d
pulp
pd
pdl
B
Bsp-/-
d
pulp
pd
pdl
C
Molar root cell counts (# cells)
70
60
50
40
30
20
10
0
Buccal
Lingual
WT
Bsp-/-
D
pdl
WT
ff
d
E
pdl
Bsp-/-
ff
d
WT
Bsp-/-
F
OPN
G
d
pdl
ac
b
H
OPN
I
d
pdl
ac
b
J
TNAP
K
d
pdl
ac
b
L
TNAP
M
d
pdl
ac
b

Figure 2.6. Exploration of potential causative factors for lack of acellular cementum formation in *Bsp*$^{-/-}$ mice.

Comparison of dentin mineralization, cementoblast number, collagen fringe fiber distribution, and tissue nonspecific alkaline phosphatase (TNAP) activity were performed. Von Kossa staining on undecalcified **(A)** WT and **(B)** *Bsp*$^{-/-}$ molars at 14 dpn indicated *Bsp*$^{-/-}$ dentin mineralization (black-stained regions) was comparable to WT. **(C)** Cell counts for putative cementoblast root-lining cells performed at 14 dpn revealed no difference in cell numbers of *Bsp*$^{-/-}$ vs. WT first molar teeth. Picrosirius red staining under polarized light indicated that fringe fibers (ff) of the PDL (high intensity yellowish fibers; indicated by white arrows) were similar in density and distribution in **(D)** WT vs. **(E)** *Bsp*$^{-/-}$ mouse molars. OPN localized to the acellular cementum (ac) of **(F, G)** WT and **(H, I)** *Bsp*$^{-/-}$ molars at 14 dpn. TNAP was not altered in the periodontia of **(J, K)** WT vs. **(L, M)** *Bsp*$^{-/-}$ mouse molars at 14 dpn. Abbreviations: pd=predentin; d=dentin; pdl=periodontal ligament; ac=acellular cementum. Scale bar is 200 μm in panels F, H, J, and L (original 100X), and 50 μm in panels A, B, G, I, K, and M (original 400X).

Table 2.1. Serum biochemistry for *Bsp*$^{-/-}$ and WT mice.

Below are serum calcium, inorganic phosphorus, and alkaline phosphatase activity in male mice at 3, 4, and 8 weeks postnatal.

Age	Genotype	Sample size	Calcium, mmol/L	Phosphorus, mmol/L	Alkaline phosphatase, U/L
3 wks	WT	4	2.62 ± 0.09	3.50 ±0.41	257.25 ± 45.09
	Bsp$^{-/-}$	5	2.64 ± 0.12	3.53 ± 0.19	358.20 ± 65.95
4 wks	WT	3	2.79 ± 0.60	4.50 ± 1.05	290.00 ± 61.02
	Bsp$^{-/-}$	3	2.57 ± 0.33	4.37 ± 0.96	294.67 ± 93.94
8 wks	WT	6	2.38 ± 0.04	2.52 ± 0.19	119.00 ± 7.21
	Bsp$^{-/-}$	6	2.37 ± 0.06	2.49 ± 0.27	163.67 ± 12.68 *

* indicates $p < 0.01$ by independent samples (Student's) t-test

2.3.3 Periodontal breakdown in *Bsp*$^{-/-}$ mice

Defective acellular cementum in *Bsp*$^{-/-}$ mice preceded a progressive breakdown of periodontal organization at later ages. WT molars at 26 dpn displayed dense and highly organized collagen fiber insertions in the cervical root, visualized by picrosirius red staining under polarized light (Figure 2.7A-B). Conversely, *Bsp*$^{-/-}$ molars lost PDL organization in the cervical root by this age (Figure 2.7C-D), a condition that degenerated further over time (Figure 2.8). Defective cementum-PDL attachment in *Bsp*$^{-/-}$ molars allowed for significant down-growth of gingival epithelial tissues into the periodontal region, initiating a long junctional epithelium (Figure 2.7E-F; Figure 2.9). Periodontal disarray in *Bsp*$^{-/-}$ mice was accompanied by increased incidence of root resorption by 60 dpn (Figure 2.7G-J), and appearance of osteoclast-like cells, RANKL immunostaining, and bone resorption in alveolar bone (Figure 2.7K-N). There was no indication that inflammation played a significant role in the periodontal breakdown, based on histology and lack of neutrophil infiltration into the periodontia (Figure 2.10).

Tooth and bone resorption were documented further by SEM and microCT. SEM revealed extensive pitting in *Bsp*$^{-/-}$ versus WT molars, concentrated in the cervical roots (Figure 2.11A-F). Lack of acellular cementum was indicated by clearly visible dentinal tubules on the external surface of *Bsp*$^{-/-}$ molar roots. MicroCT analysis revealed extensive reduction in alveolar bone height in *Bsp*$^{-/-}$ vs. WT mandibles, particularly along the lingual aspect (Figure 2.11G-J).

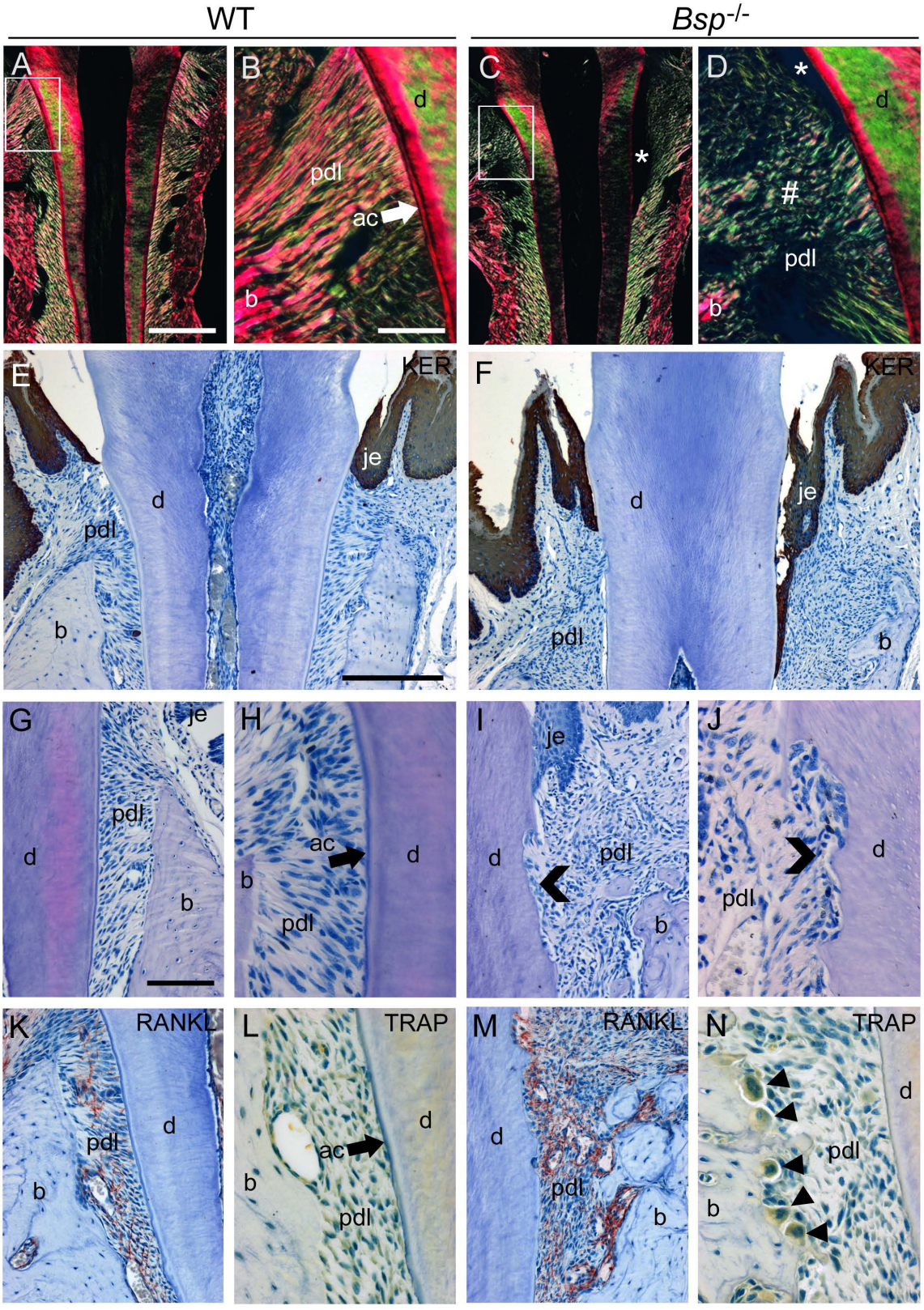
WT
Bsp-/-
A
B
C
D
d
pdl
ac
b
*
#
E
F
KER
je
G
H
I
J
K
L
M
N
RANKL
TRAP

Figure 2.7. Periodontal breakdown in *Bsp*$^{-/-}$ mice.

(A, B) Picrosirius red stained sections viewed under polarized light reveal a high degree of organization and directionality (indicated by high intensity yellowish fibers) of periodontal ligament (pdl) collagen fibrils between acellular cementum (ac) and bone (b) in WT molars at 26 dpn. The dark space represents either empty space or disorganized collagen fiber. **(C, D)** *Bsp*$^{-/-}$ molars at 26 dpn feature loss of organization of collagen fibers in cervical PDL region (#) where detachment (*) is also present. **(E)** Pan-keratin immunohistochemistry (red-brown color) indicates a well maintained junctional epithelium (je) in WT molars at 60 dpn, whereas **(F)** *Bsp*$^{-/-}$ molars feature down-growth and establishment of a long junctional epithelium in association with loss of PDL attachment. Compared to **(G, H)** WT molars at 60 dpn, **(I, J)** *Bsp*$^{-/-}$ molar teeth feature extensive root resorption (chevrons). Compared to **(K, L)** WT molars, *Bsp*$^{-/-}$ molars at 60 dpn showed **(M)** localization of receptor activator of nuclear factor kappa-B ligand (RANKL) near tooth and bone surfaces, and **(N)** numerous osteoclast-like cells (arrow heads; large, multinucleated, tartrate resistant acid phosphatase (TRAP) positive) on alveolar bone surfaces. Scale bar is 200 μm in panels A and C (original 100X), 50 μm in panels B, D, H, J, L, and N (original 400X), 100 μm in panels G, I, K, and M (original 200X), and 100 μm in panels E and F (original 100X). n=3

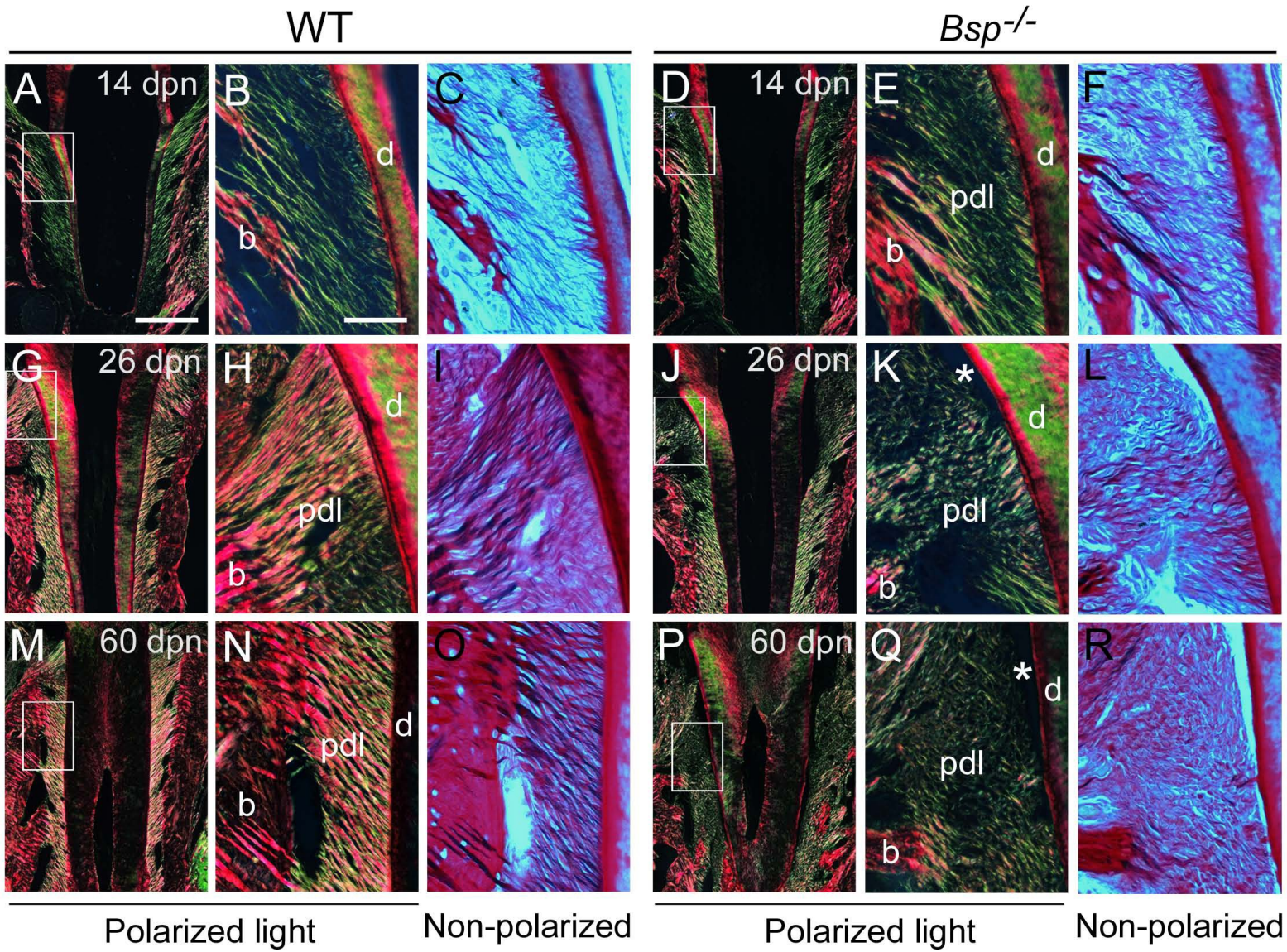
WT
Bsp-/-
A
14 dpn
B
d
b
C
D
14 dpn
E
d
pdl
b
F
G
26 dpn
H
d
pdl
b
I
J
26 dpn
K
*
d
pdl
b
L
M
60 dpn
N
pdl
d
b
O
P
60 dpn
Q
*
d
pdl
b
R
Polarized light
Non-polarized
Polarized light
Non-polarized

Figure 2.8. Progressive loss of PDL organization in *Bsp*$^{-/-}$ mice.

Picrosirius red staining viewed under polarized light was used to reveal organization and directionality (indicated by high intensity yellowish fibers) of periodontal ligament (pdl) collagen fibrils over the course of root development. The same sections photographed under non-polarized light are shown to illustrate presence of collagen (pink-red) regardless of organization. At 14 dpn, a similar level of PDL organization is present in the nascent roots of **(A-C)** WT and **(D-F)** *Bsp*$^{-/-}$ mouse molars. At 26 dpn, cervical PDL of **(G-I)** WT molars is highly organized, with directional collagen fibers radiating from the root surface. The cervical-most PDL of **(J-L)** *Bsp*$^{-/-}$ molars at this age is disorganized and features periodontal detachment (*). At the advanced age of 60 dpn, **(M-O)** WT molar PDL is very highly organized, while **(P-R)** *Bsp*$^{-/-}$ PDL has become increasingly disorganized over the cervical portion. Scale bar is 200 μm in panels A, D, G, J, M, and P (original 100X), and 50 μm in panels B, C, E, F, H, I, K, L, N, O, Q, and R (original 400X). n=6

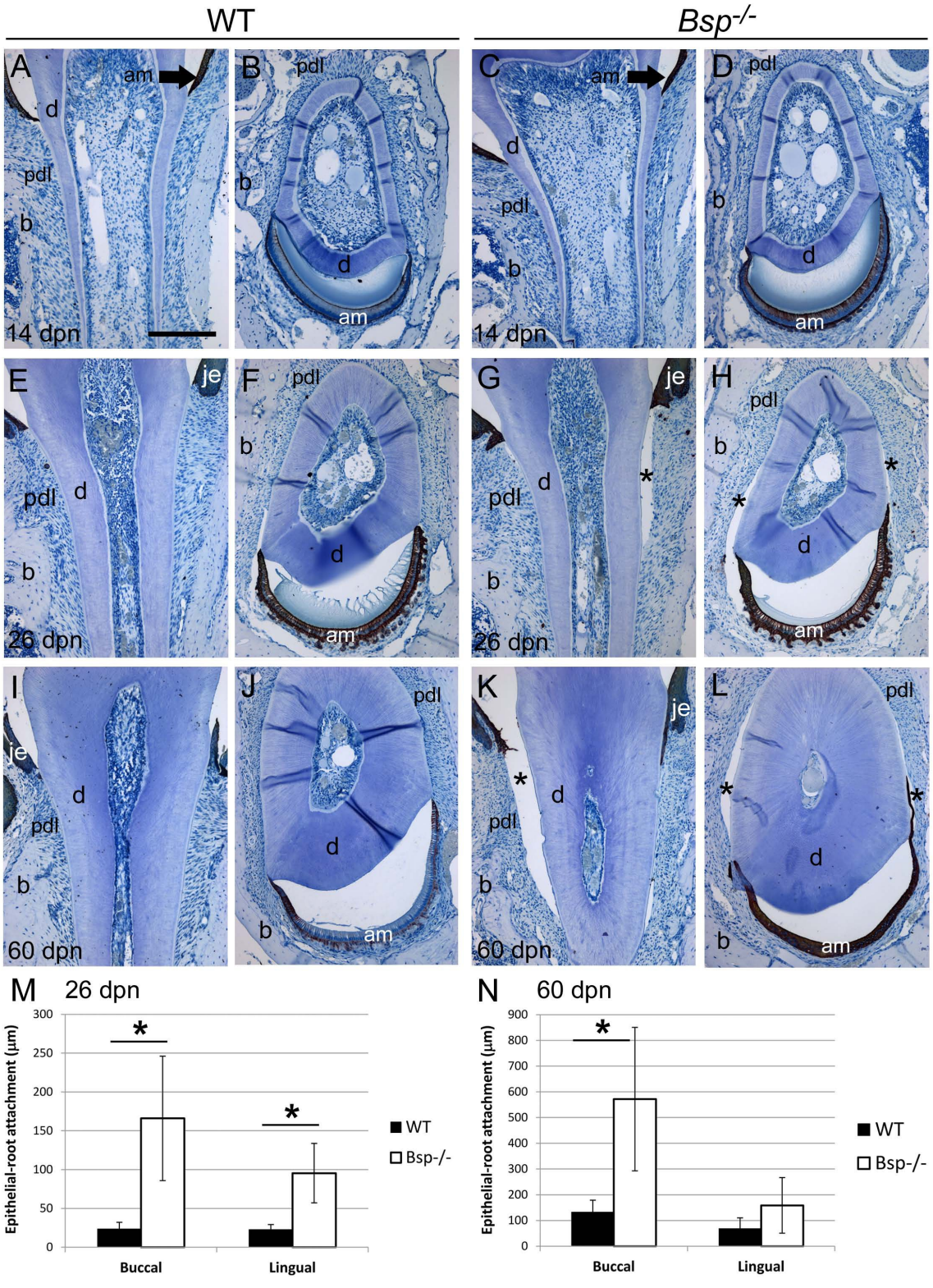
WT
Bsp-/-
A
am
d
pdl
b
14 dpn
B
pdl
b
d
am
C
am
d
pdl
b
14 dpn
D
pdl
b
d
am
E
je
pdl
d
b
26 dpn
F
pdl
b
d
am
G
je
d
*
pdl
b
26 dpn
H
pdl
b
*
*
d
am
I
je
d
pdl
b
60 dpn
J
pdl
d
b
am
K
je
*
d
pdl
b
60 dpn
L
pdl
*
*
d
b
am
M
26 dpn
Epithelial-root attachment (µm)
300
250
200
150
100
50
0
*
*
Buccal
Lingual
WT
Bsp-/-
N
60 dpn
Epithelial-root attachment (µm)
900
800
700
600
500
400
300
200
100
0
*
Buccal
Lingual
WT
Bsp-/-

Figure 2.9. Progressive epithelial in-growth in *Bsp*$^{-/-}$ mouse molars and incisors.

Pan-keratin immunohistochemistry was employed to visualize the dental epithelium (reddish-brown color) over the course of root development. In the **(A)** unerupted molar and **(B)** incisor of WT mice at 14 dpn, ameloblasts (am) of the enamel organ are positively labeled by pan-keratin antibodies. **(C, D)** Junctions of epithelium and the nascent root of *Bsp*$^{-/-}$ teeth are well maintained at this early time point. Junctional epithelium (je) is established in erupted **(E)** WT molars by 26 dpn, and **(F)** incisors feature a well maintained labial-lingual epithelial junction. **(G)** *Bsp*$^{-/-}$ molars display abnormal thickening of the junctional epithelium at 26 dpn, in association with detachment (*) of periodontal ligament (pdl). **(H)** *Bsp*$^{-/-}$ incisors at this age display epithelial in-growth to the periodontal region of the lingual root analogue, in association with periodontal detachment (*). While WT **(I)** molars and **(J)** incisors display well maintained epithelial junctions at 60 dpn, *Bsp*$^{-/-}$ **(K)** molars feature dramatic epithelial down-growth into regions of periodontal detachment (*), and **(L)** incisors also display extensive detachment (*) and epithelial invasion into the periodontal compartment. Measurement of epithelial attachment at **(M)** 26 and **(N)** 60 dpn indicated a significant and progressive increase in epithelial down growth in *Bsp*$^{-/-}$ versus WT molars ($p<0.05$ by ANOVA and post-hoc Tukey test). Abbreviations: d=dentin; b=bone. Scale bar is 200 μm for all panels A-L (original 100X). n=6

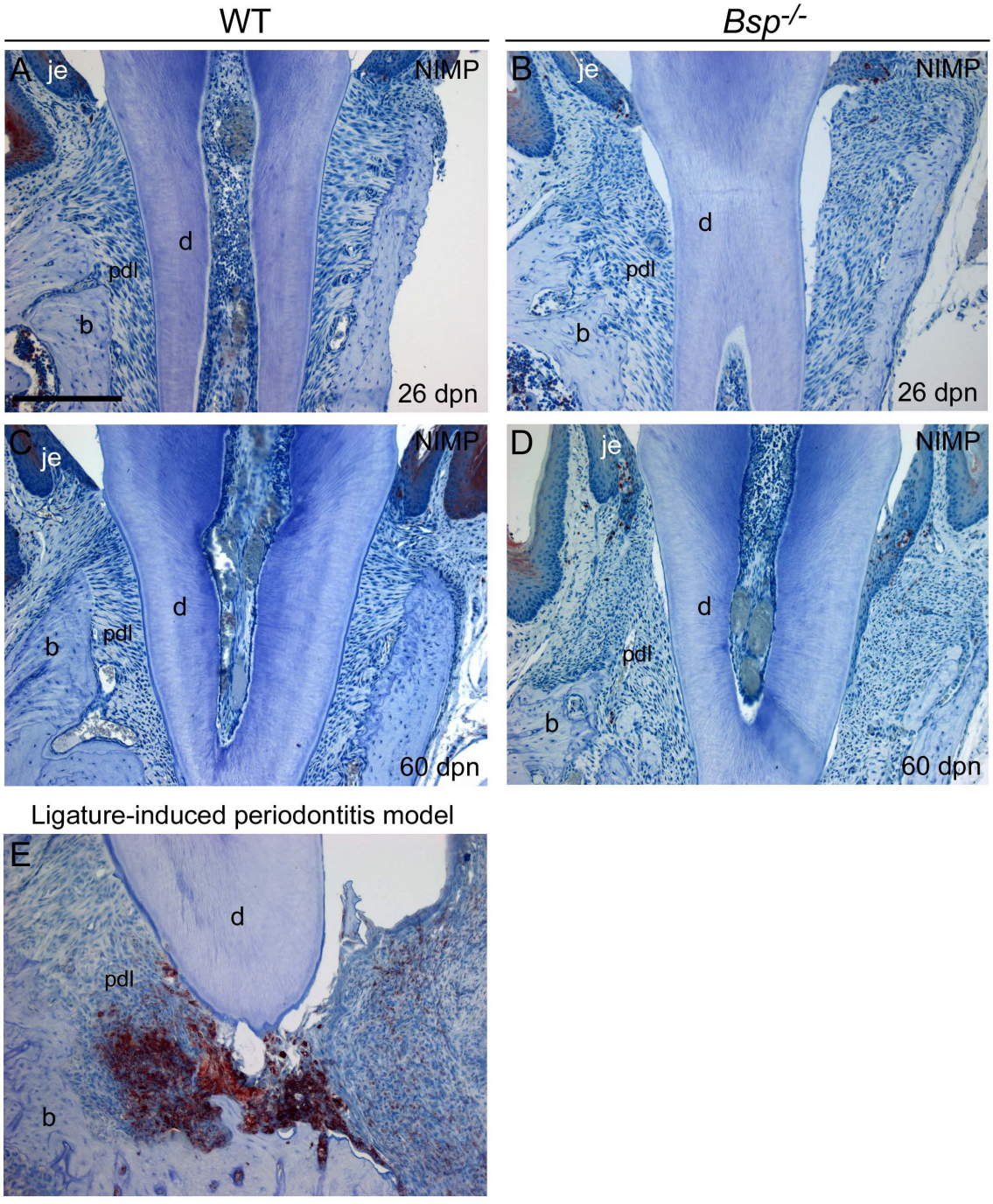
WT
Bsp-/-
A
je
NIMP
d
pdl
b
26 dpn
B
je
NIMP
d
pdl
b
26 dpn
C
je
NIMP
d
b
pdl
60 dpn
D
je
NIMP
d
pdl
b
60 dpn
Ligature-induced periodontitis model
E
d
pdl
b

Figure 2.10. Lack of inflammation during periodontal breakdown in *Bsp*$^{-/-}$ mice.

Immunohistochemistry was used to localize neutrophils (reddish color) in periodontal tissues. Despite severe bone and tooth resorption (See Figures 2.7 and 2.11), *Bsp*$^{-/-}$ mice did not feature greater presence of neutrophils in the periodontal compartment, compared to WT at ages 26 dpn (**B** vs. **A**) and 60 dpn (**D** vs. **C**). **(E)** Neutrophil staining around a first molar root in a ligature-induced murine model for peridontitis is included as a positive control for increased neutrophil infiltration associated with bone destruction. One month old mouse first mandibular molars were tied with a cotton ligature until tissue harvest 15 days later. Abbreviations: je=junctional epithelium; d=dentin; b=bone. Scale bar is 200 μm for all panels A-E (original 100X).

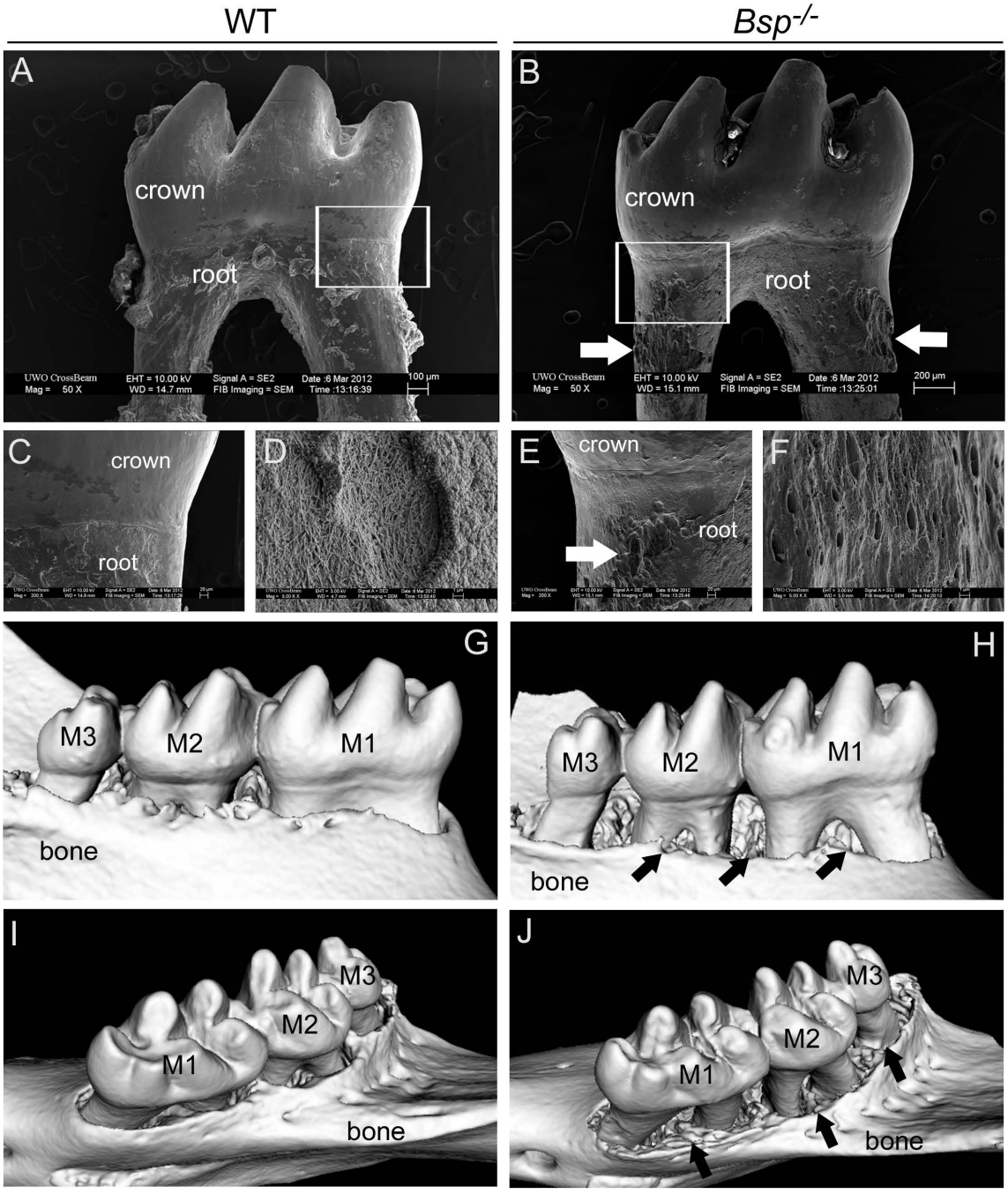
WT
Bsp-/-
A
crown
root
UWO CrossBeam
Mag = 50 X
EHT = 10.00 kV
WD = 14.7 mm
Signal A = SE2
FIB Imaging = SEM
Date :6 Mar 2012
Time :13:16:39
100 µm
B
crown
root
UWO CrossBeam
Mag = 50 X
EHT = 10.00 kV
WD = 15.1 mm
Signal A = SE2
FIB Imaging = SEM
Date :6 Mar 2012
Time :13:25:01
200 µm
C
crown
root
D
E
crown
root
F
G
M3
M2
M1
bone
H
M3
M2
M1
bone
I
M3
M2
M1
bone
J
M3
M2
M1
bone

Figure 2.11. Increased tooth root and alveolar bone resorption in *Bsp*$^{-/-}$ mice.

Compared to the smooth surface of **(A, C)** 10-week old WT molars viewed by backscattered SEM, **(B, E)** *Bsp*$^{-/-}$ teeth exhibit abundant pitting (white arrows in B and E) of the root surface consistent with external root resorption, concentrated on the cervical portion of the root surface. White boxes in A and B indicate regions shown at higher magnification in C and E, respectively. Compared to the **(D)** WT molar root surface at high magnification, **(F)** *Bsp*$^{-/-}$ molar roots display exposed dentinal tubules, indicating absence of cementum in regions of root resorption. MicroCT revealed that compared to **(G, I)** WT mandibles, **(H, J)** *Bsp*$^{-/-}$ mandibles display extensive reduction in alveolar bone height, especially on the lingual aspect (black arrows in H and J). Abbreviations: M1=first molar; M2=second molar; M3=third molar. Scale bar is 100 μm in panels A and B (original 50X), 20 μm in panels C and E (original 2,00X), and 1 μm in panels D and F (original 5,000X). n=3

2.4 DISCUSSION

BSP is an extracellular matrix protein present in bone and cementum. Here we demonstrate for the first time that lack of BSP inhibited formation and mineralization of acellular cementum. Further, reduction and loss-of-function of the acellular cementum in *Bsp*$^{-/-}$ mice led to structural defects in the cementum-PDL interface, PDL disorganization, down-growth of epithelium, and increased tooth and bone resorption. Results collected here demonstrated that BSP plays a non-redundant role in acellular cementum formation, likely involved in initiating mineralization and/or promoting appositional cementum growth. Because of its importance to cementum formation, BSP is essential for formation of a functional periodontium.

2.4.1 Acellular cementum as a mineralization-sensitive tissue

Lack of BSP led to a severe developmental inhibition of acellular cementum formation, shown here by histology, histochemistry, immunohistochemistry, and SEM. As a late stage in odontogenesis, cementum formation depends on a number of prior developmental stages. Our results suggested that the defect did not result from defective dentin, lack of migration/position of precursor cells, or root surface collagen fringe fibers [considered the extracellular matrix proper for acellular cementum (Bosshardt and Schroeder, 1996)]. Local TNAP deficiency (by IHC), hypophosphatemia, and hypocalcemia were ruled out as causes of cementum inhibition in *Bsp*$^{-/-}$ mice. It is notable that acellular cementum formation is similarly inhibited in the *Alpl*$^{-/-}$ mouse model featuring loss of TNAP function (Beertsen et al., 1999; Foster et al., 2012; McKee et al., 2011). *Alpl*$^{-/-}$ mice harbor increased levels of the mineral inhibitor pyrophosphate (PP_i) and serve as a model of hypophosphatasia (HPP), where lack of acellular cementum predisposes to tooth loss (van den Bos et al., 2005). We have demonstrated that reduction of PP_i, in turn, promotes increased acellular cementum formation (Foster et al., 2011; Foster et al., 2012), and hypothesized that acellular cementum represents a tissue strongly regulated at the physicochemical level of mineralization, i.e. hydroxyapatite nucleation and growth. Cellular cementum size was undiminished by loss of BSP,

though mineralization was delayed at earlier ages; functional consequences of this are under study. Cellular cementum was unaffected in *Alpl*$^{-/-}$ mice (Beertsen et al., 1999) and in mice where acellular cementum increased via decreased PP_i (Foster et al., 2012), supporting the view that these tissues are subject to different developmental influences.

Acellular cementum forms as a progressive mineralization of the PDL collagen fiber bundles inserting into the root surface. We have previously shown BSP binds collagen with high affinity (Tye et al., 2005), mediates hydroxyapatite formation (Harris et al., 2000; Hunter and Goldberg, 1993), and that hydroxyapatite nucleation potency is increased 10-fold when BSP is incubated with collagen (Baht et al., 2010). Considering BSP is localized across the width of the acellular cementum (Bosshardt et al., 1998; McKee et al., 1996), and based on our past and present findings, it is likely that BSP is critical for proper cementum formation and function.

Another SIBLING protein, OPN, was present at *Bsp*$^{-/-}$ root surfaces, as in WT controls. OPN functions as an inhibitor of hydroxyapatite crystal growth *in vitro* and *in vivo* (Boskey et al., 2002; Hunter et al., 1994). Presence of OPN in the absence of BSP may additionally tip the balance toward inhibition of cementum mineralization. It is also possible that another function of BSP (e.g. cell adhesion, signaling, etc.) may contribute to the cementum phenotype of the *Bsp*$^{-/-}$ mouse, and this is currently under study.

2.4.2 Absence of BSP leads to periodontal breakdown

A functional periodontal complex depends on stable insertion of PDL collagen fibers into the acellular cementum, as well as ability for remodeling on the bone surface of the PDL space. We propose that lack of acellular cementum in *Bsp*$^{-/-}$ mice led to a progressive degradation of periodontal integrity over time. Lack of PDL-tooth anchorage was followed by PDL disorganization, epithelial down-growth, and tooth and alveolar bone resorption. These are hallmarks of periodontal breakdown associated with periodontal disease, however this phenotype developed without an apparent inflammatory response in the periodontal compartment, suggesting failure of function/adaptation of the

periodontium. Similar examples of periodontal degradation have resulted in transgenic mouse models with compromised periodontal function, e.g. *Dmp1* null (Ye et al., 2008) and *periostin* null (Rios et al., 2008) mice. Substitution of a soft diet for pelletized chow is currently being studied to determine the contribution of occlusal stress to incidence of periodontal breakdown and incisor malocclusion.

An unexpected finding was the increased incidence of tooth and alveolar bone resorption in *Bsp*$^{-/-}$ mice. Previous studies employing *Bsp*$^{-/-}$ mice showed that BSP deficiency impairs osteoclastogenesis and bone resorption *in vivo* and *in vitro* (Boudiffa et al., 2010; Malaval et al., 2008). Conversely, BSP over-expression increased osteoclastic activity (Valverde et al., 2008). We propose that increased resorption in the periodontal compartment of *Bsp*$^{-/-}$ mice is the result of local loss of integrity and function in a tissue that functions under high mechanical stress and depends on rapid remodeling for proper maintenance. While increased presence of RANKL and TRAP-positive osteoclast-like cells was noted in periodontia *of Bsp*$^{-/-}$ mice, the cause for increased tooth and bone resorption is being explored further in this model.

In summary, results from these studies show for the first time that BSP is critical for acellular cementum formation and periodontal attachment. The role of BSP in acellular cementogenesis is likely to be in promoting mineralization at the root surface, to anchor PDL fibers and provide strong attachment of the tooth to the alveolar bone. Loss-of-function of BSP may predispose to periodontal disease through defective cementum-PDL attachment. Ongoing studies will further elucidate potential roles of BSP in cementum formation and regeneration, and in wider periodontal biology.

2.5 REFERENCES

Baht GS, O'Young J, Borovina A, Chen H, Tye CE, Karttunen M *et al.* (2010). Phosphorylation of Ser136 is critical for potent bone sialoprotein-mediated nucleation of hydroxyapatite crystals. *Biochem J* 428(3)*:*385-395.

Beertsen W, VandenBos T, Everts V (1999). Root development in mice lacking functional tissue non-specific alkaline phosphatase gene: inhibition of acellular cementum formation. *J Dent Res* 78(6)*:*1221-1229.

Boskey AL, Spevak L, Paschalis E, Doty SB, McKee MD (2002). Osteopontin deficiency increases mineral content and mineral crystallinity in mouse bone. *Calcif Tissue Int* 71(2)*:*145-154.

Bosshardt D, Schroeder H (1996). Cementogenesis reviewed: a comparison between human premolars and rodent molars. *Anat Rec* 245(2)*:*267-292.

Bosshardt D, Zalzal S, McKee M, Nanci A (1998). Developmental appearance and distribution of bone sialoprotein and osteopontin in human and rat cementum. *Anat Rec* 250(1)*:*13-33.

Bosshardt D (2005). Are cementoblasts a subpopulation of osteoblasts or a unique phenotype? *J Dent Res* 84(5)*:*390-406.

Boudiffa M, Wade-Gueye NM, Guignandon A, Vanden-Bossche A, Sabido O, Aubin JE *et al.* (2010). Bone sialoprotein deficiency impairs osteoclastogenesis and mineral resorption in vitro. *J Bone Miner Res* 25(12)*:*2669-2679.

Claes L, Recknagel S, Ignatius A. (2012). Fracture healing under healthy and inflammatory conditions. Nat Rev Rheumatol. 8(3):133-143.

Einhorn TA, Gerstenfeld LC. (2015). Fracture healing: mechanisms and interventions. Nat Rev Rheumatol. 11(1):45-54.

Everts V, Niehof A, Tigchelaar-Gutter W, Beertsen W (2012). Transmission electron microscopy of bone. *Methods Mol Biol* 816(351-363.

Fisher L, Fedarko N (2003). Six genes expressed in bones and teeth encode the current members of the SIBLING family of proteins. *Connect Tissue Res* 44 Suppl 1(33-40.

Foster BL, Popowics TE, Fong HK, Somerman MJ (2007). Advances in defining regulators of cementum development and periodontal regeneration. *Curr Top Dev Biol* 78(47-126.

Foster BL, Nagatomo KJ, Bamashmous SO, Tompkins KA, Fong H, Dunn D *et al.* (2011). The progressive ankylosis protein regulates cementum apposition and extracellular matrix composition. *Cells Tissues Organs* 194(5)*:*382-405.

Foster BL (2012). Methods for studying tooth root cementum by light microscopy. *Int J Oral Sci* 4(3)*:*119-128.

Foster BL, Nagatomo KJ, Nociti FH, Fong H, Dunn D, Tran AB *et al.* (2012). Central role of pyrophosphate in acellular cementum formation. *PLoS One* 7(6)*:*e38393.

Ganss B, Kim R, Sodek J (1999). Bone sialoprotein. *Crit Rev Oral Biol Med* 10(1)*:*79-98.

Harris NL, Rattray KR, Tye CE, Underhill TM, Somerman MJ, D'Errico JA *et al.* (2000). Functional analysis of bone sialoprotein: identification of the hydroxyapatite-nucleating and cell-binding domains by recombinant peptide expression and site-directed mutagenesis. *Bone* 27(6)*:*795-802.

Hunter GK, Goldberg HA (1993). Nucleation of hydroxyapatite by bone sialoprotein. *Proc Natl Acad Sci U S A* 90(18)*:*8562-8565.

Hunter GK, Kyle CL, Goldberg HA (1994). Modulation of crystal formation by bone phosphoproteins: structural specificity of the osteopontin-mediated inhibition of hydroxyapatite formation. *Biochem J* 300 (Pt 3)(723-728.

Kacena MA, Troiano NW, Wilson KM, Coady CE, Horowitz MC (2004). Evaluation of two different methylmethacrylate processing, infiltration, and embedding techniques on the histological, histochemical, and immunohistochemical analysis of murine bone samples. *J Histotechnol* 27(2)*:*119-130.

Macneil R, Sheng N, Strayhorn C, Fisher L, Somerman M (1994). Bone sialoprotein is localized to the root surface during cementogenesis. *J Bone Miner Res* 9(10)*:*1597-1606.

MacNeil R, Berry J, D'Errico J, Strayhorn C, Piotrowski B, Somerman M (1995). Role of two mineral-associated adhesion molecules, osteopontin and bone sialoprotein, during cementogenesis. *Connect Tissue Res* 33(1-3)*:*1-7.

Malaval L, Wade-Guéye NM, Boudiffa M, Fei J, Zirngibl R, Chen F *et al.* (2008). Bone sialoprotein plays a functional role in bone formation and osteoclastogenesis. *J Exp Med* 205(5)*:*1145-1153.

Marsell R, Einhorn TA. (2011). The biology of fracture healing. Injury. 42(6):551-555.

McKee M, Zalzal S, Nanci A (1996). Extracellular matrix in tooth cementum and mantle dentin: localization of osteopontin and other noncollagenous proteins, plasma proteins, and glycoconjugates by electron microscopy. *Anat Rec* 245(2)*:*293-312.

McKee MD, Nakano Y, Masica DL, Gray JJ, Lemire I, Heft R *et al.* (2011). Enzyme Replacement Therapy Prevents Dental Defects in a Model of Hypophosphatasia. *J Dent Res*.

Rios H, Ma D, Xie Y, Giannobile W, Bonewald L, Conway S *et al.* (2008). Periostin is essential for the integrity and function of the periodontal ligament during occlusal loading in mice. *J Periodontol* 79(8)*:*1480-1490.

Somerman M, Shroff B, Agraves W, Morrison G, Craig A, Denhardt D *et al.* (1990). Expression of attachment proteins during cementogenesis. *J Biol Buccale* 18(3)*:*207-214.

Tye CE, Hunter GK, Goldberg HA (2005). Identification of the type I collagen-binding domain of bone sialoprotein and characterization of the mechanism of interaction. *J Biol Chem* 280(14)*:*13487-13492.

Valverde P, Zhang J, Fix A, Zhu J, Ma W, Tu Q *et al.* (2008). Overexpression of bone sialoprotein leads to an uncoupling of bone formation and bone resorption in mice. *J Bone Miner Res* 23(11)*:*1775-1788.

van den Bos T, Handoko G, Niehof A, Ryan L, Coburn S, Whyte M *et al.* (2005). Cementum and dentin in hypophosphatasia. *J Dent Res* 84(11)*:*1021-1025.

White DR (1978). Tissue substitutes in experimental radiation physics. *Med Phys* 5(6)*:*467-479.

Ye L, Zhang S, Ke H, Bonewald LF, Feng JQ (2008). Periodontal breakdown in the Dmp1 null mouse model of hypophosphatemic rickets. *J Dent Res* 87(7)*:*624-629.

CHAPTER 3

3 Mechanical Forces Exacerbate Periodontal Defects in *Bsp*-null Mice

3.1 INTRODUCTION

Bone sialoprotein (BSP) is a multifunctional phosphoprotein belonging to the Small Integrin Binding Ligand N-Linked Glycoprotein (SIBLING) family (Fisher and Fedarko, 2003). BSP localizes primarily to mineralized tissues, including bone, calcified cartilage, dentin and cementum, where its expression is up-regulated at the onset of mineralization (Macneil et al., 1994; McKee et al., 1996). *In vitro* studies have demonstrated that the integrin-binding RGD sequence in BSP promotes cell attachment, signaling, and migration (Ganss et al., 1999; Goldberg and Hunter, 2012). In addition, BSP binds collagen (Baht et al., 2008; Tye et al., 2005) and hydroxyapatite with high affinity (Goldberg et al., 2001) and promotes mineral formation (Hunter and Goldberg, 1993). Analysis of the *Bsp*$^{-/-}$ mouse, during development and repair, revealed decreased growth and mineralization of long-bones (Holm et al., 2015; Malaval et al., 2008; Malaval et al., 2009). Lack of BSP also affected osteoclast formation and recruitment negatively, leading to reduced long-bone turnover (Boudiffa et al., 2010; Malaval et al., 2008).

Previously, we reported that loss of BSP causes inhibition of functional acellular cementum on molar and incisor tooth roots, hypomineralization of cellular cementum, and detachment and disorganization of the periodontal ligament (PDL) (Foster et al., 2013b). In contrast to reduced bone turnover reported in femurs and tibias (Malaval et al., 2008), we reported increased osteoclastic resorption in alveolar bone of *Bsp*$^{-/-}$ mice, associated with increased presence of receptor activator of nuclear factor kappa-B ligand (RANKL) in the periodontium, increased numbers of TRAP-positive osteoclast-like cells, cervical resorption of molars, substantial alveolar bone loss, and increased incidence of incisor malocclusion (Foster et al., 2013b). Collectively, these data support the interpretation that lack of acellular cementum is the primary defect, leading to PDL detachment, epithelial downgrowth, and alveolar bone destruction. We hypothesized that defective periodontal attachment due to lack of acellular cementum played a central role in the periodontal breakdown observed in *Bsp*$^{-/-}$ mice, and forces generated by occlusion contributed to these pathological changes in dentoalveolar tissues. In this study, we aimed to determine whether reducing masticatory forces through use of soft diet would ameliorate periodontal dysfunction and malocclusion in *Bsp*$^{-/-}$ mice. To elucidate the

pathological mechanisms involved, changes in molar and incisor teeth were analyzed by micro-computed tomography (microCT) and histology over time.

3.2 MATERIALS AND METHODS

3.2.1 Animals

Animal care followed guidelines of the Canadian Council on Animal Care and Veterinary Services at the University of Western Ontario. Preparation and genotyping of *Bsp*$^{-/-}$ and wild-type (WT) mice, maintained on a mixed 129/CD1 background, were performed as described previously (Malaval et al., 2008). At 3 weeks of age, *Bsp*$^{-/-}$ and WT littermates, offspring from heterozygous mice mating, were randomly assigned to groups fed a diet (2018 Tekland Global 18% protein, Harlan Laboratories, Indianapolis, IN) either in the form of hard pellets (hard diet; HD) or soft powder (soft diet; SD) and had access to water *ad libitum*. Mice were weighed weekly (3-9 weeks). Experimental endpoints for histological and radiographic analysis were 4, 8, and 20 weeks.

The mice were observed on a weekly basis to determine onset of malocclusion. Any form of incisor misalignment was considered a malocclusion. For classification of a severe malocclusion phenotype, both incisor misalignment and overgrowth need to be present.

3.2.2 Blood chemistry

Animals were anesthetized with isoflurane gas and whole blood collected by cardiac puncture. Blood samples were transferred to BD Vacutainer® SST™ tubes and allowed to coagulate at room temperature for 20 min. After centrifugation at 3,000g for 10 min at 4°C, sera supernatants were collected and stored at -20°C. Serum biochemistry was analyzed at the NIH Veterinary Services Clinical Chemistry (Bethesda, MD).

3.2.3 Histology

Long-bones and mandibles used for microCT were harvested, fixed in 10% neutral-buffered formalin solution overnight and stored in calcium-free Hanks' buffered saline solution. Procedures for histology and analysis of hemi-mandibles were previously described (Foster, 2012).

3.2.4 Micro-computed tomography

MicroCT analysis of hemi-mandibles was performed using eXplore Locus SP at 80 kVp, 80 µA, with 0.508mm Al filter and exposure time of 1600 msec/frame at 4 frames/view to obtain 900 views. These images were reconstructed at 13 µm spatial resolution with calibration and data analysis as described previously (Foster et al., 2013b). Long-bone images were acquired with eXplore Locus Ultra to obtain 1000 views at 120 kVp, 20 µA, and 16 msec/view exposure time. Data were reconstructed at 154 µm spatial resolution. Long-bone lengths were measured between the tips of the medial condyle and greater trochanter (femurs) or medial malleolus (tibias).

For analysis of hemi-mandibles, regions of interest (ROIs) were identified at three anatomical positions along the length incisor: alveolar crest, first molar (mesial root), and third molar. These anatomical positions are relative position of the mandible to the length of the incisor as shown in Figure 3.3A. Coronal sections at these positions were used to measure the mineral density, thickness, and areas of incisor enamel, labial dentin and lingual dentin. For the first molar analysis, ROIs were determined at three positions: crown enamel and dentin, and root dentin. For all mineral density measurements, 3D cubical volumes of interest (VOIs; 10 isotropic voxel size) were defined within the ROIs. Three separate measurements were obtained and averaged for each ROI. The 2D area of interest was defined by manually drawn contours along the boundaries of the incisors.

For mandibular molars, mesial root exposure was determined by comparing the distance between buccal/lingual alveolar ridge crest and cemento-enamel junction to the total root length. All measurements were performed at the midline of mesial root of first and second molars. As an indicator of bone loss, the PDL width in the furcation region of first and second molars was measured.

3.2.5 Measurement of incisor eruption rate

At 8 weeks, WT and *Bsp*$^{-/-}$ mice (3 mice per group) were anesthetized by isoflurane gas. Lingual surfaces of mandibular incisors were etched with phosphoric acid gel etchant (Kerr Corporation, Orange, CA) for 30 sec, then cleaned by wiping with moist gauze. Incisors were dried completely using gauze, then bonding agent (OptiBond Solo Plus; Kerr Corporation) was applied to the etched surface and light cured for 20 sec. Dental composite resin (Premise Flowable; Kerr Corporation) was applied to the incisors and a small (1-2 mm) piece of stainless steel wire was fixed to the incisors near the socket margin. Composite was polymerized by UV light. The affixed stainless steel wires are monitored for 9 days to determine the incisor eruption rate; based on the change in distance from the fixed wire to the socket margin. A cabinet X-ray (Faxitron X-ray Corp., Chicago, IL, USA) was used for radiographic analysis of skulls, and a dissecting stereomicroscope (StereoDiscovery.V8) and digital camera (MRc5, Carl Zeiss Microscopy Gmbh, Jena, Germany) were used to capture images and make measurements.

3.2.6 Statistical analyses

Quantitative data are expressed as mean ± standard error. Statistical analyses between experimental groups were performed using two-way analysis of variance and Bonferroni post-tests with Prism 5 version 5.03 (GraphPad, La Jolla, CA).

3.3 RESULTS

3.3.1 Soft diet normalized body weight, long-bone length, and incisor malocclusion of *Bsp*$^{-/-}$ mice

In order to analyze the role of masticatory forces on the periodontal phenotype of *Bsp*$^{-/-}$ mice, WT and *Bsp*$^{-/-}$ mice were assigned to hard (HD) or soft (SD) diet groups. From 3-9 weeks of age, *Bsp*$^{-/-}$(HD) mice weighed significantly less than WT(HD) (Figure 3.1A), consistent with studies on 8-week-old (Bouleftour et al., 2014) and 4-month-old mice (Malaval et al., 2008). However, WT(SD) and *Bsp*$^{-/-}$(SD) groups were not statistically different in weight. While weight of WT mice fed either diet were not significantly different, weight of *Bsp*$^{-/-}$(SD) was significantly greater than *Bsp*$^{-/-}$(HD) at 3-5 weeks, but not in older mice, suggesting differences become less pronounced with age. These data suggest that soft diet, at least partially, rescues the reduced body weight phenotype of *Bsp*$^{-/-}$ mice. *Bsp*$^{-/-}$ mice did not exhibit any abnormalities in behavior, fertility, breeding, and nursing capabilities.

Bsp$^{-/-}$ mandibular incisors featured chalky white enamel, in contrast to the normal yellow-brown coloration in WT and heterozygous mice (Figure 3.1C). Regardless of diet, *Bsp*$^{-/-}$ mice developed malocclusion, with mandibular incisors rotated in a lingual-to-labial direction compared to WT (Figure 3.1C insets). Over the course of 8 weeks, ~30% of *Bsp*$^{-/-}$(HD) but only ~3% of *Bsp*$^{-/-}$(SD) developed severe malocclusion affecting maxillary and mandibular incisors, causing overgrowth and resulting in dysfunction (Figure 3.1C,D). The onset of these severe malocclusion occurs within the first 5 weeks post weaning (Table 3.1). WT and heterozygous mice fed either diet did not develop malocclusion (data not shown). *Bsp*$^{-/-}$(HD) mice with severe incisor malocclusion weighed significantly less than *Bsp*$^{-/-}$(HD) with milder incisor malocclusion (Figure 3.1B), suggesting that severe malocclusion, with corresponding malnutrition, may contribute to the observed bone phenotype.

Previous studies reported shortening of long-bones in *Bsp*$^{-/-}$ mice fed normal hard pellet diet at 4 and 16 months of age (Malaval et al., 2008), consistent with our findings at 8

weeks (Figure 3.1E). However, when fed SD, femur and tibia lengths of *Bsp*$^{-/-}$ and WT mice were not significantly different. Further, increased serum alkaline phosphatase (ALP) activity, a marker of skeletal activity, in *Bsp*$^{-/-}$ mice (Foster et al., 2013b), was also normalized with SD (Figure 3.1F). Other blood-chemistry markers, including calcium, phosphorus, magnesium, sodium, chloride, glucose, albumin, and protein triglycerides were similar for all groups (Table 3.2). Thus, SD normalized body weight, long-bone length, serum ALP, and reduced severe malocclusion in *Bsp*$^{-/-}$ mice.

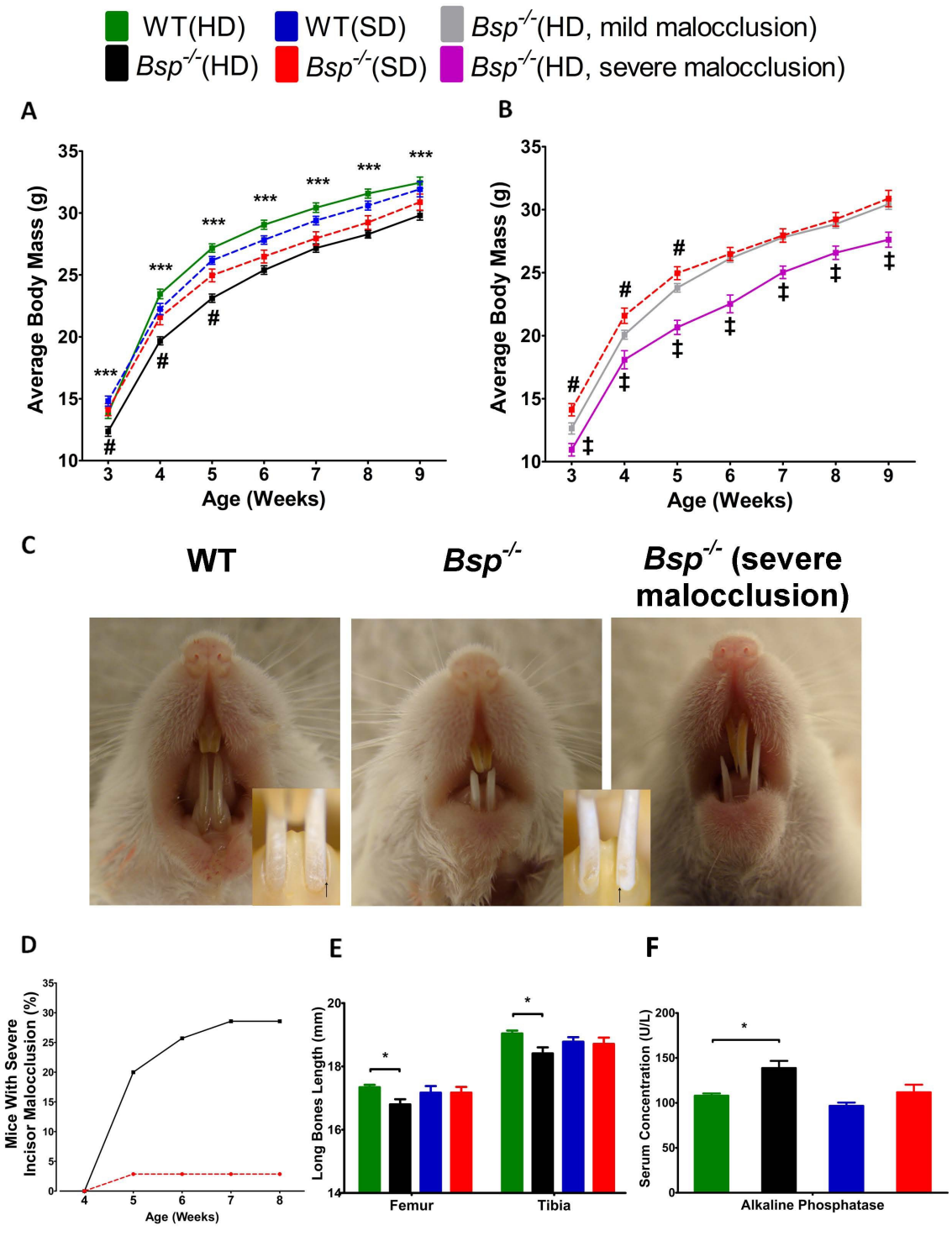
WT(HD)
WT(SD)
Bsp-/-(HD, mild malocclusion)
Bsp-/-(HD)
Bsp-/-(SD)
Bsp-/-(HD, severe malocclusion)
A
B
Average Body Mass (g)
Age (Weeks)
C
WT
Bsp-/-
Bsp-/- (severe malocclusion)
D
Mice With Severe Incisor Malocclusion (%)
Age (Weeks)
E
Long Bones Length (mm)
Femur
Tibia
F
Serum Concentration (U/L)
Alkaline Phosphatase

Figure 3.1. Soft diet normalizes body weight, bone length, and incisor malocclusion in *Bsp*$^{-/-}$ mice.

(A) Between 3 and 9 weeks, *Bsp*$^{-/-}$ mice fed with hard diet (*Bsp*$^{-/-}$(HD)) weigh significantly less (*) than the WT counterpart (WT(HD)) (n=35-58 for week 3-8; n=27 at week 9). However, WT and *Bsp*$^{-/-}$ mice fed soft diet (WT(SD) and *Bsp*$^{-/-}$(SD)) are not statistically different in weight. Between 3 and 5 weeks, *Bsp*$^{-/-}$(SD) weigh significantly greater (#) than *Bsp*$^{-/-}$(HD), but not in older mice. (**B**) *Bsp*$^{-/-}$(HD) with severe malocclusion weigh significantly less (‡) than *Bsp*$^{-/-}$(HD) with milder malocclusion, suggesting this phenotype might be caused by dental dysfunction and malnutrition. **(C)** *Bsp*$^{-/-}$ mice, regardless of diet, developed some degree of malocclusion that is associated with labial rotation of the incisors, observed by altered location of the cemento-enamel junction (black arrow in insets). Severe malocclusion of maxillary and mandibular incisors is prominent in *Bsp*$^{-/-}$ mice fed hard diet. (**D**) Over 8 weeks, 10 out of 35 (~30%) *Bsp*$^{-/-}$(HD) mice develop severe incisor malocclusion, a feature evident in only 1 out of 35 (~3%) *Bsp*$^{-/-}$(SD) mice. **(E)** In the HD groups, femurs and tibias are significantly shorter in 8-week old *Bsp*$^{-/-}$ mice compared to WT, however no differences were apparent between the two SD groups (n=6). **(F)** The increased serum alkaline phosphatase (ALP) activity in *Bsp*$^{-/-}$ vs. WT is normalized in the SD groups (n=5). For **A, B, E and F**, values shown represent means ± SEM; *$p < 0.05$, **$p<0.01$, ***$p<0.001$. **Note: (A)** The average body mass for *Bsp*$^{-/-}$(HD) mice includes all mice regardless of degree of malocclusion.

Table 3.1. The effect of diet on the onset of severe malocclusion in *Bsp*$^{-/-}$ mice.

Bsp$^{-/-}$ and wild type littermates were fed either a hard or soft diet from the time of weaning. Each week animals were examined for evidence of severe malocclusion of the incisors. The onset of malocclusion for *Bsp*$^{-/-}$ mice were observed within 5 week post weaning. For each *Bsp*$^{-/-}$ mouse, the first observation of severe malocclusion was recorded. No malocclusion was observed in any of the wild type mice.

	Number of mice that have first indication of malocclusion per week							
***Bsp*$^{-/-}$ Mice Diet**	**N**	**Week 4**	**Week 5**	**Week 6**	**Week 7**	**Week 8**	**Total**	**Malocclusion Rate (%)**
Hard Diet	35	0	7	2	1	0	10	28.6
Soft Diet	35	0	1	0	0	0	1	2.9

Table 3.2. Serum biochemistry for *Bsp*$^{-/-}$ and WT mice.

Below are various chemical activity analysis of 8-week-old, which include calcium, phosphorus, magnesium, sodium, chloride, glucose, albumin, alkaline phosphatase, and protein triglycerides. n = 4 mice per group.

Genotype and Diet	Sodium, mmol/L	Chloride, mmol/L	Calcium, mmol/L	Magnesium, mmol/L
WT (HD)	462.00 ± 4.24	409.50 ± 5.20	2.03 ± 0.14	0.85 ± 0.04
WT (SD)	464.25 ± 1.50	413.25 ± 2.87	2.18 ± 0.08	0.87 ± 0.05
Bsp$^{-/-}$ (HD)	463.50 ± 5.20	413.5 ± 4.50	2.17 ± 0.07	0.83 ± 0.11
Bsp$^{-/-}$ (SD)	465.00 ± 4.90	412.50 ± 1.73	2.27 ± 0.15	0.83 ± 0.09

Genotype and Diet	Phosphorous, mg/dL	Glucose, mg/dL	Blood Urea Nitrogen (BUN), mg/dL	Uric acid, mg/dL
WT (HD)	7.88 ± 0.62	253.50 ± 7.55	2.03 ± 0.14	1.20 ± 0.24
WT (SD)	7.95 ± 0.39	212.25 ± 17.73	2.18 ± 0.08	1.28 ± 0.29
Bsp$^{-/-}$ (HD)	8.10 ± 1.49	240.75 ± 40.50	2.17 ± 0.07	1.13 ± 0.29
Bsp$^{-/-}$ (SD)	8.18 ± 1.28	237.75 ± 16.68	2.27 ± 0.15	1.73 ± 0.51

Genotype and Diet	Albumin, g/dL	Cholestrol, mg/dL	Triglycerides, mg/dL	Alkaline Phosphatase, U/L
WT (HD)	2.85 ± 0.39	147.00 ± 11.75	144.00 ± 61.73	108.00 ± 5.48
WT (SD)	2.93 ± 0.15	138.00 ± 9.49	138.75 ± 23.03	96.75 ± 7.89
Bsp$^{-/-}$ (HD)	2.93 ± 0.15	135.75 ± 19.81	120.00 ± 57.60	138.75 ± 17.73 *
Bsp$^{-/-}$ (SD)	2.70 ± 0.24	141.75 ± 17.56	151.50 ± 41.10	111.75 ± 18.87

Genotype and Diet	Aspartate Trans, U/L	Amylase, U/L	Total Protein, mg/dL
WT (HD)	63.00 ± 19.44	2347.50 ± 223.41	4.65 ± 0.17
WT (SD)	60.75 ± 35.53	2415.75 ± 262.32	4.58 ± 0.15
Bsp$^{-/-}$ (HD)	45.00 ± 10.68	2386.50 ± 255.60	4.65 ± 0.17
Bsp$^{-/-}$ (SD)	57.00 ± 17.83	2680.50 ± 447.30	4.58 ± 0.15

* indicates $p < 0.05$ by two-way analysis of variance and Bonferroni post-tests.

3.3.2 Altered dentin and enamel formation in incisors of *Bsp*$^{-/-}$ mice

At 4 weeks of age, *Bsp*$^{-/-}$ incisors appeared similar to WT (Figure 3.2A). However, by 8 weeks, microCT and histology revealed increased dentin thickness and decreased pulp volume in *Bsp*$^{-/-}$ mouse incisors compared to WT (Figure 3.2B,C,E,G,I, and Figure 3.3A,B). Incisor dentin thickness measured at the first and third molar increased by 85% in *Bsp*$^{-/-}$ mice (Figure 3.3B), whereas enamel thickness was normal at all positions (Figure 3.4). At first, the incisors appeared to have enhanced mineralization of both dentin and enamel in the unerupted portion compared to WT incisors (Figure 3.2B, 3.3C-D). At the site of eruption (at the alveolar crest), dentin and enamel mineral densities were equivalent in *Bsp*$^{-/-}$ and WT. Mineral density of *Bsp*$^{-/-}$ molar crown and root dentin were comparable to WT, however, enamel mineral density was elevated by 12.4% (Figure 3.3E).

Due to these alterations in dentinogenesis and enamel mineralization in *Bsp*$^{-/-}$ mice, irrespective of diet type, we analyzed the incisor rate of eruption. *Bsp*$^{-/-}$ mouse incisors erupted at a significantly reduced rate compared to WT, 141 vs. 323 μm/day, respectively (Figure 3.5). Therefore, relative alterations in dentin and enamel mineral densities near incisor apices are likely due to reduced rate of eruption in *Bsp*$^{-/-}$ mice.

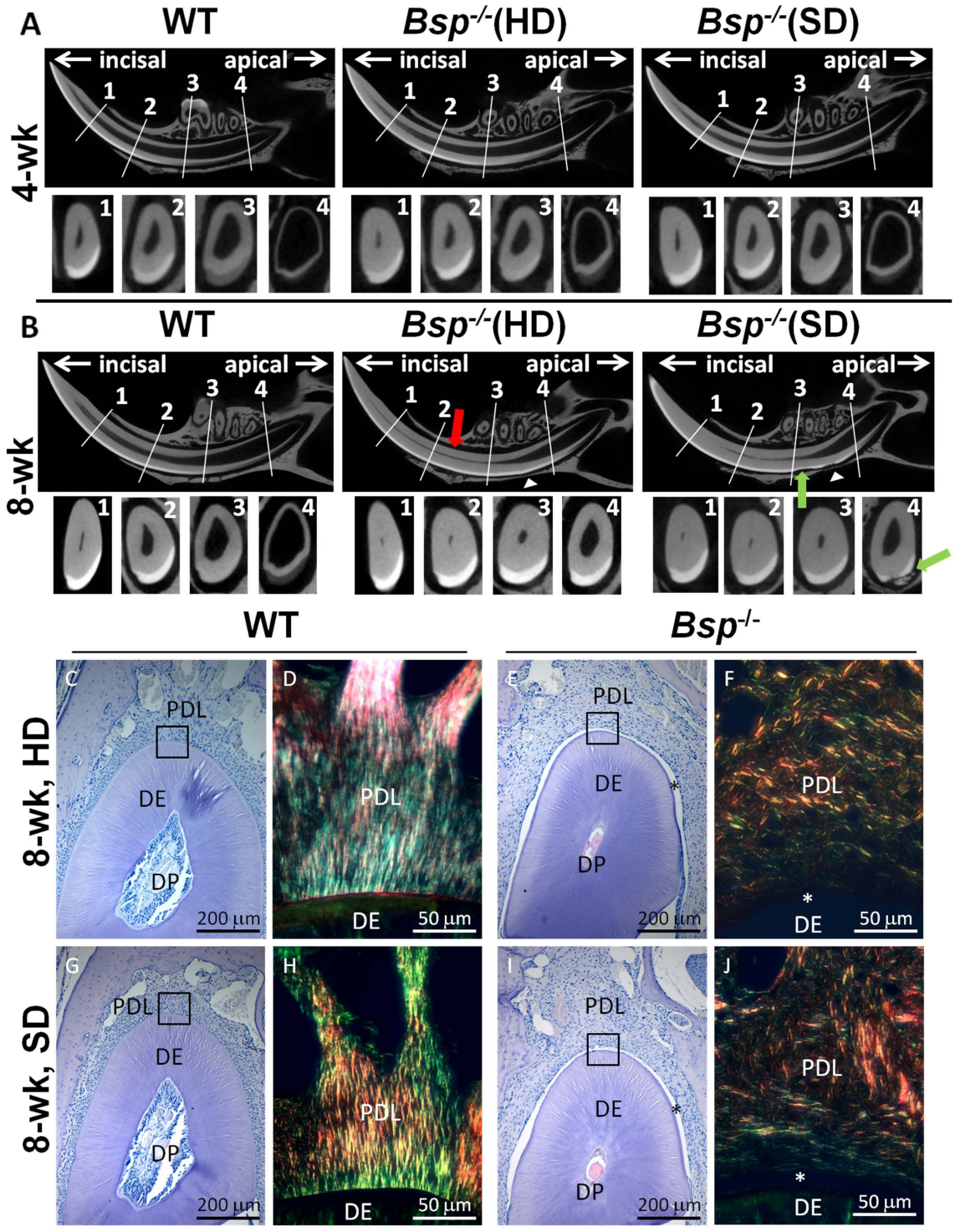
A
WT
Bsp-/-(HD)
Bsp-/-(SD)
4-wk
incisal
apical
1
2
3
4
B
8-wk
WT
Bsp-/-
8-wk, HD
8-wk, SD
C
D
E
F
G
H
I
J
PDL
DE
DP
200 μm
50 μm

Figure 3.2. Altered incisor dentin and enamel formation in *Bsp*$^{-/-}$ mice.

For microCT analysis, 4 different landmarks were chosen: (1) alveolar crest, (2) mental foramen, (3) first molar, and (4) third molar. The WT images in **(A and B)** are representative of both WT(HD) and WT(SD) since no apparent differences in phenotype were observed between these WT groups. **(A)** At 4 weeks of age, microCT analysis indicates no striking difference in incisors of *Bsp*$^{-/-}$ mice compared to WT. **(B)** By 8 weeks of age, microCT images reveal increased dentin thickness (red arrow) and decreased pulp volume towards the apical end of the incisors in *Bsp*$^{-/-}$ mice compared to WT, regardless of diet. In addition, regardless of diet, resorption of enamel and dentin (green arrow) and incisor-associated bone (white arrowhead) can be seen in *Bsp*$^{-/-}$ mice. **(C, E, G, I)** Histology (H&E stain) confirms increased dentin (DE) thickness and decreased dental pulp (DP) space in *Bsp*$^{-/-}$ mouse incisors compared to WT. **(D, F, H, J)** Detachment (*) and disorganization of periodontal ligament (PDL) collagen-fiber bundles in *Bsp*$^{-/-}$ mouse incisors with Picrosirius red (PR) staining under polarized light. Soft diet does not normalize dentinogenesis, or PDL attachment in *Bsp*$^{-/-}$ mouse incisors. The histological tissues were sectioned at a position relative to the mental foramen (position 2).

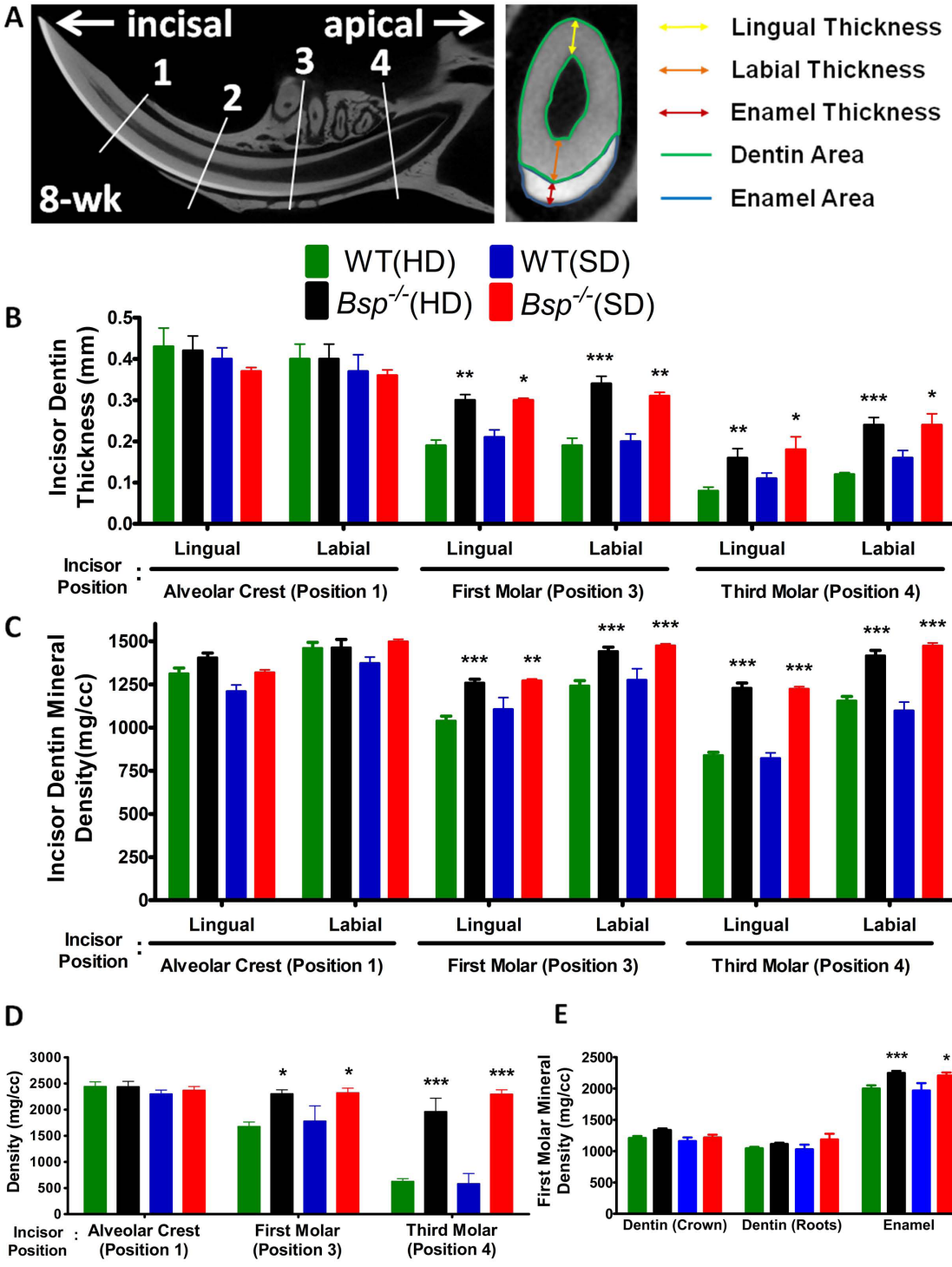
A
incisal
apical
1
2
3
4
8-wk
Lingual Thickness
Labial Thickness
Enamel Thickness
Dentin Area
Enamel Area
WT(HD)
WT(SD)
Bsp-/-(HD)
Bsp-/-(SD)
B
Incisor Dentin Thickness (mm)
0.5
0.4
0.3
0.2
0.1
0.0
Lingual
Labial
Incisor Position :
Alveolar Crest (Position 1)
First Molar (Position 3)
Third Molar (Position 4)
C
Incisor Dentin Mineral Density(mg/cc)
1500
1250
1000
750
500
250
0
D
Incisor Enamel Mineral Density (mg/cc)
3000
2500
2000
1500
1000
500
0
Alveolar Crest (Position 1)
First Molar (Position 3)
Third Molar (Position 4)
E
First Molar Mineral Density (mg/cc)
Dentin (Crown)
Dentin (Roots)
Enamel

Figure 3.3. Increased incisor dentinogenesis and enamel mineralization in *Bsp*$^{-/-}$ mice.

(A) Using microCT incisor dentin thickness, area, and mineral density were analyzed at: (1) alveolar crest, (2) mental foramen, (3) first molar and (4) third molar. Linear measurements were also performed to determine thickness of incisor enamel, labial and lingual dentin, as well as cross-sectional area of the dentin and enamel. By 8 weeks of age, microCT analysis reveals significantly increased dentin thickness **(B)** and mineral density **(C)** in the apical end of the *Bsp*$^{-/-}$ mouse incisors (incisor position 3 and 4) compared to WT, regardless of diet. **(D)** Similar to dentin, the enamel mineral density is increased significantly at both incisor positions 3 and 4 of the *Bsp*$^{-/-}$ mice, regardless of diet. Interestingly, both enamel and dentin mineral density at position 3 and 4 are equivalent to the erupted incisor tissue densities (position 1) in both WT and *Bsp*$^{-/-}$ mice, regardless of diet. **(E)** First molar crown and root dentin densities are not different in *Bsp*$^{-/-}$ compared to WT mice; however, the enamel mineral density is significantly increased in *Bsp*$^{-/-}$ molars compared to WT, regardless of diet. For **B-E**, values shown represent means ± SEM; n=5; *$p < 0.05$, **$p<0.01$, ***$p<0.001$. **Note:** Measurements of thickness and mineral density determined at positions 1 and 2 were similar to each other, and showed no significant difference between WT and *Bsp*$^{-/-}$ groups, thus only measurements at position 1 are shown.

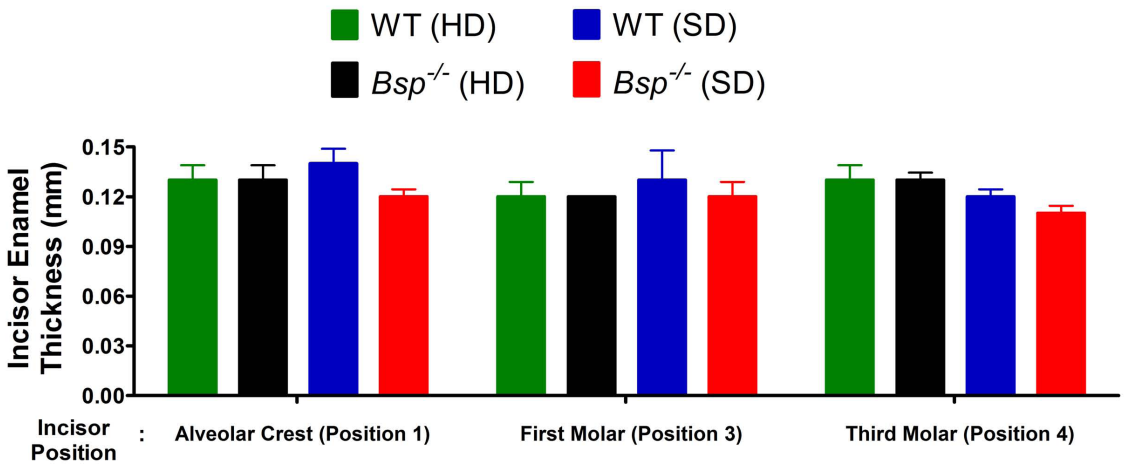
WT (HD)
WT (SD)
Bsp-/- (HD)
Bsp-/- (SD)
Incisor Enamel Thickness (mm)
0.15
0.12
0.09
0.06
0.03
0.00
Incisor Position :
Alveolar Crest (Position 1)
First Molar (Position 3)
Third Molar (Position 4)

Figure 3.4. Similar enamel thickness was observed between experimental groups.

Using microCT incisor dentin thickness, area, and mineral density were analyzed at: (1) alveolar crest, (2) mental foramen, (3) first molar and (4) third molar. Linear measurements were also performed to determine thickness of incisor enamel. No significant difference in enamel thickness were observed between the mice groups.

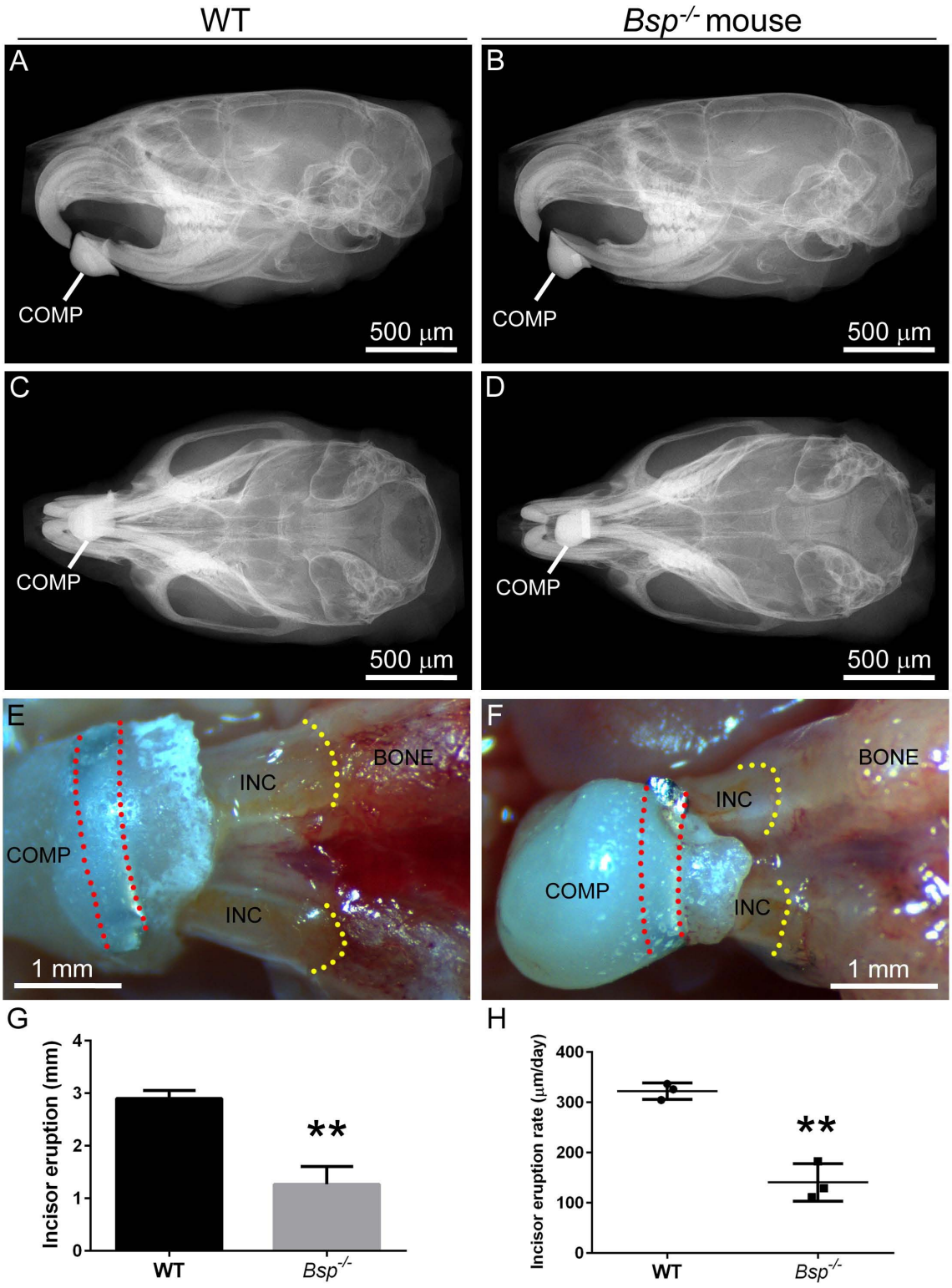
WT
Bsp-/- mouse
A
COMP
500 μm
B
COMP
500 μm
C
COMP
500 μm
D
COMP
500 μm
E
BONE
INC
COMP
INC
1 mm
F
BONE
INC
COMP
INC
1 mm
G
Incisor eruption (mm)
4
3
2
1
0
**
WT
Bsp-/-
H
Incisor eruption rate (μm/day)
400
300
200
100
0
**
WT
Bsp-/-

Figure 3.5. *Bsp*$^{-/-}$ mice feature reduced rates of incisor eruption.

WT and *Bsp*$^{-/-}$ mice at 8 weeks old were fixed with dental composite to affix a small length of stainless steel wire to the labial surface of the mandibular incisors near the socket margin. **(A-D)** Radiographs of skulls taken after 9 days indicate the placement of the composite (COMP) on the incisors. **(E, F)** Stereomicroscope images show the labial incisor (INC) surfaces, including the mass of composite, the embedded wire (outlined in red), and the socket margin (outlined in yellow). Measurements made between the socket margin and middle of the wire were used to calculate incisor eruption distance and rate. **(G)** *Bsp*$^{-/-}$ mice featured a significantly reduced incisor eruption distance over 9 days, **(H)** corresponding to a more than 2-fold significantly reduced rate of eruption, compared to WT incisors. Graph in (G) shows mean ± SD and graph in (H) shows individual measurements and mean ± SD. ** indicates $p < 0.01$ for unpaired *t*-test (n=3 for each group).

This page was intentionally left blank

3.3.3 Soft diet does not rescue periodontal defects in *Bsp*$^{-/-}$ mice

Defects noted in acellular cementum, PDL and alveolar bone in *Bsp*$^{-/-}$ mice prompted us to determine the role of masticatory forces on these periodontal manifestations. SD did not rescue PDL detachment and disorganization, and resorption of incisor enamel, dentin, or associated bone in *Bsp*$^{-/-}$ mice (Figure 3.2C,E,G,I). Furthermore, between 4 and 20 weeks of age, *Bsp*$^{-/-}$ mice in both diet groups exhibited similar dramatic loss of alveolar bone, extensive cervical root resorption (Figure 3.6A), PDL detachment, and epithelial downgrowth (Figure 3.6B-I). The reduced periodontal structure contributed to premature loss of teeth, especially third molars, as the *Bsp*$^{-/-}$ mice aged.

Periodontal structures were analyzed quantitatively at 8 and 20 weeks, including exposure of molar roots (an indicator of alveolar bone reduction) and width of PDL in the interradicular region (Figure 3.7A). MicroCT analysis confirmed increased root exposure for all *Bsp*$^{-/-}$ molars compared to WT, regardless of diet type (Figure 3.7B). At 20 weeks, additional loss of alveolar bone in *Bsp*$^{-/-}$ mice was apparent, especially on the lingual side (Figure 3.8). At both 8 and 20 weeks, *Bsp*$^{-/-}$ mice exhibited significantly wider PDL in the interradicular regions of first and second molars (Figure 3.7C), reflecting bone loss in that region as well. However, at 8 weeks, *Bsp*$^{-/-}$(SD) featured significantly less of a width increase in PDL than *Bsp*$^{-/-}$(HD), indicating diet-associated amelioration of bone loss in this region. The altered periodontal structure, evidenced by reduced alveolar bone and wider PDL space (Figure 3.7D), is likely responsible for the observed molar malocclusion by 8 weeks of age (Figure 3.7E).

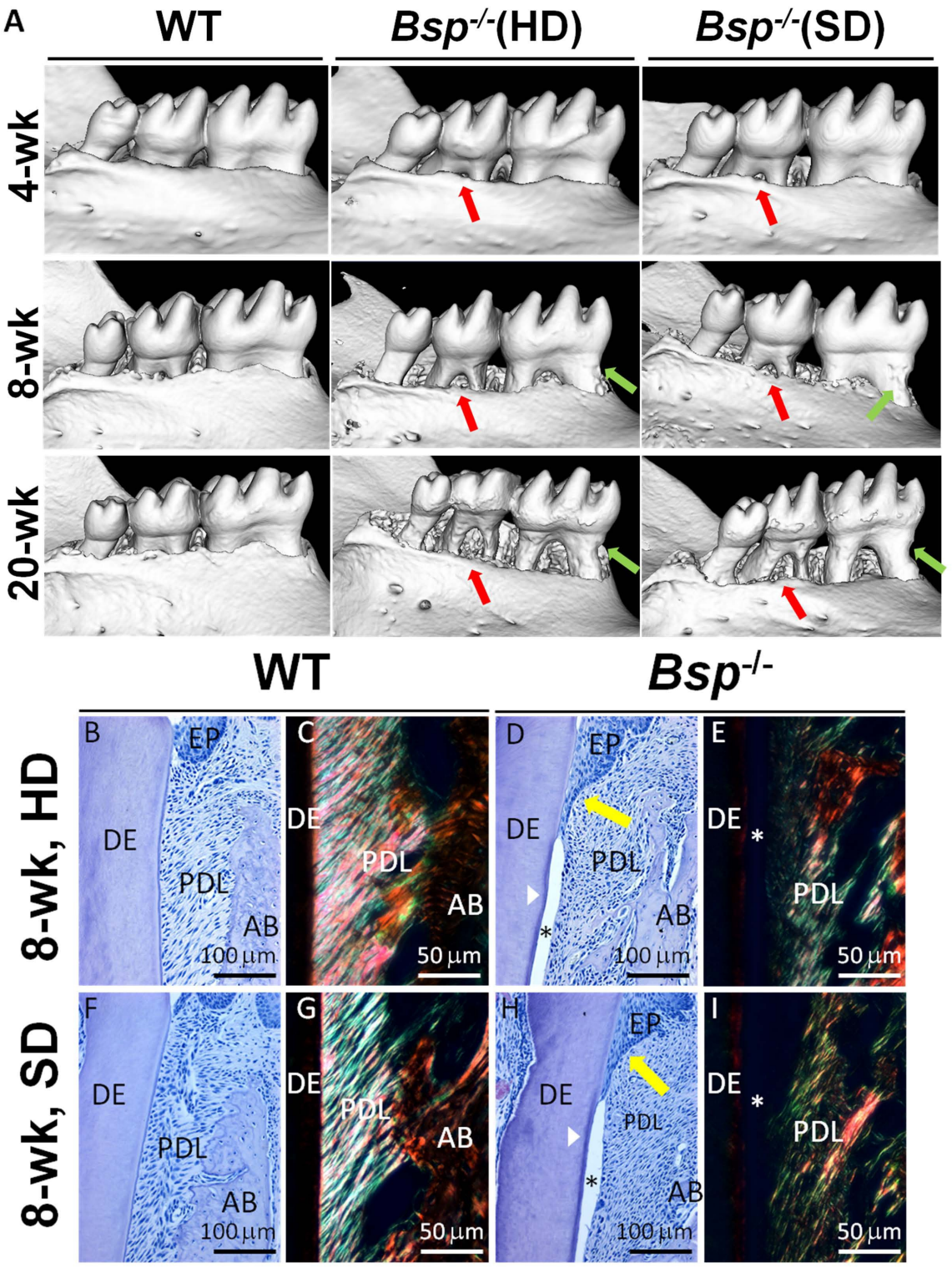
A
WT
Bsp-/-(HD)
Bsp-/-(SD)
4-wk
8-wk
20-wk
WT
Bsp-/-
8-wk, HD
8-wk, SD
B
C
D
E
F
G
H
I
EP
DE
PDL
AB
100 µm
50 µm

Figure 3.6. Soft diet does not rescue periodontal phenotype in *Bsp*$^{-/-}$ mice.

(A) MicroCT images demonstrate progressive tooth root resorption (green arrow) and alveolar bone (AB) loss (red arrow) in both *Bsp*$^{-/-}$ diet groups at 8 and 20 weeks. **(B, D, F, H)** H&E stained first-molar sections in 8-week-old mice reveal that *Bsp*$^{-/-}$ mice in both diet groups feature identical phenotypes marked by lack of acellular cementum (white arrowhead), PDL detachment (*), and epithelial (EP) downgrowth (yellow arrow). **(C, E, G, I)** Picrosirius red (PR) stained sections under polarized light microscopy demonstrate loss of PDL collagen organization in both *Bsp*$^{-/-}$ diet groups.

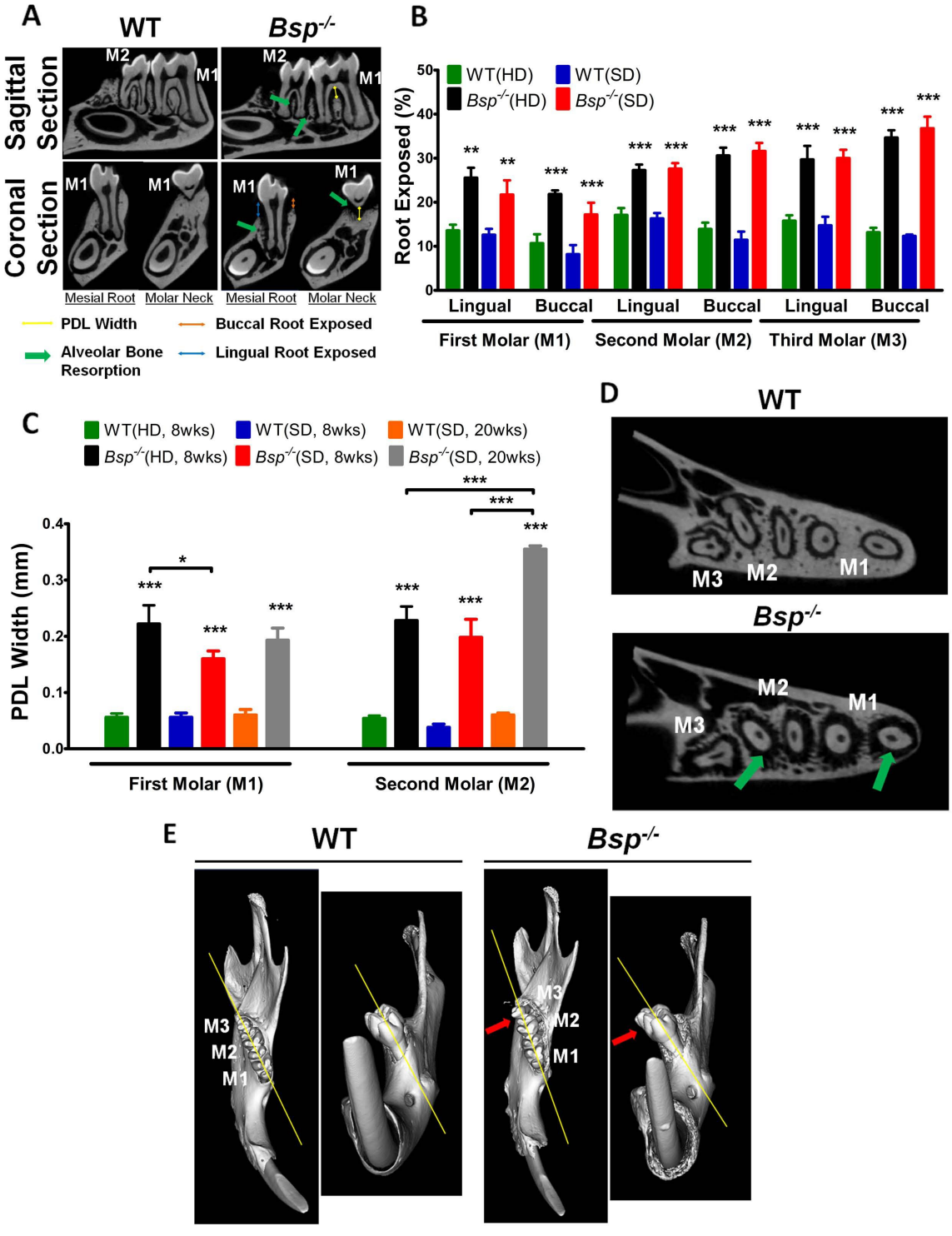
A
WT
Bsp-/-
Sagittal Section
Coronal Section
M1
M2
Mesial Root
Molar Neck
PDL Width
Alveolar Bone Resorption
Buccal Root Exposed
Lingual Root Exposed
B
WT(HD)
WT(SD)
Bsp-/-(HD)
Bsp-/-(SD)
Root Exposed (%)
Lingual
Buccal
First Molar (M1)
Second Molar (M2)
Third Molar (M3)
C
WT(HD, 8wks)
WT(SD, 8wks)
WT(SD, 20wks)
Bsp-/-(HD, 8wks)
Bsp-/-(SD, 8wks)
Bsp-/-(SD, 20wks)
PDL Width (mm)
First Molar (M1)
Second Molar (M2)
D
WT
Bsp-/-
M3
M2
M1
E
WT
Bsp-/-
M3
M2
M1

Figure 3.7. Progressive periodontal breakdown in mandibles of *Bsp*$^{-/-}$ mice.

(A) MicroCT cross-sectional images reveal alveolar bone loss around molar roots (green arrows). For all three molars (M1-M3), root exposure on buccal (blue arrow) and lingual (orange arrow) aspects, and PDL width in the interradicular region (yellow line) were determined. **(B)** MicroCT analysis confirms significantly increased molar root exposure in all three molars in 8-week-old *Bsp*$^{-/-}$ mice, with no difference in root exposure observed between both *Bsp*$^{-/-}$ diet groups. **(C)** At both 8 and 20 weeks, *Bsp*$^{-/-}$ mice exhibited significantly wider PDL in the interradicular regions of first and second molars compared to WT, regardless of diet. At 8 weeks, *Bsp*$^{-/-}$ mice in the SD group exhibit significantly less increase in PDL width than the HD group, indicating diet-associated amelioration of bone loss in this region. As expected, *Bsp*$^{-/-}$(SD) showed further widening of PDL width at 20 weeks compared to 8 weeks due to progressive alveolar bone loss. At 8 weeks, **(D)** extensive alveolar bone loss around the molar roots (green arrows**)** contributes to loss of periodontal support that lead to **(E)** molar malocclusion (red arrows). For **B and C**, values represent means ± SEM; n=5; *p < 0.05.**p<0.01, ***p<0.001. Abbreviations: M1 = first molar; M2 = second molar; M3 = third molar.

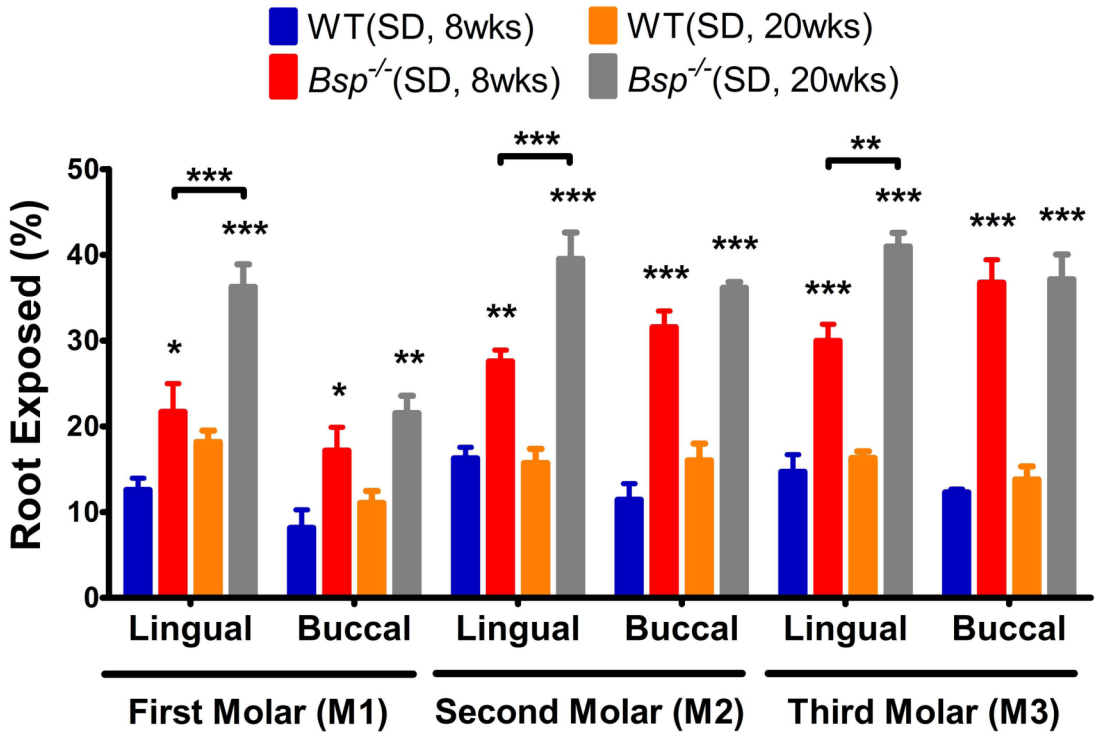

Figure 3.8. Further extensive alveolar bone resorption is seen in older *Bsp*$^{-/-}$ mice.

Quantitative microCT analysis of 20-week-old *Bsp*$^{-/-}$(SD) mice revealed continuing progressive loss of alveolar bone, with more profound bone loss on the lingual aspects of M1-M3. Values represent means ± SEM; n=5; *p<0.05, **p<0.01, *** p<0.001.

3.4 DISCUSSION

We hypothesized that the periodontal manifestations in *Bsp*$^{-/-}$ mice resulted from absence of acellular cementum, with the resulting loss of PDL attachment and associated abnormal mechanical forces leading to tooth dysfunction and periodontal tissue destruction. We tested this hypothesis using a diet designed to reduce masticatory forces, thus reducing mechanical stress on the periodontal apparatus. Soft diet was unable to diminish periodontal breakdown associated with *Bsp*$^{-/-}$ mouse molars, including PDL detachment and disorganization, severe and progressive alveolar bone loss, and resorption of tooth root surfaces, indicating that masticatory forces are not primary factors in those pathological changes. However, SD almost eliminated severe incisor malocclusion in *Bsp*$^{-/-}$ mice, supporting the hypothesis that occlusal loading contributed to the malocclusion phenotype. Surprisingly, SD normalized body weight, long-bone length, and serum ALP activity in *Bsp*$^{-/-}$ mice, suggesting that tooth dysfunctions predispose *Bsp*$^{-/-}$ mice to feeding problems and nutritional deficits that affect body and skeletal growth, and that provision of SD improves post-weaning nutrition. Another surprising finding was *Bsp*$^{-/-}$ incisor phenotype of enhanced dentinogenesis and enamel mineralization that is likely due to a slower eruption rate. This study demonstrates the importance of BSP in maintaining proper periodontal function and alveolar bone remodeling, and points to dental dysfunction as causative factor of skeletal defects observed in *Bsp*$^{-/-}$ mice.

3.4.1 Role of altered mechanotransduction in *Bsp*$^{-/-}$ mice periodontal breakdown

In this study, we demonstrated a progressive and severe alveolar bone loss in *Bsp*$^{-/-}$ mice, in contrast to reduced long-bone turnover *in vivo* and reduced osteoclast activation *in vitro* reported previously (Malaval et al., 2008). We propose two potential causal factors to account for the discrepancy in turnover between long-bone and alveolar bone in *Bsp*$^{-/-}$

mice: (1) excessive traumatic forces, or (2) unloading of alveolar bone resulting in altered mechanotransduction.

In normal function, alveolar bone undergoes frequent loading during mastication and is subject to continuous remodeling to accommodate tooth function (Sodek and McKee, 2000). The PDL is a mechanosensitive tissue that provides connection between tooth root and supportive alveolar bone acting as a pool of progenitor cells, a source of vascularity and innervation, and, importantly, as a shock-absorber helping to prevent tissue damage under the forces generated by tooth use (Beertsen et al., 1997). Alveolar bone operates as a functional unit with the non-mineralized PDL, and proper mechanical and biological signals between PDL and alveolar bone are critical to maintain functional homeostasis of the periodontal apparatus (Ho et al., 2013; Wise and King, 2008). Masticatory forces are transmitted through the PDL generally in an occlusal-apical direction before being distributed to the surrounding alveolar bone (Meikle, 2006; Milne et al., 2009), including buccal and lingual alveolar ridges, interdental bone, and interradicular bone in multi-rooted teeth.

Alveolar bone resorption can result from excessive compression forces or occlusal stress by stimulation of osteoclastogenesis through local up-regulation of RANKL, such as directed resorption on the compression side during orthodontic tooth movement (Kook et al., 2011; Sanuki et al., 2010; Walker et al., 2008; Wise and King, 2008). Up-regulation of RANKL, often associated with inflammatory-mediated bone resorption (Yoshinaga et al., 2007), was evident in the PDL region of *Bsp*$^{-/-}$ mice, although inflammatory cells were not observed (Foster et al., 2013b). Furthermore, loss of PDL attachment and epithelial downgrowth in *Bsp*$^{-/-}$ mice compromises the shock-absorbing function of the PDL, disturbing the stress-distribution function of the periodontium, and subjecting the bony socket to increased and possibly traumatic compression forces during mastication. Extensive resorption of alveolar bone in *Bsp*$^{-/-}$ mice was most evident in the cervical root, where load-bearing horizontal and oblique PDL fibers enter bone as Sharpey's fibers. In contrast, traumatic hyperocclusion in mouse molars is more associated with bone and tooth resorption near the apex and in the interradicular bone (Walker et al., 2008).

Secondly, alveolar bone resorption can also result from absence of mechanotransduction from the PDL. Alveolar bone formation occurs as the tooth root forms and remodels in response to changes in tooth use (e.g. orthodontics), and disappears in the absence of teeth (e.g. edentulous ridges) (Hansson and Halldin, 2012; Wise and King, 2008). These processes are regulated by the PDL, as both a mechanotransductor supplying mechanical stimuli to bone, and as cellular source of biological signals including regulators of bone homeostasis (e.g. RANKL and osteoprotegerin (OPG)). The tooth-PDL-alveolar bone functional unit can be understood through application of the mechanostat theory introduced by Harold Frost (Frost, 1987), which proposes that proper functional loading is necessary to maintain structural integrity in bone through balanced resorption and formation. Similar to edentulous ridges, where lack of mechanical stimuli leads to osteopenia and alveolar ridge resorption (Hansson and Halldin, 2012), *Bsp*$^{-/-}$ mice may experience alveolar bone loss as a result of disturbance of tooth attachment and reduced functional loading.

The inability of SD to ameliorate periodontal breakdown in *Bsp*$^{-/-}$ mice supports the hypothesis that loss of PDL attachment and altered mechanotransduction are contributors to reduction in alveolar bone in *Bsp*$^{-/-}$ mice. Limitations of the study include inability to measure true mechanical forces in mouse periodontia, and inability to control chewing of other hard materials (e.g. cage wires, bedding) that could introduce unrecognized occlusal trauma into the SD group.

3.4.2 Malocclusion and altered incisor formation in *Bsp*$^{-/-}$ mice

While SD did not alter periodontal breakdown around molar teeth, it almost completely rescued the severe incisor malocclusion in *Bsp*$^{-/-}$ mice. This finding strongly supports non-physiological distribution of occlusal forces as a causative factor for incisor malocclusion. We also demonstrate, for the first time, evidence of molar misalignment and malocclusion in *Bsp*$^{-/-}$ mice, likely due to PDL detachment coupled with occlusal stress, similar to the incisor.

These data favor dental dysfunction and malnutrition as factors contributing to low body weight, reduced long-bone length, and elevated serum ALP in *Bsp*$^{-/-}$ mice. Previous studies have demonstrated *Bsp*$^{-/-}$ mice fed on normal hard pellet diet were smaller with shorter long-bones (Bouleftour et al., 2014; Malaval et al., 2008), and increased serum ALP (Foster et al., 2013b). These parameters were normalized with provision of SD to *Bsp*$^{-/-}$ mice. Studies on periostin-null mice, which exhibit a similar periodontal breakdown and incisor malocclusion, also report similar rescue with SD in body weight and long-bone length (Rios et al., 2005). Additionally, pain associated with tooth dysfunction in enamelin-null mice resulted in malnutrition and reduced body weight, which was rescued by SD (Chan et al., 2013). These parallel observations support the interpretation that post-weaning malnutrition from malocclusion contributes to the bone and weight phenotype in *Bsp*$^{-/-}$ mice. However, all bone changes in *Bsp*$^{-/-}$ mice, do not necessarily stem from tooth dysfunction and malnutrition. We and others have shown early delays in long-bone ossification in *Bsp*$^{-/-}$ mice (Bouleftour et al., 2014; Holm et al., 2015). Serum ALP is a commonly used biomarker for bone formation and mineralization (Yadav et al., 2012). In the *Bsp*$^{-/-}$ mice, elevation of ALP activity may serve as a compensatory mechanism for the demonstrated skeletal hypomineralization described in (Bouleftour et al., 2014). SD helps to reduce the severe malocclusion in *Bsp*$^{-/-}$ mice, ameliorating the skeletal defect, which in turn is reflected by normalized serum ALP.

Another surprising insight is related to the rapid incisor dentin and enamel mineralization in *Bsp*$^{-/-}$ mice. Dentin is reported to include BSP (Fujisawa et al., 1993; Qin et al., 2001), yet *Bsp*$^{-/-}$ molar dentin appeared normal (Foster et al., 2013b), and confirmed by microCT analysis in this report. Enamel is formed from dental epithelium and suspected to include BSP (Chen et al., 1998). The question arises as to why the incisor is so dramatically affected by loss of BSP. We determined that *Bsp*$^{-/-}$ incisors erupt at a slower rate than WT, causing the appearance of enhanced or accelerated dentinogenesis and enamel mineralization towards the apex. Alterations in *Bsp*$^{-/-}$ incisor eruption could result from periodontal dysfunction due to lack of cementum and also, indirectly, chronic occlusal trauma. Previous studies indicate that migration of PDL fibroblasts contributes to the

continuously erupting rodent incisor (Beertsen et al., 1997). Several other mouse models have similar incisor enamel and/or dentin phenotype including periostin-null mice (Rios et al., 2005; Rios et al., 2008), OPG-null mice (Sheng et al., 2010), Vitamin D receptor-null mice (Zhang et al., 2009), and integrin α11β1-null mice (Popova et al., 2007). We propose that periodontal dysfunction and resulting lower rates of incisor eruption may underlie dentin and enamel changes in all of these models.

3.4.3 Limiting factors of the studies

The use of SD reduces the occlusal forces during mastication in comparison to hard diet. However, to address the role of occlusal forces on acellular cementum in the *Bsp*$^{-/-}$ mice we can incorporate a similar strategy used in the periostin null mice. This method requires weekly trimming of one side of the mandibular incisors using surgical clippers. The other side of the mandibular incisors will be used for comparison (Rios et al., 2008). Using this model they demonstrated that occlusal hypofunction was achieved. In the study, the reduced incisors were able to rescue the enamel and dentin resorption observed in the incisors of periostin-null mice. However, for our study, the surgical trimming of the incisors will introduces additional forces, which may have an effect on the integrity of the cementum-pdl interface of the *Bsp*$^{-/-}$ incisor.

3.5 CONCLUSION

This study provides new insights into the role of BSP in the formation and maintenance of the periodontium, confirming the importance of BSP for acellular cementum formation that cannot be corrected by diet.

3.6 REFERENCES

Baht GS, Hunter GK, Goldberg HA. 2008. Bone sialoprotein–collagen interaction promotes hydroxyapatite nucleation. Matrix Biol. 27(7):600-608.

Beertsen W, McCulloch CAG, Sodek J. 1997. The periodontal ligament: a unique, multifunctional connective tissue. Periodontol 2000. 13(1):20-40.

Boudiffa M, Wade-Gueye NM, Guignandon A, Vanden-Bossche A, Sabido O, Aubin JE, Jurdic P, Vico L, Lafage-Proust MH, Malaval L. 2010. Bone sialoprotein deficiency impairs osteoclastogenesis and mineral resorption in vitro. J Bone Miner Res. 25(12):2669-2679.

Bouleftour W, Boudiffa M, Wade-Guéye NM, Bouët G, Cardelli M, Laroche N, Vanden-Bossche A, Thomas M, Bonnelye E, Aubin JE et al. 2014. Skeletal development of mice lacking bone sialoprotein (BSP) - impairment of long bone growth and progressive establishment of high trabecular bone mass. PLoS One. 9(5):e95144.

Chan AHL, Lertlam R, Simmer JP, Wang C-N, Hu JCC. 2013. Bodyweight assessment of enamelin null mice. Biomed Res Int. 2013(246861).

Chen J, Sasaguri K, Sodek J, Aufdemorte TB, Jiang H, Thomas HF. 1998. Enamel epithelium expresses bone sialoprotein (BSP). Eur J Oral Sci. 106(S1):331-336.

Fisher LW, Fedarko NS. 2003. Six genes expressed in bones and teeth encode the current members of the SIBLING family of proteins. Connect Tissue Res. 44(1):33-40.

Foster BL. 2012. Methods for studying tooth root cementum by light microscopy. Int J Oral Sci. 4(3):119-128.

Foster BL, Soenjaya Y, Nociti FH, Holm E, Zerfas PM, Wimer HF, Holdsworth DW, Aubin JE, Hunter GK, Goldberg HA et al. 2013. Deficiency in acellular cementum and periodontal attachment in Bsp null mice. J Dent Res. 92(2):166-172.

Frost HM. 1987. Bone "mass" and the "mechnostat': a proposal. Anat Rec. 219(1):1-9.

Fujisawa R, Butler WT, Brunn JC, Zhou HY, Kuboki Y. 1993. Differences in composition of cell-attachment sialoproteins between dentin and bone. J Dent Res. 72(8):1222-1226.

Ganss B, Kim RH, Sodek J. 1999. Bone sialoprotein. Crit Rev Oral Biol Med. 10(1):79-98.

Goldberg HA, Warner KJ, Hunter GK. 2001. Binding of bone sialoprotein, osteopontin and synthetic polypeptides to hydroxyapatite. Connect Tissue Res. 42(1):25-37.

Goldberg HA, Hunter GK. 2012. Functional domains of bone sialoprotein.In: Phosphorylated extracellular matrix proteins of bone and dentin. Goldberg M, editor. Oak Park (IL): Bentham Science Publishers; vol.2, p. 266-282.

Hansson S, Halldin A. 2012. Alveolar ridge resorption after tooth extraction: A consequence of a fundamental principle of bone physiology. J Dent Biomech. 3(1758736012456543).

Ho SP, Kurylo MP, Grandfield K, Hurng J, Herber R-P, Ryder MI, Altoe V, Aloni S, Feng JQ, Webb S et al. 2013. The plastic nature of the human bone–periodontal ligament–tooth fibrous joint. Bone. 57(2):455-467.

Holm E, Aubin JE, Hunter GK, Beier F, Goldberg HA. 2015. Loss of bone sialoprotein leads to impaired endochondral bone development and mineralization. Bone. 71(0):145-154.

Hunter GK, Goldberg HA. 1993. Nucleation of hydroxyapatite by bone sialoprotein. Proc Natl Acad Sci U S A. 90(18):8562-8565.

Kook S-H, Jang Y-S, Lee J-C. 2011. Human periodontal ligament fibroblasts stimulate osteoclastogenesis in response to compression force through TNF-α-mediated activation of CD4+ T cells. J Cell Biochem. 112(10):2891-2901.

Macneil RL, Sheng N, Strayhorn C, Fisher LW, Somerman MJ. 1994. Bone sialoprotein is localized to the root surface during cementogenesis. J Bone Miner Res. 9(10):1597-1606.

Malaval L, Wade-Guéye NM, Boudiffa M, Fei J, Zirngibl R, Chen F, Laroche N, Roux J-P, Burt-Pichat B, Duboeuf F et al. 2008. Bone sialoprotein plays a functional role in bone formation and osteoclastogenesis. J Exp Med. 205(5):1145-1153.

Malaval L, Monfoulet L, Fabre T, Pothuaud L, Bareille R, Miraux S, Thiaudiere E, Raffard G, Franconi J-M, Lafage-Proust M-H et al. 2009. Absence of bone sialoprotein (BSP) impairs cortical defect repair in mouse long bone. Bone. 45(5):853-861.

McKee MD, Zalzal S, Nanci A. 1996. Extracellular matrix in tooth cementum and mantle dentin: Localization of osteopontin and other noncollagenous proteins, plasma proteins, and glycoconjugates by electron microscopy. Anat Rec. 245(2):293-312.

Meikle MC. 2006. The tissue, cellular, and molecular regulation of orthodontic tooth movement: 100 years after Carl Sandstedt. Eur J Orthod. 28(3):221-240.

Milne TJ, Ichim I, Patel B, McNaughton A, Meikle MC. 2009. Induction of osteopenia during experimental tooth movement in the rat: alveolar bone remodelling and the mechanostat theory. Eur J Orthod. 31(3):221-231.

Popova SN, Barczyk M, Tiger C-F, Beertsen W, Zigrino P, Aszodi A, Miosge N, Forsberg E, Gullberg D. 2007. α11β1 integrin-dependent regulation of periodontal ligament function in the erupting mouse incisor. Mol Cell Biol. 27(12):4306-4316.

Qin C, Brunn JC, Jones J, George A, Ramachandran A, Gorski JP, Butler WT. 2001. A comparative study of sialic acid-rich proteins in rat bone and dentin. Eur J Oral Sci. 109(2):133-141.

Rios H, Koushik SV, Wang H, Wang J, Zhou H-M, Lindsley A, Rogers R, Chen Z, Maeda M, Kruzynska-Frejtag A et al. 2005. Periostin null mice exhibit dwarfism, incisor enamel defects, and an early-onset periodontal disease-like phenotype. Mol Cell Biol. 25(24):11131-11144.

Rios HF, Ma D, Xie Y, Giannobile WV, Bonewald LF, Conway SJ, Feng JQ. 2008. Periostin is essential for the integrity and function of the periodontal ligament during occlusal loading in mice. J Periodontol. 79(8):1480-1490.

Sanuki R, Shionome C, Kuwabara A, Mitsui N, Koyama Y, Suzuki N, Zhang F, Shimizu N, Maeno M. 2010. Compressive force induces osteoclast differentiation via prostaglandin E2 production in MC3T3-E1 cells. Connect Tissue Res. 51(2):150-158.

Sheng Z-F, Ye W, Wang J, Li C-H, Liu J-H, Liang Q-C, Li S, Xu K, Liao E-Y. 2010. OPG knockout mouse teeth display reduced alveolar bone mass and hypermineralization in enamel and dentin. Arch Oral Biol. 55(4):288-293.

Sodek J, McKee MD. 2000. Molecular and cellular biology of alveolar bone. Periodontol 2000. 24(1):99-126.

Tye CE, Hunter GK, Goldberg HA. 2005. Identification of the Type I collagen-binding domain of bone sialoprotein and characterization of the mechanism of interaction. J Biol Chem. 280(14):13487-13492.

Walker CG, Ito Y, Dangaria S, Luan X, Diekwisch TGH. 2008. RANKL, osteopontin, and osteoclast homeostasis in a hyperocclusion mouse model. Eur J Oral Sci. 116(4):312-318.

Wise GE, King GJ. 2008. Mechanisms of tooth eruption and orthodontic tooth movement. J Dent Res. 87(5):414-434.

Yadav MC, de Oliveira RC, Foster BL, Fong H, Cory E, Narisawa S, Sah RL, Somerman M, Whyte MP, Millán JL. 2012. Enzyme replacement prevents enamel defects in hypophosphatasia mice. J Bone Miner Res. 27(8):1722-1734.

Yoshinaga Y, Ukai T, Abe Y, Hara Y. 2007. Expression of receptor activator of nuclear factor kappa B ligand relates to inflammatory bone resorption, with or without occlusal trauma, in rats. J Periodontal Res. 42(5):402-409.

Zhang X, Rahemtulla F, Zhang P, Li X, Beck P, Thomas HF. 2009. Normalisation of calcium status reverses the phenotype in dentin, but not in enamel of VDR-deficient mice. Arch Oral Biol. 54(12):1105-1110.

CHAPTER 4

4 Healing of rat calvarial defects with nano-hydroxyapatite/ poly(ester-urethane) scaffolds loaded with low dose rhBMP-2

4.1 INTRODUCTION

Large bone defect repair generally requires surgical intervention and the use of biomaterials, combined with growth factors, as a temporary filler to promote *de novo* bone formation. Various biomaterials such as autologous bone, allogeneic devitalized bone, resorbable ceramics, polymers, and ceramic/polymer composite have been used in clinical and research settings to enhance bone repair. In general, biomaterials need to provide structure, rigidity, and a medium that enables cell and blood vessel infiltration.

Due to the lack of osteoinductive property of most synthetic biomaterials, recombinant human bone morphogenetic protein-2 (rhBMP-2), which is one of the most prevalent growth factor used clinically due to its high potency to induce bone formation, are commonly added to scaffolds to promote tissue regeneration. Of relevance, various studies have shown that the addition rhBMP-2 is effective in promoting the in-growth of cells and bone tissue regeneration (Brown et al., 2011; Fricain et al., 2013; Kim and Hollinger, 2012; Li et al., 2009). Since rhBMP-2 has been shown to be primarily activated during fracture healing (Yu et al., 2010), it is important to maintain the presence of rhBMP-2 at the defect site during the bone repair process. For clinical application, in 2002, the Federal Drug Administration approved the InFUSE^{TM} bone graft, which is a porous collagen sponge that acts as a vehicle to deliver 12 mg of rhBMP-2. However, this high dose of rhBMP-2 is required to be clinically effective due to the poor retention of the growth factor in the collagen sponge. Not only is rhBMP-2 costly, but at high doses, patients would be at potential risks of adverse side effects that includes heterotopic bone formation, unnecessary immune response and even cancer (Carragee et al., 2011; Epstein, 2013). Since retention and slow release from scaffolds would be optimum, it is important to develop a strategy that utilizes appropriate biomaterials with the right properties as a carrier of low dose rhBMP-2, without compromising its effectiveness. Here, for the first time, we investigate the effectiveness of a novel poly(ester-urethane) (PU) scaffolds incorporated with nano-sized hydroxyapatite (nHA) as the carrier of rhBMP-2, and mediator of bone repair.

In recent years, PU-based scaffolds have been extensively developed and shown to have potential applications for the tissue regeneration. Various studies have demonstrated

success using PU-based scaffold for tissue repairs in bone (Hofmann et al., 2008; Kavlock et al., 2007; Li et al., 2009), cartilage (Dresing et al., 2014; Lee et al., 2005), and other soft tissues (Gogolewski et al., 2008; Guan et al., 2005; Guelcher, 2008; Guelcher et al., 2008). The PU-based scaffolds used in this study were designed to have porous interconnected network that allows for cell and blood vessel infiltration (Laschke et al., 2009; Laschke et al., 2013). In addition, the scaffolds are biocompatible and have viscoelastic property for easy physical fitting into the bone defects, as shown in previous studies (Hofmann et al., 2008; Laschke et al., 2009; Laschke et al., 2013; Lee et al., 2005; Pirvu et al., 2015). Furthermore, the incorporation of nHA particles into the PU matrix was able to improve its material stiffness (Boissard et al., 2009) and increased its capacity to bind proteins such as serum albumin and fibrinogen (Laschke et al., 2010b). The incorporation of nHA particles did not appear to affect the scaffolds' biocompatibility and ability to allow for angiogenesis to proceed within its porous network (Laschke et al., 2009).

In this study, *in vitro* experiments were done on the novel nano-sized hydroxyapatite-incorporated poly(ester-urethane) (nHA/PU) scaffolds to determine the ability of the biomaterial to support osteoblastic cell culture. In addition, a well-established rat calvarial defect model (Cacciafesta et al., 2001; Kim et al., 2008; Mardas et al., 2008; Sawyer et al., 2009) was also utilized to validate the effectiveness of the nHA/PU scaffolds in delivering low-dose rhBMP-2 for guided bone regeneration. The bone repair were assessed using micro-computed tomography (microCT), histology and mechanical testing.

4.2 MATERIALS AND METHODS

4.2.1 Scaffold preparation

The biodegradable PU solution was synthesized in a one-step solution polycondensation as previously described in detail (Laschke et al., 2010b). The process involved the use of 1,6-hexamethylene diisocyanate (Sigma-Aldrich, Milwaukee, WI), poly(ε-caprolactone)

diol (M_W = 530 g mol^{-1}, Sigma-Aldrich, Milwaukee, WI), and 1,4,3,6-dianhydro-D-sorbitol as reactants. Dibutyltin dilaurate (Fluka, Buchs, CH) was used a catalyst for the reaction and N,N-dimethylformaide (Fluka, Buchs, CH) was used as a solvent. To create nHA/PU solution, nHA (Biomaterials US, Ltd., USA) particles, ranging in size from 50 to 200 nm, were dispersed into a PU solution. The nHA mass fraction added was 10 wt.% of the PU solution. Prior to usage, the nHA particles were washed with ethanol and dried at 100°C under vacuum (Laschke et al., 2010b). The nHA/PU scaffolds were prepared using a salt leaching-phase inverse process as previously described (Boissard et al., 2009; Gorna and Gogolewski, 2006; Laschke et al., 2010b). This method involved a vigorous mixing of nHA/PU solution with porogen (sodium phosphate heptahydrate dibasic salt; Fluka, Buchs, CH) until a homogeneous paste was obtained. The paste was then poured into a cylindrical mould and left in air to allow for slow evaporation of the solvents. The salt was leached out by extensive washing in water, which created porous nHA/PU sponges. In order to produce scaffolds of consistent thickness, the sponges were cut using a water jet system. In this study, the scaffolds were prepared with a circular dimension of 5.5 mm and 1 mm thickness with pore sizes ranging from 90 to 300 μm. The scaffolds were washed in ethanol, dried under vacuum, and sterilized in ethylene oxide prior to use in the studies.

4.2.2 *In vitro* rhBMP-2 release kinetics

Three nHA/PU scaffolds were each incubated with 1 μg of rhBMP-2 (R&D systems, Minneapolis, MN) diluted into 25 μl of saline solution for 24 h at 4°C. Control scaffolds were incubated in an equal volume of saline. After 24 h incubation, each scaffold was immersed and agitated in 1 ml of phosphate buffered saline (PBS) to remove unbound rhBMP-2. To determine the release kinetics of the bound rhBMP-2 from the nHA/PU scaffolds, the samples were further incubated at 37°C in 1 ml PBS in microcentrifuge tubes. At 3, 24 and 72 h, the PBS solutions were replaced with fresh PBS and 100 μl of the supernatant used to quantify the concentration of the rhBMP-2 using a Human BMP-2 Quantikine ELISA kit (R&D systems, Minneapolis, MN) according to the

manufacturer's instructions. The accumulated rhBMP-2 release kinetics were expressed as percentage of the rhBMP-2 bound to the nHA/PU scaffold.

4.2.3 Cell isolation, culture conditions and cell viability

Bone marrow was isolated from male Sprague-Dawley rats (Charles River Laboratories International, Wilmington, MA) aged 11-12 weeks (325-375 g) by flushing the tibia and femur marrow canal with culture medium consisting of Iscove's Modified Dulbecco's Medium (IMDM) supplemented with 10% fetal bovine serum (FBS), 1% penicillin-streptomycin and 1% L-glutamine (Life Technologies, Carlsbad, CA). The recovered cells enriched in mesenchymal stromal cells (MSC) were cultured in culture medium in 75 mm^2 flasks (NUNC) at 37°C in 5% CO_2 for 3 days, and then sub-cultured using 0.05% Trypsin-EDTA solution. Cells at passage 2 were used for subsequent studies.

Prior to cell seeding, the nHA/PU scaffolds (n=3 for each group; experiment conducted in triplicate) were incubated for 24 h at 4°C with either 25 µl saline solution or 1 µg of rhBMP-2 in 25 µl saline solution. In addition, nHA/PU scaffolds that were pretreated with 1 µg rhBMP-2 and used in the 72 h rhBMP2 release kinetics study were also used in the studies outlined below. Rat MSC were seeded onto the control and rhBMP2-pretreated nHA/PU scaffolds at a density of 3.5×10^5 cells/scaffold and incubated in 24-well plates (NUNC). After 1 h incubation, the MSC-seeded scaffolds were placed between a sandwich construct consisting of 2 Teflon-rings in a clean 24-well plate in order to fully immerse the scaffolds in culture medium. The MSC-seeded scaffolds were then cultured in osteoblast differentiating medium consisting of culture medium supplemented with 50 µg/ml ascorbic acid and 2 mM β-glycerophosphate. The mineralizing medium was changed every 2 days for the duration of the culture. For a control group, nHA/PU scaffolds with no cells were also incubated with differential media.

After 4 weeks of culture, the scaffolds were washed with Hank's Balanced Salt Solution (HBSS) three times, fixed with 4% paraformaldehyde for 20 min, and processed for cryo-

section. In order to determine the relative level of matrix mineralization, the cryosectioned scaffolds were stained for calcium mineral deposition with Alizarin red staining solution (1% w/v, Ricca Chemical company, Arlington, TX) for 20 min at room temperature. To remove excess dye, the sections were washed with deionized water three times (5 min incubation time for each wash).

4.2.4 Scanning Electron Microscopy (SEM) analysis

nHA/PU scaffolds cultured with MSC for up to 4 weeks were fixed with 4% glutaraldehyde solution (Sigma-Aldrich, Oakville, ON) for 15 min, after which the scaffolds were gently rinsed three times with Phosphate Buffered Saline (PBS) solution. Samples were dehydrated in a series of ethanol dilutions (25%, 50%, 75%, 90% and 100%) for 5 min at each concentration and then air-dried. The samples were osmium-coated, and imaged with a Leo 1540 XB FIB/SEM using secondary electron mode at 1-20 kV (Carl Zeiss, Western Nanofabrication Facility, University of Western Ontario, London, ON).

4.2.5 Animals and surgery

Male Sprague-Dawley rats aged 11-12 weeks (325-375 g) were maintained on a standard rat diet (5P00-Prolab RMH 3000; LabDiet, St. Louis, MO). Animal experiments were conducted in accordance with guidelines of the Canadian Council on Animal Care (CCAC) and Animal Care and Veterinary Services (ACVS), University of Western Ontario.

Animals were anaesthetized with isoflurane gas and the heads positioned in a stereotaxic frame. The dorsal part of the cranium was shaved, aseptically prepared, and a midline incision of approximately 20 mm created. The skin flaps were kept opened using a retractor and the underlying periosteum was removed. A 5-mm stainless steel trephine drill (Salvin Dental Specialties, Charlotte, NC) was used to create circular defects on

each of the parietal bones, thus creating 2 defects in each rat. The diameter of the wound is usually slightly larger at approximately between 5.1 to 5.3 mm. Caution was exercised to prevent damage to the dura membrane by adding a custom-made stainless steel sleeve (1.5 mm depth shorter) around the trephine drill. In addition, in order to prevent heat damage of the host bone, irrigation with saline solution was done throughout the procedure. The nHA/PU or rhBMP-2 (1 μg) treated nHA/PU (nHA/PU/rhBMP-2) scaffolds without any cells were then implanted and secured in place by double crossing 4-0 Vicryl suture attached to the temporalis muscles. The amount of rhBMP-2 used per scaffold in the study was determined by previous studies that used low dose of rhBMP-2 (La et al., 2010; Schofer et al., 2011b). For the negative control group, the defect holes were left empty without any double crossing suture. In order to prevent any contamination, both defects in each rat were implanted with scaffolds of the same treatment group. The skin was closed using 4-0 Silk sutures. Antibiotics and analgesic were administered to the animals and they were allowed to recover for up to 12 weeks post surgery, after which they were euthanized with CO_2 gas inhalation according to CCAC and ACVS guidelines. At 6 and 12 weeks post-op, the implants and surrounding bone were recovered, fixed with 10% buffered formalin overnight at 4°C and prepared for histology. Samples for mechanical testing were not fixed but stored in HBSS containing 0.10% sodium azide.

4.2.6 In vivo micro-computed tomography analysis

At 0, 2, 6, 12 weeks post-op, animals were anaesthetized with isoflurane gas and placed in a microCT scanner (eXplore speCZT; GE Healthcare, London, ON). The scans were performed using a standardized live-animal protocol (90 kVp, 40 μA, 900 views, 16 ms per view). Images were reconstructed at a spatial resolution of 50 μm and calibrated with a cortical bone phantom (SB3; Gammex RMI, Middleton, WI) having a hydroxyapatite equivalent of 1,100 mg/cc (White, 1978). Data were analyzed with MicroView ABA version 2.2 (GE Healthcare).

In order to visually determine the new bone formation, the 2D Maximum Intensity Projection (MIP) and 3D isosurface images of the rat calvarial bones defect sites were constructed. As for the quantification of the newly formed bone, a cylindrical region of interest (ROI, 5 mm x 1.5 mm) was positioned within the center of each defect site. The bone mineral content (BMC) within the ROI was determined linearly by assigning a value threshold for air (-1000 Hounsfield unit (HU)), water (0 HU), soft tissues (below 700 HU), trabecular bone (above 700 HU), cortical bone (above 1700 HU) and SB3 phantom (2700 HU). The total new bone volume (BV) formation was determined by adding all the voxels with HU value above 700 within the ROI. Bone-to-total tissue volume ratio (BV/TV) was determined by calculating the ratio of total voxels with HU value above 700 over the total voxels of the ROI. As for the cortical bone volume (CBV), only voxels with HU above 1700 were considered for calculation. Twenty calvarial defects were measured at 2 and 6 weeks and twelve calvarial defects were measured at 12 weeks for each group (nHA/PU and nHA/PU/rhBMP-2 up to 12 weeks; empty control only up to 6 weeks).

4.2.7 **Histological Analysis**

The parietal bones were fixed with 10% formalin for 24 h and then decalcified in 0.65 M ethylenediaminetetraacetic acid (EDTA) disodium salt dihydrate, pH 7.4, at 37°C for 2 weeks. After dehydration, the samples were embedded in paraffin, and sectioned at 5 μm thickness. The sagittal sections were stained with hematoxylin and eosin (H&E) and Masson's Trichrome (MT). The percentage of new bone area in the defect was quantified for each treatment group by comparing pixel quantities using image J. Color threshold tools in Image J were used to differentiate pixels correspond to new bone or other non-mineralized soft tissue.

4.2.8 Mechanical Testing

The implants with surrounding parietal bones were recovered (undecalcified) , stored in HBSS containing 0.10% sodium azide overnight and then tested on an Instron machine (ElectroPuls E1000, Instron, Norwood, MA). Native bone samples were also used for comparison. For the mechanical testing, a custom-made stainless steel push-out test jig was made. The base and cap had a 5.5-mm hole in the center to allow for the penetration of the cylindrical punch during testing. Each specimen was then mounted with cyanoacrylate adhesive onto the base and adjusted to make sure that the center of the implant was aligned with the center of the hole. The cap was then placed and tightened in order to prevent bowing of the specimen during testing.

Indentation tests on the center of implants were performed using the Instron machine with a 100-N load cell and 1-mm diameter indenter in order to assess the quality of the newly formed bone within the defects. The rate of indentation was 1 mm/min to a maximum load of 2N (± 0.003N). The load and displacement data were recorded during the testing procedure and the elastic modulus was calculated with the following formula used in previous studies. (McKee et al., 2011a; McKoy et al., 1999):

$$E = S(1 - v^2)/d$$

Where S is the indentation stiffness or the slope of the load-displacement in its linear region (N/mm) and d (mm) is the diameter of the indenter. The Poisson's ratio (v) of bone was assumed to be 0.3 (Busa et al., 2005). Five to eight specimens were used for each group.

Push-out tests were conducted to evaluate the osteointegration of the implant with the surrounding host calvarial bone using the Instron machine with a 2-kN load cell and 1 mm/min rate. An indenter probe of 5-mm diameter with a flat polished end was fabricated for the test. Load and displacement data were recorded during the testing procedure and all specimens were tested to failure. Five to seven specimens were used for each group.

For both mechanical test, intact native rat parietal bones of the same age were used as controls.

4.2.9 Statistical Analyses

Quantitative data were expressed as means ± standard error. Statistical analyses among groups were performed using two-way analysis of variance (ANOVA) and Bonferroni post-tests with Prism 5 version 5.03 (GraphPad Software, La Jolla, CA). $p<0.05$ was considered to be statistically significant.

4.3 RESULTS

4.3.1 Cells adhesion and nHA/PU scaffold properties

The sponge-like nHA/PU scaffolds are comprised of a network of multi inter-connected channels with pore sizes that varied from 90-300 μm (Figure 4.1 A1-E1). To determine whether cells attach, spread out and thrive in the scaffold, rat long bone MSC cells at passage 2 were seeded onto the scaffold and cultured for 2 or 4 weeks, fixed and observed by SEM. The images demonstrate cells adhering to the wall of the internal pores in the scaffolds (Figure 4.1 C2 and C3). In addition, collagen fibrils are also evident (Figure 4.1 E2 and E3). These data showed that the nHA/PU scaffold is a biocompatible surface that permits MSC attachment and secretion of extracellular matrix.

4.3.2 *In vitro* bioactivity of bound rhBMP-2

In order to determine whether the nHA/PU scaffolds binds rhBMP-2 and releases it over time, the release profiles of rhBMP-2 from the scaffolds were determined (Figure 4.2). Of the 1 μg added to the scaffold, approximately 8.77 ± 1.25% of the rhBMP-2 was not bound. After a 3 h incubation period, approximately 5% of the originally bound rhBMP-

2 was released into the incubation medium. At 24 and 72 h incubation period, only very low levels (a total of less than 2%) of the growth factor were released. These results imply that the nHA/PU scaffolds were able to retain the bound rhBMP-2 very well.

After the 72 h incubation period, no direct measurement of bound rhBMP-2 was attempted due to the harsh demineralizing and denaturing solutions that would be required to recover the rhBMP-2 from the scaffold. However, to confirm the presence of bioactivity of the growth factor, these nHA/PU/rhBMP-2 scaffolds, after the 72 h incubation and buffer exchanges, were seeded with MSC and cultured in differentiation media for 4 weeks. The control groups included untreated scaffolds and scaffolds treated with fresh 1 μg rhBMP-2 incubated overnight at 4°C without washing, prior to MSC seeding. Both rhBMP-2 treated scaffold groups appeared to have enhanced mineralization based on Alizarin Red staining, compared to the control untreated scaffold group with or without cells (Figure 4.3 A and B). Minimal red staining were observed in groups without any cells seeded after 4 weeks cultured with differential media. These results suggest that even after incubation for 72 h, with buffer exchanges, the rhBMP-2 treated scaffolds still retained activity consistent with the presence of rhBMP-2.

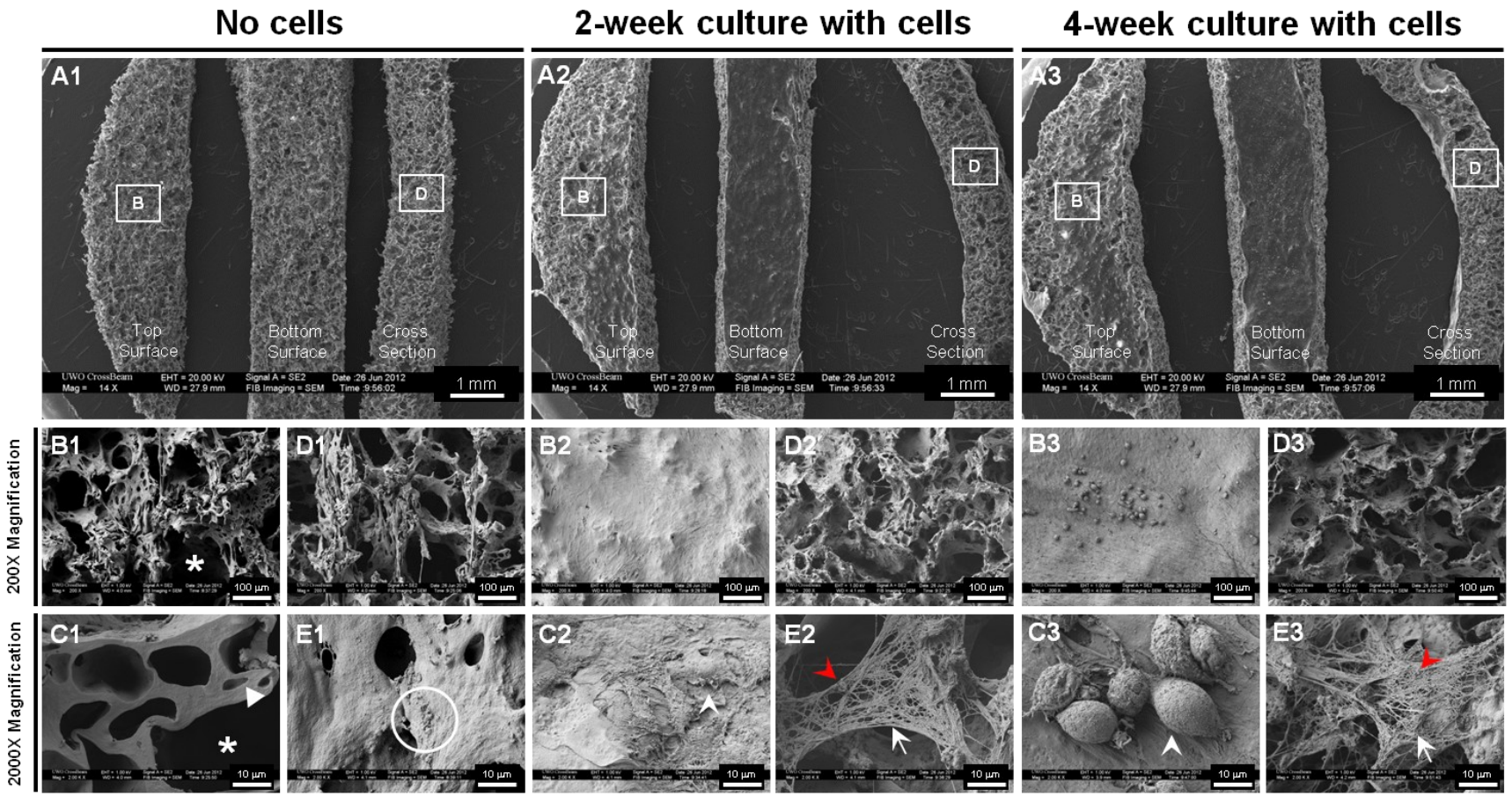
No cells
2-week culture with cells
4-week culture with cells
A1
A2
A3
B
D
Top Surface
Bottom Surface
Cross Section
1 mm
200X Magnification
2000X Magnification
B1
D1
B2
D2
B3
D3
C1
E1
C2
E2
C3
E3
100 µm
10 µm

Figure 4.1. SEM images of nHA/PU scaffolds incubated with mesenchymal stromal cells (MSC).

Panels **A1-3** are representative images of the surface and cross-sectional area of the nHA/PU scaffold with or without cell culture. Panels **B1-3** and **D1-3** are 200X magnification of the area marked by white boxes as shown in panel **A**. At higher magnification **(C1, E1),** inter-connected pores can be seen in the nHA/PU scaffolds. Macro (white star) and micro (white triangle) pores ranging from 90 to 300 μm and aggregates of hydroxyapatite nanoparticles (white circle) are evident in the nHA/PU scaffold. By 2 weeks, extracellular matrix made by the cells can be observed covering the surface of the scaffold **(B2,B3)**. At 2 (**C2, E2)** and 4 weeks **(C3, E3)**, cells (white arrow head) were seen adhering on the walls of the nHA/PU scaffolds. Collagen fibrils (white arrow) secreted by the cells and aggregates of hydroxyapatite (red arrow head) were observed on the walls and across the pores of the nHA/PU scaffolds.

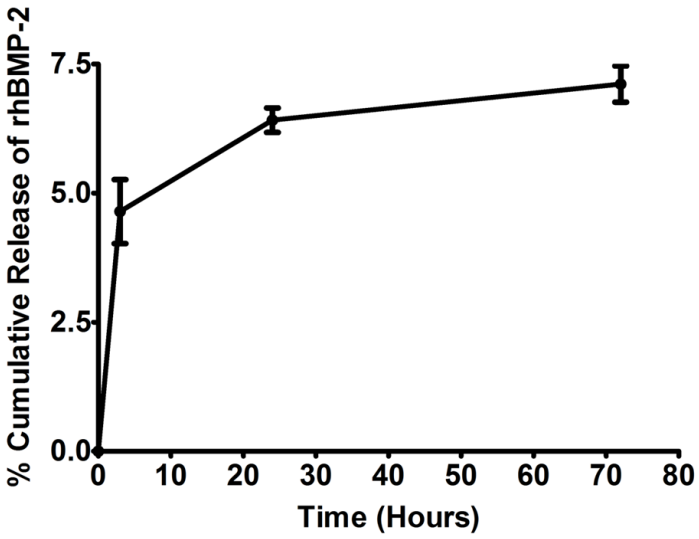

Figure 4.2. ***In vitro*** **cumulative release of rhBMP-2 from nHA/PU scaffolds.**

At 72 h, only approximately 7% of the originally bound rhBMP-2 was released from the scaffold. n=3

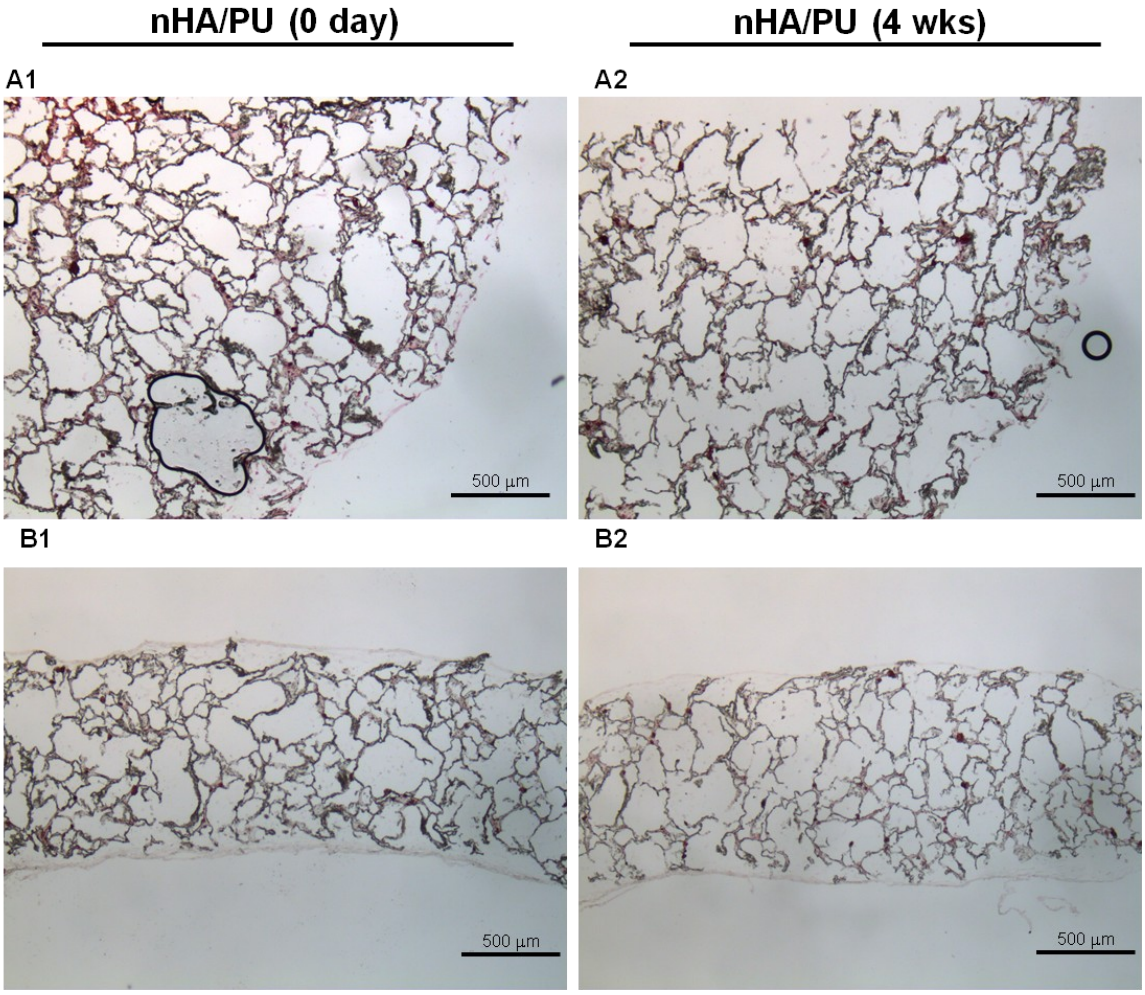

Figure 4.3A. Control nHA/PU scaffolds show minimal alizarin red staining.

The images in panel A1-2 and B1-2 represent transverse and cross-sectional sections, respectively, of control nHA/PU scaffolds without cells stained with alizarin red. The nHA/PU scaffolds were incubated with differential media for 0 day and 4 weeks. At both time point, minimal red staining was observed.

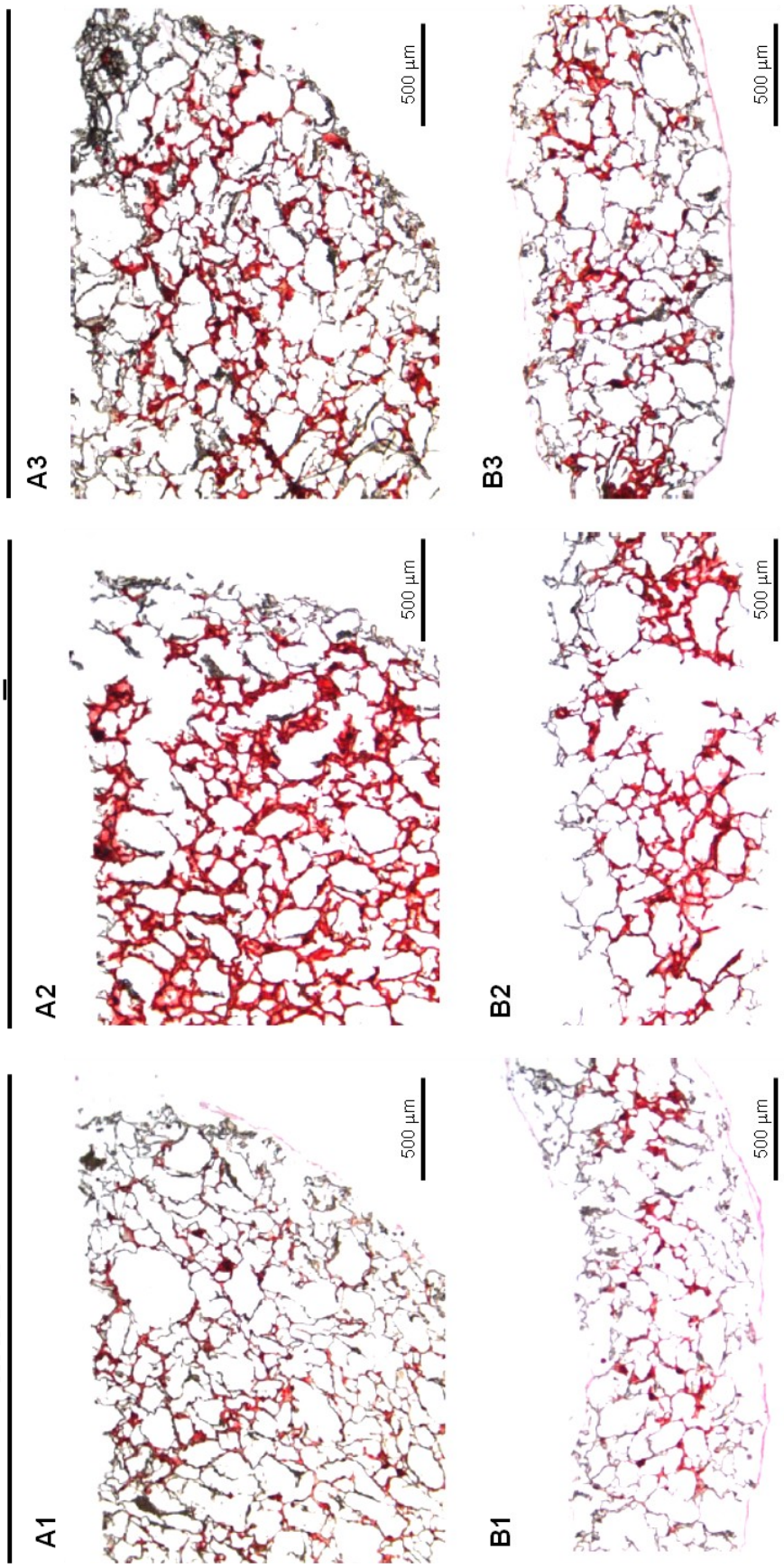
nHA/PU
nHA/PU/rhBMP-2_72hrs
nHA/PU/rhBMP-2
A1
A2
A3
B1
B2
B3
500 µm
500 µm
500 µm
500 µm
500 µm
500 µm

Figure 4.3B. The presence of rhBMP-2 in nHA/PU scaffold increased matrix mineralization when cultured with MSC cells.

The images in panel A1-3 and B1-3 represent transverse and cross-sectional sections, respectively, of treated and control nHA/PU scaffolds stained with alizarin red. The histology sections of nHA/PU/rhBMP-2_72h group appears to have similar quantity of alizarin red staining compared to nHA/PU/rhBMP-2 group, which confirms that a significant proportion of the rhBMP-2 remains associated with the nHA/PU scaffolds even after 72 h of incubation and 3 washes. Both nHA/PU groups treated with rhBMP-2 qualitatively appear to have elevated alizarin red staining compared to nHA/PU control group.

4.3.3 rhBMP-2 treated nHA/PU scaffolds promote bone repair

An established rat calvarial defect model was used to determine whether the rhBMP-2 treated nHA/PU scaffolds (nHA/PU/rhBMP-2) promotes *in vivo* bone repair. At 2 weeks post-op, bone in-growth into the defects from host bone and some island-like bone spicules were observed in the nHA/PU/rhBMP-2 group, indicated by faint grey coloring in the MIP images that filled the defects (Figure 4.4). This was not observed in the untreated nHA/PU control group. At 6 weeks, the defect sites of the rhBMP-2 treated group were filled with apparent bone, whereas minimal bone formation was observed in the untreated nHA/PU control group. Even after 6 weeks, for the group with empty hole, no new bone formation was observed in the middle of the defects (data not shown). Most of the very limited bone in growth was from the periphery of the defects. Therefore no further measurement was conducted for this group.

The bone mineral content (BMC), new total bone volume (BV), percentage of bone-to-tissue volume (BV/TV) and cortical bone volume (CBV) of the nHA/PU/rhBMP-2 group were significantly higher compared to nHA/PU group at all three time points (Figure 4.5A to D). Interestingly, between 6 and 12 weeks, no significant increase in new bone formation was observed in either group as shown in Figure 5B and C. However, the BMC values at 12 weeks were significantly higher compared to values at 6 weeks, which was likely due to the continuous process of remodeling and densification of the newly formed bone. This was confirmed by the observed significant increase in percentage of CBV between the three time points for both nHA/PU/rhBMP-2 and control groups (Figure 4.5D).

Detailed histological analysis confirmed that rhBMP-2 treated nHA/PU scaffolds enhanced bone formation *in vivo* compared to the control scaffolds (Figure 4.6). At 6 weeks, compared to the control group, the nHA/PU/rhBMP-2 group demonstrated significantly more new bone formation. This is indicated by union bone formation adjacent to the dura-membrane and island-like bone spicules throughout the defect sites. At higher resolution, fibrous tissue and individual island-like bone spicules, of which some appeared to contain osteons, can be seen forming in the defects of both groups.

However, the amount of fibrous tissue appears to be greater in the control group compared to the nHA/PU/rhBMP-2 group (Figure 4.6, panels C and D). Quantitative measurements on histological sections were also done to determine the amount of new bone formed in the defects. At both 6 and 12 weeks, nHA/PU/rhBMP-2 group showed significantly more new bone area compared to nHA/PU group (Figure 4.7). However, similar to microCT analysis, the histological analysis demonstrated that similar amount of total bone formation was observed for both groups. This result confirmed that, after 6 weeks post-op, minimal increase of new bone formation was observed for both groups.

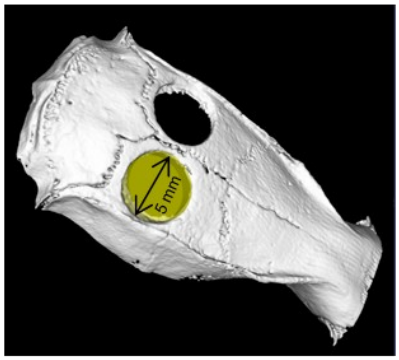
5 mm

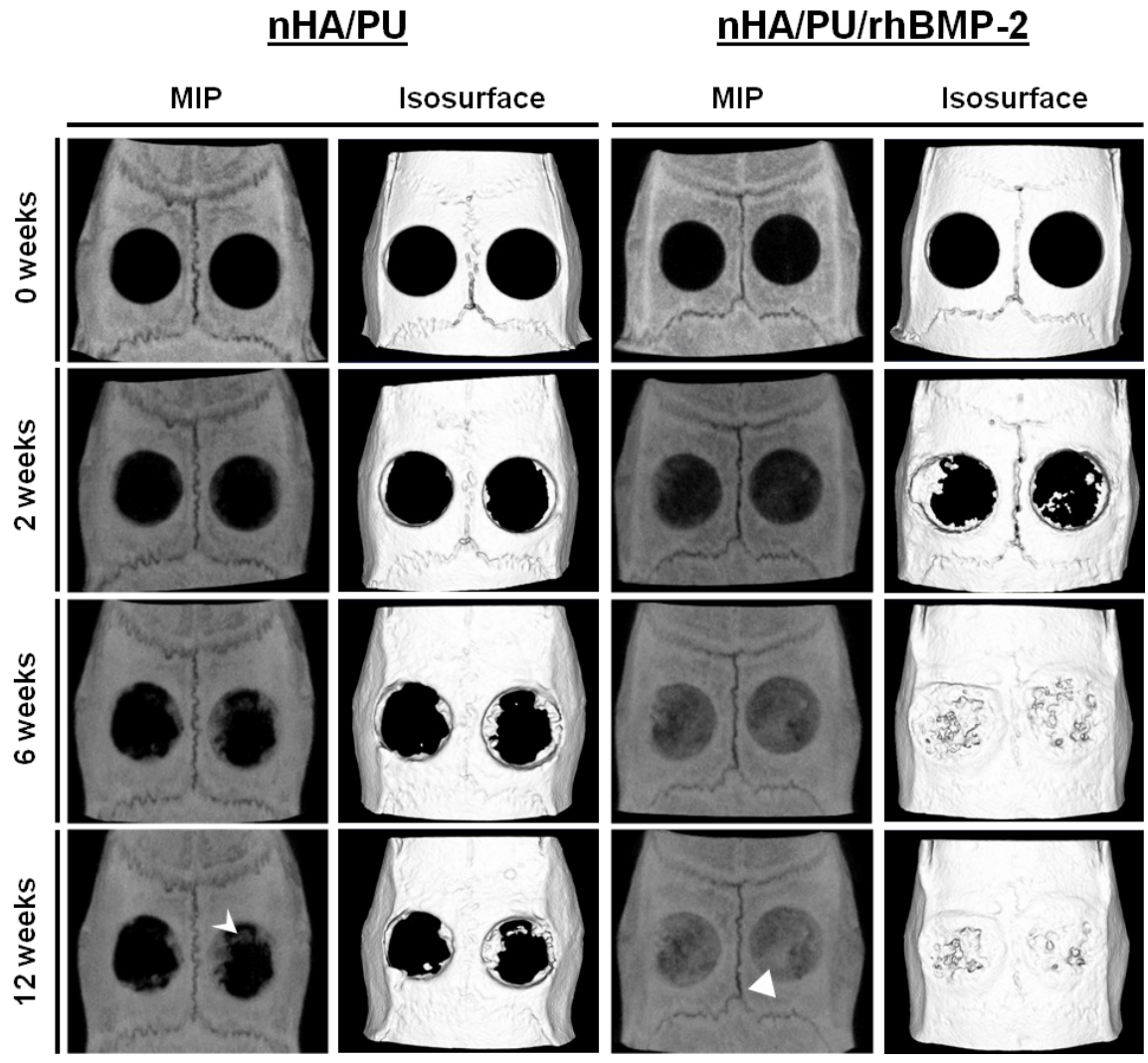
nHA/PU
nHA/PU/rhBMP-2
MIP
Isosurface
MIP
Isosurface
0 weeks
2 weeks
6 weeks
12 weeks

Figure 4.4. MicroCT images of bone repair for nHA/PU and nHA/PU/rhBMP-2 groups.

Maximum Intensity Projection (MIP) and 3D isosurface images of rat calvarial defects indicate that the presence of rhBMP-2 enhanced bone formation in the calvarial defect sites. By 6 weeks, new bone fills most of the defect site in the nHA/PU/rhBMP-2 scaffold group and the radiodensity of the newly formed bones also appeared to be more dense over time, which is an indication of increasing mineral content. The image on the left describes the cylindrical region of interest (ROI), coloured yellow to highlight area that was analyzed. (n=12 for 2 and 6 weeks, n=20 for 12 weeks)

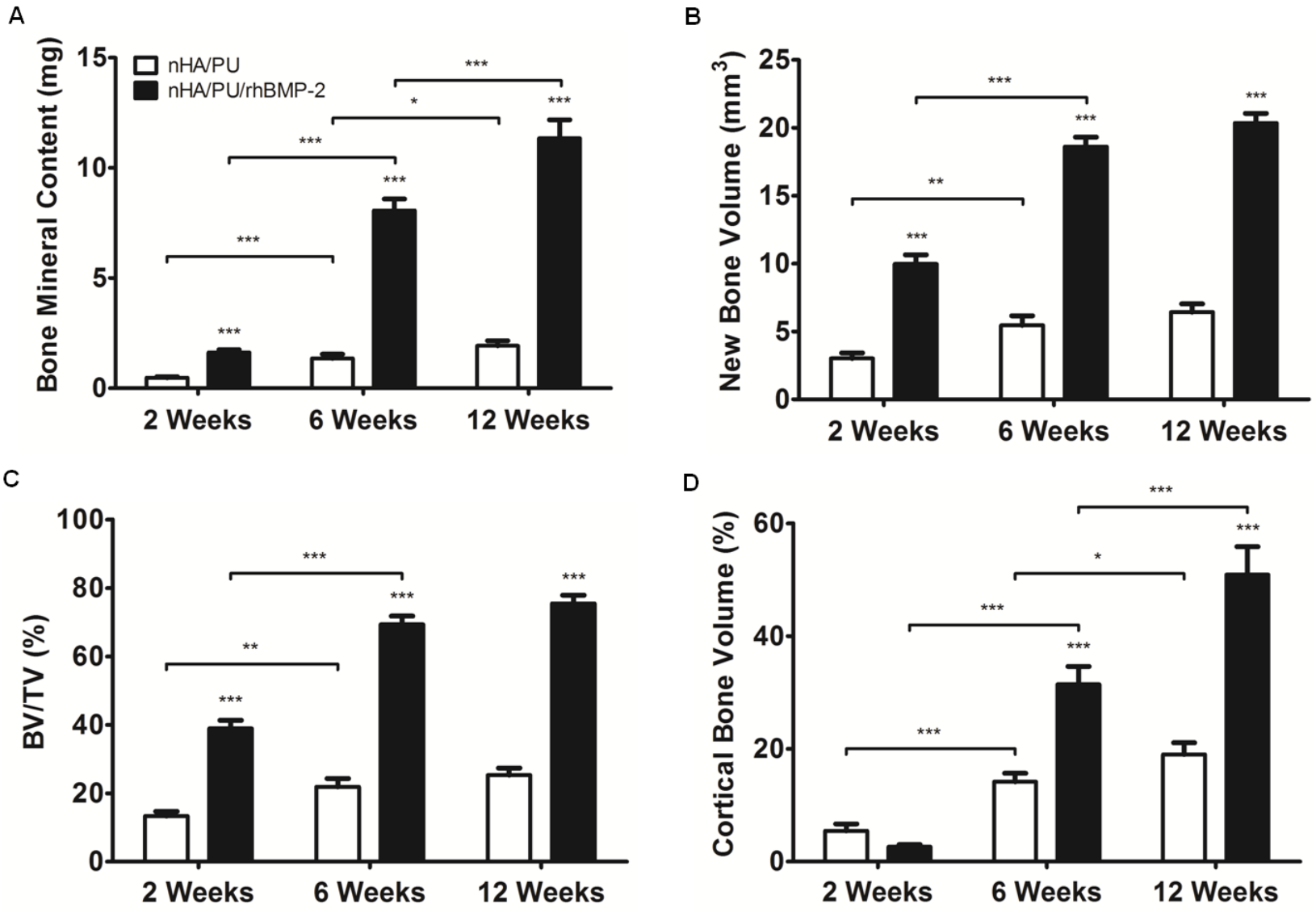
A
Bone Mineral Content (mg)
nHA/PU
nHA/PU/rhBMP-2
2 Weeks
6 Weeks
12 Weeks
B
New Bone Volume (mm3)
C
BV/TV (%)
D
Cortical Bone Volume (%)

Figure 4.5. Quantitative microCT analysis of bone repair.

MicroCT analysis showed that **(A)** bone mineral content (BMC); **(B)** new bone volume (BV); **(C)** percentage of bone-to-tissue volume (BV/TV) and **(D)** percentage of cortical bone volume, were enhanced in nHA/PU/rhBMP-2 scaffold group compared to nHA/PU scaffold group at 6 and 12 weeks. Data represents mean ± standard error (n=20 for 2 and 6 weeks, n=12 for 12 weeks, *$p<0.05$, **$p<0.01$, ***$p<0.001$).

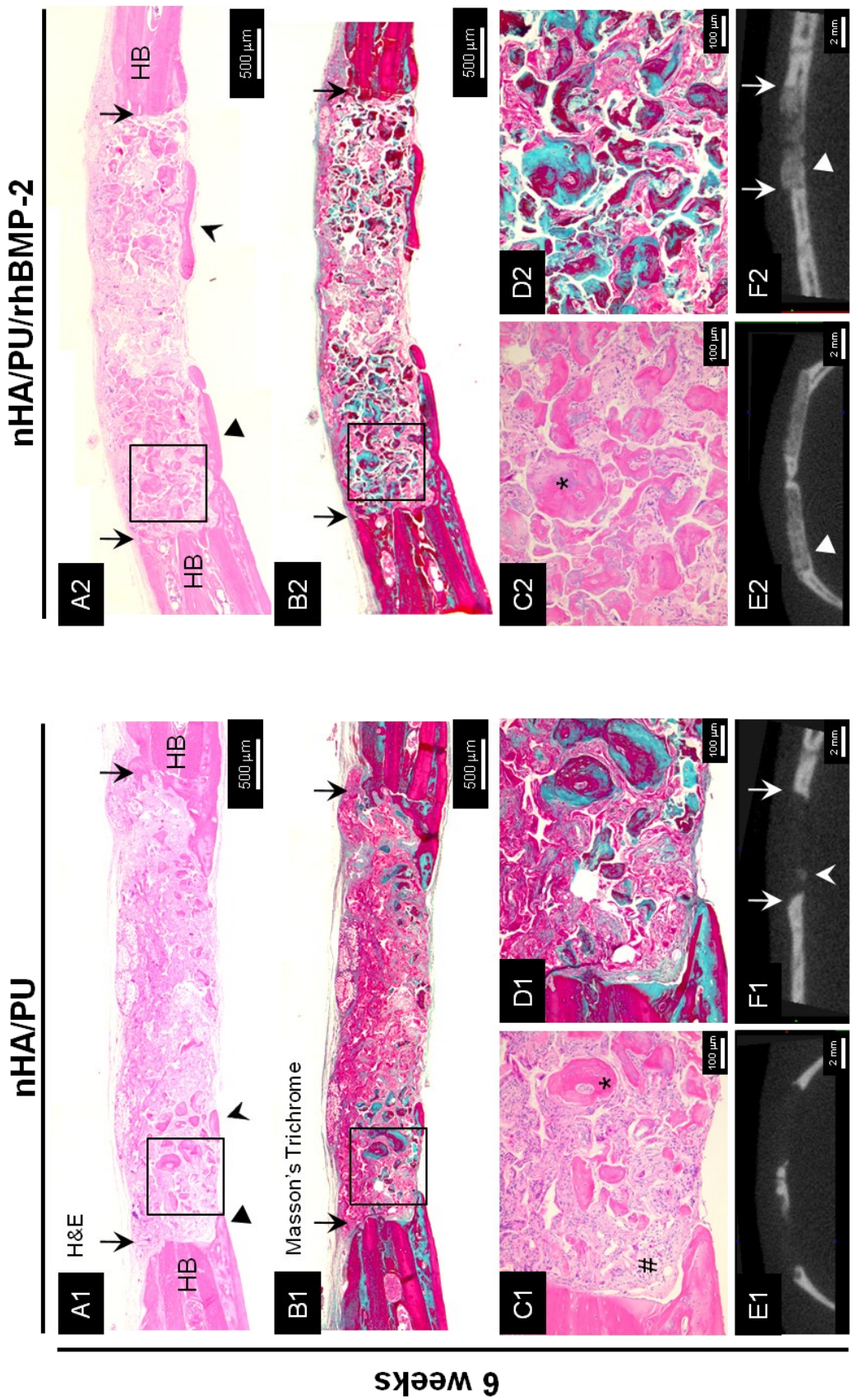
nHA/PU
nHA/PU/rhBMP-2
6 weeks
A1
H&E
HB
HB
500 µm
B1
Masson's Trichrome
500 µm
C1
*
#
100 µm
D1
100 µm
E1
2 mm
F1
2 mm
A2
HB
HB
500 µm
B2
500 µm
C2
*
100 µm
D2
100 µm
E2
2 mm
F2
2 mm

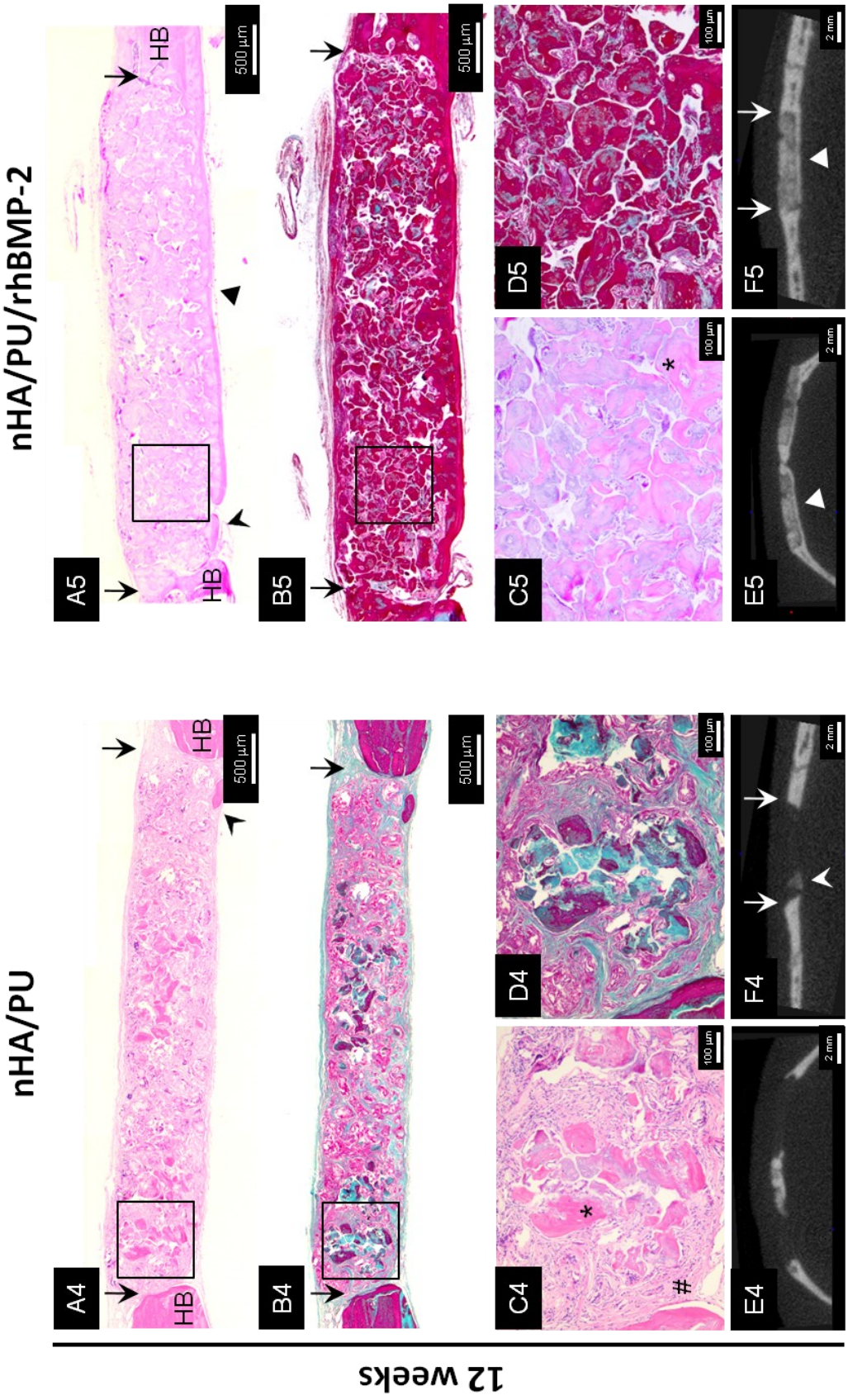
nHA/PU
nHA/PU/rhBMP-2
12 weeks
A4
B4
C4
D4
E4
F4
A5
B5
C5
D5
E5
F5
HB
500 µm
100 µm
2 mm
*
#

Figure 4.6. Histology and microCT analysis of rat calvaria at 6 and 12 weeks.

Both microCT and histology analyses confirmed that the presence of rhBMP-2 in nHA/PU scaffolds enhanced bone formation *in vivo*. **(Panel A and B)** Sagittal sections of nHA/PU/rhBMP-2 group showed extensive bone healing compared to nHA/PU group. Staining consists of H&E (Panel A and C; dark pink – mineralized bone) and Masson's Trichrome (**Panel B and D**; teal – collagen and less mineralized bone, dark purple red – mature bone). Arrows indicate edge of the bone defect adjacent to host bone (HB). Arrowheads indicate island-like new bone formation in the defect sites. Triangle indicates continuous in-growth of new bone formation from the host bone adjacent to the dura membrane. **(Panel C and D)** At a higher magnification, defects containing nHA/PU scaffolds are predominately filled with fibrous tissue (#); however, mineralized bone (*) can also be observed. For the nHA/PU/rhBMP-2 scaffold group, island-like bone formation can be seen throughout the defect; especially at 12 weeks post-implantation. MicroCT images of coronal **(Panel E)** and sagittal **(Panel F)** sections confirm the demonstration of new bone formation indicated by histology.

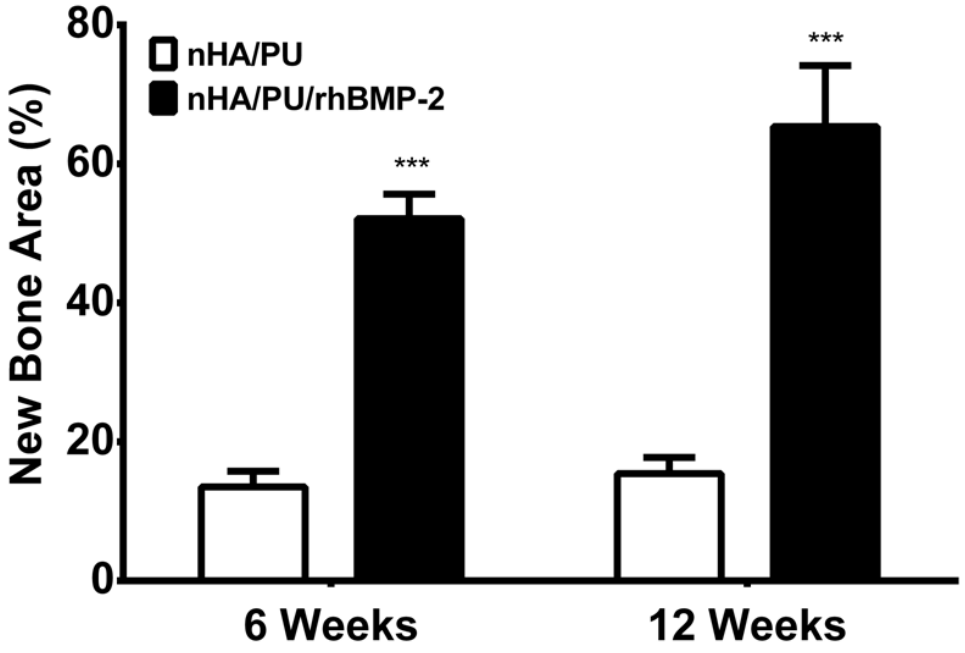

Figure 4.7. Quantitative histological analysis of explanted tissues at 6 and 12 week.

For both time points, nHA/PU/rhBMP-2 group have significantly higher amount of new bone area within the original defect compared to nHA/PU group. Data represents mean ± standard error (n=8 for both 6 and 12 weeks, ***$p<0.001$).

4.3.4 Mechanical test analysis

To test the mechanical property of the newly formed bone and degree of osteointegration of implant-host bone, push-out and indentation tests were performed on the bone repair sites. Based on the indentation experiments, at 6 weeks, the elastic modulus was significantly higher (15-fold) for the nHA/PU/rhBMP-2 group compared to the untreated nHA/PU control group; however, the value was still significantly lower compared to native bone (Figure 4.8A). By 12 weeks, the elastic modulus of the nHA/PU/rhBMP-2 had doubled, and interestingly, the level was statistically similar to native bone modulus at 6 weeks but not at 12 weeks. The modulus for the untreated nHA/PU group remained unchanged over time (Figure 8A). The push-out tests indicates that at 6 weeks, approximately 50% more load was required to fracture the bone-implant osteointegration region of the nHA/PU/rhBMP-2 group compared to the untreated control and no scaffold groups (Figure 4.8B). This suggests that the new bone in-growth from the host bone integrated well with the scaffold within the defect site. Interestingly, the no scaffold group also registered similar fracture load compared to untreated control group, which was likely due to the in-growth of new bone from the host bone around the defect. The similarity in fracture load for the nHA/PU control and no scaffold group indicates that the presence of the nHA/PU scaffold did not hinder the bone in-growth from the host tissue. This result suggests that the nHA/PU scaffold is biocompatible and well tolerated *in vivo*. Unexpectedly, at 12 weeks, the required load to fracture the bone of the untreated nHA/PU control and nHA/PU/rhBMP-2 groups were similar to those at 6 weeks, which indicates that the bone-implant osteointegration region strength had potentially peaked (Figure 4.8B). This value was approximately 30% lower compared to native bone strength.

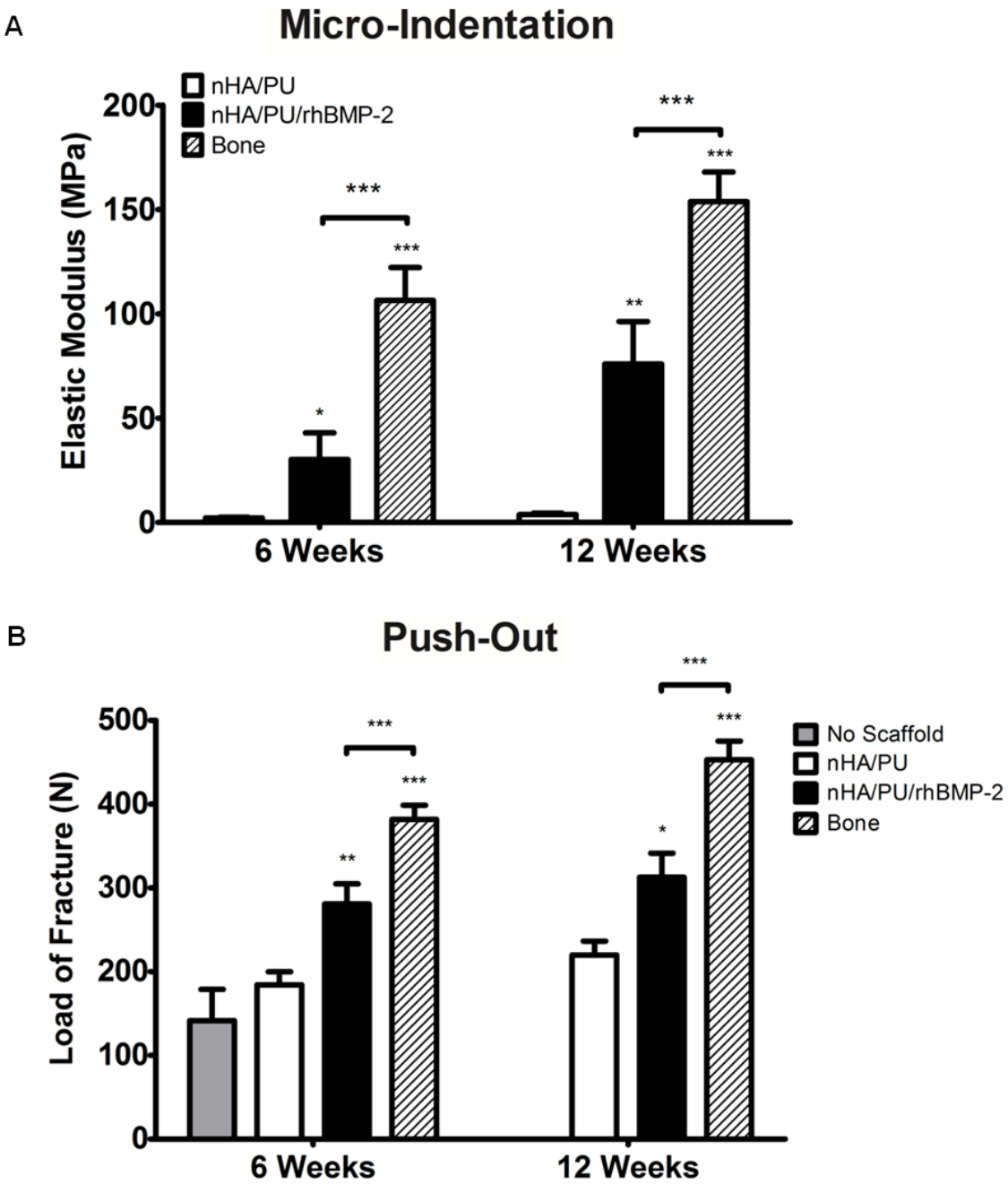
A
Micro-Indentation
nHA/PU
nHA/PU/rhBMP-2
Bone
Elastic Modulus (MPa)
200
150
100
50
0
6 Weeks
12 Weeks
B
Push-Out
Load of Fracture (N)
500
400
300
200
100
0
No Scaffold
nHA/PU
nHA/PU/rhBMP-2
Bone
6 Weeks
12 Weeks

Figure 4.8. Mechanical testing of rat calvarias at 6 and 12 weeks.

(A) Micro-indentation tests indicated that the stiffness of newly formed bone in nHA/PU/rhBMP-2 group was significantly higher compared to nHA/PU group at both time points. **(B)** Push-out tests showed a significant difference in load of fracture for nHA/PU/rhBMP-2 group compared to the nHA/PU group. The bone-control was done on undamaged calvarial bone. Data represents mean ± standard error (micro-indentation test: n = 6 for bone groups and n= 8 and 5 for all other groups at 6 and 12 weeks, respectively; push-out test: n = 5 for no scaffold group and n=7 for all other groups; *$p<0.05$, **$p<0.01$, ***$p<0.001$).

4.4 DISCUSSION

In tissue engineering, biocompatibility, degradation rate, osteoconductive, and osteoinductive are important properties of effective biomaterials for bone repair. However, most biomaterials are not osteoinductive in nature; thus, the addition of various growth factors or bioactive proteins is a common practice. Clinically, rhBMP-2 is the most prevalent growth factor for bone tissue regeneration due to its high potency in driving osteoprogenitor cell differentiation to osteoblastic cells, which leads to *de novo* bone formation. A high dose of rhBMP-2 is usually required in the clinical setting to ensure the enhancement of bone repair. Bone repair studies in small animals have also demonstrated that increasing the dose of rhBMP-2 enhances the rate and amount of bone formed (Angle et al., 2012; Ben-David et al., 2013; Murakami et al., 2002). However, there are potential side effects due to the high levels of growth factor that include excessive bone formation, adverse immune responses, and cancer (Carragee et al., 2011; Epstein, 2013). Therefore, delivery strategies that utilize low levels of rhBMP-2 and still achieve sufficient bone formation are required. In this study, we demonstrate that the novel nHA/PU scaffold loaded with low-dose rhBMP-2 is effective in promoting bone regeneration. In addition, rhBMP-2 appeared to bind well onto the nHA/PU scaffold as indicated by the low concentration of rhBMP-2 released from the scaffold after 72 hr incubation.

4.4.1 nHA/PU scaffold supports cell attachment and binding of rhBMP-2

Previous studies have shown that the inter-connective pore networks in PU scaffolds allow for the in-growth of cells and blood vessels (REF). Furthermore, these scaffolds have an inherent mechanical stiffness and viscoelastic properties, which are important for bone tissue engineering applications (Boissard et al., 2009; Gogolewski et al., 2008). In addition, the PU scaffolds have good angiogenic properties and are effective in supporting cell attachment, growth, and differentiation (Hofmann et al., 2008; Laschke et al., 2010a; Laschke et al., 2012; Laschke et al., 2013). The addition of nHA to PU

scaffolds allow for improved mechanical stiffness and enhanced binding of proteins (Laschke et al., 2010b). SEM images demonstrated that even though most of the mineral crystals appear to be embedded, some are found on the surface including the walls of the pores as shown in Figure 1.

Hydroxyapatite has been shown to effectively bind proteins as demonstrated in its use as a chromatography resin (Matsumoto et al., 2004; Shen et al., 2008; Xie et al., 2010). Thus, this property of HA likely contributes to the binding of rhBMP-2 to the nHA/PU scaffold. Of relevance, rhBMP-2 was shown to have higher binding to HA-coated ceramic surfaces than uncoated surfaces and, more importantly, be released at a slower rate (Autefage et al., 2009). Our *in vitro* study indicates that approximately 7% of the initial bound rhBMP-2 to the HA/PU scaffold was released by 72 hrs, which is a similar release rate described in previous studies that utilized methods of rhBMP-2 entrapment within nano/micro-particle vehicles for controlled release (Li et al., 2009; Li et al., 2015; Xie et al., 2010).

rhBMP-2 has been shown to promote differentiation of osteoprogenitor cells to osteoblastic cells which in turn leads to increased matrix formation with subsequent calcification. This osteoinductive property of the rhBMP-2 is crucial for promoting bone repair, including the parietal bones which undergo intramembranous ossification. Previous studies have indicated that intramembranous ossification begins within the first few days of fracture and BMP expression is up-regulated in the proliferating osteoprogenitors during this process (Sfeir et al., 2005). Therefore, the presence of rhBMP-2 within the interconnected porous network of the scaffold may promote osteogenic differentiation, which in turn will speed up the bone repair process.

In order to confirm the bioactivity of the bound rhBMP-2, the treated nHA/PU scaffolds were seeded with MSC and cultured. Based on alizarin red staining, the rhBMP-2 treated nHA/PU scaffolds qualitatively appeared to have higher amount of matrix mineralization compared to untreated nHA/PU scaffolds. Interestingly, nHA/PU/rhBMP-2 that were incubated and washed in media for 72 h prior to the addition of the MSC, also appeared to have similar levels of mineralization compared to the nHA/PU scaffolds treated with

fresh rhBMP-2. This result confirmed that rhBMP-2 was present and active even after the 72 h incubation period that included multiple washes.

A limitation of our study was the difficulty to quantify certain metrics from the 3D cell cultures in the porous scaffolds. Analysis using microscopic techniques quantifying cell numbers or mineral content require reproducible and representative sections of the 3D scaffolds with equivalent cell numbers spread evenly through the structure. Staining of the polymers for cells, for example, showed an uneven distribution, with few cells found at or near the surface of the polymers. Furthermore, histological sections through the scaffold show inconsistent pore sizes and distribution.

In order to determine cell numbers in the scaffold, we tried to quantify DNA content. Unfortunately, no reliable data was obtained. For example, using TRIzol reagent, inadequate levels of DNA was extracted from the scaffolds, whereas measureable levels were extracted from cultures in the absence of scaffolds.

4.4.2 nHA/PU scaffold treated with low dose rhBMP-2 enhanced repair of calvarial bone defects

MicroCT analyses have been reliably used to quantify level of mineralization with regards to the spatial distribution of new bone within the calvarial defects (Cowan et al., 2007; Sawyer et al., 2009; Umoh et al., 2009). In agreement with these studies, our μCT bone volume measurements and histological analyses both demonstrated increased formation of new bone in the nHA/PU/rhBMP-2 scaffolds compared to untreated scaffolds. A number of studies have shown that the addition of rhBMP-2 to various scaffold materials promotes bone repair. In studies that used the rat calvarial defect model, large doses (5 μg or more) of rhBMP-2 were loaded into each scaffold of various compositions, which includes synthetic materials such as β-tricalcium phosphate, polylactic and polyglycolic acid gel, and poly ε-caprolactone/tricalcium phosphate, as

well as natural materials such as collagen and autogenous bone chips (Luvizuto et al., 2011; Sawyer et al., 2009; Schwarz et al., 2009). In comparison, our nHA/PU scaffold was only loaded with 1 µg of rhBMP-2 and was shown to be as good if not better in generating new bone. In our study, the percentage of bone covering the defect volume (BV/TV) for the rhBMP-2 treated group was 75.48 ± 8.36 % at 12 weeks, which is greater than the findings reported by Sawyer *et al* and Luvizuto *et al* (Luvizuto et al., 2011; Sawyer et al., 2009). Of relevance, other studies using the calvarial defect model have also demonstrated that lower doses (174 - 500 ng) of rhBMP-2 per scaffold (polylactic acid based) can achieve relatively moderate bone formation covering approximately 20-45% of the defect volume (La et al., 2010; Schofer et al., 2011b). The length of time in which rhBMP-2 is present in the scaffold during bone repair has been noted to be crucial for bone formation. Previous studies have demonstrated that long-term delivery of rhBMP-2 (1 µg or greater) promoted greater amount of bone formation compared to a short-term delivery method. However at a very low dose of rhBMP-2 (500 ng of less), both delivery methods resulted in the same amount of bone formation (La et al., 2010). In our system, the effectiveness of nHA/PU/rhBMP-2 scaffold in bone repair is likely attributed to its porous interconnected network that allows for in-growth of cells and vascularization system, and also its ability to absorb and bind growth factors and other bioactive proteins. The slow release of rhBMP-2 from nHA/PU scaffold contributed to the high percentage of new bone volume seen in this study. Of relevance, most studies that used high dose of rhBMP-2 usually have a fast rhBMP-2 release profile from the scaffold. For example, Sawyer et al. indicated that almost all of the bound rhBMP-2 was released from the poly ε-caprolactone/tricalcium phosphate/collagen scaffold within 10 hours of incubation (Sawyer et al., 2009).

No adverse inflammatory response was observed in any of the treatment groups, supporting that the nHA/PU scaffold is biocompatible as previously shown (Dresing et al., 2014; Laschke et al., 2010b). The mode of healing between the rhBMP-2 treated scaffolds appears to differ compared to the control scaffold group. In the control group, containing only the untreated scaffold, minimal new bone formation was observed, with most observed at the edge of the defect and some island-like bone formation in the interior of the scaffold. In contrast, use of the rhBMP-2 treated scaffold resulted in

widespread healing throughout the defect site. This result also confirmed our *in vitro* study, which showed that the rhBMP-2 treated nHA/PU scaffold was effective in promoting cell migration and differentiation within the scaffold.

At all three time points, we found that BMC, BV, BV/TV of rhBMP-2 treated nHA/PU scaffolds were significantly higher compared to those of the control scaffold group. By 6 weeks, the BV/TV analyses indicated that approximately 70% of the defects were filled with bone. However, this BV/TV value was statistically similar to that at 12 weeks, which suggests that the rate of bone formation was significantly reduced after 6 weeks and likely approaching the limits of bone growth. Other studies have also shown that new bone growth was significantly reduced after 8 weeks. (Schofer et al., 2011a). In comparison, the average BMC and the percentage of cortical bone volume in the defect were significantly higher at 12 weeks compared to 6 weeks. Together with the BV/TV values, these data indicate that bone remodeling was likely the main process during this post 6-week repair period. Thus, this data highlights the importance of promoting and maximizing new bone growth at early stages of the bone repair.

Of relevance, previous *in vivo* studies using a subcutaneous model demonstrated that BMPs induced both chondrogenesis and osteogenesis (Kuboki et al., 2001; Wang et al., 1990). Similarly, *in vitro* studies also have shown that BMP induces cartilage formation using muscle-derived cells (Sampath and Reddi, 1983; Sato and Urist, 1984). However, it is possible that the type of ossification during bone repair depends on location and type of bone. For example, the parietal bones are known to be formed via intramembranous ossification and during the bone repair, however in this study we did not analyze for markers of cartilage formation within the calvarial defects.

Mechanical testing on the repaired bone defects was also performed in this study since it is another parameter that is crucial in evaluating the quality of new bone. Two types of mechanical test models were utilized: micro-indentation and push-out test. The micro-indentation test has previously been shown to be useful in determining the elastic modulus of newly formed bone (Sawyer et al., 2009). At both 6 and 12 weeks, the elastic modulus of the newly formed bone at the center of the defect were significantly higher

for the nHA/PU/rhBMP-2 group compared to the control scaffold group, though it is still lower than that of native bone. The latter was expected since histological and microCT analyses suggest that the newly formed bone had not been fully remodeled even by 12 weeks. In order to determine the quality and strength of the osteointegration, the load of fracture at the implant-bone boundary was obtained using the push-out test. The results indicate that significant higher load of fracture was required for the nHA/PU/rhBMP-2 group compared to control group; but this value was still lower compared to that of native bone. Interestingly, the control group has a similar load of fracture value compared to the no-scaffold group, which indicates that the mechanical strength at the osteointegration boundary is mainly due to the normal bone in-growth at the periphery of the defect.

In conclusion, this study demonstrated that the nHA/PU scaffold has a high binding affinity with rhBMP-2. Combined with low dose rhBMP-2, the nHA/PU scaffold was able to effectively promote bone repair by 6 weeks. This data indicates that nHA/PU is an ideal scaffold for bone tissue engineering.

4.5 REFERENCES

Angle SR, Sena K, Sumner DR, Virkus WW, Virdi AS (2012). Healing of rat femoral segmental defect with bone morphogenetic protein-2: a dose response study. *J Musculoskelet Neuronal Interact* 12(1)*:*28-37.

Autefage H, Briand-Mésange F, Cazalbou S, Drouet C, Fourmy D, Gonçalvès S *et al.* (2009). Adsorption and release of BMP-2 on nanocrystalline apatite-coated and uncoated hydroxyapatite/β-tricalcium phosphate porous ceramics. *Journal of Biomedical Materials Research Part B: Applied Biomaterials* 91B(2)*:*706-715.

Ben-David D, Srouji S, Shapira-Schweitzer K, Kossover O, Ivanir E, Kuhn G *et al.* (2013). Low dose BMP-2 treatment for bone repair using a PEGylated fibrinogen hydrogel matrix. *Biomaterials* 34(12)*:*2902-2910.

Boissard CIR, Bourban PE, Tami AE, Alini M, Eglin D (2009). Nanohydroxyapatite/poly(ester urethane) scaffold for bone tissue engineering. *Acta Biomaterialia* 5(9)*:*3316-3327.

Brown KV, Li B, Guda T, Perrien DS, Guelcher SA, Wenke JC (2011). Improving Bone Formation in a Rat Femur Segmental Defect by Controlling Bone Morphogenetic Protein-2 Release. *Tissue Engineering Part A* 17(13-14)*:*1735-1746.

Busa B, Miller LM, Rubin CT, Qin YX, Judex S (2005). Rapid Establishment of Chemical and Mechanical Properties during Lamellar Bone Formation. *Calcif Tissue Int* 77(6)*:*386-394.

Cacciafesta V, Dalstra M, Carles, Melsen B, Andreassen TT (2001). Growth hormone treatment promotes guided bone regeneration in rat calvarial defects. *The European Journal of Orthodontics* 23(6)*:*733-740.

Carragee EJ, Hurwitz EL, Weiner BK (2011). A critical review of recombinant human bone morphogenetic protein-2 trials in spinal surgery: emerging safety concerns and lessons learned. *The Spine Journal* 11(6)*:*471-491.

Cowan CM, Aghaloo T, Chou Y, Walder B, Zhang T, Soo C *et al.* (2007). MicroCT Evaluation of Three-Dimensional Mineralization in Response to BMP-2 Doses In Vitro and in Critical Sized Rat Calvarial Defects. *Tissue Engineering Part A* 13(3)*:*501-512.

Dresing I, Zeiter S, Auer J, Alini M, Eglin D (2014). Evaluation of a press-fit osteochondral poly(ester-urethane) scaffold in a rabbit defect model. *Journal of Materials Science: Materials in Medicine* 25(7)*:*1691-1700.

Epstein NE (2013). Complications due to the use of BMP/INFUSE in spine surgery: The evidence continues to mount. *Surgical Neurology International* 4(Suppl 5)*:*S343-S352.

Fricain JC, Schlaubitz S, Le Visage C, Arnault I, Derkaoui SM, Siadous R *et al.* (2013). A nano-hydroxyapatite – Pullulan/dextran polysaccharide composite macroporous material for bone tissue engineering. *Biomaterials* 34(12)*:*2947-2959.

Gogolewski S, Gorna K, Zaczynska E, Czarny A (2008). Structure–property relations and cytotoxicity of isosorbide-based biodegradable polyurethane scaffolds for tissue repair and regeneration. *Journal of Biomedical Materials Research Part A* 85A(2)*:*456-465.

Gorna K, Gogolewski S (2006). Biodegradable porous polyurethane scaffolds for tissue repair and regeneration. *Journal of Biomedical Materials Research Part A* 79A(1)*:*128-138.

Guan J, Fujimoto KL, Sacks MS, Wagner WR (2005). Preparation and characterization of highly porous, biodegradable polyurethane scaffolds for soft tissue applications. *Biomaterials* 26(18)*:*3961-3971.

Guelcher SA (2008). Biodegradable polyurethanes: synthesis and applications in regenerative medicine. *Tissue Eng Part B Rev* 14(1)*:*3-17.

Guelcher SA, Srinivasan A, Dumas JE, Didier JE, McBride S, Hollinger JO (2008). Synthesis, mechanical properties, biocompatibility, and biodegradation of polyurethane networks from lysine polyisocyanates. *Biomaterials* 29(12)*:*1762-1775.

Hofmann A, Ritz U, Verrier S, Eglin D, Alini M, Fuchs S *et al.* (2008). The effect of human osteoblasts on proliferation and neo-vessel formation of human umbilical vein endothelial cells in a long-term 3D co-culture on polyurethane scaffolds. *Biomaterials* 29(31)*:*4217-4226.

Kavlock KD, Pechar TW, Hollinger JO, Guelcher SA, Goldstein AS (2007). Synthesis and characterization of segmented poly(esterurethane urea) elastomers for bone tissue engineering. *Acta Biomater* 3(4)*:*475-484.

Khadra M, Kasem N, Haanæs HR, Ellingsen JE, Lyngstadaas SP (2004). Enhancement of bone formation in rat calvarial bone defects using low-level laser therapy. *Oral surgery, oral medicine, oral pathology, oral radiology, and endodontics* 97(6)*:*693-700.

Kim J, Hollinger JO (2012). Recombinant human bone morphogenetic protein-2 released from polyurethane-based scaffolds promotes early osteogenic differentiation of human mesenchymal stem cells. *Biomedical Materials* 7(4)*:*045008.

Kim S-S, Gwak S-J, Kim B-S (2008). Orthotopic bone formation by implantation of apatite-coated poly(lactide-co-glycolide)/hydroxyapatite composite particulates and bone morphogenetic protein-2. *Journal of Biomedical Materials Research Part A* 87A(1)*:*245-253.

La WG, Kang SW, Yang HS, Bhang SH, Lee SH, Park JH *et al.* (2010). The efficacy of bone morphogenetic protein-2 depends on its mode of delivery. *Artif Organs* 34(12)*:*1150-1153.

Laschke MW, Strohe A, Scheuer C, Eglin D, Verrier S, Alini M *et al.* (2009). In vivo biocompatibility and vascularization of biodegradable porous polyurethane scaffolds for tissue engineering. *Acta Biomaterialia* 5(6)*:*1991-2001.

Laschke MW, Mussawy H, Schuler S, Eglin D, Alini M, Menger MD (2010a). Promoting external inosculation of prevascularised tissue constructs by pre-cultivation in an angiogenic extracellular matrix. *European Cells & Materials* 20(356-366.

Laschke MW, Strohe A, Menger MD, Alini M, Eglin D (2010b). In vitro and in vivo evaluation of a novel nanosize hydroxyapatite particles/poly(ester-urethane) composite scaffold for bone tissue engineering. *Acta Biomaterialia* 6(6)*:*2020-2027.

Laschke MW, Kleer S, Scheuer C, Schuler S, Garcia P, Eglin D *et al.* (2012). Vascularisation of porous scaffolds is improved by incorporation of adipose tissue-derived microvascular fragments. *European Cells & Materials* 24(266-277.

Laschke MW, Schank TE, Scheuer C, Kleer S, Schuler S, Metzger W *et al.* (2013). Three-dimensional spheroids of adipose-derived mesenchymal stem cells are potent initiators of blood vessel formation in porous polyurethane scaffolds. *Acta Biomaterialia* 9(6)*:*6876-6884.

Lee C, Grad S, Gorna K, Gogolewski S, Goessl A, Alini M (2005). Fibrin–Polyurethane Composites for Articular Cartilage Tissue Engineering: A Preliminary Analysis. *Tissue Engineering* 11(9-10)*:*1562-1573.

Li B, Yoshii T, Hafeman AE, Nyman JS, Wenke JC, Guelcher SA (2009). The effects of rhBMP-2 released from biodegradable polyurethane/microsphere composite scaffolds on new bone formation in rat femora. *Biomaterials* 30(35)*:*6768-6779.

Li L, Zhou G, Wang Y, Yang G, Ding S, Zhou S (2015). Controlled dual delivery of BMP-2 and dexamethasone by nanoparticle-embedded electrospun nanofibers for the efficient repair of critical-sized rat calvarial defect. *Biomaterials* 37(0)*:*218-229.

Luvizuto ER, Tangl S, Zanoni G, Okamoto T, Sonoda CK, Gruber R *et al.* (2011). The effect of BMP-2 on the osteoconductive properties of β-tricalcium phosphate in rat calvaria defects. *Biomaterials* 32(15)*:*3855-3861.

Mardas N, Stavropoulos A, Karring T (2008). Calvarial bone regeneration by a combination of natural anorganic bovine-derived hydroxyapatite matrix coupled with a synthetic cell-binding peptide (PepGen™): an experimental study in rats. *Clin Oral Implants Res* 19(10)*:*1010-1015.

Matsumoto T, Okazaki M, Inoue M, Yamaguchi S, Kusunose T, Toyonaga T *et al.* (2004). Hydroxyapatite particles as a controlled release carrier of protein. *Biomaterials* 25(17)*:*3807-3812.

McKee CT, Last JA, Russell P, Murphy CJ (2011). Indentation versus tensile measurements of Young's modulus for soft biological tissues. *Tissue Eng Part B Rev* 17(3)*:*155-164.

McKoy BE, Kang Q, An YH (1999). Indentation testing of bone. In: Mechanical testing of bone and the bone-implant interface. YH An and RA Draughn editors: CRC Press, pp. 233-240.

Murakami N, Saito N, Horiuchi H, Okada T, Nozaki K, Takaoka K (2002). Repair of segmental defects in rabbit humeri with titanium fiber mesh cylinders containing recombinant human bone morphogenetic protein-2 (rhBMP-2) and a synthetic polymer. *J Biomed Mater Res* 62(2)*:*169-174.

Osathanon T, Linnes ML, Rajachar RM, Ratner BD, Somerman MJ, Giachelli CM (2008). Microporous nanofibrous fibrin-based scaffolds for bone tissue engineering. *Biomaterials* 29(30)*:*4091-4099.

Pirvu T, Blanquer SBG, Benneker LM, Grijpma DW, Richards RG, Alini M *et al.* (2015). A combined biomaterial and cellular approach for annulus fibrosus rupture repair. *Biomaterials* 42(0)*:*11-19.

Sawyer AA, Song SJ, Susanto E, Chuan P, Lam CXF, Woodruff MA *et al.* (2009). The stimulation of healing within a rat calvarial defect by mPCL–TCP/collagen scaffolds loaded with rhBMP-2. *Biomaterials* 30(13)*:*2479-2488.

Schofer MD, Roessler PP, Schaefer J, Theisen C, Schlimme S, Heverhagen JT *et al.* (2011a). Electrospun PLLA nanofiber scaffolds and their use in combination with BMP-2 for reconstruction of bone defects. *PLoS ONE* 6(9)*:*e25462.

Schofer MD, Veltum A, Theisen C, Chen F, Agarwal S, Fuchs-Winkelmann S *et al.* (2011b). Functionalisation of PLLA nanofiber scaffolds using a possible cooperative

effect between collagen type I and BMP-2: impact on growth and osteogenic differentiation of human mesenchymal stem cells. *J Mater Sci Mater Med* 22(7)*:*1753-1762.

Schwarz F, Ferrari D, Sager M, Herten M, Hartig B, Becker J (2009). Guided bone regeneration using rhGDF-5- and rhBMP-2-coated natural bone mineral in rat calvarial defects. *Clin Oral Implants Res* 20(11)*:*1219-1230.

Sfeir C, Ho L, Doll BA, Azari K, Hollinger JO (2005). Fracture Repair. In: Bone Regeneration and Repair: Biology and Clinical Applications. JR Lieberman and GE Friedlaender editors. Totowa, NJ: Humana Press Inc, pp. 21-44.

Shen J-W, Wu T, Wang Q, Pan H-H (2008). Molecular simulation of protein adsorption and desorption on hydroxyapatite surfaces. *Biomaterials* 29(5)*:*513-532.

Umoh JU, Sampaio AV, Welch I, Pitelka V, Goldberg HA, Underhill TM *et al.* (2009). In vivo micro-CT analysis of bone remodeling in a rat calvarial defect model. *Phys Med Biol* 54(7)*:*2147.

Wang EA, Rosen V, D'Alessandro JS, Bauduy M, Cordes P, Harada T, Israel DI, Hewick RM, Kerns KM, LaPan P *et al*. (1990). Recombinant human bone morphogenetic protein induces bone formation. Proc Natl Acad Sci U S A. 87(6):2220-2224.

White D (1978). Tissue substitutes in experimental radiation physics. *Med Phys* 5(6)*:*467-479.

Xie G, Sun J, Zhong G, Liu C, Wei J (2010). Hydroxyapatite nanoparticles as a controlled-release carrier of BMP-2: absorption and release kinetics in vitro. *J Mater Sci Mater Med* 21(6)*:*1875-1880.

Yu YY, Lieu S, Lu C, Miclau T, Marcucio RS, Colnot C (2010). Immunolocalization of BMPs, BMP antagonists, receptors, and effectors during fracture repair. *Bone* 46(3)*:*841-851.

CHAPTER 5

5 Effect of bone sialoprotein treated nano-hydroxyapatite/ poly(ester-urethane) scaffolds on bone formation

5.1 INTRODUCTION

BSP is an acidic phosphoprotein highly expressed in mineralized tissues such as skeleton and dentition (Fisher and Fedarko, 2003; Ganss et al., 1999). It is also a member of Small Integrin-Binding Ligand, N-Linked Glycoprotein (SIBLING) group and a major component of non-collagenous proteins in bone. Similar to other SIBLING proteins, BSP contains several highly conserved functional domains. These included a collagen-binding domain, two hydroxyapatite nucleation regions and an integrin recognition site (RGD motif, which is involved in cell attachment, migration and signaling) (Goldberg and Hunter, 2012). BSP has been previously shown to be a potent nucleator of hydroxyapatite (HA) (Hunter and Goldberg, 1993). In addition, the attached phosphate has been demonstrated to be an important modification that regulates the HA nucleation potency, in particular at the Serine-136 position (Baht et al., 2010).

Mice with *Bsp* gene ablated ($Bsp^{-/-}$) have impaired bone growth and mineralization. Early studies by the Malaval group have shown $Bsp^{-/-}$ mice to have shortened long bones, decreased bone mineral density, delayed mineral formation, thinner cortical bone thickness, and greater trabecular bone volume, as well as reduction in osteoclast formation and activity, which resulted in low bone turnover compared to wild type (WT) mice (Boudiffa et al., 2010; Malaval et al., 2008). In femoral defect model, $Bsp^{-/-}$ mice also displayed delayed bone repair compared to WT control (Malaval et al., 2009; Monfoulet et al., 2010). All these defects seen in $Bsp^{-/-}$ mice suggest that BSP plays a crucial role in bone development and mineralization. Furthermore, studies reported by Wang and Glimcher indicate that BSP promoted new bone formation *in vivo* (Wang et al., 2006; Xu et al., 2007). In these studies, the collagen-BSP scaffolds were able to induce some mineral formation along the dura membrane within 4 days of implantation in rat calvarial defect. In addition, by day 7, cell proliferation, matrix mineralization, and angiogenesis were found within the BSP-treated implant.

The physiological importance of BSP and its functional importance in skeletal development has been the main focus of research on BSP. However, minimal research has been done testing BSP as a potential therapeutic reagent for promoting bone repair. In this study, we investigate the effectiveness of BSP-treated poly(ester-urethane) (PU)

scaffolds in promoting bone repair. PU based scaffolds have been extensively studied and shown to have potential tissue engineering applications in tissues such as bone (Hofmann et al., 2008; Kavlock et al., 2007; Li et al., 2009), cartilage (Dresing et al., 2014; Lee et al., 2005), and other soft tissue (Gogolewski et al., 2008; Guan et al., 2005; Guelcher, 2008; Guelcher et al., 2008) regeneration. The PU scaffolds are biocompatible, biodegradable and have viscoelastic properties for easy physical fitting into the bone defects (Hofmann et al., 2008; Laschke et al., 2009; Laschke et al., 2013; Lee et al., 2005; Pirvu et al., 2015). For bone tissue engineering application, nano-sized hydroxyapatite (nHA) particles were incorporated into the PU-based (nHA/PU) scaffolds to improve the material stiffness (Boissard et al., 2009) and also to increase its capacity to bind proteins such as albumin and fibrinogen (Laschke et al., 2010b).

In this study, *in vitro* experiments were conducted to determine the amount of BSP that can bind onto the nHA/PU scaffolds. Furthermore, the BSP-treated nHA/PU scaffolds were cultured with MSC to validate whether the presence of BSP can improved cells attachment. In addition, rat calvarial defect model will be utilized to validate the effectiveness of BSP-treated nHA/PU scaffolds in promoting bone repair. Micro-computed tomography (microCT) and histological analysis will be used to monitor the rate of bone repair.

5.2 MATERIALS AND METHODS

5.2.1 Scaffold preparation

The biodegradable PU solution was synthesized in a one-step solution polycondensation as previously described in detail (Laschke et al., 2010b). The process involved the use of 1,6-hexamethylene diisocyanate (Sigma-Aldrich, Milwaukee, WI), poly(ε-caprolactone) diol (M_W = 530 g mol^{-1}, Sigma-Aldrich, Milwaukee, WI), and 1,4,3,6-dianhydro-D-sorbitol as reactants. Dibutyltin dilaurate (Fluka, Buchs, CH) was used a catalyst for the reaction and N,N-dimethylformaide (Fluka, Buchs, CH) was used as a solvent. To create

nHA/PU solution, nHA (Biomaterials US, Ltd., USA) particles, ranging in size from 50 to 200 nm, were dispersed into a PU solution. The nHA mass fraction added was 20 wt.% of the PU solution. Prior to usage, the nHA particles were washed with ethanol and dried at 100°C under vacuum (Laschke et al., 2010b). Both PU and nHA/PU scaffolds were prepared using a salt leaching-phase inverse process as previously described (Boissard et al., 2009; Gorna and Gogolewski, 2006; Laschke et al., 2010b). This method involved a vigorous mixing of PU or nHA/PU solution with porogen (sodium phosphate heptahydrate dibasic salt; Fluka, Buchs, CH) until a homogeneous paste was obtained. The paste was then poured into a cylindrical mould and left exposed to air to allow for slow evaporation of the solvents. The salt was leached out by extensive washing in water, which created porous PU or nHA/PU sponges. In order to produce consistent thickness scaffolds, the sponges were cut using water jet system. In this study, the scaffolds were prepared with a circular dimension of 5.5 mm and 1 mm thickness with pore sizes ranging from 90 to 300 μm. The scaffolds were washed in ethanol, dried under vacuum, and sterilized in ethylene oxide prior to use in the studies.

5.2.2 BSP expression and purification

Recombinant rat BSP (rBSP) was expressed in *Escherichia coli* strain BL21(DE3) cells and purified by fast protein liquid chromatography (FPLC) as described previously (Baht et al., 2010; Tye et al., 2003). To phosphorylate the protein, rBSP was treated with casein kinase 2 (CK2) in reaction buffer [150 mM sodium chloride (NaCl), 10 mM magnesium chloride ($MgCl_2$), 1 mM dithiothreitol (DTT), 0.1 mM adenosine triphosphate (ATP) and 50 mM tris(hydroxymethyl)aminomethane-hydrochloride (Tris-HCl); pH 7.4] as described previously (Baht et al., 2010). Phosphate content was determined by matrix-assisted laser desorption/ionization (MALDI) mass spectrometry (Department of Biochemistry, UWO, London, ON).

Native bovine BSP (bBSP) was purified from the long bones of a still-born calf. The procedure followed methods previously described in detail for purification of native rat BSP (ratBSP) (Goldberg and Sodek, 1994). In brief, bone chips were first washed 3

times with phosphate buffered saline (PBS) containing proteinase inhibitor (PI) [100 mM amino caproic acid, 5 mM benzamidine HCl, 5 mM N-ethyl maleimide, and 1 mM phenylmethylsulfonyl fluoride (PMSF)] solutions followed by a series (3-4 times) of freeze-thaw cycles for 24 h in order to fracture the bone to allow for removal of inner blood and cells from bone cavities. Then the bone chips were incubated in chloroform-methanol solution overnight in order to dissolve and remove fats and lipids. The next step involved the extraction of the bone chips with 4.0 M guanidine hydrochloride/Tris-HCl buffer containing PI (4 x 24 h incubations) to remove unwanted proteins not associated with bone mineral. Finally, the mineral-associated proteins were extracted with 0.5M ethylenediaminetetraacetic acid (EDTA)/Tris-HCl buffer containing PI solutions (4 x 24 h incubations).

The extracted protein solution was concentrated using an Amicon ultrafiltration cell and YM10 membranes (cut-off, 10 KDa) (EMD Millipore, Etobicoke, ON) with at least 2 buffer exchanges with Q-buffer A (50 mM Tris-HCl, 7 M urea, pH7.4) chromatography solution. The concentrated protein solution was diluted with Q-buffer A solution and then passed through Q Sepharose Fast Flow (Fast Q) column (1 x 10 cm; Pharmacia Biotech, GE Healthcare Life Sciences, Mississauga, ON) connected to an FPLC system to separate the proteins based on charge. The proteins were eluted with a linear gradient of NaCl (0 - 1.2 M) at a flow rate of 2.5 ml/min. The fractions containing the proteins of interest were then collected and pooled together. Aliquots of the fractions were also run on 12.5% polyacrylamide gels using the Phastgel system (Amersham Biosciences, GE Healthcare Life Sciences, Mississauga, ON) to confirm the presence of the protein. After electrophoresis, the gels were stained with Stains-All and silver nitrate (Goldberg and Warner, 1997). The proteins were re-chromatographed on Fast Q column and then finally by gel filtration using a Superdex 200 PG column (1.6 x 60 cm; Pharmacia Biotech, GE Healthcare Life Sciences, Mississauga, ON) with S-buffer [50 mM Tris/HCl, 0.2 M NaCl, and 4 M urea; pH 7.4] to separate proteins based on molecular size, as described previously (Goldberg and Sodek, 1994). The fractions enriched with BSP were pooled and dialyzed with 10 mM ammonium bicarbonate for 72 h at 4°C using Spectra/Por dialysis membrane (cut-off, 12-14 kDa) (Spectrum Laboratories, Rancho Dominguez, CA). After dialysis, the final solutions were aliquoted and lyophilized. The

purity and quantity of the protein samples were determined using Bicinchoninic acid (BCA) assay (ThermoFisher Scientific, Burlington, ON), amino acid analysis (Macromolecular Crystallography Facility, Department of Biochemistry, UWO, London, ON), and MALDI mass spectrometry (Bruker® Reflex IV MALDI TOF MS, MALDI Mass Spectrometry Facility, Department of Biochemistry, UWO, London, ON).

5.2.3 *In vitro* prBSP binding experiment

PU and nHA/PU scaffolds were first incubated in 500 μl of phosphate buffered saline (PBS) solution for 1 h. The scaffolds were then transferred and incubated with either 5, 10 or 20 μg of phosphorylated rBSP (prBSP) diluted into 60 μl of PBS solution for 24 h at 4°C. After 24 h of incubation, the scaffolds were centrifuged and the supernatants collected to determine (by sodium dodecyl sulfate - polyacrylamide gel electrophoresis (SDS-PAGE) analysis) the amount of unbound prBSP. The scaffolds were then washed with 60 μl of PBS solution (4 times, 5 min each time) and 60 μl of 0.5 M NaCl solution (for 5 min) to remove loosely bound prBSP. Finally, the prBSP scaffolds were eluted from the scaffolds using 60 μl of SDS loading buffer. For SDS-PAGE analysis, 10 μl of the 60 μl supernatants from each step were collected and mixed with 10 μl of 2 times concentrated SDS loading buffer. The solutions were denatured at 95°C for 5 min prior to loading onto the gels. The amount of bound prBSP (that were eluted with SDS-PAGE loading buffer) was estimated by comparing the relative pixel-to-intensity ratio of the stained protein bands with the total of unbound, washed, and eluted bands on the acrylamide gels after electrophoresis.

5.2.4 Cell isolation, culture conditions and cell viability

As previously mentioned, BSP has a RGD motif which plays a role in cell signaling and attachment. In this study, we would like to verify that the presence of BSP on the nHA/PU scaffolds may increased the amount of cells bind onto the scaffolds.

Three *in vitro* experiments were done in the study. In the first experiment, C3H10T1/2 cells were used to determine the effect of prBSP on cell attachment. Each nHA/PU scaffold was incubated for 24 h at 4°C with either 150 µl of PBS solution or 150 µl of prBSP-PBS solution (containing 20 µg of prBSP). Approximately 1.2 x 10^6 of C3H10T1/2 cells were seeded onto the scaffold and incubated for 1 h in culture media. The scaffolds were then fixed with 4% paraformaldehyde, sectioned (10 µm) and imaged using confocal microscopy to determine the number of attached cells. Three sections from each scaffold were assessed for cell numbers with the field of view being approximately 1.16 mm^2. The total surface area for the scaffold was estimated to be approximately 23.76 mm^2. Therefore, in order to determine the total numbers of cells, the average cells per section was multiplied with the number of sections (in this case equal to 100 since the thickness of the scaffold is 1 mm). A limitation of the technique is that the polymer scaffolds are porous and have irregular pore size, which are factors that we are unable to include in our total surface area or volume calculation.

The second experiment involved the use of mesenchymal stromal cells (MSC). Bone marrow was isolated from male Sprague-Dawley rats (Charles River Laboratories International, Wilmington, MA) aged 11-12 weeks (325-375 g) by flushing the tibia and femur marrow canal with culture medium consisting of Iscove's Modified Dulbecco's Medium (IMDM) supplemented with 10% fetal bovine serum (FBS), 1% penicillin-streptomycin and 1% L-glutamine (Life Technologies, Carlsbad, CA). The MSC were cultured in culture medium in 75 mm^2 (NUNC) flasks at 37°C in 5% CO_2 for 3 days, and then sub-cultured using 0.05% trypsin-EDTA solution. Cells at passage 2 were used for subsequent studies.

Prior to cell seeding, the nHA/PU scaffolds were incubated for 24 h at 4 °C with either 25 µl of saline solution or 25 µl of prBSP-saline solution (containing 20 µg of prBSP). Rat MSC were seeded onto the control and pretreated nHA/PU scaffolds at a density of 3.5 x 10^5 cells/scaffold and incubated in 24-well plates (NUNC). After 1 h incubation, the MSC-seeded scaffolds were placed between a sandwich construct consisting of 2 Teflon-rings in a clean 24-well plate in order to fully immerse the scaffolds in culture medium. The MSC-seeded scaffolds were then cultured in differentiating medium consisting of

culture medium supplemented with 50 µg/ml ascorbic acid and 2 mM β-glycerophosphate. The mineralizing media were changed every 2 days for the duration of the culture.

After 4 weeks of culture, the scaffolds were washed with Hank's Balanced Salt Solution (HBSS) three times, fixed with 4% paraformaldehyde for 20 min, and processed for cryosectioning. In order to determine the relative level of matrix mineralization, the cryosectioned samples were stained for calcium mineral deposition with Alizarin red staining solution (1% w/v, Ricca Chemical company, Arlington, TX) for 20 min at room temperature. To remove excess dye, the samples were washed with deionized water for three times (5 min incubation time for each wash).

The third experiment used the same method as the second experiment; however, instead of prBSP, bBSP was used.

5.2.5 Animals and surgery

Male Sprague-Dawley rats (Charles River Laboratories International, Wilmington, MA) aged 11-12 weeks (325-375 g) were maintained on a standard rat diet (5P00-Prolab RMH 3000; LabDiet, St. Louis, MO, USA). Animal experiments were conducted in accordance with guidelines of the Canadian Council on Animal Care (CCAC) and Animal Care and Veterinary Services (ACVS), University of Western Ontario.

Animals were anaesthetized with isoflurane gas and the heads positioned in a stereotaxic frame. The dorsal part of the cranium was shaved, aseptically prepared, and a midline incision of approximately 20 mm created. The skin flaps were kept opened using a retractor and the underlying periosteum was removed. A 5-mm stainless steel trephine drill (Salvin Dental Specialties, Charlotte, NC) was used to create circular defects on each of the parietal bones, thus creating 2 defects in each rat. Caution was exercised to prevent damage to the dura membrane by adding a custom-made stainless steel sleeve (1.5 mm depth shorter) around the trephine drill. In addition, in order to prevent heat

damage of the host bone, irrigation with saline solution was done throughout the procedure. The nHA/PU or bBSP treated nHA/PU (nHA/PU/bBSP) scaffolds without cells were then implanted and secured in place by double crossing 4-0 Vicryl suture attached to the temporalis muscles. In order to prevent any contamination, both defects in each rat were implanted with scaffolds of the same treatment group. The skin was closed using 4-0 Silk suture. Antibiotics and analgesic were administered to the animals and they were allowed to recover for up to 12 weeks post surgery, after which they were euthanized with CO_2 gas inhalation according to CCAC and ACVS guidelines. At 0, 2, 6 and 12 weeks, *in vivo* microCT analysis was performed, as described below. In addition, at 6 and 12 weeks, the rats were euthanized with CO_2 and then the implants with surrounding bone were collected, fixed with 10% buffered formalin overnight at 4°C, and prepared for histology.

5.2.6 *In vivo* micro-computed tomography analysis

At intervals of 2 weeks, animals were anaesthetized with isoflurane gas and placed in a microCT scanner (eXplore speCZT; GE Healthcare, London, ON). The scans were performed using a standardized live-animal protocol (90 kVp, 40 µA, 900 views, 16 ms per view). Images were reconstructed at a spatial resolution of 50 µm and calibrated with a cortical bone phantom (SB3; Gammex RMI, Middleton, WI) having a hydroxyapatite equivalent of 1,100 mg/cc (White, 1978). Data were analyzed with MicroView ABA version 2.2 (GE Healthcare).

In order to visually determine new bone formation, the 2D Maximum Intensity Projection (MIP) and 3D isosurface images of the rat calvarial bones defect sites were constructed. As for the quantification of the newly formed bone, a cylindrical region of interest (ROI, 5 mm x 1.5 mm) was positioned within the center of each defect site. The bone mineral content (BMC) within the ROI was determined linearly by assigning a value threshold for air (-1000 Hounsfield unit (HU)), water (0 HU), soft tissues (below 700 HU), trabecular bone (above 700 HU), cortical bone (above 1700 HU) and SB3 phantom (2700 HU). The total new bone volume (BV) formation was determined by adding all the voxels with HU

value above 700 within the ROI. Bone-to-total tissue volume ratio (BV/TV) was determined by calculating the ratio of total voxels with HU value above 700 over the total voxels of the ROI. As for the cortical bone volume (CBV), only voxels with HU above 1700 were considered for calculation. Twenty calvarial defects were measured at 2 and 6 weeks and twelve calvarial defects were measured at 12 weeks for each group.

5.2.7 Histological Analysis

The parietal bones were fixed with 10% formalin for 24 h and then decalcified in 0.65 M ethylenediaminetetraacetic acid (EDTA) disodium salt dihydrate, pH 7.4, at 37°C for 2 weeks. After dehydration, the samples were embedded in paraffin, and sectioned at 5 μm thickness. The sagittal sections were stained with hematoxylin and eosin (H&E). The amount of bone formation was quantified at the center sections of the implants.

5.2.8 Statistical Analyses

Quantitative data were expressed as mean ± standard error. Statistical analyses among groups were performed using two-way analysis of variance (ANOVA) and Bonferroni post-tests with Prism 5 version 5.03 (GraphPad Software, La Jolla, CA). $p<0.05$ was considered to be statistically significant.

5.3 RESULTS

5.3.1 bBSP expression and purification

The extracted protein solution from the bovine bone was first passed through Fast Q column and eluted with a linear NaCl gradient in order to separate the proteins based on

charge. At pH 7.0, bovine osteopontin (bOPN) and bBSP enriched fractions (proteins are eluted in overlapping peaks) were collected (Figure 5.1). PhastGel electrophoresis was performed to confirm the presence of bOPN and bBSP in the fractions (data not shown). The collected fractions, with the highest concentration of bBSP, were pooled, concentrated, and re-chromatographed on Fast Q Sepharose column to further purify the protein (data not shown). The bBSP enriched fractions were pooled, concentrated, and applied to a Superdex gel filtration column to separate proteins based on molecular size (Figure 5.2). Based on the SDS-PAGE analysis, fractions (14-19) with the highest concentration of bBSP were pooled, concentrated and re-chromatographed on the Superdex 200 PG column to increase the purity of bBSP (Figure 5.3). Fractions 14-18 from the second Superdex run were combined, dialyzed and lyophilized. Aliquots were analyzed by amino acid analysis to determine protein content, and relative purity.

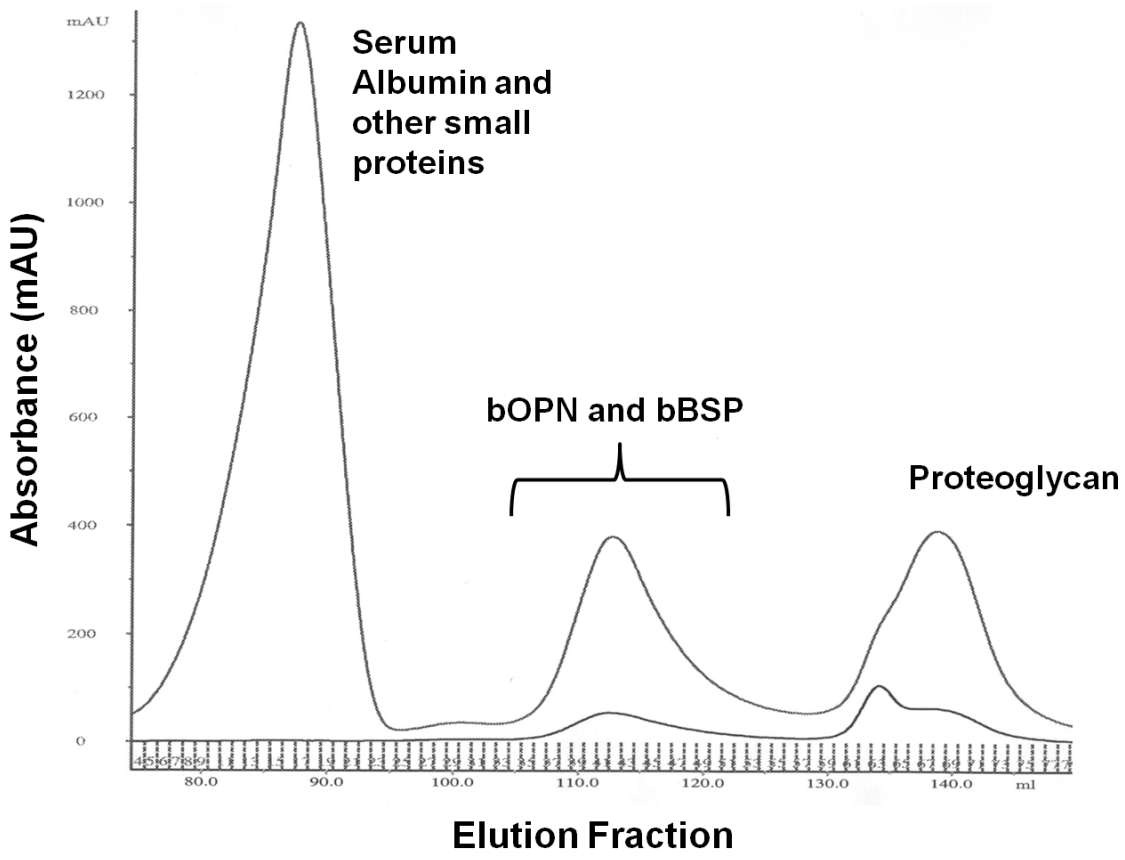

Figure 5.1. Separation of bone proteins by ion exchange chromatography.

Extracted solution containing various bone proteins were passed through Q Sepharose Fast Flow column connected to the FPLC system. The proteins were eluted with a linear gradient of NaCl (0-1.2M). Fractions containing bBSP and bOPN were collected, pooled, and re-chromatographed on the Q-Sepharose column. The bBSP and bOPN were eluted when the concentration of the NaCl at approximately 0.40-0.45M. Absorbance at 230 and 280 nm were determined.

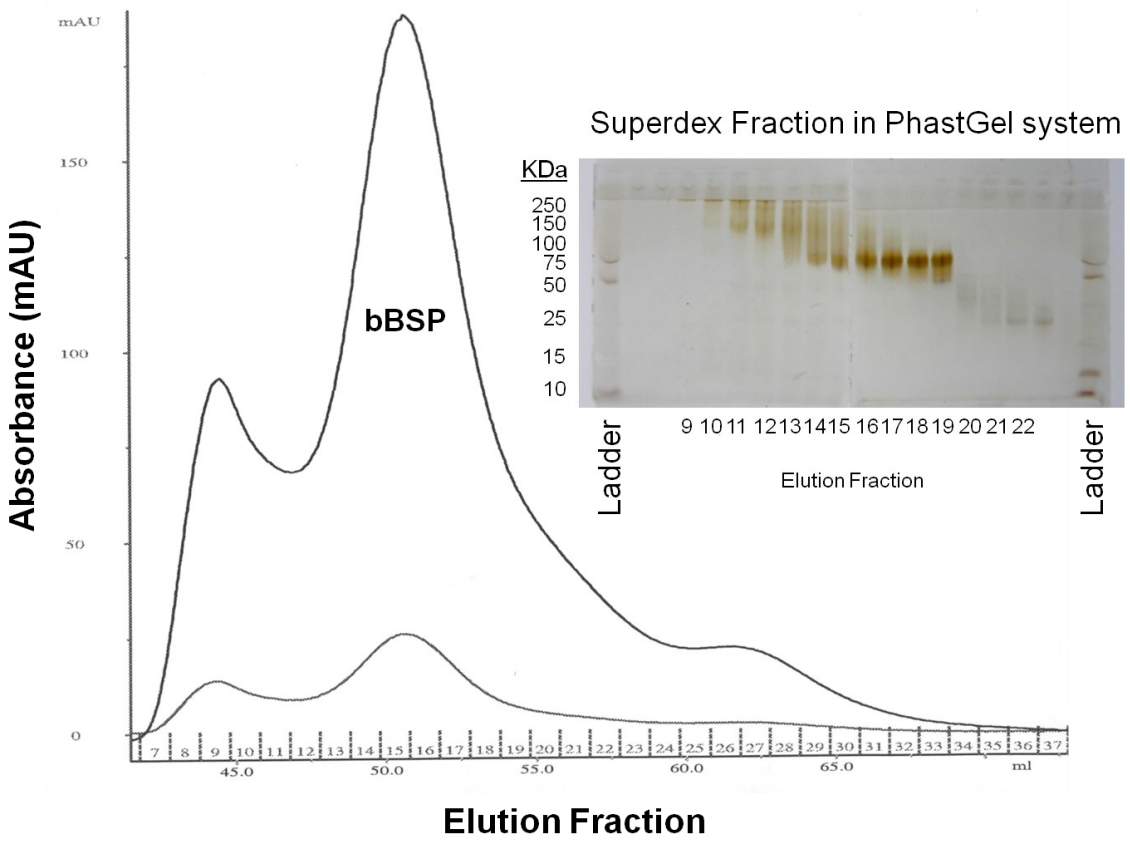

Figure 5.2. Separation of bBSP using Superdex 200 PG gel filtration column.

The fractions from Q-Sepharose chromatography enriched in bBSP were pooled and run on a Superdex gel filtration column. Fractions enriched in bBSP (Fractions 14-19; ~75KDa) were pooled, concentrated and rechromatographed on the gel filtration column (Fig.2.3) Absorbances at 230 and 280 nm were measured.

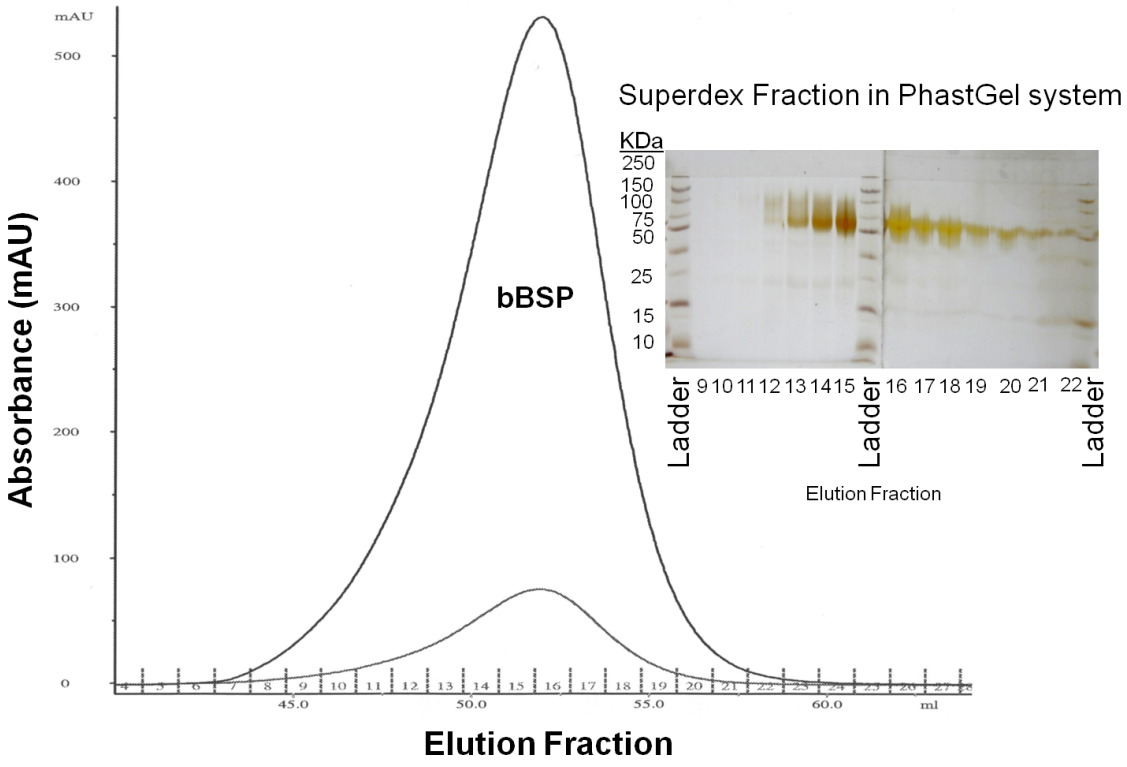

Figure 5.3. Re-purification of bBSP using Superdex 200 PG gel filtration column.

The pooled fractions, which contain mainly bBSP were re-chromatographed on Superdex 200 PG column, and samples analyzed by SDS-PAGE (inset). Fractions 14-18 representing the 'cleanest' fractions enriched in bBSP were pooled and used for future study.

5.3.2 Addition of nHA improved prBSP binding to the PU-based scaffold

To be generally effective in tissue regeneration, scaffolds should demonstrate a propensity to bind and slowly release the added factors. Our binding experiments demonstrated that prBSP are able to bind well to PU-based scaffolds. The PU scaffolds were incubated with prBSP, followed by elution with 0.5 M NaCl which was unable to elute the bound prBSP (Figure 5.4). Based on the relative intensity for both 5 and 10 μg prBSP loading onto scaffold, it was estimated that maximum binding to the PU scaffold was approximately 2.5 μg of prBSP (Table 5.1 and Figure 5.4). The addition of nHA to the PU scaffold was able to increase the binding capacity. Approximately 7 μg of bound prBSP appears to be the limit for nHA/PU scaffolds since loading 10 or 20 μg of prBSP gave similar binding capacity (Table 5.1 and Figure 5.5).

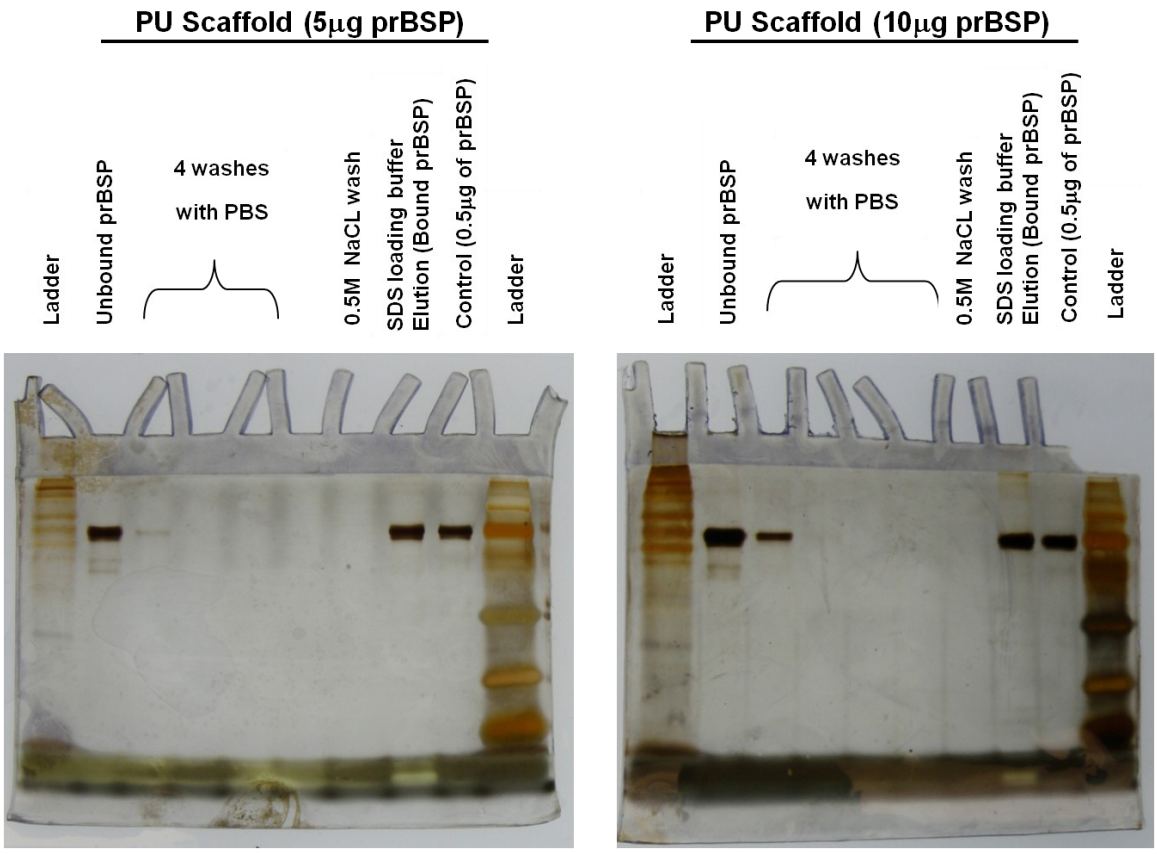

Figure 5.4. SDS-PAGE analysis of prBSP binding to PU scaffold.

The binding capacity of the prBSP on the PU scaffold was determined using a SDS-PAGE based assay. During the assay, a series of washes as indicated was done on the prBSP-treated PU scaffold to remove unbound or weakly bound prBSP. Two concentrations of prBSP - 5 μg (Left image) and 10 μg (Right image) were used. The amount of bound prBSP was estimated by comparing the relative pixel to intensity ratio of the SDS-eluted prBSP band with the total of unbound and from washes, and the intensity to the control 0.5μg of prBSP.

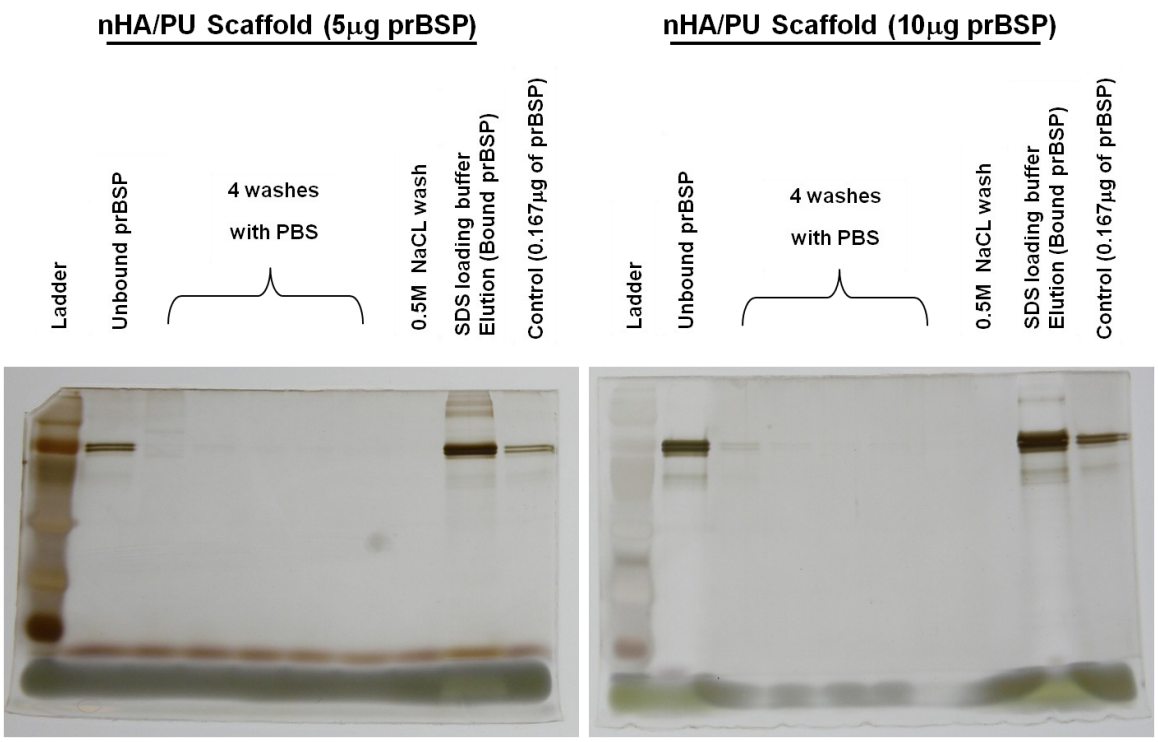

Figure 5.5. SDS-PAGE analysis of prBSP binding to nHA/PU scaffold.

The binding capacity of the prBSP on the nHA/PU scaffold was determined using a SDS-PAGE-based assay. During the assay, a series of washes was done on the prBSP treated nHA/PU scaffold to remove unbound or weakly bound prBSP. Two concentrations of prBSP - 5 μg (Left image) and 10 μg (Right image) were used. The amount of bound prBSP was estimated by comparing the relative pixel to intensity ratio of the SDS-eluted prBSP band with the total of unbound and washes and the intensity to the control 0.167μg of prBSP.

Table 5.1. Estimation of bound prBSP for each treatment group.

The amount of bound prBSP was estimated by comparing the relative pixel to intensity ratio of the SDS eluted prBSP band with the total of unbound, washed, and the control prBSP sample. The assumption was that the total amount of prBSP loaded equaled the combined pixels to intensity ratio of unbound, washed, and eluted prBSP.

	Number of pixels			**Intensity (Mean)**			**Pixels to intensity ratio**			
Sample	**Unbound prBSP**	**Washed prBSP**	**Eluted prBSP**	**Unbound prBSP**	**Washed prBSP**	**Eluted prBSP**	**Unbound prBSP**	**Washed prBSP**	**Eluted prBSP**	**Bound prBSP (µg)**
PU + 5 µg prBSP	4245	1731	4156	30.22	134.05	29.14	140.47	12.91	142.62	2.41
PU + 10 µg prBSP	5911	1451	3889	15.28	24.58	25.38	386.85	59.03	187.84	2.56
nHA/PU + 5 µg prBSP	1535	-	5341	66.48	-	45.56	23.09	-	117.23	4.18
nHA/PU + 10 µg prBSP	4914	-	8075	79.86	-	48.4	61.53	-	166.84	7.31
nHA/PU + 20 µg prBSP	9775	4670	8389	*105.54*	*154.28*	*117.95*	92.62	30.27	71.12	7.33

5.3.3 The addition of BSP improved cell attachment and appeared to have increased mineral formation

The C3H10T11/2 mouse cell line was used to study cell attachment and mineral formation in the HA/PU scaffolds. After only 1 h of incubation, the presence of prBSP increased the number of cells attached to the scaffold by a factor of 5 (Figure 5.6, Table 5.2). Other *in vitro* studies have shown that the addition of recombinant human BSP (rhBSP) to MSC, in the presence of osteogenic media, drive osteogenic differentiation into osteoblasts (Xia et al., 2011). Our experiments with MSC culture demonstrated that the presence of prBSP or bBSP on nHA/PU scaffold appeared to have enhanced mineral formation compared to their respective control groups (Figure 5.7 and 5.8). In addition, these result also indicate that due to the highly conserved nature of BSP, its functional properties are similar regardless of the species source.

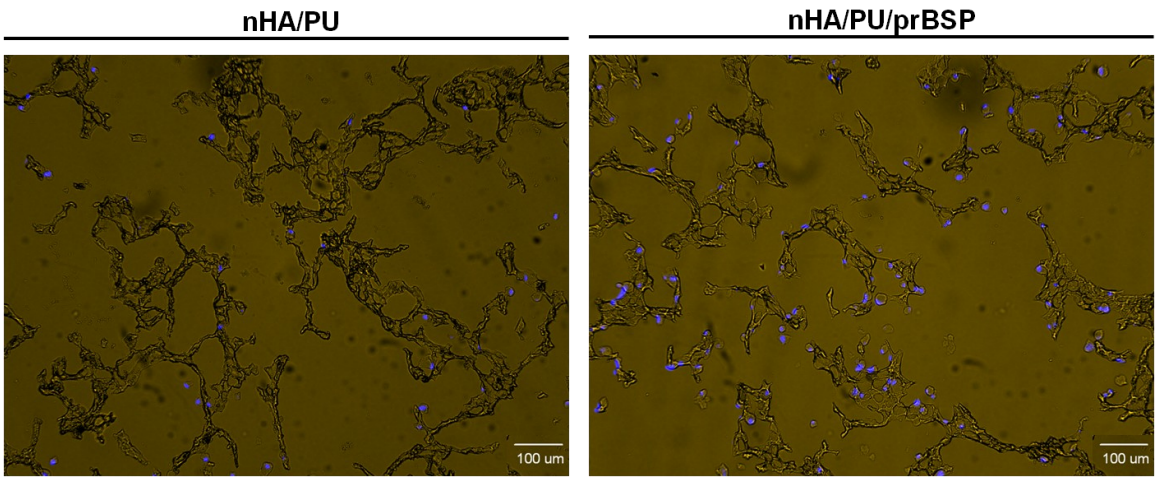

Figure 5.6. The effect of prBSP treated nHA/PU scaffold cultured with C3H10T1/2 cells.

nHA/PU scaffolds were either untreated or treated with 150 µl of prBSP-PBS solution (containing 20 µg of prBSP). Approximately, 1.2 x 10^6 C3H10T1/2 cells were seeded onto the scaffold and then incubated for 1 hr and fixed with 4% PFA. Confocal image of the sectioned scaffold suggests that prBSP treated nHA/PU scaffolds had higher cell attachment compared to control group. Blue is DAPI staining of cell nuclei.

Table 5.2. The effect of BSP on cell attachment to the nHA/PU scaffold.

The presence of BSP increased the number of attached cell to the nHA/PU scaffold.

Treatment group	Total number of cell in the polymer (10^5)	Percentage of cell attached (%)
nHA/PU	0.70	5.80
nHA/PU/prBSP	3.42	28.50

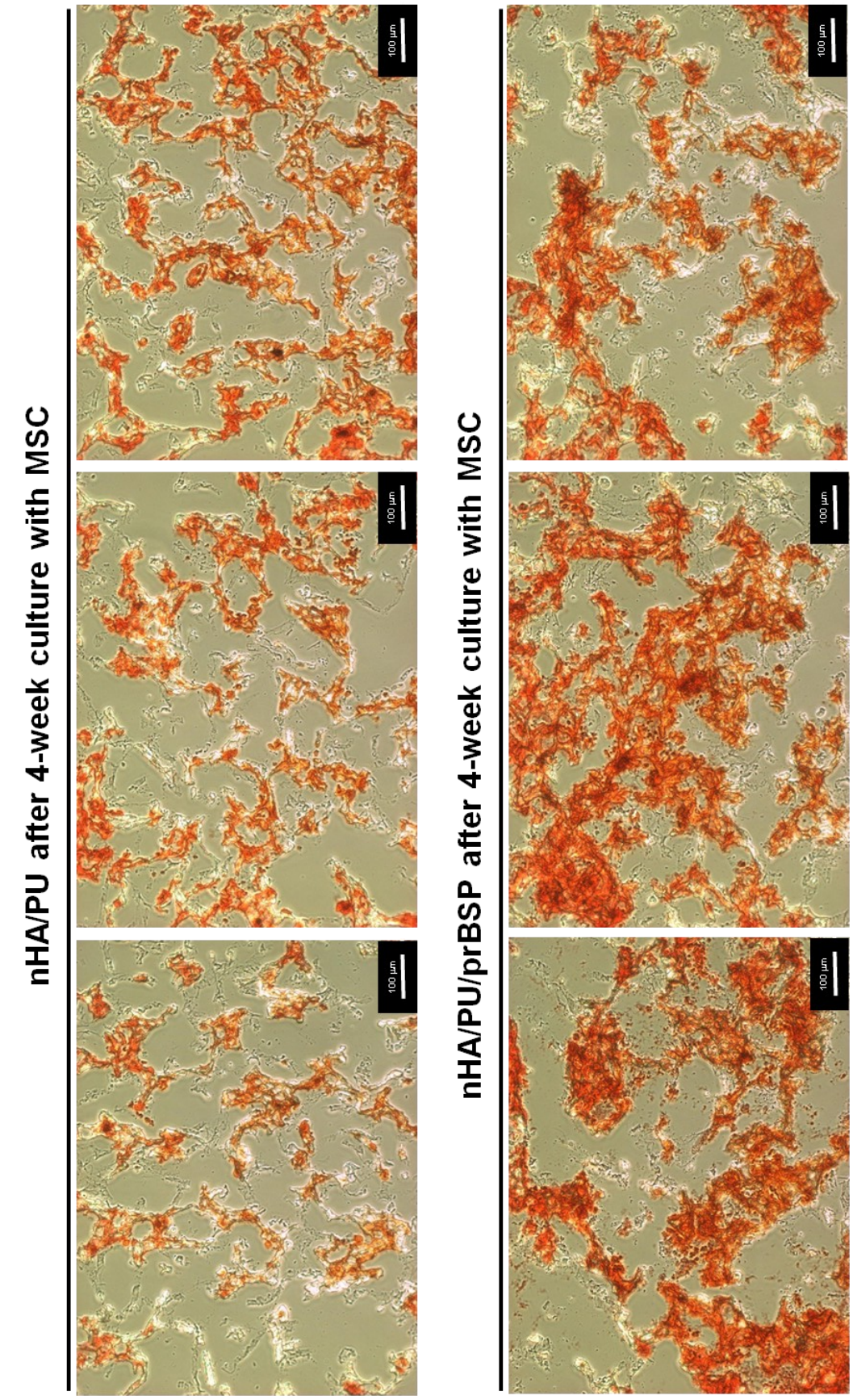
nHA/PU after 4-week culture with MSC
nHA/PU/prBSP after 4-week culture with MSC
100 µm

Figure 5.7. Effect of prBSP on nHA/PU cultured with MSC for 4 weeks.

After 4 weeks, the scaffolds were fixed, cryosectioned, and stained with alizarin red. Compared to the control group, the nHA/PU/prBSP group appeared to demonstrate more alizarin red staining, which suggest an increased in mineral formation. Note: The three images in each group are from different scaffolds.

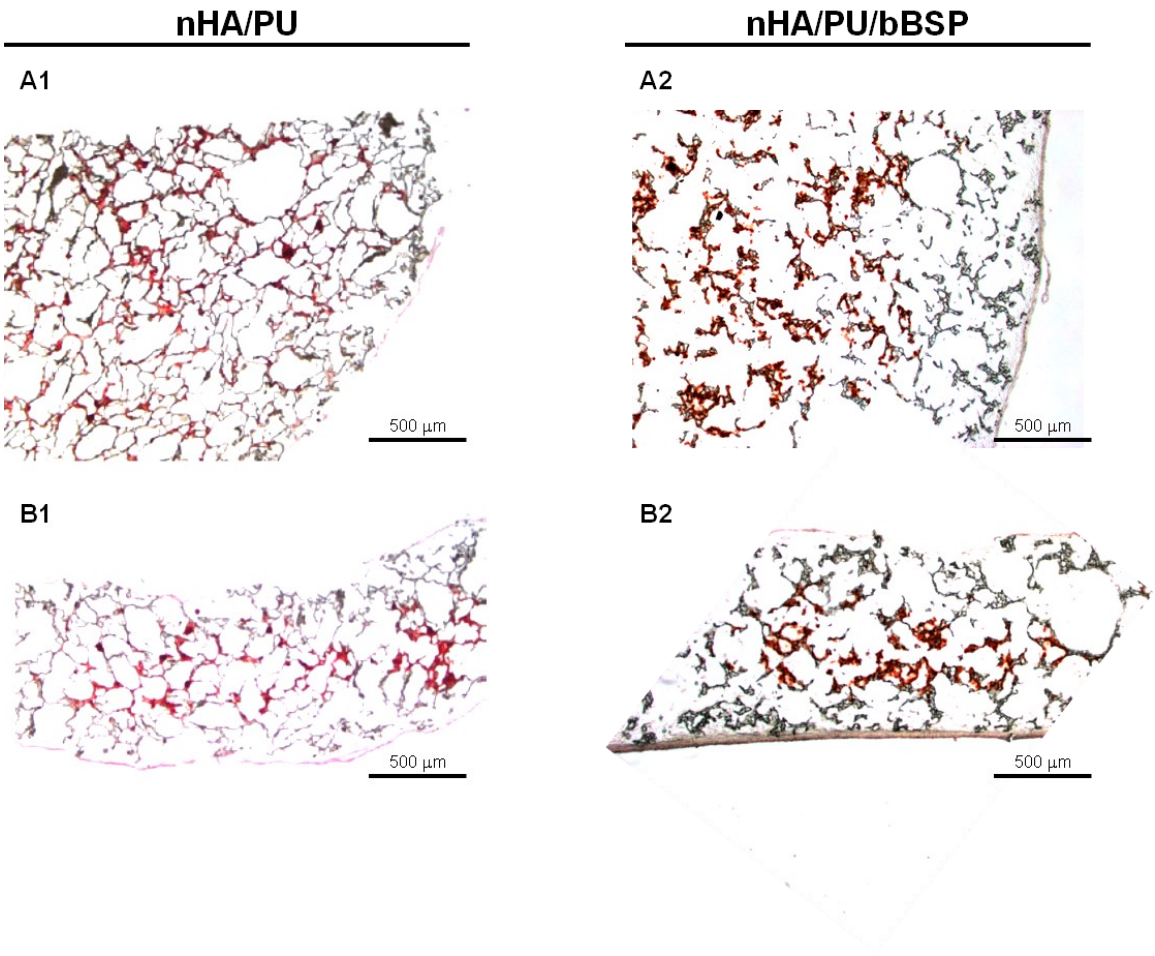

Figure 5.8. Effect of bBSP on nHA/PU cultured with MSC for 4 weeks.

The images in panel A1-2 and B1-2 represent transverse and cross-sectional sections, respectively, of control and bBSP treated nHA/PU scaffolds stained with alizarin red. After 4 weeks, the scaffolds were fixed, cryosectioned, and stained with alizarin red. Compared to the control group, the nHA/PU/bBSP cryosections qualitatively appeared to have more alizarin red staining, which may be due to an increase in osteogenic mineralization.

5.3.4 bBSP treated nHA/PU scaffolds are not effective in promoting bone repair

An established calvarial defect model was used to determine the effectiveness of the bBSP treated nHA/PU scaffolds in promoting *in vivo* bone repair. At 2, 6, and 12 weeks after implantation, the nHA/PU/bBSP group showed similar bone mineral content (BMC), new total bone volume (BV), percentage of bone-to-tissue volume (BV/TV), and percentage of cortical bone volume compared to the control group (Figure 5.9). In both groups, minimal bone in-growth into the defects from host bone and some island-like bone spicules were observed (Figure 5.10). Occasionally, higher bone formation was observed in nHA/PU/bBSP group; however, this was also observed in the control group (Figure 5.11). In agreement with the microCT data, the histological analysis of nHA/PU/bBSP groups also indicated a similar observation compared to control group (Figure 5.12). In contrast, the rhBMP-2 treated nHA/PU group, which is the positive control group was able to promote bone repair as indicated in Chapter 4.

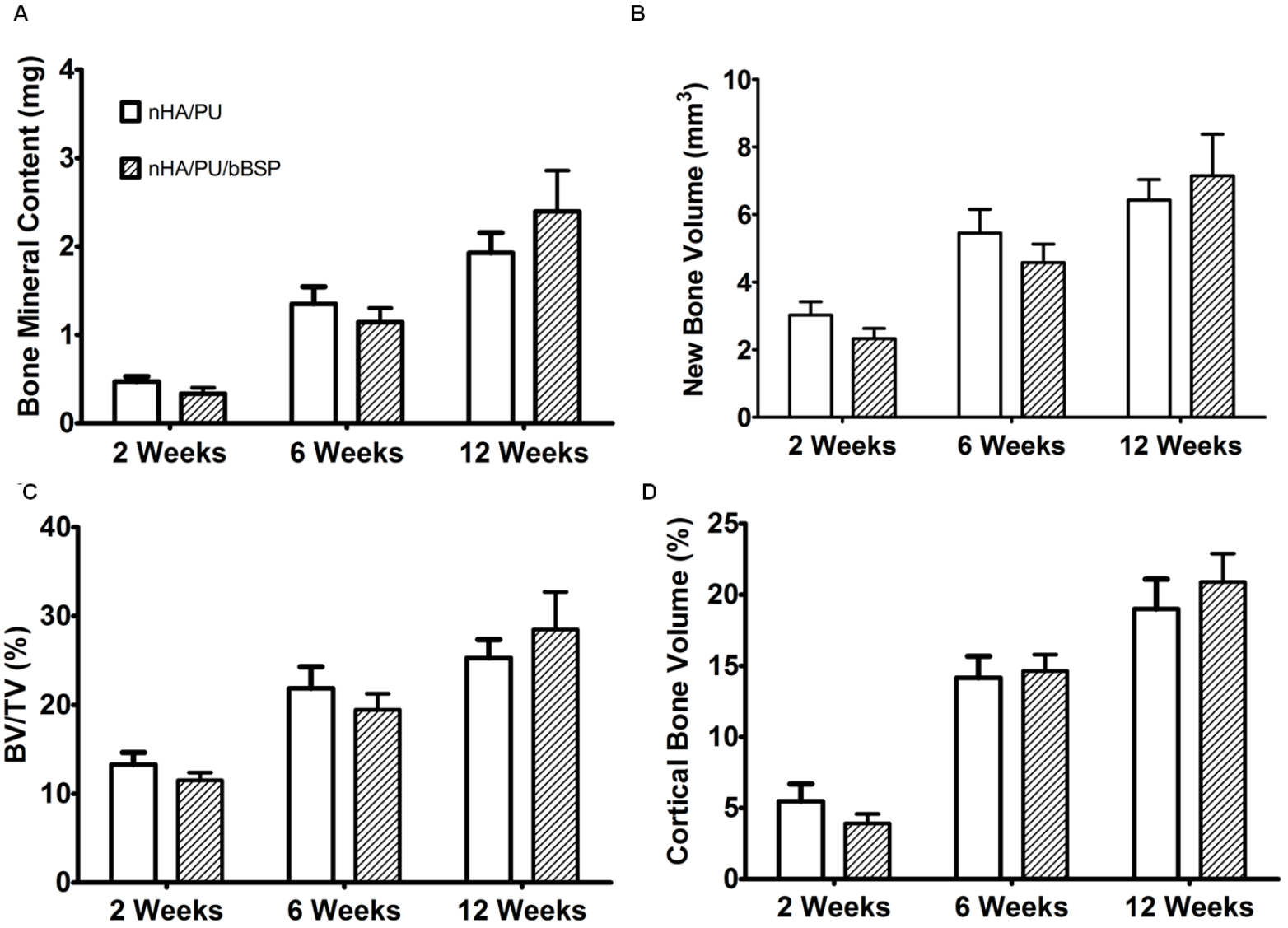
A
Bone Mineral Content (mg)
nHA/PU
nHA/PU/bBSP
0
1
2
3
4
2 Weeks
6 Weeks
12 Weeks
B
New Bone Volume (mm3)
0
2
4
6
8
10
2 Weeks
6 Weeks
12 Weeks
C
BV/TV (%)
0
10
20
30
40
2 Weeks
6 Weeks
12 Weeks
D
Cortical Bone Volume (%)
0
5
10
15
20
25
2 Weeks
6 Weeks
12 Weeks

Figure 5.9. Quantitative microCT analysis of bone repair.

The microCT analysis of **(A)** bone mineral content (BMC); **(B)** new bone volume; **(C)** percentage of bone-to-tissue volume and **(D)** percentage of cortical bone volume were similar for both nHA/PU/bBSP group and nHA/PU group at 2, 6, and 12 weeks. The data suggest that bBSP are not effective in promoting bone repair. Data represents mean ± standard error (n=20 for 2 and 6 weeks, n=12 for 12 weeks)

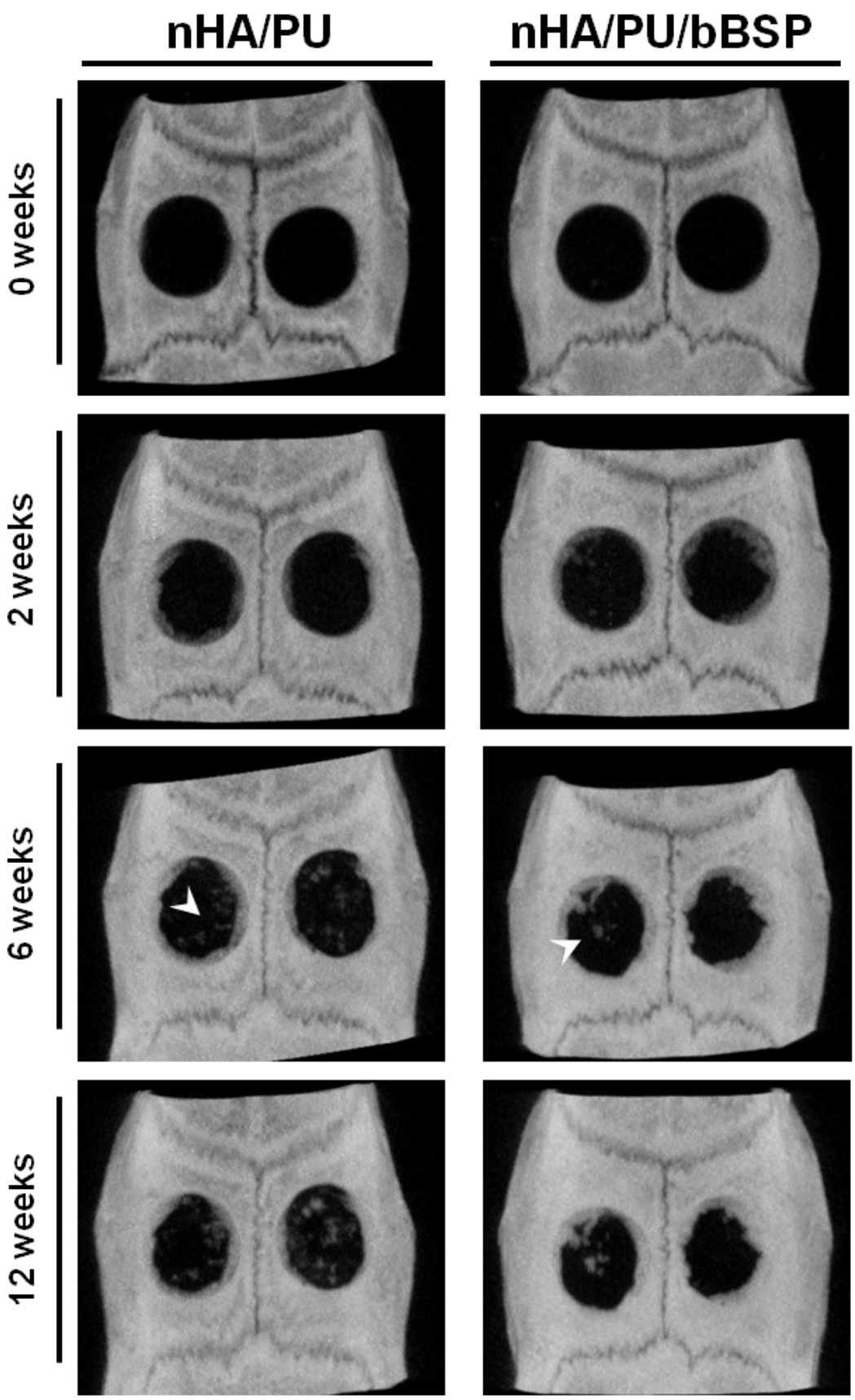
nHA/PU
nHA/PU/bBSP
0 weeks
2 weeks
6 weeks
12 weeks

Figure 5.10. MicroCT images of bone repair in rat calvarial defects from 0 to 12 weeks post-op.

Maximum intensity projection (MIP) images of both nHA/PU and nHA/PU/bBSP demonstrated a similar healing pattern. Both groups often demonstrated variable results as presented in the two representative images for each group. The white arrowheads referred to the island-like bone formation seen in the defect.

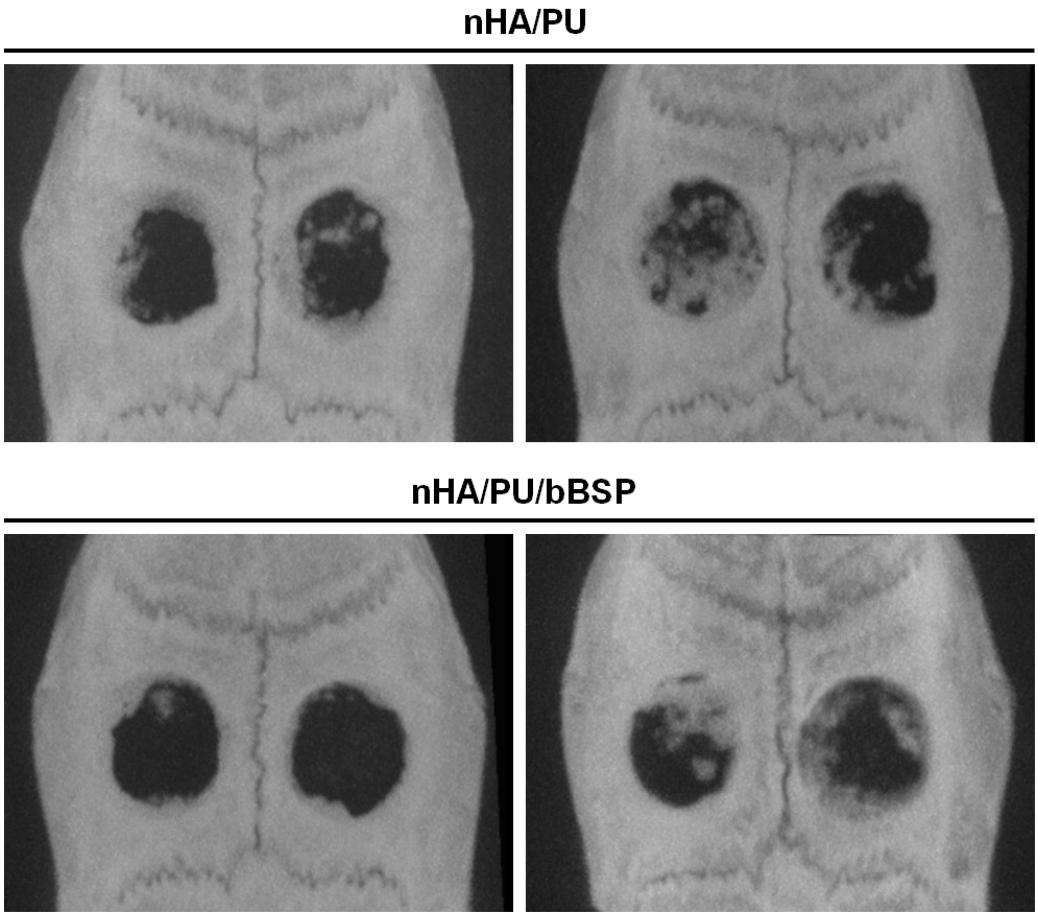

Figure 5.11. MicroCT images of bone repair in rat calvarial defects after 12 weeks post-op.

Maximum intensity projection images of both nHA/PU and nHA/PU/bBSP demonstrated a similar healing pattern. These are additional images from 2 different pair of rats. Both groups demonstrated variable results in bone formation.

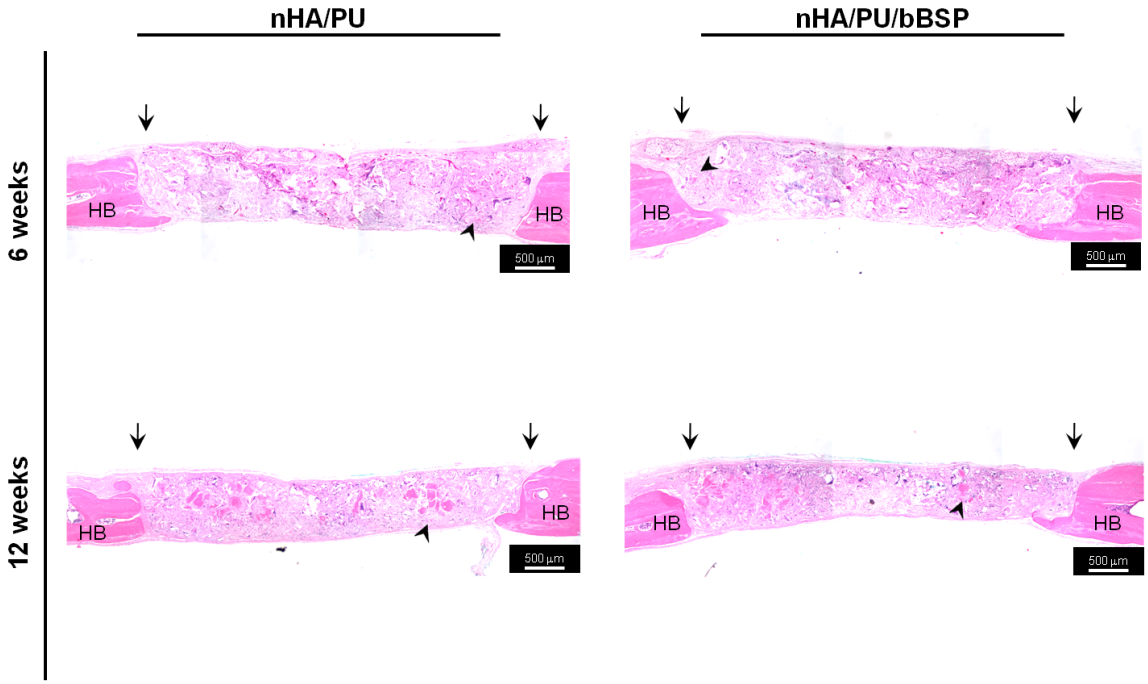

Figure 5.12. Histological analysis of rat calvaria at 12 weeks.

H&E stained sectioned of nHA/PU/bBSP and nHA/PU groups demonstrated similar bone repair response even after 12 weeks post-op. Minimal island-like new bone formation are observed in the defect site as marked by black arrows. No apparent major inflammation can be seen in any of the groups. These results suggest that BSP is not a potent promoter of bone repair.

5.4 DISCUSSION

In tissue engineering, prevalent strategies to enhance bone repair utilize osteoconductive biomaterials in combination with osteoinductive growth factors or bioactive proteins. This study was designed to evaluate the effectiveness of BSP-treated nHA/PU scaffolds for guided bone regeneration using a rat calvarial defect model. BSP is an extracellular matrix protein present in mineralized tissue such as bone and dentition. The expression of BSP in mineralized tissues is upregulated at the onset of mineralization. Previous studies have shown that the presence of BSP enhances osteoblast differentiation and HA nucleation *in vitro* (Cooper et al., 1998; Zhou et al., 1995). In addition, other studies have also provided evidence for the role of BSP in bone formation, in which the authors demonstrate that the presence of BSP enhanced bone repair *in vivo* (Wang et al., 2006; Xu et al., 2007).

The presence of BSP in the PU based scaffold is able to promote cell attachment and differentiation, which in turn led to the improved overall osteogenic mineralization *in vitro*. The addition of nHA was able to significantly improve the PU-based scaffold capability to bind BSP. These results confirmed the effectiveness of nHA/PU scaffold as a carrier for bioactive proteins. Unfortunately, in spite of the promising *in vitro* results, our data indicated that, in our model, the presence of BSP was not effective in promoting bone regeneration *in vivo*; suggesting that BSP is not a potent promoter of bone repair.

5.4.1 The presence of BSP enhanced mineral formation *in vitro;* however, BSP is not effective for bone repair in our *in vivo* model.

In the literature, there are few studies on the potential role of BSP as a therapeutic reagent to promote bone repair. However, over the years, various *in vitro* studies have postulated for an important role of BSP in biomineralization and bone development. Previous studies including from our group were able to identify the three functional regions of BSP [collagen binding, HA nucleation, and integrin recognition (RGD)] that play important

roles in biomineralization as described in (Goldberg and Hunter, 2012). In addition, various *in vitro* studies were able to demonstrate that BSP promotes cell proliferation and differentiation to osteoblasts, which led to increase osteogenic mineralization in culture (Cooper et al., 1998; Gordon et al., 2007; Xia et al., 2011; Zhou et al., 1995). *In vivo* studies demonstrated that *Bsp*$^{-/-}$ mice have a bone phenotype, which include lower bone density, shorter long bone length, thinner femoral cortical bone (Malaval et al., 2008), and slower bone repair process (Malaval et al., 2009; Monfoulet et al., 2010). Furthermore, the use of BSP bound to native but not denatured collagen in an *in vivo* bone repair model was effective in promoting bone repair (Wang et al., 2006; Xu et al., 2007). These latter authors indicated that bovine BSP-treated collagen scaffold in rat calvarial defects was able to promote early mineral deposition within the first 4 days, followed by new bone formation over time. These findings led us to believe that BSP can be a good therapeutic reagent for bone repair since it plays an important role in mineralization and maintains homeostasis during bone remodeling (Ganss et al., 1999; Goldberg and Hunter, 2012).

In our study, we investigated the potential use of BSP-treated nHA/PU scaffolds in bone repair. Previous studies indicated that long term delivery of growth factors such as bone morphogenetic-2 (BMP-2) has resulted in greater amount of bone formation compared to a shorter term delivery (La et al., 2010). The authors showed the importance of continuous presence of the BMP-2 in the system during bone repair. For this study, we believed that the presence of BSP throughout the bone repair was also crucial; therefore increasing the BSP binding capability of the PU scaffold was determined to be a necessity. Previous studies had shown that the addition of nHA improved the adsorption of bovine serum albumin, fibrinogen, and other proteins derived from fetal calf serum to the scaffold (Laschke et al., 2010b). Our results confirmed that the addition of nHA particles also increased the level of BSP bound to the nHA/PU scaffold. Furthermore, our binding studies demonstrated that the elution step with high salt was unable to remove the additional BSP from the nHA modified PU scaffolds, suggesting that the BSP was tightly bound to the exposed hydroxyapatite. Of relevance, hydroxyapatite is a well-established material used in chromatographical purification since it has significant protein

binding properties (Matsumoto et al., 2004; Shen et al., 2008; Xie et al., 2010). The data from the binding studies suggest that nHA/PU scaffold is an effective carrier for BSP.

The addition of either prBSP or bBSP to the scaffolds was able to enhance cell attachment and mineral formation in our *in vitro* cultures compared to the control group. The integrin recognition region (RGD sequence) near the C-terminus of BSP likely contributed to the recruitment and attachment of cells onto the scaffold. RGD motifs are known to mediate cell attachment and signaling for differentiation and migration since it interacts with the $\alpha_v\beta_3$ integrin, a cell-surface receptor present in both osteoblasts (Oldberg et al., 1988) and osteoclasts (Helfrich et al., 1992). Furthermore, other *in vitro* studies also indicated that the addition of BSP was found to improve the overall osteoconductivity of implants made from various materials such as titanium, ceramic, and synthetic polymer and enhanced cell attachment (Graf et al., 2008; O'Toole et al., 2004). These *in vitro* results were promising and together with previous demonstration of BSP promoting *in vivo* bone repair (Wang et al., 2006), led us to perform *in vivo* experiments using rat calvarial defect model to monitor the effect of BSP in bone repair.

Analysis of the implanted BSP-treated nHA/PU scaffolds in rat calvarial defects resulted in no significant differences in new bone formation compared to the control group. The results of both prBSP and bBSP-treated scaffold were variable, in which moderate amount of island-like bone formation were observed on occasion in the defect site; however, most of the time only minimal bone formation were observed. These surprising results prompted us to look at the use of collagen scaffold instead of nHA/PU scaffold to re-confirm the positive result from previous published studies (Wang et al., 2006; Xu et al., 2007). However, similar to BSP-treated nHA/PU scaffold, BSP-treated collagen scaffold did not enhance bone formation compared to the respective control group (data not shown, n=4). Of relevance, other *in vivo* studies also indicate that the presence of BSP did not significantly enhanced the efficiency of bone formation (Schaeren et al., 2010) or improved the strength of implant-bone integration (O'Toole et al., 2004). Similar to our study, the authors demonstrated that in the *in vitro* setting the presence of BSP induced cell differentiation and osteogenic mineralization. However, in their *in vivo* system, BSP was not effective in enhancing bone repair.

In order to understand how the Glimcher group (Wang et al., 2006; Xu et al., 2007) was able to show that BSP promoted bone repair *in vivo*, we contacted the authors responsible for the study (Glimcher is deceased). In contrast to what was indicated in their manuscripts (Wang et al., 2006; Xu et al., 2007), succinimide was added to the BSP-collagen incubation solution, which immobilized the BSP through covalent linkage to the collagen (E. Salih, personal communication). The use of succinimide, which is a potent cross-linking agent was not indicated in the relevant manuscripts. Confirmation of this knowledge, as well as additional information regarding the relatively poor potency of BSP and collagen mixtures to promote bone repair *in vivo* was also obtained (J. Wang, personal communication). It has been documented that immobilization of anionic peptides or proteins to a surface promotes nucleation since the overall negative charges of the protein will attract and bind calcium, which will initiate mineral formation by itself. For example, phosphorylated acidic peptides have been demonstrated to act as nucleators of HA when immobilized on a surface (Saito et al., 1997). It is well known that the implantation of mineral in bone defects, either hydroxyapatite or calcium carbonate, is relatively effective in initiating bone repair (Fu et al., 2013; Parizi et al., 2013). Thus the initiation of mineral deposition in the calvarial defects that was evident in the Wang et al. study, may have been the required prerequisite to initiate the remodeling sequence that would ultimately drive the bone repair that was observed in their study. While BSP binds tightly to collagen, it is quite possible that the HA nucleating regions in BSP are less susceptible to blood derived enzymatic activity if crosslinked to collagen. Enzymatic activity would normally be elevated during the initial stages of repair.

Our recent studies have shown that some of the *Bsp*$^{-/-}$ mice bone defects reported by the Malaval group are related to malnourishment (Soenjaya et al., 2015). The absence of BSP resulted in defective acellular cementum formation (Foster et al., 2013b), which in turn destabilized the periodontium, causing periodontal breakdown and tooth malocclusion. As a result the *Bsp*$^{-/-}$ mice were not able to feed properly. When given a soft food diet, many of the bone phenotypes were reversible. These results suggested that *Bsp*$^{-/-}$ mice do not have a major bone phenotype as described in the previous studies done by the Malaval's group. In spite of the ineffectiveness of BSP in enhancing bone repair in our study, BSP has still been shown to be relevant for bone development since delayed

mineralization were observed in fetal or young long bones (Holm et al., 2015) and craniofacial bones (Foster et al., 2015) of *Bsp*$^{-/-}$ mice. In addition, absence of BSP was also shown to negatively affect the rate of bone repair and cause reduced osteoclast activity (Malaval et al., 2008; Monfoulet et al., 2010). Therefore, there is a possibility that BSP may be more relevant in promoting osteoclast formation and maintaining osteoclast activity. If this process is delayed, then bone turnover will also be delayed.

In summary, this study showed that BSP can bind effectively onto the nHA/PU scaffold and the presence of BSP resulted in improved cell attachment and osteogenic mineralization *in vitro*. These results confirmed that nHA/PU scaffold is an effective carrier for bioactive proteins. However, in spite of the encouraging observation in the *in vitro* experiments, our *in vivo* studies using the calvarial defect model indicate that BSP by itself is not an effective therapeutic reagent for enhancing bone repair.

5.5 REFERENCES

Baht GS, O'Young J, Borovina A, Chen H, Tye CE, Karttunen M *et al.* (2010). Phosphorylation of Ser^{136} is critical for potent bone sialoprotein-mediated nucleation of hydroxyapatite crystals *Biochem J* 428(385-395.

Boissard CIR, Bourban PE, Tami AE, Alini M, Eglin D (2009). Nanohydroxyapatite/poly(ester urethane) scaffold for bone tissue engineering. *Acta Biomaterialia* 5(9)*:*3316-3327.

Boudiffa M, Wade-Gueye NM, Guignandon A, Vanden-Bossche A, Sabido O, Aubin JE *et al.* (2010). Bone sialoprotein deficiency impairs osteoclastogenesis and mineral resorption in vitro. *J Bone Miner Res* 25(12)*:*2669-2679.

Cooper LF, Yliheikkila PK, Felton DA, Whitson SW (1998). Spatiotemporal assessment of fetal bovine osteoblast culture differentiation indicates a role for BSP in promoting differentiation. *J Bone Miner Res* 13(4)*:*620-632.

Dresing I, Zeiter S, Auer J, Alini M, Eglin D (2014). Evaluation of a press-fit osteochondral poly(ester-urethane) scaffold in a rabbit defect model. *Journal of Materials Science: Materials in Medicine* 25(7)*:*1691-1700.

Fisher LW, Fedarko NS (2003). Six genes expressed in bones and teeth encode the current members of the SIBLING family of proteins. *Connect Tissue Res* 44(1)*:*33-40.

Foster BL, Soenjaya Y, Nociti FH, Holm E, Zerfas PM, Wimer HF *et al.* (2013). Deficiency in acellular cementum and periodontal attachment in Bsp null mice. *J Dent Res* 92(2)*:*166-172.

Foster BL, Ao M, Willoughby C, Soenjaya Y, Holm E, Lukashova L *et al.* (2015). Mineralization defects in cementum and craniofacial bone from loss of bone sialoprotein. *Bone* 78(150-164.

Fu K, Xu Q, Czernuszka J, Triffitt JT, Xia Z (2013). Characterization of a biodegradable coralline hydroxyapatite/calcium carbonate composite and its clinical implementation. *Biomed Mater* 8(6)*:*065007.

Ganss B, Kim RH, Sodek J (1999). Bone sialoprotein. *Crit Rev Oral Biol Med* 10(1)*:*79-98.

Gogolewski S, Gorna K, Zaczynska E, Czarny A (2008). Structure–property relations and cytotoxicity of isosorbide-based biodegradable polyurethane scaffolds for tissue repair and regeneration. *Journal of Biomedical Materials Research Part A* 85A(2)*:*456-465.

Goldberg HA, Sodek J (1994). Purification of mineralized tissue-associated osteopontin. *Methods in Cell Science* 16(3)*:*211-215.

Goldberg HA, Warner KJ (1997). The staining of acidic proteins on polyacrylamide gels: enhanced sensitivity and stability of "Stains-all" staining in combination with silver nitrate. *Anal Biochem* 251(2)*:*227-233.

Goldberg HA, Hunter GK (2012). Functional domains of bone sialoprotein. In: Phosphorylated extracellular matrix proteins of bone and dentin. M Goldberg editor. Oak Park (IL): Bentham Science Publishers, pp. 266-282.

Gordon JAR, Tye CE, Sampaio AV, Underhill TM, Hunter GK, Goldberg HA (2007). Bone sialoprotein expression enhances osteoblast differentiation and matrix mineralization in vitro. *Bone* 41(3)*:*462-473.

Gorna K, Gogolewski S (2006). Biodegradable porous polyurethane scaffolds for tissue repair and regeneration. *Journal of Biomedical Materials Research Part A* 79A(1)*:*128-138.

Graf HL, Stoeva S, Armbruster FP, Neuhaus J, Hilbig H (2008). Effect of bone sialoprotein and collagen coating on cell attachment to TICER® and pure titanium implant surfaces. *Int J Oral Maxillofac Surg* 37(7)*:*634-640.

Guan J, Fujimoto KL, Sacks MS, Wagner WR (2005). Preparation and characterization of highly porous, biodegradable polyurethane scaffolds for soft tissue applications. *Biomaterials* 26(18)*:*3961-3971.

Guelcher SA (2008). Biodegradable polyurethanes: synthesis and applications in regenerative medicine. *Tissue Eng Part B Rev* 14(1)*:*3-17.

Guelcher SA, Srinivasan A, Dumas JE, Didier JE, McBride S, Hollinger JO (2008). Synthesis, mechanical properties, biocompatibility, and biodegradation of polyurethane networks from lysine polyisocyanates. *Biomaterials* 29(12)*:*1762-1775.

Helfrich MH, Nesbitt SA, Dorey EL, Horton MA (1992). Rat osteoclasts adhere to a wide range of RGD (Arg-Gly-Asp) peptide-containing proteins, including the bone sialoproteins and fibronectin, via a beta 3 integrin. *J Bone Miner Res* 7(3)*:*335-343.

Hofmann A, Ritz U, Verrier S, Eglin D, Alini M, Fuchs S *et al.* (2008). The effect of human osteoblasts on proliferation and neo-vessel formation of human umbilical vein endothelial cells in a long-term 3D co-culture on polyurethane scaffolds. *Biomaterials* 29(31)*:*4217-4226.

Holm E, Aubin JE, Hunter GK, Beier F, Goldberg HA (2015). Loss of bone sialoprotein leads to impaired endochondral bone development and mineralization. *Bone* 71(0)*:*145-154.

Hunter GK, Goldberg HA (1993). Nucleation of hydroxyapatite by bone sialoprotein. *Proc Natl Acad Sci U S A* 90(18)*:*8562-8565.

Kavlock KD, Pechar TW, Hollinger JO, Guelcher SA, Goldstein AS (2007). Synthesis and characterization of segmented poly(esterurethane urea) elastomers for bone tissue engineering. *Acta Biomater* 3(4)*:*475-484.

La WG, Kang SW, Yang HS, Bhang SH, Lee SH, Park JH *et al.* (2010). The efficacy of bone morphogenetic protein-2 depends on its mode of delivery. *Artif Organs* 34(12)*:*1150-1153.

Laschke MW, Strohe A, Scheuer C, Eglin D, Verrier S, Alini M *et al.* (2009). In vivo biocompatibility and vascularization of biodegradable porous polyurethane scaffolds for tissue engineering. *Acta Biomaterialia* 5(6)*:*1991-2001.

Laschke MW, Strohe A, Menger MD, Alini M, Eglin D (2010). In vitro and in vivo evaluation of a novel nanosize hydroxyapatite particles/poly(ester-urethane) composite scaffold for bone tissue engineering. *Acta Biomaterialia* 6(6)*:*2020-2027.

Laschke MW, Schank TE, Scheuer C, Kleer S, Schuler S, Metzger W *et al.* (2013). Three-dimensional spheroids of adipose-derived mesenchymal stem cells are potent initiators of blood vessel formation in porous polyurethane scaffolds. *Acta Biomaterialia* 9(6)*:*6876-6884.

Lee C, Grad S, Gorna K, Gogolewski S, Goessl A, Alini M (2005). Fibrin–Polyurethane Composites for Articular Cartilage Tissue Engineering: A Preliminary Analysis. *Tissue Engineering* 11(9-10)*:*1562-1573.

Li B, Yoshii T, Hafeman AE, Nyman JS, Wenke JC, Guelcher SA (2009). The effects of rhBMP-2 released from biodegradable polyurethane/microsphere composite scaffolds on new bone formation in rat femora. *Biomaterials* 30(35)*:*6768-6779.

Malaval L, Wade-Guéye NM, Boudiffa M, Fei J, Zirngibl R, Chen F *et al.* (2008). Bone sialoprotein plays a functional role in bone formation and osteoclastogenesis. *J Exp Med* 205(5)*:*1145-1153.

Malaval L, Monfoulet L, Fabre T, Pothuaud L, Bareille R, Miraux S *et al.* (2009). Absence of bone sialoprotein (BSP) impairs cortical defect repair in mouse long bone. *Bone* 45(5)*:*853-861.

Matsumoto T, Okazaki M, Inoue M, Yamaguchi S, Kusunose T, Toyonaga T *et al.* (2004). Hydroxyapatite particles as a controlled release carrier of protein. *Biomaterials* 25(17)*:*3807-3812.

Monfoulet L, Malaval L, Aubin JE, Rittling SR, Gadeau AP, Fricain J-C *et al.* (2010). Bone sialoprotein, but not osteopontin, deficiency impairs the mineralization of regenerating bone during cortical defect healing. *Bone* 46(2)*:*447-452.

O'Toole GC, Salih E, Gallagher C, FitzPatrick D, O'Higgins N, O'Rourke SK (2004). Bone sialoprotein-coated femoral implants are osteoinductive but mechanically compromised. *J Orthop Res* 22(3)*:*641-646.

Oldberg A, Franzen A, Heinegard D, Pierschbacher M, Ruoslahti E (1988). Identification of a bone sialoprotein receptor in osteosarcoma cells. *J Biol Chem* 263(36)*:*19433-19436.

Parizi AM, Oryan A, Shafiei-Sarvestani Z, Bigham-Sadegh A (2013). Effectiveness of synthetic hydroxyapatite versus Persian Gulf coral in an animal model of long bone defect reconstruction. *J Orthop Traumatol* 14(4)*:*259-268.

Pirvu T, Blanquer SBG, Benneker LM, Grijpma DW, Richards RG, Alini M *et al.* (2015). A combined biomaterial and cellular approach for annulus fibrosus rupture repair. *Biomaterials* 42(0)*:*11-19.

Saito T, Arsenault AL, Yamauchi M, Kuboki Y, Crenshaw MA (1997). Mineral induction by immobilized phosphoproteins. *Bone* 21(4)*:*305-311.

Schaeren S, Jaquiéry C, Wolf F, Papadimitropoulos A, Barbero A, Schultz-Thater E *et al.* (2010). Effect of bone sialoprotein coating of ceramic and synthetic polymer materials on in vitro osteogenic cell differentiation and in vivo bone formation. *Journal of Biomedical Materials Research Part A* 92A(4)*:*1461-1467.

Shen J-W, Wu T, Wang Q, Pan H-H (2008). Molecular simulation of protein adsorption and desorption on hydroxyapatite surfaces. *Biomaterials* 29(5)*:*513-532.

Soenjaya Y, Foster BL, Nociti FH, Jr., Ao M, Holdsworth DW, Hunter GK *et al.* (2015). Mechanical Forces Exacerbate Periodontal Defects in Bsp-null Mice. *J Dent Res* 94(9)*:*1276-1285.

Tye CE, Rattray KR, Warner KJ, Gordon JAR, Sodek J, Hunter GK *et al.* (2003). Delineation of the Hydroxyapatite-nucleating Domains of Bone Sialoprotein. *J Biol Chem* 278(10)*:*7949-7955.

Wang J, Zhou H-Y, Salih E, Xu L, Wunderlich L, Gu X *et al.* (2006). Site-Specific *In Vivo* Calcification and Osteogenesis Stimulated by Bone Sialoprotein. *Calcif Tissue Int* 79(3)*:*179-189.

White D (1978). Tissue substitutes in experimental radiation physics. *Med Phys* 5(6)*:*467-479.

Xia B, Wang J, Guo L, Jiang Z (2011). Effect of bone sialoprotein on proliferation and osteodifferentiation of human bone marrow-derived mesenchymal stem cells in vitro. *Biologicals* 39(4)*:*217-223.

Xie G, Sun J, Zhong G, Liu C, Wei J (2010). Hydroxyapatite nanoparticles as a controlled-release carrier of BMP-2: absorption and release kinetics in vitro. *J Mater Sci Mater Med* 21(6)*:*1875-1880.

Xu L, Anderson AL, Lu Q, Wang J (2007). Role of fibrillar structure of collagenous carrier in bone sialoprotein-mediated matrix mineralization and osteoblast differentiation. *Biomaterials* 28(4)*:*750-761.

Zhou HY, Takita H, Fujisawa R, Mizuno M, Kuboki Y (1995). Stimulation by bone sialoprotein of calcification in osteoblast-like MC3T3-E1 cells. *Calcif Tissue Int* 56(5)*:*403-407.

CHAPTER 6

6 Discussion

6.1 DISCUSSION

Development and repair of skeletal tissue and its subsequent mineralization involve complex processes and cell-cell interaction. During the onset of mineralization, the expression of bone sialoprotein (BSP) is up-regulated in mineralized tissues such as the bones and teeth (Fisher and Fedarko, 2003; Ganss et al., 1999). Our previous studies have been focused on determining the functional roles of BSP in biomineralization. These include the demonstration that BSP has three highly conserved functional regions: 1) collagen-binding region, 2) two HA-nucleation regions, and 3) an integrin recognition region (Goldberg and Hunter, 2012). However, we still have yet to determine which one or combination of the three functional regions is the most critical for biomineralization and bone formation. The nucleating regions of BSP were found to not only contribute as HA nucleation sites (Hunter and Goldberg, 1993) but also allow for binding to HA (Goldberg et al., 2001; Stubbs et al., 1997). The phosphorylation of BSP was verified to be a very important modification of BSP since this regulated the HA nucleation potency, especially at the Serine-136 position (Baht et al., 2010). Additional studies demonstrated that the HA nucleation potency of BSP is further enhanced when it is bound to collagen (Baht et al., 2008). This suggests that the combination of collagen binding and HA nucleation regions might potentially be important for bone formation. The integrin binding region (RGD motif) of BSP has been previously shown to mediate cell attachment to the matrix and cell signaling as well as contributing to differentiation of osteoprogenitor cells to osteoblasts and their migration (Gordon et al., 2007). The RGD motif is recognized by cell-surface receptors, in particular the $\alpha_v\beta_3$ integrin, which are present in both osteoblasts (Oldberg et al., 1988) and osteoclasts (Helfrich et al., 1992).

In recent years, the physiological relevance of BSP in skeletal development has also been investigated by other research groups using the *Bsp*$^{-/-}$ mouse model. In various *in vivo* studies, *Bsp*$^{-/-}$ mice were found to have impaired bone growth and mineralization. The observed bone phenotype includes: shortened long bone, delayed mineral formation, reduced bone mineral density, and thinner cortical bone thickness compared to WT mice (Malaval et al., 2008). The absence of BSP was also found to negatively affect osteoclast formation and activities (Boudiffa et al., 2010; Malaval et al., 2008), which in turn

reduced bone turnover. As a result, *Bsp*$^{-/-}$ mice also displayed delayed bone repair compared to WT mice (Malaval et al., 2009; Monfoulet et al., 2010). Furthermore, previous studies had indicated that BSP is a promising therapeutic reagent for bone repair. Using a rat calvarial model, the authors were able to induce osteoprogenitor cell recruitment and early mineralization at the defect site when it was implanted with BSP-treated collagen scaffold (Wang et al., 2006; Xu et al., 2007). All of these studies provided strong evidence for BSP playing an important role in bone development and mineralization.

Bone is not the only mineralized tissue that expresses BSP. Studies have shown that BSP is also present in both acellular and cellular cementum (Macneil et al., 1994; McKee et al., 1996), however the role of BSP in cementum development is undefined. The acellular cementum is a thin layer of mineralized tissue that covers the cervical portion of the tooth root. This tissue layer has been shown to be important in maintaining the attachment of the periodontal ligament (PDL) to the tooth root surface (Bosshardt, 2005; Foster et al., 2007). In contrast, the cellular cementum is a bone-like tissue covering the apical portions of the tooth root. During normal root formation, cementoblasts express and secrete BSP which led us to postulate that it likely contributes to cementum formation and mineralization (Macneil et al., 1995; Somerman et al., 1990).

The purpose of this thesis project was to further understand the role of BSP in the periodontal development and its potential as a therapeutic reagent for bone repair. The information gained from these studies will allow us to potentially design a new novel therapeutic peptide, based on BSP functional regions, for use in enhancing periodontal and bone repair.

Role of BSP in mineralized tissue development

In the absence of BSP, we demonstrated that acellular cementum formation is severely affected (chapters 2 and 3). *Bsp*$^{-/-}$ mice have severe periodontal tissue breakdown, marked by defective acellular cementum on both of the molar and incisor roots. The

acellular cementum appeared hypomineralized and detachment was observed at the acellular cementum-PDL interface (Foster et al., 2013b). The PDL detachment from the cementum likely contributed to the observed disorganization of PDL Sharpey's fibers, increased epithelial down-growth into the detached space, and tooth malocclusion. The destabilization of the periodontium eventually resulted in extensive root and alveolar bone resorption (Foster et al., 2013b). In comparison, under normal conditions, PDL fibers inserted into the cementum, anchor and stabilize the tooth. Previously, our group demonstrated that BSP has a high binding affinity site to collagen (Tye et al., 2005), and its HA nucleation potency is significantly increased (10-fold) when bound to collagen (Baht et al., 2010). Thus, BSP may function as a glue at the cementum-PDL interface while promoting proper mineralization of the tissue, which in turn, provides stabilization of the tissue. Histological analyses indicated that the structural defect only occurs at the acellular cementum-PDL interface. The alveolar bone-PDL interface appears to be unaffected by the absence of BSP (Foster et al., 2015); which may be due to the cellular nature of bone and presence of possible compensatory mechanisms in bone but not in acellular cementum. Of relevance, the phenotype of the *Alpl*$^{-/-}$ mouse was also that of deficient acellular cementum formation due to the loss of TNAP function that led to increased levels of pyrophosphate, which is a potent inhibitor of mineralization (Beertsen et al., 1999; Foster et al., 2013a; McKee et al., 2011b). In addition, other studies have demonstrated that the reduction in the level of pyrophosphate promotes acellular formation (Foster et al., 2011; Foster et al., 2013a). Similar to that in bone matrix, the presence of various growth factors such as transforming growth factor-β, bone morphogenetic proteins (BMPs), and fibroblast growth factor were also observed in the cementum matrix. However, the acellular cementum, which lacks cementocytes, does not have a similar distribution of these growth factors compared to cellular cementum and bone (Bosshardt, 2005). These findings suggest that the acellular cementum is strongly regulated by the physicochemical level of mineralization. Thus, the absence of BSP, which binds well with collagen and is involved in hydroxyapatite nucleation and growth, likely has directly weakened the acellular cementum that led to PDL detachment observed in *Bsp*$^{-/-}$ mice.

Periodontal tissue breakdown is usually associated with periodontal disease due to infection. However, in the *Bsp*$^{-/-}$ mice no apparent inflammatory response was observed in the periodontal ligament or adjacent tissues, suggesting that the defect was likely due to failure in the function of the periodontium. These findings prompted us to investigate whether occlusal stress contributes to the periodontal breakdown and tooth malocclusion observed in *Bsp*$^{-/-}$ mice.

All of the mice in this study were fed either the standard hard diet (HD) or powdered soft diet (SD), which should reduce the stress applied to the periodontium during mastication. As expected, similar to previous study (chapter 2), *Bsp*$^{-/-}$ mice fed with HD were found to have higher incident of tooth malocclusion, were smaller in size [long bone length and body weight], and had elevated serum alkaline phosphatase (ALP) activity compared to WT mice. The substitution of SD was able to reduce the severe incisor malocclusion rate by a factor of 10-fold, suggesting that excessive occlusal loading contributed to the malocclusion phenotype of *Bsp*$^{-/-}$ mice. In addition, the *Bsp*$^{-/-}$ mice fed with SD appeared to have normal body weight, long bone length, and serum ALP activity compared to WT mice. These results indicated that *Bsp*$^{-/-}$ mice do not have a major bone phenotype as previously described by Malaval's group. These bone phenotypes are likely related to malnourishment due to difficulty of the mice to consume standard HD (Soenjaya et al., 2015). Another factor to consider is that litter mate controls were used in all of our studies; in contrast, Malaval's group did not, as indicated by different color mice (between groups) used in their recent study (Bouleftour et al., 2014), but also evident in their other publications. Other studies have demonstrated that undernutrition negatively influences immune function (Chan et al., 1996), growth (Lifshitz, 2009) and offspring neurodevelopment (Akitake et al., 2015), behavior and fertility (Rios et al., 2005), and intuitively breeding and nursing capabilities. We did not observe any significant issues with these characteristics in our *Bsp*$^{-/-}$ mouse colony. However, in contrast, Malaval's group have reported uncharacteristic nesting behavior of their *Bsp*$^{-/-}$ mice colony compared to WT mice (Bouleftour et al., 2014), presumably due to malnutrition.

Changing the diet was not able to prevent PDL detachment, tooth malocclusion, and periodontal breakdown in *Bsp*$^{-/-}$ mice. Furthermore, regardless of diet group, *Bsp*$^{-/-}$ mice

have lower rates of incisor eruption compared to WT mice, which is likely due to lack of acellular cementum formation and the associated periodontal detachment. In addition, a small preliminary study on older *Bsp*$^{-/-}$ mice (above 1 yr old), indicate that odontoma-like nodules are present at the apical end of the incisors (data not shown). These unusual features are not yet fully understood, however, we postulate that it is caused by the inability of the mouse incisor to properly erupt due to the defects at the PDL-acellular cementum interface. Over time, the cumulative occlusal stress from mastication possibly has caused the cementum-PDL interface to become progressively weaker, and thus less resistant to the forces. This might have pushed the continually developing incisor inward or into the socket, which resulted in the continuously forming dentin and enamel to be deposited around the apical end of the incisor. These results demonstrate the importance of BSP in maintaining proper periodontal structure and function and alveolar bone remodeling, and point to dental dysfunction as causative factor of skeletal defects observed in *Bsp*$^{-/-}$ mice.

Potential use of nHA/PU scaffold and BSP for bone regeneration therapy

The second half of the thesis [Chapter 4 and 5] focused on the role of BSP as a therapeutic reagent to enhance bone repair. As mentioned before, previous studies done by the Glimcher's group indicated that the addition of BSP in a collagen scaffold was able to promote early mineralization in rat calvarial defect model and promoted bone repair that was evident after a month (Wang et al., 2006; Xu et al., 2007). For our study, a similar rat calvarial defect model was used. However, novel PU and nHA/PU scaffolds developed by our collaborators, David Eglin and Mauro Alini (AO Foundation) were used instead of collagen scaffolds. The first step of the study was to determine whether the scaffolds could be effective carriers for growth factor and bioactive proteins. Both the PU and the nHA/PU scaffolds have previously been demonstrated to be biocompatible and effective for tissue regeneration (Hofmann et al., 2008; Laschke et al., 2009; Laschke et al., 2010b). The PU-based scaffold has been shown to be osteoconductive and also able to bind bioactive proteins. The addition of nHA particles

was found to be have additional capacity to bind serum proteins (Boissard et al., 2009). Our *in vitro* experiments verified that nHA/PU scaffolds had a threefold higher binding capacity for BSP than PU scaffolds alone. Of relevance, other studies have shown that during bone repair, long term delivery of growth factor resulted in a greater amount of bone formation than a scaffold that would release the factor over a shorter time period (La et al., 2010). Thus, the use of a scaffold with higher binding capacity, and potentially with increased affinity, was relevant in our bone repair model. Furthermore, previous studies have also demonstrated that the PU scaffolds were able to promote angiogenesis *in vivo* (Hofmann et al., 2008; Laschke et al., 2010b), which is critical in the normal bone remodeling sequence that occurs in bone repair.

In this study, recombinant human morphogenetic protein-2 (rhBMP-2) was used as a positive control group. rhBMP-2 is the most common growth factor used in the clinical setting due to its high potency to drive osteoprogenitor cell differentiation to osteoblasts which subsequently leads to increased new bone formation. However, a main concern is that clinically high doses of rhBMP-2 are usually required to ensure successful bone repair. Various studies have demonstrated that there are potential side effects when high levels of BMPs are used, including excessive bone formation, adverse immune responses, and increased risk in developing cancer (Carragee et al., 2011; Epstein, 2013). Therefore, to avoid these complications, we decided to use a low-dose rhBMP-2 to determine whether this would achieve a similar positive outcome in regards to new bone formation. Our *in vitro* study showed that nHA/PU scaffold was able to bind well with both rhBMP-2 and BSP. Both rhBMP-2 and BSP treated nHA/PU scaffold in cell culture appeared to have elevated amount of mineral formation. In our calvarial *in vivo* system, the presence of low dose rhBMP-2 was able to significantly enhance bone repair compared to the scaffold-only control group. MicroCT analyses suggested that approximately 70% of the defects were filled with bone by 6 weeks. This result was very promising since other studies that utilized larger dose of rhBMP-2 were shown to achieve either a lower or similar amount of new bone formation by 6-8 weeks post-op (Luvizuto et al., 2011; Sawyer et al., 2009; Schwarz et al., 2009). Unfortunately, BSP-treated nHA/PU scaffold group was not able to significantly enhance *in vivo* bone repair even after 12 weeks. In the BSP-treated group, moderate island-like bone formation were found in the defect sites

on occasion; however, most of the time only minimal bone formation was observed in the defect sites. Similar observations were also found in the scaffold-only control group.

In summary, this study showed that nHA/PU scaffold is able to bind both rhBMP-2 and BSP. Even though on its own, BSP is not effective as a promoter of bone repair in our model, various mineralized tissue phenotypes observed in the *Bsp*$^{-/-}$ mice provide strong support that BSP is still important for mineralized tissue development.

6.2 FUTURE DIRECTION

Role of BSP in mineralized tissue development

To further understand which part of the functional regions of BSP is important for cementum development, a preliminary study was done by injecting BSP into *Bsp*$^{-/-}$ mice in order to determine whether the acellular cementum phenotype could be rescued. Subcutaneous injections (daily for the first 3 time points, every 2 days for the next 4 time points, and every three days for the last 3 time points) of native and recombinant rat BSP were done beginning with 5 day old *Bsp*$^{-/-}$ mice. At 6 weeks, microCT images revealed a slight delay in periodontal breakdown (data not shown). However, no significant conclusions could be derived using this method possibly due to the limited amounts of BSP that could be injected (10 µl or less; using a 1mg/ml BSP-PBS solution) into the young pups. In addition, it is likely that only a small percentage of the injected BSP would be carried by the circulatory system to the periodontium. Future studies should utilize an adeno-associated virus (AAV) linked to the *Bsp* gene (wild type full length, or full length with altered functional domains) to rescue the acellular cementum deficiency in the *Bsp*$^{-/-}$ mice. This method should be a more effective way to determine the potential use of BSP to repair or rescue the structural defects seen in cementum-PDL interface of *Bsp*$^{-/-}$ mice. In addition, the use of functional mutants may provide critical new information on the roles of these domains *in vivo*, and insight into the mechanism of BSP action. Of relevance, other studies have also used AAV-mediated systemic gene therapy

method in order to effectively treat a transgenic mouse model. The authors demonstrated that AAV-mediated gene therapy was able to successfully rescue the severe bone phenotype seen in hypophosphatasia mice (Matsumoto et al., 2011).

As part of the Goldberg's group objective, as a side project, we also investigated the potential role of BSP in other mineralized tissue development. Other than bone and dentition, mineralized tissues are also found within the enthesis, which is composed of four transitional zones, including tendon connective tissue, un-calcified fibrocartilage, calcified fibrocartilage (CF), and bone, that connects tendon to bone. Using an anti-BSP antibody, our preliminary study demonstrated for the first time that BSP is present in the CF zone of the enthesis, which is found adjacent to the bone. Therefore, it is postulated that BSP also plays an important role in the enthesis development and fibrocartilage mineralization. All of the mice used for this study were fed with SD to reduce malocclusion and prevent malnourishment. Initial mechanical tensile tests indicated that the *Bsp*$^{-/-}$ mouse patellar tendon appeared to fail at a lower mechanical load compared to that of WT mice. Based on these results, a more complete analysis of the quadriceps tendon (QCT) and supraspinatus tendon (SST) entheses of 15-week old *Bsp*$^{-/-}$ mice were performed (Marinovich, Soenjaya et al., 2016). In the QCT enthesis, the CF zone of the *Bsp*$^{-/-}$ mice was 28% greater in length compared to WT mice. This lengthening of the CF appeared to increase as the *Bsp*$^{-/-}$ mice aged. By 14 months of age, the length of the CF zone was determined to be 41% greater than that of WT mice. However, no apparent difference in the lengths of CF zone were observed in the SST enthesis of *Bsp*$^{-/-}$ and WT mice. Other studies have indicated that the CF zone helps to anchor the tendons or ligaments to the bone and withstand tensile and shear loads under minimal movement (Benjamin and McGonagle, 2001). The enthesis fibrocartilage is a dynamic tissue that responds to mechanical load. Thus, the observed increased length of the CF zone is likely a compensation to strengthen the CF-bone interface and also restrict movement of the enthesis to prevent injury. Further analysis revealed that the cross sectional area of *Bsp*$^{-/-}$ patellar tendon is 7.5% larger compared to WT mice. Both *Bsp*$^{-/-}$ and WT patellar tendon failed at a similar load, which suggests that the increased cross sectional area of the *Bsp*$^{-/-}$ patellar tendon likely act as a compensatory mechanism to allow for greater dissipation of stress along the enthesis to prevent failure. In addition, the study also

indicated that no significant difference in mineral distribution and collagen organization were observed between *Bsp*$^{-/-}$ and WT mice (Marinovich, Soenjaya et al., 2016). As previously mentioned, *Bsp*$^{-/-}$ mice fed with soft diet have normal bone phenotypes such as bone length and bone mineral density. Other studies from our groups have also indicated that all of the bone phenotype occurred at the early stage of development. For example, recent studies have indicate that the absence of BSP delayed the mineralization of the fetal long-bones (Holm et al., 2015) and craniofacial bones (Foster et al., 2015). However, these bone phenotypes become less apparent as the *Bsp*$^{-/-}$ mice aged, which suggest that the role of BSP is likely being compensated by other related mechanisms. Thus, future studies should focus on the role of BSP in early enthesis development and mineralization.

Potential use of BSP for bone regeneration therapy

In terms for future studies, one potential suggestion is that BSP may be more effective if used in combination with a growth factor such as rhBMP-2. In order to confirm this hypothesis, we performed a preliminary study (n=2) that used nHA/PU scaffold treated with a combination of 0.25 µg of rhBMP-2 and 20 µg of BSP in a rat calvaria defect model. The initial results showed that the BSP-rhBMP-2 treated group appeared to have increased bone formation compared to 0.25µg rhBMP2 treated group. Furthermore, the amount of bone formation in BSP-rhBMP-2 treated group appeared to be approaching of that observed in nHA/PU scaffold group treated with 1 µg of rhBMP-2 (data not shown). However, for the pilot study the animal sample size were too small for proper statistical analyses. Therefore, a more complete study should be done to determine the best BSP-rhBMP-2 cocktail concentration that will gives the optimal bone repair.

Another potential study is the concept of permanently immobilizing BSP to the nHA/PU scaffold, which was a technique used by the Glimcher's group to crosslink BSP to collagen scaffold. It will be interesting to verify whether covalently cross-linked BSP to nHA/PU scaffold can promote bone repair.

As for *in vitro* studies, future directions, experiments with rhBMP-2 and BSP should be done to confirm any up-regulation of osteoblastic differentiation markers such as alkaline phosphatase, collagen I, osterix and osteocalcin. The results will confirm whether the presence of rhBMP-2 or BSP in the nHA/PU scaffolds can promote osteogenic differentiation. Another suggestion is to look at other markers related to bone repair such as angiogenesis. It will also be interesting to verify whether the presence of BSP (covalently cross-linked) or rhBMP-2 treated nHA/PU scaffold can enhanced angiogenesis in our calvarial defect model.

PicoGreen DNA quantification assay has been demonstrated to be a useful technique to determine total DNA from scaffolds cultured with cells (Ng et al., 2005). This assay can potentially be used in our *in vitro* culture system to quantify the approximate amount of cells in the nHA/PU scaffold in the presence of BSP or rhBMP-2. Previous studies have shown that DNA binds tightly to HA; the bound DNA are found to be more resistant to degradation compared to unbound DNA (Brundin et al., 2013). Thus, after the cell lysis, an additional step would need to be considered for extraction of DNA from mineralized tissue using decalcification step with EDTA as previously described in previous studies (Malaver and Yunis, 2003).

In conclusion, these future studies will further demonstrate the importance of BSP in mineralized tissue development and also verify BSP potential role in enhancing bone repair.

6.3 REFERENCES

Abe E (2006). Function of BMPs and BMP antagonists in adult bone. *Ann N Y Acad Sci* 1068(41-53.

Akitake Y, Katsuragi S, Hosokawa M, Mishima K, Ikeda T, Miyazato M *et al.* (2015). Moderate maternal food restriction in mice impairs physical growth, behavior, and neurodevelopment of offspring. *Nutrition Research* 35(1)*:*76-87.

Angle SR, Sena K, Sumner DR, Virkus WW, Virdi AS (2012). Healing of rat femoral segmental defect with bone morphogenetic protein-2: a dose response study. *J Musculoskelet Neuronal Interact* 12(1)*:*28-37.

Asamura S, Mochizuki Y, Yamamoto M, Tabata Y, Isogai N (2010). Bone regeneration using a bone morphogenetic protein-2 saturated slow-release gelatin hydrogel sheet: evaluation in a canine orbital floor fracture model. *Ann Plast Surg* 64(4)*:*496-502.

Aubin JE (2001). Regulation of osteoblast formation and function. *Rev Endocr Metab Disord* 2(1)*:*81-94.

Autefage H, Briand-Mésange F, Cazalbou S, Drouet C, Fourmy D, Gonçalvès S *et al.* (2009). Adsorption and release of BMP-2 on nanocrystalline apatite-coated and uncoated hydroxyapatite/β-tricalcium phosphate porous ceramics. *Journal of Biomedical Materials Research Part B: Applied Biomaterials* 91B(2)*:*706-715.

Baht GS, Hunter GK, Goldberg HA (2008). Bone sialoprotein–collagen interaction promotes hydroxyapatite nucleation. *Matrix Biol* 27(7)*:*600-608.

Baht GS, O'Young J, Borovina A, Chen H, Tye CE, Karttunen M *et al.* (2010). Phosphorylation of Ser^{136} is critical for potent bone sialoprotein-mediated nucleation of hydroxyapatite crystals *Biochem J* 428(385-395.

Baron R, Neff L, Louvard D, Courtoy PJ (1985). Cell-mediated extracellular acidification and bone resorption: evidence for a low pH in resorbing lacunae and localization of a 100-kD lysosomal membrane protein at the osteoclast ruffled border. *J Cell Biol* 101(6)*:*2210-2222.

Bartlett JD (2013). Dental enamel development: proteinases and their enamel matrix substrates. *ISRN Dent* 2013(684607.

Bauer TW, Muschler GF (2000). Bone graft materials. An overview of the basic science. *Clin Orthop Relat Res* 371)*:*10-27.

Beertsen W, McCulloch CAG, Sodek J (1997). The periodontal ligament: a unique, multifunctional connective tissue. *Periodontol 2000* 13(1)*:*20-40.

Beertsen W, VandenBos T, Everts V (1999). Root Development in Mice Lacking Functional Tissue Non-specific Alkaline Phosphatase Gene: Inhibition of Acellular Cementum Formation. *J Dent Res* 78(6)*:*1221-1229.

Bellahcene A, Merville MP, Castronovo V (1994). Expression of bone sialoprotein, a bone matrix protein, in human breast cancer. *Cancer Res* 54(11)*:*2823-2826.

Bellahcene A, Maloujahmoum N, Fisher LW, Pastorino H, Tagliabue E, Menard S *et al.* (1997). Expression of bone sialoprotein in human lung cancer. *Calcif Tissue Int* 61(3)*:*183-188.

Bellahcene A, Castronovo V, Ogbureke KU, Fisher LW, Fedarko NS (2008). Small integrin-binding ligand N-linked glycoproteins (SIBLINGs): multifunctional proteins in cancer. *Nat Rev Cancer* 8(3)*:*212-226.

Bellahcène A, Bonjean K, Fohr B, Fedarko NS, Robey FA, Young MF *et al.* (2000). Bone Sialoprotein Mediates Human Endothelial Cell Attachment and Migration and Promotes Angiogenesis. *Circ Res* 86(8)*:*885-891.

Ben-David D, Srouji S, Shapira-Schweitzer K, Kossover O, Ivanir E, Kuhn G *et al.* (2013). Low dose BMP-2 treatment for bone repair using a PEGylated fibrinogen hydrogel matrix. *Biomaterials* 34(12)*:*2902-2910.

Benjamin M, McGonagle D (2001). The anatomical basis for disease localisation in seronegative spondyloarthropathy at entheses and related sites. *J Anat* 199(Pt 5)*:*503-526.

Bianco P, Fisher LW, Young MF, Termine JD, Robey PG (1991). Expression of bone sialoprotein (BSP) in developing human tissues. *Calcif Tissue Int* 49(6)*:*421-426.

Bianco P, Riminucci M, Silvestrini G, Bonucci E, Termine JD, Fisher LW *et al.* (1993). Localization of bone sialoprotein (BSP) to Golgi and post-Golgi secretory structures in osteoblasts and to discrete sites in early bone matrix. *J Histochem Cytochem* 41(2)*:*193-203.

Blair HC, Kahn AJ, Crouch EC, Jeffrey JJ, Teitelbaum SL (1986). Isolated osteoclasts resorb the organic and inorganic components of bone. *J Cell Biol* 102(4)*:*1164-1172.

Boissard CIR, Bourban PE, Tami AE, Alini M, Eglin D (2009). Nanohydroxyapatite/poly(ester urethane) scaffold for bone tissue engineering. *Acta Biomaterialia* 5(9)*:*3316-3327.

Bonewald LF (2006). Mechanosensation and Transduction in Osteocytes. *Bonekey Osteovision* 3(10)*:*7-15.

Bosshardt DD, Selvig KA (1997). Dental cementum: the dynamic tissue covering of the root. *Periodontol 2000* 13(41-75.

Bosshardt DD (2005). Are cementoblasts a subpopulation of osteoblasts or a unique phenotype? *J Dent Res* 84(5)*:*390-406.

Bostman O, Hirvensalo E, Makinen J, Rokkanen P (1990). Foreign-body reactions to fracture fixation implants of biodegradable synthetic polymers. *J Bone Joint Surg Br* 72(4)*:*592-596.

Bostrom MP, Lane JM, Berberian WS, Missri AA, Tomin E, Weiland A *et al.* (1995). Immunolocalization and expression of bone morphogenetic proteins 2 and 4 in fracture healing. *J Orthop Res* 13(3)*:*357-367.

Boudiffa M, Wade-Gueye NM, Guignandon A, Vanden-Bossche A, Sabido O, Aubin JE *et al.* (2010). Bone sialoprotein deficiency impairs osteoclastogenesis and mineral resorption in vitro. *J Bone Miner Res* 25(12)*:*2669-2679.

Bouleftour W, Boudiffa M, Wade-Guéye NM, Bouët G, Cardelli M, Laroche N *et al.* (2014). Skeletal development of mice lacking bone sialoprotein (BSP) - impairment of long bone growth and progressive establishment of high trabecular bone mass. *PLoS One* 9(5)*:*e95144.

Boyle WJ, Simonet WS, Lacey DL (2003). Osteoclast differentiation and activation. *Nature* 423(6937)*:*337-342.

Brown KV, Li B, Guda T, Perrien DS, Guelcher SA, Wenke JC (2011). Improving Bone Formation in a Rat Femur Segmental Defect by Controlling Bone Morphogenetic Protein-2 Release. *Tissue Engineering Part A* 17(13-14)*:*1735-1746.

Brundin M, Figdor D, Sundqvist G, Sjogren U (2013). DNA binding to hydroxyapatite: a potential mechanism for preservation of microbial DNA. *J Endod* 39(2)*:*211-216.

Busa B, Miller LM, Rubin CT, Qin YX, Judex S (2005). Rapid Establishment of Chemical and Mechanical Properties during Lamellar Bone Formation. *Calcif Tissue Int* 77(6)*:*386-394.

Cacciafesta V, Dalstra M, Carles, Melsen B, Andreassen TT (2001). Growth hormone treatment promotes guided bone regeneration in rat calvarial defects. *The European Journal of Orthodontics* 23(6)*:*733-740.

Cahill KS, Chi JH, Day A, Claus EB (2009). Prevalence, complications, and hospital charges associated with use of bone-morphogenetic proteins in spinal fusion procedures. *JAMA* 302(1)*:*58-66.

Canalis E, Economides AN, Gazzerro E (2003). Bone morphogenetic proteins, their antagonists, and the skeleton. *Endocr Rev* 24(2)*:*218-235.

Carragee EJ, Hurwitz EL, Weiner BK (2011). A critical review of recombinant human bone morphogenetic protein-2 trials in spinal surgery: emerging safety concerns and lessons learned. *The Spine Journal* 11(6)*:*471-491.

Caton J, Tucker AS (2009). Current knowledge of tooth development: patterning and mineralization of the murine dentition. *J Anat* 214(4)*:*502-515.

Chan AHL, Lertlam R, Simmer JP, Wang C-N, Hu JCC (2013). Bodyweight assessment of enamelin null mice. *Biomed Res Int* 2013(246861.

Chan J, Tian Y, Tanaka KE, Tsang MS, Yu K, Salgame P *et al.* (1996). Effects of protein calorie malnutrition on tuberculosis in mice. *Proceedings of the National Academy of Sciences* 93(25)*:*14857-14861.

Chau JF, Leong WF, Li B (2009). Signaling pathways governing osteoblast proliferation, differentiation and function. *Histol Histopathol* 24(12)*:*1593-1606.

Chen D, Zhao M, Mundy GR (2004). Bone morphogenetic proteins. *Growth Factors* 22(4)*:*233-241.

Chen G, Deng C, Li Y-P (2012). TGF-β and BMP Signaling in Osteoblast Differentiation and Bone Formation. *International Journal of Biological Sciences* 8(2)*:*272-288.

Chen J, Sasaguri K, Sodek J, Aufdemorte TB, Jiang H, Thomas HF (1998). Enamel epithelium expresses bone sialoprotein (BSP). *Eur J Oral Sci* 106(S1)*:*331-336.

Claes L, Recknagel S, Ignatius A (2012). Fracture healing under healthy and inflammatory conditions. *Nat Rev Rheumatol* 8(3)*:*133-143.

Cohen MM, Jr. (2000). Merging the old skeletal biology with the new. I. Intramembranous ossification, endochondral ossification, ectopic bone, secondary cartilage, and pathologic considerations. *J Craniofac Genet Dev Biol* 20(2)*:*84-93.

Cooper LF, Yliheikkila PK, Felton DA, Whitson SW (1998). Spatiotemporal assessment of fetal bovine osteoblast culture differentiation indicates a role for BSP in promoting differentiation. *J Bone Miner Res* 13(4)*:*620-632.

Cowan CM, Aghaloo T, Chou Y, Walder B, Zhang T, Soo C *et al.* (2007). MicroCT Evaluation of Three-Dimensional Mineralization in Response to BMP-2 Doses In Vitro and in Critical Sized Rat Calvarial Defects. *Tissue Engineering Part A* 13(3)*:*501-512.

Crockett JC, Rogers MJ, Coxon FP, Hocking LJ, Helfrich MH (2011). Bone remodelling at a glance. *J Cell Sci* 124(Pt 7)*:*991-998.

D'Errico JA, MacNeil RL, Takata T, Berry J, Strayhorn C, Somerman MJ (1997). Expression of bone associated markers by tooth root lining cells, in situ and in vitro. *Bone* 20(2)*:*117-126.

de Jesus Perez VA, Alastalo TP, Wu JC, Axelrod JD, Cooke JP, Amieva M *et al.* (2009). Bone morphogenetic protein 2 induces pulmonary angiogenesis via Wnt-beta-catenin and Wnt-RhoA-Rac1 pathways. *J Cell Biol* 184(1)*:*83-99.

Deakins M, Volker JF (1941). Amount of Organic Matter in Enamel From Several Types of Human Teeth. *J Dent Res* 20(2)*:*117-121.

Dresing I, Zeiter S, Auer J, Alini M, Eglin D (2014). Evaluation of a press-fit osteochondral poly(ester-urethane) scaffold in a rabbit defect model. *Journal of Materials Science: Materials in Medicine* 25(7)*:*1691-1700.

Ducheyne P (1987). Bioceramics: material characteristics versus in vivo behavior. *J Biomed Mater Res* 21(A2 Suppl)*:*219-236.

Einhorn TA, Gerstenfeld LC (2015). Fracture healing: mechanisms and interventions. *Nat Rev Rheumatol* 11(1)*:*45-54.

Epstein NE (2013). Complications due to the use of BMP/INFUSE in spine surgery: The evidence continues to mount. *Surgical Neurology International* 4(Suppl 5)*:*S343-S352.

Everts V, Delaissé JM, Korper W, Jansen DC, Tigchelaar-Gutter W, Saftig P *et al.* (2002). The Bone Lining Cell: Its Role in Cleaning Howship's Lacunae and Initiating Bone Formation. *J Bone Miner Res* 17(1)*:*77-90.

Fisher LW, Whitson SW, Avioli LV, Termine JD (1983). Matrix sialoprotein of developing bone. *J Biol Chem* 258(20)*:*12723-12727.

Fisher LW, Hawkins GR, Tuross N, Termine JD (1987). Purification and partial characterization of small proteoglycans I and II, bone sialoproteins I and II, and osteonectin from the mineral compartment of developing human bone. *J Biol Chem* 262(20)*:*9702-9708.

Fisher LW, Torchia DA, Fohr B, Young MF, Fedarko NS (2001). Flexible structures of SIBLING proteins, bone sialoprotein, and osteopontin. *Biochem Biophys Res Commun* 280(2)*:*460-465.

Fisher LW, Fedarko NS (2003). Six genes expressed in bones and teeth encode the current members of the SIBLING family of proteins. *Connect Tissue Res* 44(1)*:*33-40.

Foster BL, Popowics TE, Fong HK, Somerman MJ (2007). Advances in Defining Regulators of Cementum Development and Periodontal Regeneration. In: Curr Top Dev Biol. PS Gerald editor: Academic Press, pp. 47-126.

Foster BL, Nagatomo KJ, Bamashmous SO, Tompkins KA, Fong H, Dunn D *et al.* (2011). The Progressive Ankylosis Protein Regulates Cementum Apposition and Extracellular Matrix Composition. *Cells Tissues Organs* 194(5)*:*382-405.

Foster BL (2012). Methods for studying tooth root cementum by light microscopy. *Int J Oral Sci* 4(3)*:*119-128.

Foster BL, Nagatomo KJ, Tso HW, Tran AB, Nociti FH, Jr., Narisawa S *et al.* (2013a). Tooth root dentin mineralization defects in a mouse model of hypophosphatasia. *J Bone Miner Res* 28(2)*:*271-282.

Foster BL, Soenjaya Y, Nociti FH, Holm E, Zerfas PM, Wimer HF *et al.* (2013b). Deficiency in acellular cementum and periodontal attachment in Bsp null mice. *J Dent Res* 92(2)*:*166-172.

Foster BL, Ao M, Willoughby C, Soenjaya Y, Holm E, Lukashova L *et al.* (2015). Mineralization defects in cementum and craniofacial bone from loss of bone sialoprotein. *Bone* 78(150-164.

Franzen A, Heinegard D (1985). Isolation and characterization of two sialoproteins present only in bone calcified matrix. *Biochem J* 232(3)*:*715-724.

Fricain JC, Schlaubitz S, Le Visage C, Arnault I, Derkaoui SM, Siadous R *et al.* (2013). A nano-hydroxyapatite – Pullulan/dextran polysaccharide composite macroporous material for bone tissue engineering. *Biomaterials* 34(12)*:*2947-2959.

Frost HM (1987). Bone "mass" and the "mechnostat': a proposal. *Anat Rec* 219(1)*:*1-9.

Fu K, Xu Q, Czernuszka J, Triffitt JT, Xia Z (2013). Characterization of a biodegradable coralline hydroxyapatite/calcium carbonate composite and its clinical implementation. *Biomed Mater* 8(6)*:*065007.

Fujisawa R, Butler WT, Brunn JC, Zhou HY, Kuboki Y (1993). Differences in composition of cell-attachment sialoproteins between dentin and bone. *J Dent Res* 72(8)*:*1222-1226.

Ganss B, Kim RH, Sodek J (1999). Bone sialoprotein. *Crit Rev Oral Biol Med* 10(1)*:*79-98.

Geiger M, Li RH, Friess W (2003). Collagen sponges for bone regeneration with rhBMP-2. *Adv Drug Deliv Rev* 55(12)*:*1613-1629.

Gill KS, Beier F, Goldberg HA (2008). Rho-ROCK signaling differentially regulates chondrocyte spreading on fibronectin and bone sialoprotein. *Am J Physiol Cell Physiol* 295(1)*:*C38-49.

Gogolewski S, Gorna K, Zaczynska E, Czarny A (2008). Structure–property relations and cytotoxicity of isosorbide-based biodegradable polyurethane scaffolds for tissue repair and regeneration. *Journal of Biomedical Materials Research Part A* 85A(2)*:*456-465.

Goldberg HA, Sodek J (1994). Purification of mineralized tissue-associated osteopontin. *Methods in Cell Science* 16(3)*:*211-215.

Goldberg HA, Warner KJ (1997). The staining of acidic proteins on polyacrylamide gels: enhanced sensitivity and stability of "Stains-all" staining in combination with silver nitrate. *Anal Biochem* 251(2)*:*227-233.

Goldberg HA, Warner KJ, Hunter GK (2001). Binding of bone sialoprotein, osteopontin and synthetic polypeptides to hydroxyapatite. *Connect Tissue Res* 42(1)*:*25-37.

Goldberg HA, Hunter GK (2012). Functional domains of bone sialoprotein. In: Phosphorylated extracellular matrix proteins of bone and dentin. M Goldberg editor. Oak Park (IL): Bentham Science Publishers, pp. 266-282.

Goldberg M, Kulkarni AB, Young M, Boskey A (2011). Dentin: Structure, Composition and Mineralization: The role of dentin ECM in dentin formation and mineralization. *Frontiers in Bioscience (Elite Edition)* 3(711-735.

Gonçalves PF, Sallum EA, Sallum AW, Casati MZ, de Toledo S, Nociti Jr FH (2005). Dental cementum reviewed: development, structure, composition, regeneration and potential functions. *Brazilian Journal of Oral Science* 4(12)*:*651-658.

Gordon JAR, Tye CE, Sampaio AV, Underhill TM, Hunter GK, Goldberg HA (2007). Bone sialoprotein expression enhances osteoblast differentiation and matrix mineralization in vitro. *Bone* 41(3)*:*462-473.

Gorna K, Gogolewski S (2006). Biodegradable porous polyurethane scaffolds for tissue repair and regeneration. *Journal of Biomedical Materials Research Part A* 79A(1)*:*128-138.

Gorski JP, Shimizu K (1988). Isolation of new phosphorylated glycoprotein from mineralized phase of bone that exhibits limited homology to adhesive protein osteopontin. *J Biol Chem* 263(31)*:*15938-15945.

Graf HL, Stoeva S, Armbruster FP, Neuhaus J, Hilbig H (2008). Effect of bone sialoprotein and collagen coating on cell attachment to TICER® and pure titanium implant surfaces. *Int J Oral Maxillofac Surg* 37(7)*:*634-640.

Guan J, Fujimoto KL, Sacks MS, Wagner WR (2005). Preparation and characterization of highly porous, biodegradable polyurethane scaffolds for soft tissue applications. *Biomaterials* 26(18)*:*3961-3971.

Guelcher SA (2008). Biodegradable polyurethanes: synthesis and applications in regenerative medicine. *Tissue Eng Part B Rev* 14(1)*:*3-17.

Guelcher SA, Srinivasan A, Dumas JE, Didier JE, McBride S, Hollinger JO (2008). Synthesis, mechanical properties, biocompatibility, and biodegradation of polyurethane networks from lysine polyisocyanates. *Biomaterials* 29(12)*:*1762-1775.

Guo X, Wang XF (2009). Signaling cross-talk between TGF-beta/BMP and other pathways. *Cell Res* 19(1)*:*71-88.

Hansson S, Halldin A (2012). Alveolar ridge resorption after tooth extraction: A consequence of a fundamental principle of bone physiology. *J Dent Biomech* 3(1758736012456543).

Harris NL, Rattray KR, Tye CE, Underhill TM, Somerman MJ, D'Errico JA *et al.* (2000). Functional analysis of bone sialoprotein: identification of the hydroxyapatite-nucleating and cell-binding domains by recombinant peptide expression and site-directed mutagenesis. *Bone* 27(6)*:*795-802.

Helfrich MH, Nesbitt SA, Dorey EL, Horton MA (1992). Rat osteoclasts adhere to a wide range of RGD (Arg-Gly-Asp) peptide-containing proteins, including the bone sialoproteins and fibronectin, via a beta 3 integrin. *J Bone Miner Res* 7(3)*:*335-343.

Helfrich MH, Crockett JC, Hocking LJ, Coxon FP (2007). The pathogenesis of osteoclast diseases: Some knowns, but still many unknowns. *IBMS BoneKEy* 4(2)*:*61-77.

Henry JA, Simonet M, Pandit A, Neuenschwander P (2007). Characterization of a slowly degrading biodegradable polyester-urethane for tissue engineering scaffolds. *J Biomed Mater Res A* 82(3)*:*669-679.

Ho SP, Kurylo MP, Grandfield K, Hurng J, Herber R-P, Ryder MI *et al.* (2013). The plastic nature of the human bone–periodontal ligament–tooth fibrous joint. *Bone* 57(2)*:*455-467.

Hofmann A, Ritz U, Verrier S, Eglin D, Alini M, Fuchs S *et al.* (2008). The effect of human osteoblasts on proliferation and neo-vessel formation of human umbilical vein endothelial cells in a long-term 3D co-culture on polyurethane scaffolds. *Biomaterials* 29(31)*:*4217-4226.

Holm E, Aubin JE, Hunter GK, Beier F, Goldberg HA (2015). Loss of bone sialoprotein leads to impaired endochondral bone development and mineralization. *Bone* 71(0)*:*145-154.

Hunter GK, Goldberg HA (1993). Nucleation of hydroxyapatite by bone sialoprotein. *Proc Natl Acad Sci U S A* 90(18)*:*8562-8565.

Itoh S, Kikuchi M, Takakuda K, Koyama Y, Matsumoto HN, Ichinose S *et al.* (2001). The biocompatibility and osteoconductive activity of a novel hydroxyapatite/collagen composite biomaterial, and its function as a carrier of rhBMP-2. *J Biomed Mater Res* 54(3)*:*445-453.

Itoh S, Kikuchi M, Koyama Y, Takakuda K, Shinomiya K, Tanaka J (2002). Development of an artificial vertebral body using a novel biomaterial, hydroxyapatite/collagen composite. *Biomaterials* 23(19)*:*3919-3926.

Jena N, Martin-Seisdedos C, McCue P, Croce CM (1997). BMP7 null mutation in mice: developmental defects in skeleton, kidney, and eye. *Exp Cell Res* 230(1)*:*28-37.

Jernvall J, Kettunen P, Karavanova I, Martin LB, Thesleff I (1994). Evidence for the role of the enamel knot as a control center in mammalian tooth cusp formation: non-dividing cells express growth stimulating Fgf-4 gene. *Int J Dev Biol* 38(3)*:*463-469.

Jernvall J, Aberg T, Kettunen P, Keranen S, Thesleff I (1998). The life history of an embryonic signaling center: BMP-4 induces p21 and is associated with apoptosis in the mouse tooth enamel knot. *Development* 125(2)*:*161-169.

Kavlock KD, Pechar TW, Hollinger JO, Guelcher SA, Goldstein AS (2007). Synthesis and characterization of segmented poly(esterurethane urea) elastomers for bone tissue engineering. *Acta Biomater* 3(4)*:*475-484.

Kikuchi M, Itoh S, Ichinose S, Shinomiya K, Tanaka J (2001). Self-organization mechanism in a bone-like hydroxyapatite/collagen nanocomposite synthesized in vitro and its biological reaction in vivo. *Biomaterials* 22(13)*:*1705-1711.

Kim J, Hollinger JO (2012). Recombinant human bone morphogenetic protein-2 released from polyurethane-based scaffolds promotes early osteogenic differentiation of human mesenchymal stem cells. *Biomedical Materials* 7(4)*:*045008.

Kim S-S, Gwak S-J, Kim B-S (2008). Orthotopic bone formation by implantation of apatite-coated poly(lactide-co-glycolide)/hydroxyapatite composite particulates and bone morphogenetic protein-2. *Journal of Biomedical Materials Research Part A* 87A(1)*:*245-253.

Kinne RW, Fisher LW (1987). Keratan sulfate proteoglycan in rabbit compact bone is bone sialoprotein II. *J Biol Chem* 262(21)*:*10206-10211.

Kook S-H, Jang Y-S, Lee J-C (2011). Human periodontal ligament fibroblasts stimulate osteoclastogenesis in response to compression force through TNF-α-mediated activation of CD4+ T cells. *J Cell Biochem* 112(10)*:*2891-2901.

Kuboki Y, Jin Q, Takita H (2001). Geometry of carriers controlling phenotypic expression in BMP-induced osteogenesis and chondrogenesis. *J Bone Joint Surg Am* 83-A Suppl 1(Pt 2)*:*S105-115.

La WG, Kang SW, Yang HS, Bhang SH, Lee SH, Park JH *et al.* (2010). The efficacy of bone morphogenetic protein-2 depends on its mode of delivery. *Artif Organs* 34(12)*:*1150-1153.

Laschke MW, Strohe A, Scheuer C, Eglin D, Verrier S, Alini M *et al.* (2009). In vivo biocompatibility and vascularization of biodegradable porous polyurethane scaffolds for tissue engineering. *Acta Biomaterialia* 5(6)*:*1991-2001.

Laschke MW, Mussawy H, Schuler S, Eglin D, Alini M, Menger MD (2010a). Promoting external inosculation of prevascularised tissue constructs by pre-cultivation in an angiogenic extracellular matrix. *European Cells & Materials* 20(356-366.

Laschke MW, Strohe A, Menger MD, Alini M, Eglin D (2010b). In vitro and in vivo evaluation of a novel nanosize hydroxyapatite particles/poly(ester-urethane) composite scaffold for bone tissue engineering. *Acta Biomaterialia* 6(6)*:*2020-2027.

Laschke MW, Kleer S, Scheuer C, Schuler S, Garcia P, Eglin D *et al.* (2012). Vascularisation of porous scaffolds is improved by incorporation of adipose tissue-derived microvascular fragments. *European Cells & Materials* 24(266-277.

Laschke MW, Schank TE, Scheuer C, Kleer S, Schuler S, Metzger W *et al.* (2013). Three-dimensional spheroids of adipose-derived mesenchymal stem cells are potent initiators of blood vessel formation in porous polyurethane scaffolds. *Acta Biomaterialia* 9(6)*:*6876-6884.

Lee C, Grad S, Gorna K, Gogolewski S, Goessl A, Alini M (2005). Fibrin–Polyurethane Composites for Articular Cartilage Tissue Engineering: A Preliminary Analysis. *Tissue Engineering* 11(9-10)*:*1562-1573.

LeFevre ML, Manly RS (1938). Moisture, Inorganic and Organic Contents of Enamel and Dentin from Carious Teeth*. *The Journal of the American Dental Association and The Dental Cosmos* 25(2)*:*233-242.

Lementowski PW, Lucas P, Taddonio RF (2010). Acute and chronic complications of intracortical iliac crest bone grafting versus the traditional corticocancellous technique for spinal fusion surgery. *Orthopedics* 33(4).

Li B, Yoshii T, Hafeman AE, Nyman JS, Wenke JC, Guelcher SA (2009). The effects of rhBMP-2 released from biodegradable polyurethane/microsphere composite scaffolds on new bone formation in rat femora. *Biomaterials* 30(35)*:*6768-6779.

Li L, Zhou G, Wang Y, Yang G, Ding S, Zhou S (2015). Controlled dual delivery of BMP-2 and dexamethasone by nanoparticle-embedded electrospun nanofibers for the efficient repair of critical-sized rat calvarial defect. *Biomaterials* 37(0)*:*218-229.

Lifshitz F (2009). Nutrition and growth. *J Clin Res Pediatr Endocrinol* 1(4)*:*157-163.

Long F (2012). Building strong bones: molecular regulation of the osteoblast lineage. *Nat Rev Mol Cell Biol* 13(1)*:*27-38.

Lu J, Descamps M, Dejou J, Koubi G, Hardouin P, Lemaitre J *et al.* (2002). The biodegradation mechanism of calcium phosphate biomaterials in bone. *J Biomed Mater Res* 63(4)*:*408-412.

Luo G, Hofmann C, Bronckers AL, Sohocki M, Bradley A, Karsenty G (1995). BMP-7 is an inducer of nephrogenesis, and is also required for eye development and skeletal patterning. *Genes Dev* 9(22)*:*2808-2820.

Luvizuto ER, Tangl S, Zanoni G, Okamoto T, Sonoda CK, Gruber R *et al.* (2011). The effect of BMP-2 on the osteoconductive properties of β-tricalcium phosphate in rat calvaria defects. *Biomaterials* 32(15)*:*3855-3861.

Macneil RL, Sheng N, Strayhorn C, Fisher LW, Somerman MJ (1994). Bone sialoprotein is localized to the root surface during cementogenesis. *J Bone Miner Res* 9(10)*:*1597-1606.

Macneil RL, Berry J, D'errico J, Strayhorn C, Piotrowski B, Somerman MJ (1995). Role of Two Mineral-Associated Adhesion Molecules, Osteopontin and Bone Sialoprotein, during Cementogenesis. *Connect Tissue Res* 33(1-3)*:*1-7.

Malaval L, Wade-Guéye NM, Boudiffa M, Fei J, Zirngibl R, Chen F *et al.* (2008). Bone sialoprotein plays a functional role in bone formation and osteoclastogenesis. *J Exp Med* 205(5)*:*1145-1153.

Malaval L, Monfoulet L, Fabre T, Pothuaud L, Bareille R, Miraux S *et al.* (2009). Absence of bone sialoprotein (BSP) impairs cortical defect repair in mouse long bone. *Bone* 45(5)*:*853-861.

Malaver PC, Yunis JJ (2003). Different dental tissues as source of DNA for human identification in forensic cases. *Croat Med J* 44(3)*:*306-309.

Mardas N, Stavropoulos A, Karring T (2008). Calvarial bone regeneration by a combination of natural anorganic bovine-derived hydroxyapatite matrix coupled with a

synthetic cell-binding peptide (PepGen™): an experimental study in rats. *Clin Oral Implants Res* 19(10)*:*1010-1015.

Marsell R, Einhorn TA (2011). The biology of fracture healing. *Injury* 42(6)*:*551-555.

Martinovic S, Mazic S, Kisic V, Basic N, Jakic-Razumovic J, Borovecki F *et al.* (2004). Expression of bone morphogenetic proteins in stromal cells from human bone marrow long-term culture. *J Histochem Cytochem* 52(9)*:*1159-1167.

Matsumoto T, Okazaki M, Inoue M, Yamaguchi S, Kusunose T, Toyonaga T *et al.* (2004). Hydroxyapatite particles as a controlled release carrier of protein. *Biomaterials* 25(17)*:*3807-3812.

Matsumoto T, Miyake K, Yamamoto S, Orimo H, Miyake N, Odagaki Y *et al.* (2011). Rescue of severe infantile hypophosphatasia mice by AAV-mediated sustained expression of soluble alkaline phosphatase. *Hum Gene Ther* 22(11)*:*1355-1364.

McKee CT, Last JA, Russell P, Murphy CJ (2011a). Indentation versus tensile measurements of Young's modulus for soft biological tissues. *Tissue Eng Part B Rev* 17(3)*:*155-164.

McKee MD, Zalzal S, Nanci A (1996). Extracellular matrix in tooth cementum and mantle dentin: Localization of osteopontin and other noncollagenous proteins, plasma proteins, and glycoconjugates by electron microscopy. *Anat Rec* 245(2)*:*293-312.

McKee MD, Nakano Y, Masica DL, Gray JJ, Lemire I, Heft R *et al.* (2011b). Enzyme Replacement Therapy Prevents Dental Defects in a Model of Hypophosphatasia. *J Dent Res* 90(4)*:*470-476.

McKoy BE, Kang Q, An YH (1999). Indentation testing of bone. In: Mechanical testing of bone and the bone-implant interface. YH An and RA Draughn editors: CRC Press, pp. 233-240.

Meikle MC (2006). The tissue, cellular, and molecular regulation of orthodontic tooth movement: 100 years after Carl Sandstedt. *Eur J Orthod* 28(3)*:*221-240.

Metsger DS, DePhilip RM, Hayes TG (1993). An autoradiographic study of calcium phosphate ceramic bone implants in turkeys. *Clin Orthop Relat Res* 291)*:*283-294.

Milne TJ, Ichim I, Patel B, McNaughton A, Meikle MC (2009). Induction of osteopenia during experimental tooth movement in the rat: alveolar bone remodelling and the mechanostat theory. *Eur J Orthod* 31(3)*:*221-231.

Monfoulet L, Malaval L, Aubin JE, Rittling SR, Gadeau AP, Fricain J-C *et al.* (2010). Bone sialoprotein, but not osteopontin, deficiency impairs the mineralization of regenerating bone during cortical defect healing. *Bone* 46(2)*:*447-452.

Murakami N, Saito N, Horiuchi H, Okada T, Nozaki K, Takaoka K (2002). Repair of segmental defects in rabbit humeri with titanium fiber mesh cylinders containing recombinant human bone morphogenetic protein-2 (rhBMP-2) and a synthetic polymer. *J Biomed Mater Res* 62(2)*:*169-174.

Nakase T, Nomura S, Yoshikawa H, Hashimoto J, Hirota S, Kitamura Y *et al.* (1994). Transient and localized expression of bone morphogenetic protein 4 messenger RNA during fracture healing. *J Bone Miner Res* 9(5)*:*651-659.

Neovius E, Lemberger M, Docherty Skogh AC, Hilborn J, Engstrand T (2013). Alveolar bone healing accompanied by severe swelling in cleft children treated with bone morphogenetic protein-2 delivered by hydrogel. *J Plast Reconstr Aesthet Surg* 66(1)*:*37-42.

Ng KW, Leong DT, Hutmacher DW (2005). The challenge to measure cell proliferation in two and three dimensions. *Tissue Eng* 11(1-2)*:*182-191.

O'Toole GC, Salih E, Gallagher C, FitzPatrick D, O'Higgins N, O'Rourke SK (2004). Bone sialoprotein-coated femoral implants are osteoinductive but mechanically compromised. *J Orthop Res* 22(3)*:*641-646.

Oldberg A, Franzen A, Heinegard D, Pierschbacher M, Ruoslahti E (1988). Identification of a bone sialoprotein receptor in osteosarcoma cells. *J Biol Chem* 263(36)*:*19433-19436.

Olsen BR, Reginato AM, Wang W (2000). Bone development. *Annu Rev Cell Dev Biol* 16(191-220.

Onishi T, Ishidou Y, Nagamine T, Yone K, Imamura T, Kato M *et al.* (1998). Distinct and overlapping patterns of localization of bone morphogenetic protein (BMP) family members and a BMP type II receptor during fracture healing in rats. *Bone* 22(6)*:*605-612.

Palmer W, Crawford-Sykes A, Rose RE (2008). Donor site morbidity following iliac crest bone graft. *West Indian Med J* 57(5)*:*490-492.

Papakostidis C, Kontakis G, Bhandari M, Giannoudis PV (2008). Efficacy of autologous iliac crest bone graft and bone morphogenetic proteins for posterolateral fusion of lumbar spine: a meta-analysis of the results. *Spine (Phila Pa 1976)* 33(19)*:*E680-692.

Parizi AM, Oryan A, Shafiei-Sarvestani Z, Bigham-Sadegh A (2013). Effectiveness of synthetic hydroxyapatite versus Persian Gulf coral in an animal model of long bone defect reconstruction. *J Orthop Traumatol* 14(4)*:*259-268.

Pirvu T, Blanquer SBG, Benneker LM, Grijpma DW, Richards RG, Alini M *et al.* (2015). A combined biomaterial and cellular approach for annulus fibrosus rupture repair. *Biomaterials* 42(0)*:*11-19.

Popova SN, Barczyk M, Tiger C-F, Beertsen W, Zigrino P, Aszodi A *et al.* (2007). α11β1 integrin-dependent regulation of periodontal ligament function in the erupting mouse incisor. *Mol Cell Biol* 27(12)*:*4306-4316.

Poynton AR, Lane JM (2002). Safety profile for the clinical use of bone morphogenetic proteins in the spine. *Spine (Phila Pa 1976)* 27(16 Suppl 1)*:*S40-48.

Provot S, Schipani E (2005). Molecular mechanisms of endochondral bone development. *Biochem Biophys Res Commun* 328(3)*:*658-665.

Qin C, Brunn JC, Jones J, George A, Ramachandran A, Gorski JP *et al.* (2001). A comparative study of sialic acid-rich proteins in rat bone and dentin. *Eur J Oral Sci* 109(2)*:*133-141.

Quinn JM, Neale S, Fujikawa Y, McGee JO, Athanasou NA (1998). Human osteoclast formation from blood monocytes, peritoneal macrophages, and bone marrow cells. *Calcif Tissue Int* 62(6)*:*527-531.

Ramay HR, Zhang M (2004). Biphasic calcium phosphate nanocomposite porous scaffolds for load-bearing bone tissue engineering. *Biomaterials* 25(21)*:*5171-5180.

Rios H, Koushik SV, Wang H, Wang J, Zhou H-M, Lindsley A *et al.* (2005). Periostin null mice exhibit dwarfism, incisor enamel defects, and an early-onset periodontal disease-like phenotype. *Mol Cell Biol* 25(24)*:*11131-11144.

Rios HF, Ma D, Xie Y, Giannobile WV, Bonewald LF, Conway SJ *et al.* (2008). Periostin is essential for the integrity and function of the periodontal ligament during occlusal loading in mice. *J Periodontol* 79(8)*:*1480-1490.

Ritting AW, Weber EW, Lee MC (2012). Exaggerated inflammatory response and bony resorption from BMP-2 use in a pediatric forearm nonunion. *J Hand Surg Am* 37(2)*:*316-321.

Saito T, Arsenault AL, Yamauchi M, Kuboki Y, Crenshaw MA (1997). Mineral induction by immobilized phosphoproteins. *Bone* 21(4)*:*305-311.

Sanuki R, Shionome C, Kuwabara A, Mitsui N, Koyama Y, Suzuki N *et al.* (2010). Compressive force induces osteoclast differentiation via prostaglandin E2 production in MC3T3-E1 cells. *Connect Tissue Res* 51(2)*:*150-158.

Sawyer AA, Song SJ, Susanto E, Chuan P, Lam CXF, Woodruff MA *et al.* (2009). The stimulation of healing within a rat calvarial defect by mPCL–TCP/collagen scaffolds loaded with rhBMP-2. *Biomaterials* 30(13)*:*2479-2488.

Saygin NE, Giannobile WV, Somerman MJ (2000). Molecular and cell biology of cementum. *Periodontol 2000* 24(73-98.

Schaeren S, Jaquiéry C, Wolf F, Papadimitropoulos A, Barbero A, Schultz-Thater E *et al.* (2010). Effect of bone sialoprotein coating of ceramic and synthetic polymer materials on in vitro osteogenic cell differentiation and in vivo bone formation. *Journal of Biomedical Materials Research Part A* 92A(4)*:*1461-1467.

Schlesinger PH, Blair HC, Teitelbaum SL, Edwards JC (1997). Characterization of the osteoclast ruffled border chloride channel and its role in bone resorption. *J Biol Chem* 272(30)*:*18636-18643.

Schliephake H, Weich HA, Dullin C, Gruber R, Frahse S (2008). Mandibular bone repair by implantation of rhBMP-2 in a slow release carrier of polylactic acid—An experimental study in rats. *Biomaterials* 29(1)*:*103-110.

Schmitt JM, Hwang K, Winn SR, Hollinger JO (1999). Bone morphogenetic proteins: an update on basic biology and clinical relevance. *J Orthop Res* 17(2)*:*269-278.

Schofer MD, Roessler PP, Schaefer J, Theisen C, Schlimme S, Heverhagen JT *et al.* (2011a). Electrospun PLLA nanofiber scaffolds and their use in combination with BMP-2 for reconstruction of bone defects. *PLoS ONE* 6(9)*:*e25462.

Schofer MD, Veltum A, Theisen C, Chen F, Agarwal S, Fuchs-Winkelmann S *et al.* (2011b). Functionalisation of PLLA nanofiber scaffolds using a possible cooperative effect between collagen type I and BMP-2: impact on growth and osteogenic differentiation of human mesenchymal stem cells. *J Mater Sci Mater Med* 22(7)*:*1753-1762.

Schwarz F, Ferrari D, Sager M, Herten M, Hartig B, Becker J (2009). Guided bone regeneration using rhGDF-5- and rhBMP-2-coated natural bone mineral in rat calvarial defects. *Clin Oral Implants Res* 20(11)*:*1219-1230.

Sellers RS, Zhang R, Glasson SS, Kim HD, Peluso D, D'Augusta DA *et al.* (2000). Repair of articular cartilage defects one year after treatment with recombinant human bone morphogenetic protein-2 (rhBMP-2). *J Bone Joint Surg Am* 82(2)*:*151-160.

Sfeir C, Ho L, Doll BA, Azari K, Hollinger JO (2005). Fracture Repair. In: Bone Regeneration and Repair: Biology and Clinical Applications. JR Lieberman and GE Friedlaender editors. Totowa, NJ: Humana Press Inc, pp. 21-44.

Shen J-W, Wu T, Wang Q, Pan H-H (2008). Molecular simulation of protein adsorption and desorption on hydroxyapatite surfaces. *Biomaterials* 29(5)*:*513-532.

Sheng Z-F, Ye W, Wang J, Li C-H, Liu J-H, Liang Q-C *et al.* (2010). OPG knockout mouse teeth display reduced alveolar bone mass and hypermineralization in enamel and dentin. *Arch Oral Biol* 55(4)*:*288-293.

Shintani S, Kamakura N, Kobata M, Toyosawa S, Onishi T, Sato A *et al.* (2008). Identification and characterization of integrin-binding sialoprotein (IBSP) genes in reptile and amphibian. *Gene* 424(1-2)*:*11-17.

Sodek J, McKee MD (2000). Molecular and cellular biology of alveolar bone. *Periodontol 2000* 24(1)*:*99-126.

Soenjaya Y, Foster BL, Nociti FH, Jr., Ao M, Holdsworth DW, Hunter GK *et al.* (2015). Mechanical Forces Exacerbate Periodontal Defects in Bsp-null Mice. *J Dent Res* 94(9)*:*1276-1285.

Somerman MJ, Shroff B, Agraves WS, Morrison G, Craig AM, Denhardt DT *et al.* (1990). Expression of attachment proteins during cementogenesis. *J Biol Buccale* 18(3)*:*207-214.

Soucacos PN, Johnson EO, Babis G (2008). An update on recent advances in bone regeneration. *Injury* 39 Suppl 2(S1-4.

Spicer PP, Kretlow JD, Young S, Jansen JA, Kasper FK, Mikos AG (2012). Evaluation of bone regeneration using the rat critical size calvarial defect. *Nat Protoc* 7(10)*:*1918-1929.

Stubbs JT, 3rd, Mintz KP, Eanes ED, Torchia DA, Fisher LW (1997). Characterization of native and recombinant bone sialoprotein: delineation of the mineral-binding and cell adhesion domains and structural analysis of the RGD domain. *J Bone Miner Res* 12(8)*:*1210-1222.

Suh DY, Boden SD, Louis-Ugbo J, Mayr M, Murakami H, Kim HS *et al.* (2002). Delivery of recombinant human bone morphogenetic protein-2 using a compression-resistant matrix in posterolateral spine fusion in the rabbit and in the non-human primate. *Spine (Phila Pa 1976)* 27(4)*:*353-360.

Tye CE, Rattray KR, Warner KJ, Gordon JAR, Sodek J, Hunter GK *et al.* (2003). Delineation of the Hydroxyapatite-nucleating Domains of Bone Sialoprotein. *J Biol Chem* 278(10)*:*7949-7955.

Tye CE, Hunter GK, Goldberg HA (2005). Identification of the Type I collagen-binding domain of bone sialoprotein and characterization of the mechanism of interaction. *J Biol Chem* 280(14)*:*13487-13492.

Udagawa N, Takahashi N, Akatsu T, Tanaka H, Sasaki T, Nishihara T *et al.* (1990). Origin of osteoclasts: mature monocytes and macrophages are capable of differentiating

into osteoclasts under a suitable microenvironment prepared by bone marrow-derived stromal cells. *Proc Natl Acad Sci U S A* 87(18)*:*7260-7264.

Ulery BD, Nair LS, Laurencin CT (2011). Biomedical Applications of Biodegradable Polymers. *J Polym Sci B Polym Phys* 49(12)*:*832-864.

Umoh JU, Sampaio AV, Welch I, Pitelka V, Goldberg HA, Underhill TM *et al.* (2009). In vivo micro-CT analysis of bone remodeling in a rat calvarial defect model. *Phys Med Biol* 54(7)*:*2147.

Vaahtokari A, Aberg T, Jernvall J, Keranen S, Thesleff I (1996). The enamel knot as a signaling center in the developing mouse tooth. *Mech Dev* 54(1)*:*39-43.

Valverde P, Tu Q, Chen J (2005). BSP and RANKL induce osteoclastogenesis and bone resorption synergistically. *J Bone Miner Res* 20(9)*:*1669-1679.

Valverde P, Zhang J, Fix A, Zhu J, Ma W, Tu Q *et al.* (2008). Overexpression of bone sialoprotein leads to an uncoupling of bone formation and bone resorption in mice. *J Bone Miner Res* 23(11)*:*1775-1788.

Vert M, Mauduit J, Li S (1994). Biodegradation of PLA/GA polymers: increasing complexity. *Biomaterials* 15(15)*:*1209-1213.

Wagner EF, Karsenty G (2001). Genetic control of skeletal development. *Curr Opin Genet Dev* 11(5)*:*527-532.

Walker CG, Ito Y, Dangaria S, Luan X, Diekwisch TGH (2008). RANKL, osteopontin, and osteoclast homeostasis in a hyperocclusion mouse model. *Eur J Oral Sci* 116(4)*:*312-318.

Wang EA, Rosen V, D'Alessandro JS, Bauduy M, Cordes P, Harada T *et al.* (1990). Recombinant human bone morphogenetic protein induces bone formation. *Proc Natl Acad Sci U S A* 87(6)*:*2220-2224.

Wang J, Zhou H-Y, Salih E, Xu L, Wunderlich L, Gu X *et al.* (2006). Site-Specific *In Vivo* Calcification and Osteogenesis Stimulated by Bone Sialoprotein. *Calcif Tissue Int* 79(3)*:*179-189.

White D (1978). Tissue substitutes in experimental radiation physics. *Med Phys* 5(6)*:*467-479.

Williams BJ, Smith JS, Fu KM, Hamilton DK, Polly DW, Jr., Ames CP *et al.* (2011). Does bone morphogenetic protein increase the incidence of perioperative complications in spinal fusion? A comparison of 55,862 cases of spinal fusion with and without bone morphogenetic protein. *Spine (Phila Pa 1976)* 36(20)*:*1685-1691.

Winnier G, Blessing M, Labosky PA, Hogan BL (1995). Bone morphogenetic protein-4 is required for mesoderm formation and patterning in the mouse. *Genes Dev* 9(17)*:*2105-2116.

Wise GE, King GJ (2008). Mechanisms of tooth eruption and orthodontic tooth movement. *J Dent Res* 87(5)*:*414-434.

Wozney JM (2002). Overview of bone morphogenetic proteins. *Spine (Phila Pa 1976)* 27(16 Suppl 1)*:*S2-8.

Wuttke M, Muller S, Nitsche DP, Paulsson M, Hanisch FG, Maurer P (2001). Structural characterization of human recombinant and bone-derived bone sialoprotein. Functional implications for cell attachment and hydroxyapatite binding. *J Biol Chem* 276(39)*:*36839-36848.

Xia B, Wang J, Guo L, Jiang Z (2011). Effect of bone sialoprotein on proliferation and osteodifferentiation of human bone marrow-derived mesenchymal stem cells in vitro. *Biologicals* 39(4)*:*217-223.

Xie G, Sun J, Zhong G, Liu C, Wei J (2010). Hydroxyapatite nanoparticles as a controlled-release carrier of BMP-2: absorption and release kinetics in vitro. *J Mater Sci Mater Med* 21(6)*:*1875-1880.

Xu L, Anderson AL, Lu Q, Wang J (2007). Role of fibrillar structure of collagenous carrier in bone sialoprotein-mediated matrix mineralization and osteoblast differentiation. *Biomaterials* 28(4)*:*750-761.

Yadav MC, de Oliveira RC, Foster BL, Fong H, Cory E, Narisawa S *et al.* (2012). Enzyme replacement prevents enamel defects in hypophosphatasia mice. *J Bone Miner Res* 27(8)*:*1722-1734.

Yang R, Gotoh Y, Moore MA, Rafidi K, Gerstenfeld LC (1995). Characterization of an avian bone sialoprotein (BSP) cDNA: comparisons to mammalian BSP and identification of conserved structural domains. *J Bone Miner Res* 10(4)*:*632-640.

Yaszemski MJ, Payne RG, Hayes WC, Langer R, Mikos AG (1996). Evolution of bone transplantation: molecular, cellular and tissue strategies to engineer human bone. *Biomaterials* 17(2)*:*175-185.

Yoshinaga Y, Ukai T, Abe Y, Hara Y (2007). Expression of receptor activator of nuclear factor kappa B ligand relates to inflammatory bone resorption, with or without occlusal trauma, in rats. *J Periodontal Res* 42(5)*:*402-409.

You L, Temiyasathit S, Lee P, Kim CH, Tummala P, Yao W *et al.* (2008). Osteocytes as mechanosensors in the inhibition of bone resorption due to mechanical loading. *Bone* 42(1)*:*172-179.

Younger EM, Chapman MW (1989). Morbidity at bone graft donor sites. *J Orthop Trauma* 3(3)*:*192-195.

Yu YY, Lieu S, Lu C, Miclau T, Marcucio RS, Colnot C (2010). Immunolocalization of BMPs, BMP antagonists, receptors, and effectors during fracture repair. *Bone* 46(3)*:*841-851.

Zaia J, Boynton R, Heinegard D, Barry F (2001). Posttranslational modifications to human bone sialoprotein determined by mass spectrometry. *Biochemistry (Mosc)* 40(43)*:*12983-12991.

Zhang H, Bradley A (1996). Mice deficient for BMP2 are nonviable and have defects in amnion/chorion and cardiac development. *Development* 122(10)*:*2977-2986.

Zhang J, Li L (2005). BMP signaling and stem cell regulation. *Dev Biol* 284(1)*:*1-11.

Zhang Q, Domenicucci C, Goldberg HA, Wrana JL, Sodek J (1990). Characterization of fetal porcine bone sialoproteins, secreted phosphoprotein I (SPPI, osteopontin), bone sialoprotein, and a 23-kDa glycoprotein. Demonstration that the 23-kDa glycoprotein is derived from the carboxyl terminus of SPPI. *J Biol Chem* 265(13)*:*7583-7589.

Zhang X, Rahemtulla F, Zhang P, Li X, Beck P, Thomas HF (2009). Normalisation of calcium status reverses the phenotype in dentin, but not in enamel of VDR-deficient mice. *Arch Oral Biol* 54(12)*:*1105-1110.

Zhou HY, Takita H, Fujisawa R, Mizuno M, Kuboki Y (1995). Stimulation by bone sialoprotein of calcification in osteoblast-like MC3T3-E1 cells. *Calcif Tissue Int* 56(5)*:*403-407.

Appendices

Appendix A: Statement of permission for the use of animals for experimental research.

All animal experimentation was conducted in compliance with the animal use protocol 2008-092 and 2009-008 held by Dr. Harvey Goldberg, principal investigator at the Schulich School of Medicine and Dentistry and the department of Biochemistry at the University of Western Ontario in London, Ontario, Canada.

Appendix B: Appendix B: Statement of permission to re-use Figure 1.2 from A.D.A.M. Education.

The permission of re-use of Figure 1.2, which was copied from https://www.nlm.nih.gov/medlineplus/ency/imagepages/1121.htm, were acquired from A.D.A.M. Education.

AUP Number: 2009-008
PI Name: Goldberg, Harvey
AUP Title: Bone Sialoprotein As Therapeutic Reagent For Enhanced Bone Repair

Approval Date: 04/11/2013

Official Notice of Animal Use Subcommittee (AUS) Approval: Your new Animal Use Protocol (AUP) entitled "Bone Sialoprotein As Therapeutic Reagent For Enhanced Bone Repair

" has been APPROVED by the Animal Use Subcommittee of the University Council on Animal Care. This approval, although valid for four years, and is subject to annual Protocol Renewal.2009-008::5

1. This AUP number must be indicated when ordering animals for this project.

2. Animals for other projects may not be ordered under this AUP number.

3. Purchases of animals other than through this system must be cleared through the ACVS office. Health certificates will be required.

The holder of this Animal Use Protocol is responsible to ensure that all associated safety components (biosafety, radiation safety, general laboratory safety) comply with institutional safety standards and have received all necessary approvals. Please consult directly with your institutional safety officers.

Submitted by: Copeman, Laura
on behalf of the Animal Use Subcommittee
University Council on Animal Care

AUP Number: 2008-092
PI Name: Goldberg, Harvey
AUP Title: Functional Characterization Of Bone Sialoprotein Using The *Bsp*-null Mouse

Approval Date: 10/11/2012

Official Notice of Animal Use Subcommittee (AUS) Approval: Your new Animal Use Protocol (AUP) entitled "Functional Characterization Of Bone Sialoprotein Using The Bsp-null Mouse

" has been APPROVED by the Animal Use Subcommittee of the University Council on Animal Care. This approval, although valid for four years, and is subject to annual Protocol Renewal.2008-092::5

1. This AUP number must be indicated when ordering animals for this project.

2. Animals for other projects may not be ordered under this AUP number.

3. Purchases of animals other than through this system must be cleared through the ACVS office. Health certificates will be required.

The holder of this Animal Use Protocol is responsible to ensure that all associated safety components (biosafety, radiation safety, general laboratory safety) comply with institutional safety standards and have received all necessary approvals. Please consult directly with your institutional safety officers.

Submitted by: Copeman, Laura
on behalf of the Animal Use Subcommittee
University Council on Animal Care

The following email on April 27, 2016 is to confirm that I have been granted permission to use image for thesis.

"Hello Yohannes,

Thank you for choosing ADAM Images!

Please see receipt attached (Transaction ID: AR1AD406A89F, Authorized code: 671030).

You have been granted permission for use of image for thesis:

ADAM Image, 1 time use for thesis (Student), Thesis: The role of bone sialoprotein in periodontal tissue development and bone repair.

Image: //www.nlm.nih.gov/medlineplus/ency/imagepages/1121.htm (Tooth anatomy)

If you have any questions, please let me know.

Sincerely,

Deidre

Deidre Friday

A.D.A.M. Education

Direct +1 678-281-2020 x2942 | **Fax** + 1 888-214-0614

Email deidre.friday@ebix.com | **Web** www.adam.com "

Curriculum Vitae

Yohannes Soenjaya

EDUCATION

Doctor of Philosophy in Biomedical Engineering, specialization in Biomaterials
University of Western Ontario, London, Ontario, Canada
Supervisor: Dr. Harvey A. Goldberg
Co-supervisor: Dr. Robert D. Litchfield
2009-2016

Master of Engineering and Management, Biomedical Entrepreneurship Track
Case Western Reserve University, Cleveland, Ohio, USA
2006-2007

Bachelor of Science Engineering in Biomedical Engineering, specialization in Orthopedic Biomaterials
Case Western Reserve University, Cleveland, Ohio, USA
2004-2007

HONOURS and AWARDS and SCHOLARSHIP

Western Graduate Research Scholarship
(Value: ~$15,000 annually)
2009-2013

Joint Motion Program Fellowship (A Canadian Institute of Health Research (CIHR) Training Program in Musculoskeletal Health Research and Leadership)
(Value: ~$13500 annually)
2009-2013

RELATED WORK EXPERIENCE

Graduate Teaching Assistantship
Department of Mechanical and Materials Engineering, University of Western Ontario

2009: MME 3379a - Material Selection

2010: MME 4446b - Composite Materials and MME 2260a - Industrial Materials

2011-2013: ES 1050 - Introductory Engineering Design and Innovation Studio

2012: MME 9620 - Nanomaterials and nanotechnology

PUBLICATIONS AND PRESENTATIONS

A. Manuscripts

Soenjaya Y, Eglin D, Willett TL, Holdsworth DW, Alini M, Hunter GK, Goldberg HA. Healing of rat calvarial defects with nanohydroxyapatite/ poly(ester-urethane) scaffolds loaded with bone sialoprotein or low-dose rhBMP-2. (In preparation)

Baskin ZJ, **Soenjaya Y**, McMasters J, Ko A, Vasanji A, Morris N, Eppell SJ. Nanophase bone substitute for craniofacial load bearing application: pilot study in the rodent. (Submitted; *Biomaterials*)

Marinovich R, **Soenjaya Y**, Wallace GQ, Zuskov A, Dunkman A, Foster BL, Ao M, Lam V, Rizkalla A, Beier F, Somerman MJ, Holdsworth DW, Soslowsky LJ, Lagugné-Labarthet F, Goldberg HA. The role of bone sialoprotein in the tendon-none insertion. *Matrix Biol*. (2016)

Soenjaya Y, Foster BL, Nociti FH, Jr., Ao M, Holdsworth DW, Hunter GK, Somerman MJ, Goldberg HA. (2015). Mechanical forces exacerbate periodontal defects in Bsp-null mice. *J Dent Res* 94(9)*:*1276-1285.

Foster BL, Ao M, Willoughby C, **Soenjaya** Y, Holm E, Lukashova L, Tran AB, Wimer HF, Zerfas PM, Nociti FH Jr, Kantovitz KR, Quan BD, Sone ED, Goldberg HA, Somerman MJ. (2015) Mineralization defects in cementum and craniofacial bone from loss of bone sialoprotein. *Bone*. 78:150-64.

Foster BL, **Soenjaya Y**, Nociti FH Jr, Holm E, Zerfas PM, Wimer HF, Holdsworth DW, Aubin JE, Hunter GK, Goldberg HA, Somerman MJ. (2013) Deficiency in acellular cementum and periodontal attachment in Bsp-null mice. *J Dent Res*. 92(2):166-72.

Baskin JZ, Vasanji A, McMasters J, **Soenjaya Y**, Barbu AM, Eppell SJ. (2012) Nanophase bone substitute in vivo response to subcutaneous implantation. *J Biomed Mater Res A.* 100(9):462-73.

B. Invited Presentations

<u>Oral Presentation</u>
Soenjaya Y, Foster BL, Nociti FH Jr, Holm E, Kantovitz KR, Aubin JE, Holdsworth DW, Hunter GK, Somerman MJ, Goldberg HA. Mechanical forces induces mandibular

defects in the bone sialoprotein null mouse. International Association for Dental Research. Boston, Massachusetts, USA. March 11, 2015. (Presented by Goldberg HA)

Soenjaya Y, Foster BL, Nociti FH Jr, Kantovitz KR, Aubin JE, Holdsworth DW, Hunter GK, Somerman MJ, Goldberg HA. Characterization of the bone sialoprotein null (*Bsp*$^{-/-}$) mice mandibular phenotype: The influence of mechanical force in inducing mandibular defects. 20th Annual Canadian Connective Tissue Conference. London Ontario. June 8, 2014.

Eppell SJ, Tong W, **Soenjaya Y**, McMasters J, Baskin JZ, "Nanophase bone substitutes: stealing a piece of nature's design," Biological Approaches in Materials Sciences, *Schloss Ringberg* (Rottach-Egern), Germany, 2008. (Presented by Eppell SJ)

Panelist
Y.Soenjaya, J.Z. Baskin, J. Morris, J. Jankowski, J.T. Kalnay, T. Biro, K. Spilizewski, M.E. Garrity-Moses, "Bringing research to clinical practice," The midwest biomedical engineering conference: Showcasing the future of biomedical engineering. Cleveland, Ohio, November 2007.

Y. Soenjaya, J. McMasters, S.J. Eppell, "Grooming tomorrow's innovators – undergraduate educational program in BME," The BioOhio annual focus on devices & diagnostics conference: Accelerating bioscience in Ohio. Dublin, Ohio, February 2007.

C. Abstracts and Poster Presentations

Soenjaya Y, Eglin D, Willett TL, Holdsworth DW, Alini M, Hunter GK, Goldberg HA. Healing of Rat Calvarial Defects With Nanohydroxyapatite/Poly(Ester-urethane) Scaffolds Loaded With rhBMP-2. 2014 Orthopaedic Research Society Annual Meeting. New Orleans, Louisiana, USA. March 15, 2014

Zuskov A, Dunkman AA, **Soenjaya Y**, Freedman BR, Soslowsky LJ, Goldberg HA. Alterations in the Mechanical Properties of Patellar Tendons in Bone Sialoprotein-Null Mice. 2014 Orthopaedic Research Society Annual Meeting. New Orleans, Louisiana, USA. March 15, 2014

Soenjaya Y, Holm E, Foster BL, Nociti FH Jr, Zerfas PM, Holdsworth DW, Aubin JE, Hunter GK, Somerman MJ, Goldberg HA. Defects in acellular cementum, periodontal attachment, and dentin and enamel mineralization in *Bsp*$^{-/-}$ mice. CIHR Joint Motion Training Program in Musculoskeletal Health Research and Leadership Annual Retreat. University of Western Ontario, London, Ontario. May 8, 2013

Soenjaya Y, Siqueira M, Holm E, Eglin D, Alini M, Holdsworth DW, Hunter GK, Litchfield RD, Goldberg HA. Bioactive protein improves cell attachment and mineralization on biodegradable poly(ester-urethane) based scaffold. 17th Annual Canadian Connective Tissue Conference. Ecole Polytechnique, Montreal, May 29, 2011

Soenjaya Y, Siqueira M, Holm E, Eglin D, Alini M, Holdsworth DW, Hunter GK, Litchfield RD, Goldberg HA. Bioactive protein improves cell attachment and mineralization on biodegradable poly(ester-urethane) based scaffold. CIHR Joint Motion Training Program in Musculoskeletal Health Research and Leadership Annual Retreat. University of Western Ontario, London, Ontario. May 13, 2011

Soenjaya Y, Hunter GK, Holdsworth DW, Goldberg HA. *In vivo* evaluation of recombinant bone sialoprotein and its derived fusion peptide for bone regeneration using calvarial and femoral defect models. Margaret Moffat Research and Career Day, The University of Western Ontario. March 31, 2010